H24/3684

MONASH UNIVERSITY
THESIS ACCEPTED IN SATISFACTION OF THE
REQUIREMENTS FOR THE DEGREE OF
DOCTOR OF PHILOSOPHY
ON..... 16 September 2003 .....
.....[redacted].....
Sec. Research Graduate School Committee

ERRATA

p ii "1.3 The Principles of Photochemistry" for "1.2 The Principles of Photochemistry", and correspondingly for the remaining sub-sections of Chapter 1.
p xi 15th line: "leachate" for "in leachate"
p xi para 3, 3rd line: "oxide" for "oxyhydroxide"
p 2 10th line: "humic substances their" for "humic structures its"
p 5, five lines from the bottom of the page: "by a" for "a"
p 10 para 2, 2nd line: "products," for "products, and"
p 13 para 4, 2nd line: "glyoxal has" for "glyoxal in has"
p 18 para 3, last sentence: "generated hydrated electrons and" for "generated and"
p 23 para 1, 3rd last line: "ammonia for" for "ammonia after for"
p 23 para 2, 4th line: "conducted on" for "conducted to"
p 26 para 2, last sentence: "fulvic acid was" for "fulvic acid"
p 27 para 3, 3rd line: "45%" for "45 %"
p 34 3rd last line: "reaction 1.9" for "reaction 1.10"
p 48 para 1, 11th line: "substances are" for "substances occur"
p 86 2nd last line: "hours of" for "hours or"
p 102 para 3, 1st line: "here indicate that" for "here that"
p 115 Figure 4.6, y axis label "pH"
p 145 para 1, 3rd line: "assess" for "asses"

ADDENDUM

p 3 para 1, last sentence: delete "both quantity and quality" and insert " the quality, in addition to the quantity"
p 6 and throughout the thesis: UVB should be UV-B, and similar with UV-A
p 20 Add at the end of sentence 2: " if mercury-organic complexes form, leading to changes in absorbance and redox properties"
p 27 para 2: Add to the end of the paragraph "A range of possible explanations was offered, including simultaneous stimulatory and inhibitory effects, and screening of UV-B by the reaction vessels that limited the production of low molecular weight products. The rate of photomineralisation was variable between carbon sources, and depth integrated rates indicated that bacterial metabolism was the dominant mineralisation mechanism"
p 27 para 3, 10th line: insert "in pre-irradiated samples" after "production"
p 28 2nd sentence: after "chlorophyll maximum" insert "(the water level with the highest concentration of algae)"
p 32 para 2, 15th line: After "solution at pH 4" remove "." And add ", in other words, the addition of fulvic acid increased the rate at both pHs, but was unable to overcome the effect of pH on the rate"
p 33 para 1, at the end of the paragraph: delete "." and insert ", i.e. the trend of increasing oxide reactivity was different with the two reductants"
p 33 para 2, 2nd sentence: after "more variable during the day" insert "than at night"
p 35 para 1, 9th line: delete "reaction 4" and insert "equation 1.9"
p 68 Insert legend for Figure 2.10 b:

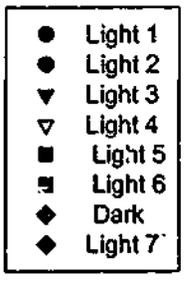

p 87 Replace Figure 3.3:

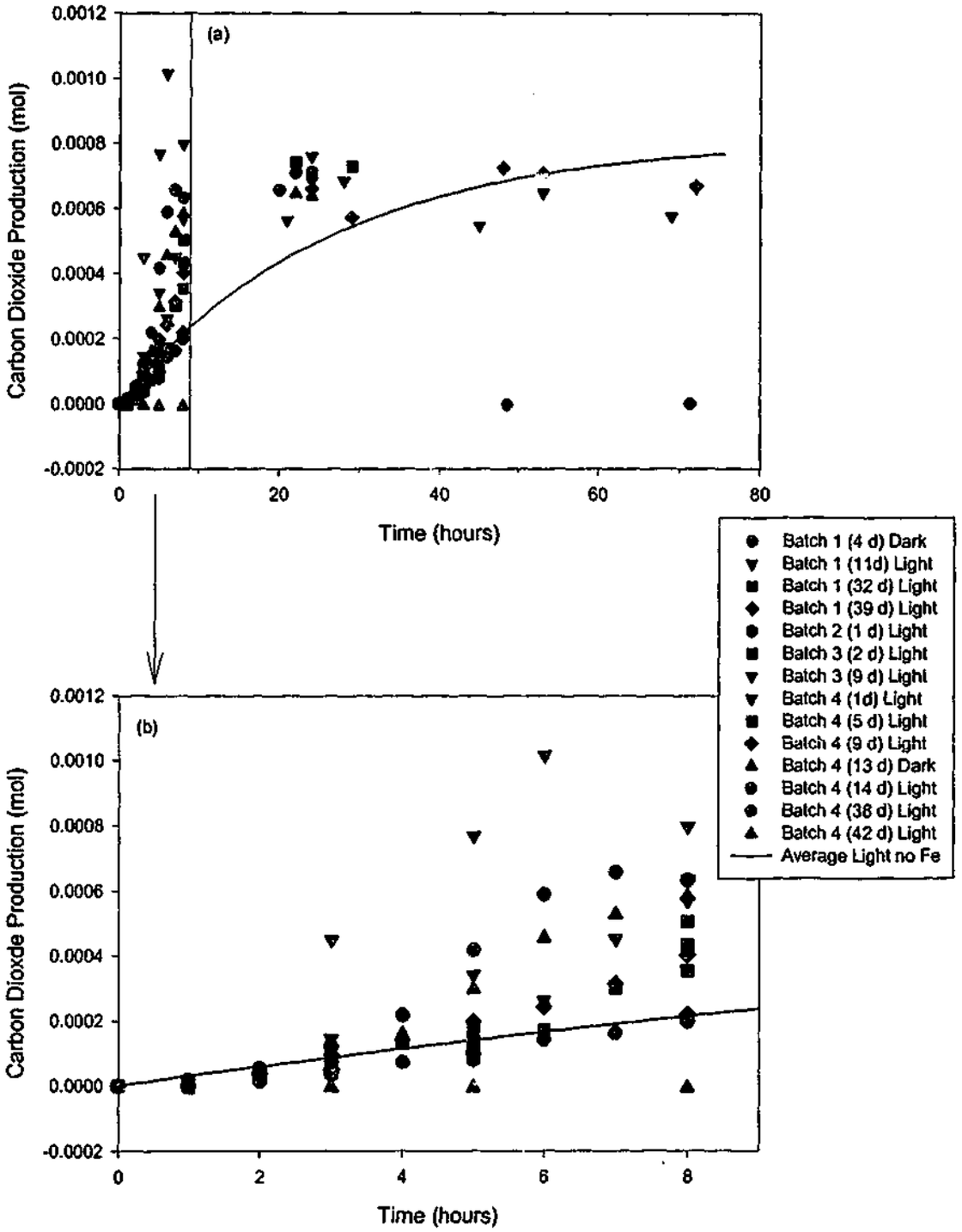

Photochemical Degradation of Aquatic Dissolved Organic Matter: the Role of Suspended Iron Oxides

Julia Alison Howitt

B. Sc. (Hons)

Water Studies Centre and School of Chemistry

Monash University

Clayton

May 2003

A thesis submitted according to the requirements for the Degree of Doctor of Philosophy at Monash University, Victoria, Australia.

Table of Contents

List of Figures

List of Tables

Abstract

Photochemical reactions can affect the cycling of organic carbon in aquatic ecosystems through direct degradation of dissolved organic matter (DOM) and changes to its availability within the food web. Suspended particles can influence these processes through changes in the light environment and interaction with the organic matter. The photochemical degradation of aquatic dissolved organic matter from billabong water samples and leachate from River Red Gum (*Eucalyptus camaldulensis)* leaves was examined. The effects of both artificial and natural light were investigated. The role of suspended iron oxides (goethite and amorphous iron oxyhydroxide) in influencing the photochemical degradation of DOM was also examined.

Irradiation of DOM with artificial UV and visible light resulted in photoproduction of carbon dioxide, traces of carbon monoxide and consumption of oxygen. The relationship between O_2 consumption and CO_2 production varied with the source of DOM and irradiation time. Substantially more CO_2 was produced than O_2 was consumed in billabong water samples, with a delay in the uptake of O_2 in some samples. In contrast, the in leachate samples showed an initial consumption of O_2 and a delay in CO_2 production. After long reaction times the molar ratio of O_2 consumed to CO_2 produced tended towards 1:1. This observation is consistent with the uptake of oxygen (via reactive oxygen intermediates such as $^1O_2$ and $HO^{\cdot}$) by the DOM to form functional groups such as -COOH and -OH. It is likely that variation in the initial DOM composition results in changes to the ratio of O_2 consumed to CO_2 produced.

The role of iron oxides in the photochemical degradation of dissolved organic matter was complex and depended on the age and structure of the iron oxide. Fresh amorphous iron oxyhydroxide increased the maximum rate of reaction in leachate samples by almost an order of magnitude. It is hypothesised that this iron oxide accelerated the rate of CO_2 production through coordination between oxygen atoms in the DOM and surface or dissolved Fe(III) atoms, providing a pathway for electron transfer reactions. This mechanism can involve a lag phase through delays in the photochemical production of functional groups containing oxygen atoms in the organic matter.

After aging, amorphous iron oxide was less effective in catalysing the photochemical interaction between leachate DOM and the oxide. For example, goethite suppressed the rate of photochemical degradation of billabong DOM, the degree of suppression being dependent on the concentration of goethite particles. This was hypothesised to be a result of reduced oxide reactivity (photochemical and/or surface adsorption) combined with increased light absorption and scattering by the oxide.

Amorphous iron oxide also increased the rate of photochemical degradation of both leachate and billabong DOM under natural sunlight irradiation. Small quantities of unidentified low-molecular-weight products were detected, these most likely being organic acids. Photochemical degradation of billabong water caused the three-dimensional fluorescence spectra to become more like that of leachate, indicating a reduction in the humic content, and potentially, an increase in the bioavailability of the remaining organic matter through a simplification of the molecular structure of the DOM. Bioavailability of the organic carbon, determined through bacteria counts and CO_2 production, appeared to increase after irradiation of billabong water, but not after irradiation of leachate.

It was shown that the photochemical reactions do alter the structure and bioavailability of DOM under environmentally relevant conditions and that the processes could be important under some environmental conditions.

Statement of Originality

This thesis contains no material that has been accepted for the award of any other degree or diploma in any university or other institution. To the best of my knowledge, this thesis contains no material previously published or written by another person, except where due reference is made in the text.

Julia Alison Howitt

Acknowledgements

I would like to thank my supervisors, Darren Baldwin and Gavin Rees from the Murray Darling Freshwater Research Centre and Barry Hart from Monash University for your support and advice on all aspects of the project, from experimental setup to the writing of this thesis. Thankyou also to Darren for providing the goethite samples used for some of the experiments.

Many others at the Murray Darling Freshwater Research Centre have also assisted with the experiments that made up this project. Alison Mitchell in particular deserves my gratitude for all her help over the last four years. Thankyou Ali, I appreciate all the time you have spent on everything from helping me battle the GC to providing moral support. Thankyou also to Trish Bowen for providing dried Eucalyptus leaves, John Pengelly for doing the TOC analyses, and Chester Merrick and Zygmunt Lorenz for your help with the light intensity measurements and Amina Price for helping with the last-minute thesis problems. Thankyou also to everyone else at the MDFRC for being a great bunch of people to work with and for taking an interest.

There are also many people at Monash University that I would like to thank: Richard Morrison for conducting the spectral analysis of the replacement Hanovia lamp and Peter Godson for lending me the lamp and everyone at the Water Studies Centre who have helped me over the years, particularly Mike Grace, Rob Seefeld, Kellie Vanderkruk, Sophie Bourgues and Pam Dickinson.

Thankyou to Diane M. McKnight and J. Robin Fulton from the University of Colorado, Boulder for advice on fluorescence corrections and Zygmunt Lorenz of the MDFRC for providing a macro on which to base the corrections. Thankyou also to the Australian Bureau of Meteorology for providing weather data for Albury.

Thankyou to Monash University, The Murray Darling Freshwater Research Centre and The Cooperative Research Centre for Freshwater Ecology for the use of equipment and financial support through an Australian Postgraduate Award and a CRC top-up scholarship.

Finally, thankyou to my family: my parents Robert and Alicia, my brothers Brett and Grant and my sister Tanya. You have been patient and supportive and I couldn't have made it without you.

1 Literature Review

1.1 Light in the Aquatic Environment

The aquatic ecosystems of inland Australia are diverse and include natural systems such as rivers, billabongs and lakes, and man-made structures such as dams, canals and weir pools. In all these environments light plays an important role by driving photosynthesis in aquatic plants, affecting visibility for aquatic animals and triggering a range of photochemical reactions that alter both the chemical and physical properties of the aquatic environment. High levels of turbidity are a common feature of Australian rivers and the high levels of suspended sediment can lead to changes in the light transmission within the waterbody, with reduced light penetration and a change from direct to diffuse light dominating the system. High organic carbon loadings are also an infrequent but important part of the inland river systems. Flooding of forested land can result in "black water" events, involving a pulse of concentrated organic matter entering the river after leaching from leaf litter on the forest floor. Concentrated organic matter is also left for extended periods in billabongs along the river course. These black water events can lead to low dissolved oxygen, diminished light penetration and may cause fish kills (Baldwin et al. 2001).

The work reported in this thesis focuses on the photodegradation of dissolved organic matter (DOM) and the effect of suspended minerals on the photochemical reactions, with a view to improving our understanding of the effects of high turbidity on organic matter degradation and its availability to microbial life. This chapter shall provide a summary of the research in this field to date, including studies on changes to the bulk properties of DOM, low-molecular-weight photoproducts, effects on nutrient cycles, the role of reactive intermediates, changes to carbon bioavailability and interactions with metals.

1.2 The Nature of Dissolved Organic Matter

Dissolved organic matter is an important light-absorbing substance and contributes a significant proportion of the colour in water bodies (Reche et al. 1999). In the order of 50-90% of the dissolved organic carbon is poorly defined and is classed as humic substances, with the remainder consisting of simple classes of compounds such as fatty acids, amino acids, carbohydrates, hydrocarbons and phenols (Morel and Hering

1993). Humic substances are polymers of a diverse range of organic building blocks and their structures are ill-defined and complex. They are yellow to brown in colour and have molecular weights ranging from about 500 D to 100,000 D (McKnight and Aiken 1998). A number of possible building blocks of humic substances have been proposed (Paciolla et al. 1999) two of which are shown in Figure 1.1.

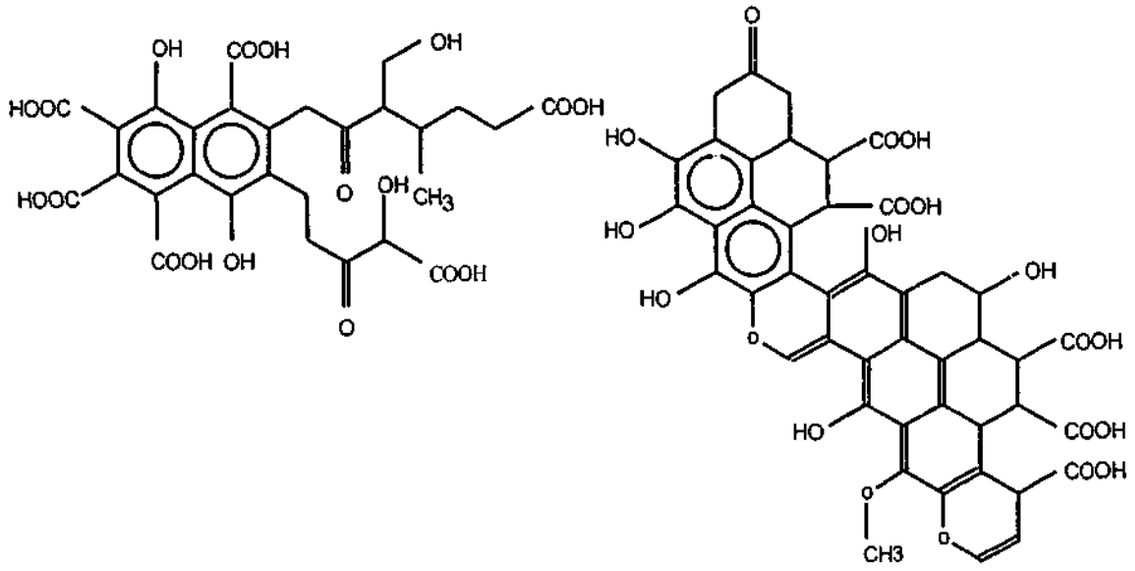

Figure 1.1: Some proposed building blocks of humic structures (Paciolla et al. 1999).

The essential features are a large number of carboxylic acid functional groups (COOH), hydroxyl groups (OH), carbonyls (C=O), aromatic rings and long chains. The structures may also contain nitrogen in various forms and be bound to metals, particularly via bonds to N and O. These building blocks link together to form the polymeric structures that give humic structures its properties. Aquatic humic substances are operationally divided into humin, humic and fulvic acids, based on separation techniques. Fulvic acids are generally defined as the fraction of the humic material that is soluble at any pH, humic acids are soluble above pH 2 and humin is insoluble at any pH. Fulvic acid is more common in the dissolved fraction and both humic and fulvic may be found in equal abundance in the suspended particulate material but humin is generally not significant in the water column (McKnight and Aiken 1998).

The non-humic fraction of the dissolved organic matter consists of relatively small molecules and these tend to be both chemically and biologically active, and can be cycled in the system on a timescale of minutes to days (Morel and Hering 1993). In contrast the humic fraction is refractory and has much slower turnover times.

Dissolved organic matter is involved in a number of important processes within aquatic ecosystems. It has been demonstrated that chromophoric dissolved organic matter controls the attenuation of ultraviolet light in high-altitude lakes (Laurion et al. 2000), except when dissolved organic matter concentration was very low and algal biomass became a significant contribution to the attenuation. Humic substances interact with a range of environmental chemicals. A number of processes can be influenced by the presence of humic substances, including: solubilization of hydrophobic organic molecules through a surfactant action, catalysing the hydrolysis of organic pollutants, effects on microbial processes, photosensitizing or quenching the degradation of non-absorbing compounds and transport of other environmental chemicals (Choudhry 1984). It has been proposed that coloured dissolved organic matter is of such importance to the functioning of lakes that coloured dissolved organic matter (CDOM) should be considered alongside the nutrient levels when considering the response of lake ecosystems to multiple stressors (Williamson et al. 1999). The authors indicate that CDOM is involved in determining the degree of autotrophy vs. heterotrophy, the temperature and oxygen gradients, and the impact of disturbances ranging from forest fires, acid rain, nutrient loads and toxic pollutants. It was also noted that the ratio of the absorbance of water samples at 320nm to the dissolved organic carbon concentration varied widely between lakes, indicating that both the quantity and quality of DOC in lakes is variable.

The photochemistry of dissolved organic matter is complex, as the complicated structures lead to a large number of possible outcomes when these molecules undergo reactions. For clarity, the various outcomes of photochemical reactions have been separated into categories, but it is important to remember that in natural systems these reactions are interlinked and many processes may be occurring simultaneously to varying proportions.

1.3 The Principles of Photochemistry

Photochemical reactions arise from the absorption of light by molecules, exciting an electron into a higher energy level (a brief explanation of energy levels and chemical bonding is included in Appendix 1). The energies of photons in the visible and ultraviolet light are comparable to the energies of chemical bonds (100 to 500

kJ/mol) (Moore 1983). The absorption of light can be described as a two-step process, the first resulting in the production of an excited state molecule:

$$M + h\nu \rightarrow M^* \qquad \text{Equation 1.1}$$

M^*, the excited state of the molecule M, is a short-lived species (10^{-8} – 10^{-9} s), which will then undergo one of a number of relaxation processes, the most common being relaxation to the ground state with the emission of heat or light (Skoog and Leary 1992). Alternatively, the excited state may undergo chemical reactions to produce new species, as the atoms are more loosely bound in the excited states (Eisberg and Resnick 1985), and these reactions are referred to as photochemical reactions. In most molecules, the absorption of a quantum of light leads to a transition from a singlet ground state to a singlet excited state, and there is usually an excited triplet state somewhere below the excited singlet (Moore 1983). The energy of the photon absorbed must match the energy difference between two orbitals, and this means that only some functional groups can absorb light of environmentally significant wavelengths. In the case of organic molecules this generally means that chromophores (the absorbing part of the molecule) require unsaturated bonds and the transitions are from non-bonding or π orbitals to π^* orbitals. The conjugation of unsaturated bonds reduces the energy of the π^* orbital and so conjugated double bonds or aromatic systems absorb light of longer wavelength. The absorption of light by transition metal complexes can occur through either the transition of an electron between *d* orbitals of differing energies or transfer of electrons between metal-based and ligand-based orbitals. These transitions tend to be in the visible part of the spectrum and lead to the strong colours of many transition metal complexes. The charge transfer absorption processes act as a form of internal redox reaction and may result in the breakdown of the excited state, leading to photochemical redox reactions (Skoog and Leary 1992). Light can also excite electrons in semiconductors. An electron within the valence band can be excited across the band gap into the conduction band. The presence of an electron in this delocalised band, and a corresponding hole in the valence band causes an increase in conductivity of the semiconductor (Ashcroft and Mermin 1976). Following photoexcitation of the semiconductor, organic molecules at the surface can either accept an electron from the conduction band and be reduced, or donate an electron into the valence band and be oxidized (Langford and Carey 1987), or an adsorbed molecule may absorb the photon,

form an excited state and inject an electron into the conduction band of the semiconductor particle and be oxidized (Wolfbauer et al. 2001).

1.4 Photochemistry of DOM: Structural Changes.

Photochemical changes to dissolved organic matter have been observed through changes in both the properties of the DOM and the concentration of low molecular weight photoproducts. Photobleaching of DOM is a phenomenon that has received attention in a number of studies over recent years, especially due to concerns over the effect of additional UV exposure of aquatic ecosystems resulting from ozone depletion (Andrews et al. 2000, Whitehead et al. 2000, Gibson et al. 2001, Osburn et al. 2001). Exposing natural waters to sunlight results in a loss of colour, suggesting changes to the chromophores in the DOM. The changes in the absorbance of lake water at 250 nm (A_{250}) and 365nm (A_{365}) have been used as an indicator to track degradation of the humic substances (De Haan 1993). The absorbances at both wavelengths were decreased by exposure of the water to natural sunlight. They proposed that an increase in the ratio of A_{250} to A_{365} suggested an increase in the proportion of smaller size molecules as it is the large, conjugated aromatic molecules that allow humic substances to absorb the longer wavelengths of light; a reduction in the size of the molecules pushes the absorbance towards the shorter wavelengths. Similar responses have been measured following the artificial irradiation of lakewater (Lindell et al. 1995) and also in fractionated and unfractionated lakewater, with the greatest increase in absorbance ratio found in the non-humic fraction (Reitner et al. 1997). Photobleaching of a dissolved soil humic acid was found to be accompanied by a reduction in the average molecular weight and an increase in acidity when photo-oxidation occurred under an O_2 atmosphere (Schmitt-Kopplin et al. 1998). They found that the ratio of A_{465} to A_{665} was inversely correlated to average molecular weight and that this ratio increases when the acid is photodegraded under oxygen. Size exclusion chromatography has also been used to determine that preferential bleaching of longer wavelengths was accompanied a decrease in the average molecular weight of the DOM (Bertilsson and Bergh 1999). Photobleaching of the coloured dissolved organic matter in the upper layer of a stratified lake has been measured in situ (Gibson et al. 2001), and a diurnal variation in the penetration of 380 nm light could be shown.

Action spectra (plots of the relative photoresponse per photon versus wavelength) for the photobleaching of seawater were prepared (Kieber et al. 1990) and when normalized to solar spectral irradiance showed that the reactions were primarily due to the action of UV-B radiation (280-320nm). The loss in water colour in samples from a humic lake was found to vary with sunlight dose and the relative loss of colour varied from 5.2 to 7.7% during the first day of exposure to sunlight (Reche et al. 1998). Another study (Reche et al. 1999) involving a comparison of photobleaching in 30 lakes, found that it was primarily an abiotic, sunlight-mediated process, demonstrating a first order relationship between sunlight exposure and photobleaching rates. UV-B (<320 nm), UV-A (320-400 nm) and photosynthetically active radiation (PAR >400 nm) all contributed to the photobleaching. Variation in photobleaching between the lakes (0-19% d^{-1}) were ascribed to differences in the chemical and trophic conditions in the lake as well as the origin and nature of the DOM. In particular, the ionic conditions were thought to influence the rate of photobleaching by changing the ratio of fulvic to humic acids or altering the conformation of the organic molecules. Other factors that correlated with the rate of photobleaching included the biological activity, DOM composition, the sum of divalent cations in the water, pH, the acid neutralizing capacity and conductivity. The water chemistry appeared to be the most important factor with the greatest photobleaching found in hardwater lakes. Similar rates of photobleaching have been found in a Finnish lake (up to 11 %) (Vähätalo et al. 2000). Up to 60% of the absorbance in the UV region of the spectrum could be lost in Mississippi River water after 28 days of sunlight exposure, with the highest levels of photobleaching occurring between 320 and 360 nm (Opsahl and Benner 1998).

In a set of mesocosm experiments using seawater (Whitehead et al. 2000), an enhancement of UVB did not cause a proportional increase in photobleaching. As this experiment retained much of the biological component of the seawater and was optically thick, the authors pointed to multiple mechanisms influencing dissolved organic matter colour and also stated that the rate of photobleaching at any wavelength is not exclusively dependent on photons absorbed at that wavelength. Evidence for the changing character of DOM during irradiation includes the apparent quantum yields for photobleaching at 310 nm changing over the course of the degradation (Andrews et al. 2000). Spectral weighting functions for a number of lakes have been calculated by using filters to exclude portions of the solar irradiance from filtered water samples

(Osburn et al. 2001). The loss absorbance at a specific wavelength was found to be the result of energy absorbed over a range of the spectrum, and the peak wavelength for photobleaching effect was 330 nm, in the UVA region although the UVB region was also found to contribute. The study also suggested that seasonal changes to the DOM may alter the photoreactivity.

A related characteristic of DOM that has been used to indicate photochemical reactions is the decrease in fluorescence observed following irradiation. Aromatic groups tend to absorb UV radiation more strongly than aliphatic groups, and since fluorescence requires the absorption of UV radiation, it is a measure of the aromatic proportion of the DOC (Lean 1998). As much as 30% of the fluorescence of a water sample can be lost by a single days exposure to sunlight. An action spectrum for fluorescence bleaching was produced that had a maximum at ~365 nm, much longer wavelengths than for absorbance photobleaching (Kieber et al. 1990). The fluorescence spectra showed broad excitation (320-380) and emission (420-480) bands, so the action spectrum maxima corresponded with the maxima for excitation. Fluorescence loss however was uniform over the range of emission and excitation. Twenty four percent of the fluorescence (excitation 365 nm, emission 470 nm) of 200 nm filtered lake-water samples was lost after two weeks of irradiation (De Haan 1993). The decrease was non-linear with time, indicating the presence of compounds with a range of photoreactivities, or the production of compounds with differing fluorescent properties. Similarly, between 10 and 20% of fluorescence was lost in Swedish lake water samples incubated at the surface of the lake for 18 hrs and 1.7% was lost at a depth of 2m (Granéli et al. 1996). The authors linked this loss of fluorescence to the production of dissolved inorganic carbon from the DOC.

The photobleaching of fluorescence (ex: 360 nm, em: 490 nm) has been found to reverse over time after irradiation of seawater with added trilinolein (a triglyceride with three linoleic acid chains) (Kieber et al. 1997). The process was enhanced by the addition of ammonia after the irradiation was complete and the fluorescence (used as a measure of humic substances) reached levels well above the starting levels. The authors proposed a mechanism of humic substance generation from trilinolein through photo-production of aldehydes followed by aldol-type condensation reactions, and the addition of nitrogen through the formation of schiff base intermediates. The importance of this work is that it indicates that exposure to sunlight can have a role in both decreasing and

increasing the humic content of aquatic dissolved organic matter and highlights the complex nature of photochemical reactions in the environment.

Photobleaching of organic matter fluorescence has also been measured at the whole-lake scale (Gibson et al. 2001). They found a linear decrease in fluorescence in the sub-arctic Canadian lake over several weeks until a rainfall event caused a sharp increase in the observed levels. Diurnal changes in fluorescence resulting from photobleaching have also been observed in the ocean (Obernosterer et al. 2001a). Photochemical processes have also been found to decrease the fluorescence lifetime of riverine DOM (Clark et al. 2002).

The information that can be obtained from fluorescence measurements at a fixed excitation wavelength and a limited emission wavelength range, while giving an indication of the changes to the humic material, does not adequately assess the changes to the total fluorescent properties of the dissolved organic matter. More information can be obtained with the technique of 3-D fluorescence contouring (or excitation-emission matrix spectroscopy). The technique has been used to characterise DOM from a variety of sources (Coble 1996). In addition to the information provided by individual fluorescence scans, 3-D fluorescence spectroscopy determined the fluorescence maximum (Ex_{max}/Em_{max})- the combination of excitation and emission wavelengths which results in maximum fluorescence. The spectra of humic substances were found to contain two maxima, one resulting from excitation in the UV region and the other from excitation in the visible region. Amongst the fluorescence properties of dissolved organic matter, Coble noted that the fluorescence maxima of extracted marine humic substances are shifted towards shorter wavelengths than the unconcentrated samples, that the relative intensity of the two maxima varies between samples, and that the maxima are blue-shifted as the salinity of the water increases (i.e. as the sample becomes more marine than riverine), but this shift was also thought to be affected by biological activity. The shifts in excitation maxima were indicative of changes in the absorption spectra of the samples. The blue-shift of the emission maxima could be the result of an increase in the energy difference between the ground and first excited states of the fluorophores. A reduction in the extent of the π-electron system, or the loss of functional groups such as carbonyl, hydroxyl or amine groups were offered as possible explanations. Fluorescence from a protein- or amino acid-like component was also present in marine surface waters and porewaters.

Absorbance correction of the spectra was found to be essential for accurate comparison of humic substance samples, especially at high concentrations (Mobed et al. 1996). Without absorbance correction, the fluorescence maxima shift to longer wavelengths with increasing concentration due to inner filtering of the emitted shorter wavelengths. Once corrections were applied, the spectra were independent of concentration and ionic strength, but were influenced by changes to pH. Dilution of estuarine water samples has been used to minimize the inner-filtering effect without making absorbance corrections (Moran et al. 2000). In this study fluorescence bleaching in light-exposed samples was slightly biased toward the region of the spectrum usually associated with terrestrial humic materials and the maxima shifted toward shorter wavelengths. Excitation/Emission matrices were used with absorbance correction for both the excitation and emission wavelengths (discussed in further detail in Appendix 2) to characterise the fluorescence properties of fulvic acids of terrestrial and microbial origins (McKnight et al. 2001). The authors found that fulvic acids derived from microbial material exhibit a sharper peak and at lower wavelengths than was found in the terrestrially derived fulvic acids. In their study it was possible to use a combination of peak location and the ratio of emission at 450 nm to 500 nm (excitation 370 nm) to differentiate between the two classes of fulvic acid. A humification index has been defined (Ohno 2002) based on the fluorescence intensity of emission in the 300-345 nm region divided by the sum of emission intensity in the 300-345 and 435-480 nm regions when the sample is excited by light of 254 nm. This study found the humification index was also concentration dependent unless corrections were made for inner filtering of the excitation and emission wavelengths.

A more comprehensive analysis of the fluorescent spectra of natural organic matter was undertaken with the development of the Spectral Fluorescent Signature technique (Marhaba et al. 2000). This technique uses the shape and locations of peaks to identify six fractions of the dissolved organic matter but was developed on a limited range of water samples and requires further validation before use on DOM from different sources.

It is clear that photochemical reactions can have significant (and sometimes contrasting) effects on the bulk properties of the dissolved organic matter and that many of these changes can be inferred from changes in the spectral properties of the mixture. Photobleaching of the absorbance and fluorescence spectra provide useful techniques to

follow changes in both the molecular weight and bonding complexity of the organic matter, provided care is taken to adjust the fluorescence data for absorbance of light within the sample to prevent concentration effects.

1.5 Photochemistry of DOM: Photoproducts.

More specific information about the photodegradation of dissolved organic matter is obtained by identifying and quantifying specific degradation products, and which can include CO_2, CO and low-molecular weight organic acids and aldehydes.

1.5.1 Dissolved Inorganic Carbon

The production of dissolved inorganic carbon (CO_2, H_2CO_3, HCO_3^- and CO_3^{2-}) is a significant route for DOM photooxidation. The production of dissolved inorganic carbon was measured in irradiated samples of humic lake water (Salonen and Vähätalo 1994). Samples were irradiated using sunlight in glass or quartz containers and the difference in photochemical dissolved inorganic carbon (DIC) production suggested that light of shorter wavelengths than 340 nm was important for DIC production. Depth profiles also indicated that UV light penetration played an important role in the rate of DIC photoproduction. Irradiation of filtered riverine, near-coastal and salt marsh water samples with simulated sunlight was found to produce DIC at a rate which was strongly correlated to the rate of photobleaching (Miller and Zepp 1995). The rate of DIC photoproduction was only slightly affected by changes to pH but was reduced by prolonged exposure to light. Dissolved inorganic carbon production was studied in five Swedish lakes by incubating quartz tubes of filter-sterilized water at varying depths for one day (Granéli et al. 1996). DIC production was equivalent to consumption of 1.7-3.7% of the DOC per day and was similar to the production of DIC caused by plankton community respiration. Photooxidation was detected at depths below the penetration of UV-B, indicating lower energy light contributed to the reactions, and depth-integrated photooxidation was independent of DOC content and colour. Loss of fluorescence was linearly related to the production if DIC. A similar study found that photochemical CO_2 production equated to ~10% of the photosynthesis rates for three lakes in Ontario during July (Lean 1998). An action spectrum produced for photochemical mineralization in a humic lake (based on measurements on filter-sterilized water in quartz tubes at varying

depths) suggested that UV-B contributed 9%, UV-A 68% and visible light contributed 23% to the photochemical DIC production in that lake (Vähätalo et al. 2000).

A study of the degradation of coastal marine dissolved organic matter found that the production of DIC accounted for up to 94% of the direct carbon loss as volatile products during photodegradation (Miller and Moran 1997). The production of DIC was strongly correlated to the loss of absorptivity in this study. The authors found the results were consistent with the production of DIC via photochemical decarboxylation of the DOM (see references within). The rate of photoproduction of DIC was found to vary seasonally in artificially irradiated lake water, with the lowest rates in late summer and early autumn, implying a seasonal change in the nature and reactivity of the DOM (Lindell et al. 2000). Both UV-A and UV-B radiation contributed to the photoreactions, however, the UV-B component of the light was found to be considerably more important than its fraction of the incident energy would imply, especially where the DOM was recalcitrant. In a comparative study of the photochemical reactivity of DOM from 38 lakes the variables that correlated to the production of DIC included: total absorbed energy, alkalinity, pH, conductivity and total iron (Bertilsson and Tranvik 2000). Only total iron had a strong positive relationship with DIC production. Alkalinity, pH and conductivity had negative effects and indicate highly productive lakes. Bertilsson concluded that autochthonous DOM is less photochemically active than allochthonous DOM. It was also found that CO_2 was not produced once oxygen dropped below 25% of saturation, suggesting an oxygen-dependent mechanism. However, this study used water samples that had been both frozen and filter-sterilized so it is possible that changes to the dissolved organic matter had occurred prior to irradiation. The trend towards increased photochemical production of DIC at lower pH was confirmed in a recent mesocosm experiment (Anesio and Granéli 2003).

These studies have highlighted the significance of DIC as a product of DOM photoreactions, and have linked its production with the reactions responsible for photobleaching of the DOM. The relative contribution of different wavelengths of light varied between studies, but ultraviolet light was generally considered to be more important than visible light. While many variables affected the rates of production including the source and aging of DOM, the measured rates indicate the photo-oxidation of DOM is a significant source of DIC in lakes and an important route for the cycling of carbon in the studied water bodies. A notable feature of these studies, is the filtration of

water samples prior to irradiation. Filtration is necessary to minimize bacterial production of CO_2, which would confound interpretation of the studies, however, filtration also removes colloidal aggregates of organic matter which may also be photoreactive, and particle surfaces that may interact with the organic matter in the environment, thereby influencing the photoreactions.

1.5.2 Carbon Monoxide

The photochemical production of carbon monoxide from irradiated seawater samples has been found to be linearly related to humic concentration and fluorescence (Mopper et al. 1991). Carbon monoxide concentrations in a eutrophic lake were found to be influenced by light- indicated by diurnal fluctuations and depth profiles (Conrad et al. 1983). The study could not isolate a mechanism, but possibilities included photooxidative processes within microbial cells or photooxidation of dissolved organic matter, particulate or dead cellular material. The rates of production of CO varied by a factor of 17 between filtered natural water samples from lakes, wetlands and coastal waters, however, rates normalized to A_{350} varied by only ± 15% (Valentine and Zepp 1993). The rates were also constant over the pH range 4-8. The authors interpreted these results to mean that the photodegradation of humic substances in the waters was the source of the CO. Normalized rates remained constant even after prolonged sunlight exposure and a 90% loss of absorbance at 350nm. This helps explain why the rates from different sites were so similar. The highest quantum yields were found for the UV-B region of the spectrum, but in terms of production UV-A and blue light were more important due to higher intensities of these bands in natural sunlight.

Another study found similar normalized rates of CO production, but noted that CO_2 was produced at a rate that was usually 20 times higher (range 10- 65 times higher) than the rate of CO production (Miller and Zepp 1995). Other studies have reported ratios that fall within this range. Carbon monoxide production has been measured at a rate linear with photobleaching and at one-tenth the rate of CO_2 generation (Lean 1998) and CO production from marine DOC was also related to light absorption and at a rate fifteen time lower than DIC production (Miller and Moran 1997).

A review by (Moran and Zepp 1997) highlighted the importance of CO as a photoproduct of DOM, both as one of the most abundant products and as a factor in carbon cycling through volatilization (CO has low solubility in water and is readily lost from aquatic ecosystems) and bacterial uptake. Carbon Monoxide photoproduction has

also been studied in a number of North American lakes (Zuo and Jones 1997). They found that CO production was a linear function of the light exposure time, and that the rate decreased by less than 10% after 14hr irradiation with a solar simulator. The rate of CO formation was the same in filtered and unfiltered samples. A good correlation was found between the rate of CO formation and DOC concentration, initial light absorbance and fluorescence, supporting the hypothesis that the CO is produced by photoreactions of the DOC, however, the role of reactive transients must also be considered. Increasing the concentration of iron was also observed to increase the production of CO. The mechanism discussed involves a photochemical cleavage of the α-carbon of carbonyl compounds. Aromatic carbonyls, phenols and α-dicarbonyls have been suggested as particularly likely to be involved and addition of these compounds to water was found to enhance the production of CO.

It is evident that the production of CO in natural waters is related to the photodegradation of DOM. Although the ratios between DIC and CO production vary widely, perhaps reflecting differences in the starting material, it is accepted that CO is an important photoproduct but produced in much lower quantities.

1.5.3 Organic Products

Low-molecular-weight (LMW) carbonyl compounds are potentially bioavailable products of DOM photodegradation. At least fourteen LMW organic molecules are known to be produced during the photoreaction of DOM (Moran and Zepp 1997). Formaldehyde, acetone, glyoxal, methylglyoxal, glyoxalate and pyruvate have been described as the major photo-produced LMW compounds (Lean 1998). The suggested mechanism for their production involves interaction with a hydroxyl radical, which can lead to the formation of a carbonyl group. Rearrangement of bonds within the organic matter can then result in the separation of a low-molecular-weight carbonyl compound from the larger organic compound.

The photochemical production of formaldehyde, acetaldehyde, acetone and glyoxal in has been measured in seawater (Mopper and Stahovec 1986). The products were found to be readily consumed by biota resulting in diurnal fluctuations of acetaldehyde and formaldehyde in the ocean as the excess photoproducts were consumed at night. Photochemical production of glyoxylic and pyruvic acids was also measured in filter-sterilized seawater irradiated with sunlight (Kieber and Mopper 1987). Unfiltered samples underwent diurnal changes due to the uptake of the acids by

biota. Oceanic profiles of these two acids suggested that glyoxalate is formed photochemically in the environment while pyruvate concentrations may depend more heavily on biological processes. A later study found that the biological uptake of pyruvate from seawater was correlated to the photochemical production and that the source of the pyruvate was high-molecular-weight organic matter (Kieber et al. 1989).

The photo-production of formaldehyde, acetaldehyde, acetone, glyoxal, methylglyoxal and glyoxalate was studied in unfiltered seawater and filtered freshwater samples (Kieber et al. 1990). Action spectra, normalized to irradiance, indicated that UV-B radiation was primarily responsible for the photoproduction of these compounds from humic substances. The production was linearly related to the initial absorbance and fluorescence of the samples and a linear relationship was also observed between the loss of absorbance and fluorescence and production of LMW compounds. Normalization of the cumulative concentrations of formaldehyde, acetaldehyde and acetone to the UV absorbance demonstrated a linear increase over time, while glyoxalate, glyoxal, and methylglyoxal plateaued after 10 hrs, probably due to the further photolysis of these products. The photochemical production of LMW carbonyl compounds was found to be higher in the surface microlayer of the ocean than in sub-surface water, and diurnal variations in the concentrations were observed (Zhou and Mopper 1997).

Acetate, citrate, formate, levulinate, pyruvate and several other fatty acids were produced in the leachate from decomposing emergent macrophytes following exposure to UV-B radiation (Wetzel et al. 1995). It was proposed that side-chain oxidations of lignin-based macromolecules could be responsible for these results. NMR spectra of UV exposed DOC indicated that the leachate contained less carbohydrate-like material than was present in the original DOC. The cinnamyl phenol derivatives of the lignin were also diminished. A study of the photochemical reactivity of dissolved lignins found that ~80% of the lignins in Mississippi water were removed after 28 days of sunlight exposure (Opsahl and Benner 1998). Only 16% were lost in the dark controls over the same period of time, most likely due to bacterial action. The decrease in concentration due to photooxidation followed an exponential decay and the fraction remaining at the end of the experiment was more recalcitrant. Absorbance bleaching was observed but did not correlate with loss of lignin. In contrast, the lignin in Pacific Ocean water was much less susceptible to photoreaction, with little loss of either lignin

or absorbance after sunlight exposure. A number of explanations for these observations were proposed: the presence of a resistant component of the original macromolecule (due to susceptible fractions having already undergone photodegradation), physical shielding by other DOM components, or the formation of stable bonds between lignin and other compounds. The loss of photosensitizers (molecules which form reactive intermediates after exposure to light and initiate reactions in other compounds) may also have reduced the rate of photodegradation. The reactions that occurred resulted in degradation of methoxyl groups, side chains and a reduction in aromaticity. There was also a marked shift in molecular size, with 90% of the lignin in the high-molecular-weight (HMW) fraction of DOM in the river sample prior to reaction and 79% in the LMW fraction following reaction. The additional LMW lignin was produced from the HMW fraction and was more refractory than the initial compounds and highly oxidized.

A decrease in average molecular weight of soil humic acid was also found during photo-oxidation under oxygen accompanied by a substantial decrease in phenolic subunits and synthesis of carboxy acids (including benzenedicarboxylic acids) and long chain alkanes (Schmitt-Kopplin et al. 1998). A selective degradation of the components of the humic acid was reported, with the lignin and lipids being most susceptible and the N compounds, alkyl aromatics and carbohydrates the most stable. Photoproduced reactive intermediates are believed to play an important role in these degradation reactions.

Oxalic, malonic, formic and acetic acids can be generated by irradiating filter-sterilized humic lake water with low intensity UV-A radiation (Dahlen et al. 1996). Succinic and butyric acid and a number of other compounds were also detected in small quantities (Bertilsson and Allard 1996). These acids were also produced during sunlight irradiation of sterile filtered lake water with formic acid accounting for about 50% of the carboxylic acid produced (Bertilsson and Tranvik 1998). The production of oxalic, malonic, formic and acetic acids (averaged over water samples from 38 lakes) was 34 % of the amount of DIC produced (Bertilsson and Tranvik 2000). However, the ratios of the four acids varied between samples from different sites. The production of individual LMW carboxylic acids occurs at rates of comparable magnitude to the rate of CO production. Photochemical production of these four organic acids has also been observed in UV-A irradiated macrophyte leachates with differences observed between

species (Farjalla et al. 2001). The further photodegradation of oxalic acids was also observed.

In contrast to the studies above, which emphasized degradation and a shift towards lower average molecular weight, it has also been found that photochemical reactions can also produce molecules with increased molecular weight and the formation of humic substances (Kieber et al. 1997). The processes studied involved an initial reduction in molecular weight via the photodegradation of unsaturated fatty acids to aliphatic aldehydes with a higher degree of saturation. The compounds with a higher degree of unsaturation were found to react at significantly higher rates. The photolysis of unsaturated fatty acids was found to result in oxidative cleavage of the double bond, producing aliphatic aldehydes and an ω-oxocarboxylic acid of lower molecular weight. The triglyceride trilinolein was also studied and produced primarily hexanal, with smaller amounts of other compounds. The degradation products matched those of its component fatty acid, linoleic acid. However, the aldehyde products have the potential to react with ammonia and organic amines, providing a pathway for the incorporation of nitrogen into humic materials. A sample of trilinolein-treated seawater, following exposure to sunlight, exhibited a photobleaching loss of fluorescence, which was then followed by a gradual increase in fluorescence back to initial levels after two weeks. The addition of ammonia produced a greater increase in humic material, with fluorescence exceeding the starting levels, and the reaction occurring at a greater rate. The ammonia concentration decreased over time and the dissolved organic nitrogen increased. The mechanism proposed for the formation of humic substances following the photodegradation of triglycerides involved an aldol condensation between the aldehyde and a carbonyl on one of the chains- increasing the level of cross-linking within the structure. Ammonia could be incorporated as a schiff base, and a variety of radically induced cross-linking and rearrangement reactions could follow, producing a humic material that contains covalently bound nitrogen.

It is evident that exposing natural dissolved organic matter to sunlight produces a variety of structural changes, many leading to smaller molecules, but also to the possibility of increased humification in some cases. The changes to DOM induced by sunlight can be followed through absorption and fluorescence changes of the sample, as well as through detection of the most common photoproducts: dissolved inorganic carbon, CO and low molecular weight carboxylic acids.

1.6 Reactions of transient oxidants.

Photochemical reactions of DOM produce a variety of transient oxidants with the potential to react with other molecules in solution in what could be described as indirect photoreactions. Three main processes are involved (Zafiriou et al. 1984):

- energy transfers such as between high-energy triplet states of chromophores and dissolved oxygen to produce singlet oxygen
- electron transfers between chromophores and non-absorbing reactants
- production of radicals and other reactive oxidants that can contribute to the degradation of non-absorbing species.

Photochemical oxygen consumption in a coloured lake decreased rapidly with depth due to decreases in light penetration (Miles and Brezonik 1981). At 0.1 m depth, the oxygen consumption in light-exposed samples was found to be three times that in dark controls. Singlet oxygen is known to be formed in surface waters (Zepp et al. 1977). The photochemical formation of singlet oxygen also occurred in a range of Dutch surface waters (Wolff et al. 1981). Oxygen consumption was measured and estimates of singlet oxygen production were reasonably correlated with total organic carbon concentration.

Components of the DOM found in seawater can act as photosensitizers for the production of singlet oxygen by energy transfer from an excited DOM triplet (Momzikoff et al. 1983). Photochemical oxygen consumption in lake and seawater was measured at levels equivalent to between 5 and 50% of photosynthetic oxygen production in those waters (Laane et al. 1985). The authors noted the involvement of UV radiation and $^1O_2$. Humic substances have been found to photosensitize the isomerization of 1,3-pentadiene and the oxygenation of 2,5-dimethylfuran- two compounds which are transparent to solar UV radiation (Zepp et al. 1985). These compounds did not bind to the humic substances and the authors proposed a mechanism which involved firstly the absorption of light by humic molecules to form excited singlets, some of which then decay by intersystem crossing to form excited triplets:

$$H + h\nu \rightarrow {}^1H^* \rightarrow {}^3H^* \qquad \text{Equation 1.2}$$

Triplets may be deactivated by a number of processes including decay to the ground state or reaction with other molecules, including O_2.

$$^3H^* + O_2 \rightarrow H + {}^1O_2 \qquad \text{Equation 1.3}$$

$$^1O_2 + A \rightarrow AO_2 \qquad \text{Equation 1.4}$$

Singlet oxygen is a strong oxidant and can react with acceptor molecules (A), such as dimethylfuran. Alternatively, $^3H^*$ could react directly with either the cis- or trans-pentadiene to form an excited triplet of pentadiene that can relax back into either isomer. The energy transfer processes require that the $^3H^*$ energy is equal to or greater than that for the energy acceptor. The energy required to excite pentadiene is greater than that required to produce singlet oxygen, so some humic triplets will be capable of undergoing either reaction path and some will only generate singlet oxygen as a result of the range of humic molecules present in solution. Up to half of the humic triplets were estimated to have energies of at least 250 kJ/mol and this is sufficient for energy transfer to occur to a large range of environmental compounds (Zepp et al. 1985).

Irradiation of fulvic acid and lake water with UV and visible light was found to generate singlet oxygen and an additional transient oxidant, most likely to be a peroxy radical. This transient oxidant was derived from the DOM and was involved in DOM sensitized oxidation of alkylphenols (Faust and Hoigné 1987). Hydrogen peroxide is also formed by irradiation of natural water samples and the rate of accumulation is related to the concentration of light-absorbing organic matter. Rates have been measured in the range of 2.7×10^{-7} to 48×10^{-7} mol L^{-1} h^{-1}, for waters with DOC concentrations of 0.53 to 18 mg L^{-1} (Cooper et al. 1988).

Laser flash photolysis studies also suggested that solvated electrons and excited radical cations can be formed from the irradiation of humic substances (Fischer et al. 1987). However, most of the photoejected electrons generated by irradiating DOM from natural waters bodies and soil re-combine with cations before escaping into the bulk solution (Zepp et al. 1987a). Sunlight irradiations generated and estimates for the production of hydrated electrons at the surface of water bodies of approx. 0.04 μmol/[(mg of DOC) h] (Zepp et al. 1987a).

The major reactive intermediates of DOM secondary photochemical reactions are (Hoigné et al. 1989):

- singlet oxygen ($^1O_2$)
- peroxy radicals ($ROO^{\cdot}$)
- H_2O_2
- solvated electron (e_{aq}^-)

- superoxide anion (O_2^-)
- humic structures excited to triplet states ($^3DOM^*$)

Nitrate and nitrite also produce hydroxyl radical ($HO^\cdot$) by photochemical processes. Of these only H_2O_2 is sufficiently long-lived to accumulate. $HO^\cdot$ is primarily consumed by fast scavenging by DOM, at rates that vary with different types of DOM. Peroxy radicals are often consumed by reaction with antioxidants, and as they are derived from diverse DOM molecules, the speciation of these radicals is complicated and unknown. The formation of superoxide can occur via direct electron transfer from excited organic molecules to O_2, through a range of mechanisms including via solvated electrons (Cooper et al. 1989). Disproportionation of superoxide generates H_2O_2. DOM is both a source and a sink for $HO^\cdot$ in the sea and the UV-B region of the spectrum is most important for its production (Mopper and Zhou 1990). The authors also found that deep-sea DOM is more readily degraded by $HO^\cdot$ than DOM from surface water samples. The generation of reactive oxygen species is summarised by Reaction Scheme 1.1 (Blough and Zepp 1995).

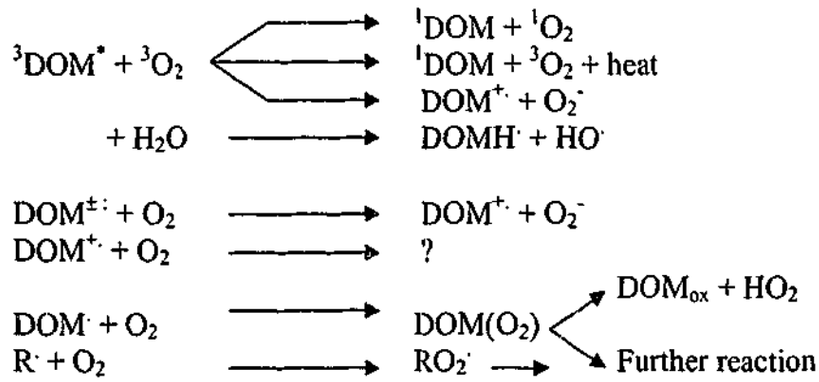

Reaction Scheme 1.1: The formation of reactive oxygen species. $^3DOM^*$, and ^1DOM are the excited triplet and ground state of DOM, respectively. $DOM^{\pm:}$ indicates a bi-radical generated via charge separation. $R^\cdot$ is an organic radical and $RO_2^\cdot$ A peroxy radical.

This reaction scheme indicates the complexity of the photochemical reactions of dissolved organic matter, indicating only primary reactions generating reactive oxygen species. Many decay routes are possible after the production of these species.

Methyl and methoxy phenols have been shown to undergo photosensitized transformation in the presence of DOM via interaction with the reactive triplet through either electron transfer or H-atom abstraction (Canonica et al. 1995). Abiotic oxygen

consumption increased with DOC content in a range of water samples following irradiation with PAR and UV-A (Lindell and Rai 1994). The experiment indicated that in humic waters oxygen consumption processes (photochemical and biological) could be more important than primary production, however, samples were poisoned with $HgCl_2$ and this could influence the photochemistry of dissolved organic matter. Substantial photochemical oxygen consumption was observed to be linear with light exposure during irradiation of lake water (Lindell et al. 1995). A study of photochemical oxygen consumption in filter-sterilized lake water found that UV-B radiation was responsible for 35 % of the reactions in unfractionated water (Reitner et al. 1997). The photochemical oxygen consumption normalized to DOC were more than twice as high in the humic fraction than the non-humic fraction.

A study of the photochemical degradation of a soil humic acid highlighted the importance of oxygen to the processes by conducting the reactions under both a nitrogen and an oxygen atmosphere (Schmitt-Kopplin et al. 1998). Reactions under an oxygen atmosphere were associated with a reduction in total organic carbon and a decreased pH, while these remained essentially unchanged under nitrogen. The O/C ratio under an O_2 atmosphere increased from 0.61 to 0.97, indicating that O_2 was incorporated into the remaining organic material. Irradiation under nitrogen did result in reduction of the average molecular weight, but the effect was more pronounced under O_2.

The quantum yield for photochemical oxygen consumption from marine water changes over the course of the irradiation (Andrews et al. 2000). The authors found that 1- 50 % of photochemical oxygen uptake could be attributed to singlet oxygen pathways, depending on absorption coefficients at 300nm. Photochemical oxygen demand in the Atlantic ocean exceeded bacterial respiration and UV-B radiation was responsible for 0-30 % of the photochemical O_2 demand (Obernosterer et al. 2001a). Diurnal variations in H_2O_2 and DOM fluorescence also occurred. The role of hydroxyl radicals in the degradation of humic substances has been examined through the use of γ-radiolysis of water (Goldstone et al. 2002). $HO^{\cdot}$ was found to produce dissolved inorganic carbon with high efficiency (~0.3 mol CO_2/mol $HO^{\cdot}$) and was involved in the production of low molecular weight organic acids. The bleaching of the DOM was relatively slow and the rates of DIC and LMW acid production were much lower than

can be expected for sunlit waters, indicating that HO· plays a minor role in the photochemical degradation of humic substances.

The importance of oxygen in thc photochemical reactions of dissolved organic matter has been established, although some degradation can occur in the absence of oxygen. It is clear that a wide range of reactive intermediates- many involving oxygen- play a role in the degradation of DOM and the formation of oxidized organic products. The photochemical degradation of DOM, therefore, not only acts as an importar: route for the cycling of carbon in the environment, but also can have a significant effect on the cycling of oxygen in aquatic environments through a range of mechansims.

1.7 Photochemistry of DOM: Effect on nutrients.

Exposing natural water samples to sunlight has the potential to affect more substances than just the carbon and oxygen cycles, for example, nitrogen and phosphorus compounds can also be affected by sunlight.

1.7.1 Phosphorus

Phosphorus concentrations in aqueous systems can be affected by sunlight through a variety of mechanisms. A large proportion of the dissolved phosphorus in an acid bog lake was found to occur as a class of high-molecular-weight (HMW) compounds that were chromatographically similar to dissolved humic materials (Francko and Heath 1982). This "HMW phosphorus" released orthophosphate when exposed to low intensity UV light. Daytime concentrations of UV-sensitive complex P were linearly related to co-chromatographing dissolved humic material (DHM) absorbance. This is consistent with the theory that DHM had formed a complex with phosphorus that could be broken down by UV-light. A diurnal variation occurred in both the concentrations of DHM and UV-sensitive P. The increase in UV-sensitive P was accompanied by an increase in Fe^{2+} suggesting the presence of organic-Fe-P complexes. The phosphate reactions were potentially linked to the reduction of Fe^{3+} associated with humic material in the water. The HMW P complex did not release orthophosphate when combined with alkaline phosphatase, providing additional evidence for an abiotic, photochemical process. The presence of UV-sensitive complex P was also observed in a later study (Francko 1986) and the addition of dissolved humic material and ferric iron influenced the processes. Addition of Fe^{3+} to lake water

labelled with $^{32}PO_4^{3-}$ increased the amount of labelled P eluting with orthophosphate following UV irradiation (Cotner and Heath 1990). Release of orthophosphate did not accompany photoreduction of Fe^{3+} on all occasions when un-amended lake water was irradiated however, suggesting that P was not always associated with Fe.

Another mechanism involves the effect of humic materials and sunlight on phosphatase (Boavida and Wetzel 1998). Phosphatases released by organisms can complex with humic substances in the water, leaving the enzyme inactive. Movement of the water can transport these complexes into the photic zone, where the phosphatases are released by UV irradiation. The enzymes are partially protected by the humic acid from direct photolysis. The binding capacity of the humic acid to the phosphatase depends on the source of the phosphatase. Thus, exposing humic acids in natural water systems, which may contain a reserve of stored enzyme, to sunlight can result in a release of phosphorus into the water through the action of the liberated enzyme.

1.7.2 Nitrogen

Nitrogen cycling in aquatic ecosystems can be affected by sunlight in a number of ways and the results of studies to date have been quite variable. Nitrate is itself photoactive, and the irradiation of nitrate can result in production of nitrite, free oxygen atoms and hydroxyl radicals, potentially influencing the photooxidation of organic matter (Zepp et al. 1987b).

The photochemical release of amino acid from a soil humic acid was examined by irradiating a humic acid solution to which ^{14}C-labelled glycine had been adsorbed/reacted (Amador et al. 1989). Increasing sunlight exposure resulted in the glycine being associated with progressively lower-molecular-weight fractions of the humic acid, and also increased the bioavailability of the complex. Photochemical reactions of unamended dissolved organic matter can also result in the release of bioavailable nitrogen (Bushaw et al. 1996).

Four hours of sunlight exposure lead to nitrogen release from a fulvic acid solution, with ammonium formation possibly occurring via a complex, multi-step mechanism. Rates of NH_4 formation, normalized to absorbance at 350 nm, were found to be similar for humic substances from different locations, however overall production appeared to be highest for samples with little previous sunlight exposure. It was proposed that the released nitrogen came from amino sugars and other nitrogen rich compounds which were associated with the humic substances and converted to

ammonium and other bioavailable compounds through photochemical processes followed by hydrolysis. Irradiation of Suwannee River humic and fulvic acids, and colloidal Bayou Trepagnier DOM samples in a solar simulator resulted in near-linear ammonia production, and the ammonia production continued for several hours after irradiation (Tarr et al. 2001). The production of free amino acids was also observed in this study. The photodegradation of the amino acids in the presence and absence of natural organic matter indicated that some, such as glycine and histidine, did not decompose to ammonia. Tryptophan broke down to ammonia in DOM independent reactions and other amino acids produced ammonia in DOM dependent reactions. The presence of hydroxyl radical was found to be important for ammonia production, although direct ammonia photoproduction from DOM and amino acids also occurs. It was hypothesised that the continuing production of ammonia after irradiation of DOM is the result of hydroxyl radical generation from H_2O_2. The continuing release of ammonia after for several hours after irradiation of humic and fulvic acids was also observed in another study (Wang et al. 2000). The release was described as involving at least a two-step process, at least one photochemical and one dark reaction.

In contrast to these studies, no measurable production of ammonia was observed following irradiation of river water samples with a UV lamp and an increase in bioavailable nitrogen was not observed (Bertilsson et al. 1999). It was suggested that the differences could have been due to these experiments being conducted to whole water samples with a high existing level of nitrogen, whereas the previous experiments were based on a humic extract. They also do not exclude the possibility of a reversible release of LMW nitrogen compounds.

Photochemically induced uptake of ammonia by humic substances has also been observed (Kieber et al. 1997). Addition of ammonia to irradiated trilinolein-treated seawater encouraged the production of humic products and the decline in ammonia was accompanied by an increase in dissolved organic nitrogen. The nitrogen containing functional groups in a soil humic acid however, were found to be relatively stable under UV irradiation (Schmitt-Kopplin et al. 1998).

Nitrite was found to be a product of the photodegradation of DOM (Kieber et al. 1999). In experiments with humic substances added to seawater, the amount of nitrite produced photochemically was correlated to the amount of added humic material and to the length of irradiation. The relationship proved to be complex in natural waters

however, and was affected by both humic substances and initial nitrite concentrations. In samples with high initial nitrite, the direct photochemical degradation of nitrite could exceed photoproduction from humic substances. Aqueous solutions of HNO_2^- and NO_2^- have also been found to undergo photoreactions and generate hydroxyl radicals (Arakaki et al. 1999).

A recent study to investigate the inconsistencies in photochemical release of labile N compounds from dissolved organic (Koopmans and Bronk 2002) found ammonia production in river and creek samples, where initial N had been primarily in the form of organic nitrogen. In contrast, groundwater samples which initially had predominantly ammonia-N had more photochemically mediated loss of ammonia than production, suggesting a dependence on the initial form of the nitrogen. The production of dissolved primary amines and NO_2^- was inconsistently observed, possibly due to the low concentration of DOM in the study.

The photochemical degradation of dissolved organic matter has the potential to alter the bioavailability of both nitrogen and phosphorus in aquatic ecosystems, through both direct and indirect mechanisms. The studies described above highlight both the complexity and potential significance of photochemical reactions on nutrient cycles in the environment.

1.8 Impact of photochemistry on the bioavailability of DOM.

Exposing dissolved organic matter to sunlight can impact on its availability to bacteria in the aquatic environment. Weak photolysis of macromolecules (molecular weight > 1,500 Da) was found to enhance the availability of the organic matter to two species of bacteria, but not to a third (Geller 1986). The results reflected changes to the bioavailability of the organic matter, but also differences in the metabolic requirements of the bacteria. Sunlight irradiation was also shown to increase the bioavailability of radiolabelled glycine associated with soil humic acid and this increased bioavailability was associated with a decrease in molecular weight of the organic matter (Amador et al. 1989).

In one study, inorganic N and P were added to lake water to avoid nutrient limitation and then it was exposed to artificial UV light (Lindell et al. 1995). Oxygen consumption and photobleaching indicated photochemical reactions had occurred. Subsequent bacterial growth experiments revealed the bacterial abundance increased

logarithmically with the duration of pre-irradiation of the sample and bacterial cell volumes also increased. The effects on bacterial abundance plateaued after 8-10 hours of light exposure. The increase in bacterial abundance was ascribed to the photo-oxidation products of the DOM. This study was however, conducted on water samples which had been autoclaved, and the DOC may not have been representative of natural samples. A similar study (Reitner et al. 1997) also observed consumption of oxygen and changes in absorbance due to photochemical reactions when lake water was exposed to sunlight. The abundance of bacteria following inoculation and incubation of this water was found to be ~46% higher than in the dark controls. Samples in which the bacteria were directly exposed to UV radiation experienced a drop in bacterial activity by ~50%, indicating that while UV degradation of the DOM is beneficial to the bacteria, the UV itself is detrimental to the organisms. UV stressed bacteria were observed to recover more rapidly when long-wavelength UV-A and PAR were present than in the dark, which suggests that the damage is done by UV-B and that a repair mechanism exists which uses the other wavelengths. An increase in bacterial growth efficiency and abundance have also been found in photobleached samples of DOC (Reche et al. 1998). Bacterial production however was decreased due to photoinhibition by the UV-A and visible radiation used in the experiment. Production was only measured during daylight hours and abundance was measured after several days, so abundance was taken as the most reliable indicator of the overall effect of sunlight exposure. It was proposed that the positive effects of photobleaching were a result of the production of low-molecular-weight substrate and changes to the DOC, and also possibly due to cometabolism (the presence of the readily available substrate assists bacterial degradation of the more resistant molecules). In these experiments insufficient P and N were released photochemically to overcome nutrient limitation; nutrient addition significantly enhanced the utilization of photobleached DOC. The relationship between photobleaching and increased bioavailability was also observed in biologically refractory estuarine water (Moran et al. 2000).

Similar bacterial growth enhancement was found in fulvic acid solutions which had either been exposed to sunlight or had glucose added (Bushaw et al. 1996). Phosphorous addition was required due to nutrient limitation, but nitrogen was not required in samples exposed to sunlight, indicating that photochemical nitrogen release was sufficient to overcome nitrogen limitation in these samples. The increase in

assimilable nitrogen was also found to increase the rate of degradation of the humic substances. The authors suggested that release of biologically available nitrogen could be a key process in regulating the microbial turnover of DOM.

The photochemical production of pyruvate in seawater was found to result from DOC with molecular weight > 500 and the biological uptake of pyruvate was found to be highly correlated to it's photochemical production (Kieber et al. 1989). The release of LMW fatty acids was also found to be responsible for the stimulation of bacterial growth following exposure of organic extracts from decomposing plants to UV-B radiation (Wetzel et al. 1995). The humic acid was more affected by the UV light than the fulvic acid, but the macromolecules in each fraction were affected to only a minor extent.

Filter-sterilized humic lake water was found to photochemically produce several carboxylic acids, and a 52-hour sunlight exposure produced a fourfold increase in total bacterial biomass (Bertilsson and Allard 1996). Microbial uptake of the carboxylic acids was observed, but the bacterial uptake of carbon was estimated to exceed the production of these compounds, indicating changes to the bioavailability of the high-molecular weight compounds also occurred. The photochemical production of three organic acids (malonic, formic and acetic) from high-molecular weight DOM from a humic lake was found to provide a major bacterial substrate, implying that organic acid production was a significant factor in the increased bioavailability of humic materials after irradiation (Bertilsson and Tranvik 1998). Another study, based on river water samples (Bertilsson et al. 1999), found that carboxylic acids could account for 10 – 72 % of the photochemically induced increase in bacterial biomass, indicating that in this study, other changes to the DOC were important for overall change to DOC bioavailability.

Alternating cycles of light exposure and microbial degradation have been found to result in more extensive degradation of DOM in coastal seawater than just microbial processes (Miller and Moran 1997). The increased degradation was due to photochemical mineralization and the production of compounds more readily consumed by bacteria. The loss of DOC through each of these processes was about the same. Changes in the optical properties during the biological degradation phase indicated that the bacteria were not only utilizing LMW photoproducts of the DOM, but that the larger molecules were available to the bacteria after exposure to sunlight. Changes in

absorbance during biological degradation were not observed in samples that had not been irradiated. Photochemical alteration of DOM from a freshwater swamp also produced more bioavailable forms of organic matter, measured as an increase in bacterial growth (Bano et al. 1998). Irradiation increased carbon utilization by up to 300%. Non-humic compounds were found to be more bioavailable per unit weight than humic compounds, both before and after irradiation, but both fractions were made significantly more bioavailable by irradiation. Despite this, calculations based on absorptivity coefficients (a_{350}) found that the humic substances would be approximately 6 times more important as a source of labile substrates in the sampled lake.

Contrasting results were observed in a study of photochemical and microbial turnover of carbon from the Amazon (Amon and Benner 1996). Despite high rates of photochemical activity, microbial activity was carbon limited and was not significantly affected by sunlight exposure.

Enhanced bacterial growth on light-exposed marine DOM was directly related to photobleaching of the samples (Obernosterer and Herndl 2000). The response varied between samples, with a 35 and 45 % increase in bacterial growth in the humic and fulvic fractions of Adriatic sea water, but a 50% increase in humic samples only was observed in North Sea samples. Adriatic Sea samples were more photochemically active and more bioavailable. In, contrast, another study of the effect of photochemical reactions on the bioavailability of marine organic matter found the response was depth dependent (Benner and Biddanda 1998). Bacterial production in pre-irradiated surface waters (to 115m) averaged 23% of the dark controls, while in the deep waters the production averaged 141% of the corresponding dark controls. The distinction between the effect of sunlight on the bioavailability of the DOM corresponded to differences in the concentration of DOC between the surface and deep waters and variations in the chemical composition. The bacterial production in the dark controls was 2-3 times greater in the surface waters than the deep waters, indicating that this fraction was already more bioavailable. Surface water exposed to sunlight, however, supported fewer bacteria than either of the dark controls or the deep water exposed to sunlight. The possible explanations of the loss of bioavailability in the surface water include the photoproduction of inhibitory chemicals, the photomineralization of the bioavailable DOM, and the production of refractory compounds. The deep water DOM however increased in bioavailability, possibly due to the production of LMW compounds.

Variable effects of UV radiation on differing sources of marine DOC were observed (Obernosterer et al. 1999), and the differences were dependent on the initial bioavailability of the organic matter. Degradation of labile organic matter was observed, both in addition experiments and in experiments on water from a chlorophyll maximum, but enhanced bioavailability was observed in deep water samples. These results indicate that the effects of photochemical reactions on DOM bioavailability will always be complex due to the potential for production of labile compounds from refractory material and the mineralization of labile material or its transformation into more refractory substances. An inverse relationship between the effects of photodegradation and initial biodegradability was also measured in water from the Southern Ocean (Obernosterer et al. 2001b). The photochemically induced increase in bioavailability was two-fold higher in the fraction of less than 20 kDa than in the bulk DOM, and this fraction was initially less biologically available. The positive effect of sunlight on bacterial production in a subtropical seagrass lagoon was found to be due to enhanced phytoplankton production (Ziegler and Benner 2000). In this case, photochemical changes to DOM were of minor importance, highlighting the complex role of light in aquatic environments.

The biodegradability of fresh algal DOC (measured as mineralization of radiolabelled carbon) was decreased by irradiation in the presence of humic substances (Tranvik and Kokalj 1998). Humic substances or irradiation alone did not affect the biodegradation of the DOC, suggesting that the source of the carbon will affect the changes to bioavailability resulting from irradiation. A study of the effect of UV irradiation on the bioavailability of LMW organic matter derived from a diatom culture, found that losses of organic matter through mineralization were counterbalanced by an increase in the bioavailability of the remaining organic matter (Naganuma et al. 2000). However, a pure bacterial culture was used and may not reflect the response of a bacterial assembly.

A difference between the effects of photodegradation on bioavailability of leachates from terrestrial plants (deciduous leaves) and aquatic macrophytes was observed (Anesio et al. 2000). In these experiments the DOC concentration was kept constant, but the colour and initial bioavailability varied widely between species. The effect of irradiation depended on the type of bioavailability measurement made (e.g. bacterial production, biomass, respiration, bacterial growth efficiency and carbon

utilization). For macrophytes, UV irradiation increased bacterial production but did not affect the other parameters, while in leachates from terrestrial plants, total carbon utilization was increased. Bacterial biomass was enriched in ^{13}C in samples grown in irradiated substrate compared to dark controls. The photochemical degradation of leachates from two macrophytes (*Phragmites australis* and *Hydrocaris morsus-ranae*) was compared and the effect on bioavailability was studied (Farjalla et al. 2001). In the *Phragmites* samples, suppression of bacterial growth was observed after irradiation, with the effect increasing with exposure time. The inhibition was less pronounced in the *Hydrocaris* leachates. Bacterial respiration was not affected. The lowest bacterial growth efficiencies in each sample corresponded to the irradiation time with the highest hydrogen peroxide concentration. A study of the photochemical and microbial degradation of DOM from forest and pasture sources did not find any significant changes to dissolved organic carbon concentration after 20-40 hours of irradiation (Wiegner and Seitzinger 2001). No change to biodegradability was observed after irradiation, but samples were stored frozen for up to two months before the microbial experiments, which may have affected the DOC.

Overall, it is clear that exposure of dissolved organic matter to sunlight has the potential to influence the microbial cycling of organic matter in the environment. However, the effects of photochemical modification of the DOM vary widely between samples, with a general trend towards increased bioavailability in samples that were previously refractory. It is not possible to predict the change in bioavailability of a particular sample after irradiation based on current understanding.

1.9 Photochemical reactions of DOM associated with metals.

1.9.1 Mechanisms for Interaction

The chemical composition of DOM is highly variable and a number of different functional groups may be included in the structure, as discussed in Section 1.2. The presence of oxygen and nitrogen within its structure gives DOM the potential to bind to metal ions and to the surface of particles. As many metal complexes are photoactive, this is another important area to consider when looking at the impact of sunlight on the chemistry of aquatic systems. As discussed in Section 1.3, organometallic compounds can undergo photochemical reactions through exchange of electrons from the excited ligand to the metal centre, or from the excited metal to the ligand, resulting in either the

oxidation or reduction of the ligand. Metal oxides are also photoactive. Sunlight of energy that exceeds the band-gap energy can create an excited state and organic molecules adsorbed to the surface of the oxide may then react with this excited state. Alternatively, it may be the adsorbed molecules that act as a photosensitizer, absorbing the light and producing an excited state leading to reaction with the oxide. The photoproduction of reactive intermediates leads to a complex variety of possible reactions resulting from exposing these systems to sunlight.

There are restricted conditions under which metal-organic compounds can undergo photoreaction. The photooxidation of the ligand is initiated by a process that involves the absorp ..n of a photon leading to the excitation of a ligand-based electron into a partially filled *d* orbital belonging to the metal (Langford and Carey 1987). The transition state formed may simply relax back into the original state unless the metal ion is readily reducible in aqueous systems and the first oxidation step for the ligand is an irreversible process. For example, carboxylate groups decompose rapidly after oxidation to give CO_2 and avoid back-reaction, and phenols form stable radicals which may survive to undergo further reaction and hence these functional groups are likely to be involved in light-induced reactions. The most likely metal ions to be involved in this process are Fe(III) and Mn(III, IV). It is also possible that metal ions will quench the photoinitiation of reactions within the humic material, so the presence of metals in natural water samples may affect the rate of photoreaction in either direction. Semiconductors, however, have several advantages over metal complexes when it comes to the prevention of back-reaction. A semiconductor in an electrolyte solution will come into electrostatic equilibrium with the solution through the transfer of charge between the solution and the particle surface (Stumm 1992). The excess charge generated in the solid is not isolated on the surface of the particle, but is distributed over a space charge region in the order of 5 nm to 0.2 μm in width (analogous to the electrical double layer in the solution). The electric field that forms in the space charge region is represented by the bending of the valance and conduction bands (downwards if the Fermi energy of the solid is higher than the solution potential, upwards if the solution potential is higher). This band bending provides a mechanism for the separation of electrons and holes after excitation of the semiconductor, electrons will move in the direction of lower potential and holes in the direction of higher potential. This charge separation increases the lifetime of the excited state and increases the

probability of reaction with an organic molecule. A typical semiconductor also has the potential to be "doped" with localised sites that capture photogenerated holes or electrons (a result of impurities in the structure), and these can also reduce the recombination of electrons and holes (Langford and Carey 1987). Efficient photoreactions rely on the presence of a reactant at the surface that can react with either electrons or holes, and this will occur most readily if the reactant is adsorbed on the surface. In colloidal semiconductors the band –bending becomes small when the radius of the colloid approaches the thickness of the space charge layer (Stumm 1992). In these cases charge separation occurs through a diffusion mechanism. When reductants and oxidants are adsorbed on the same particle both oxidative and reductive exchanges may occur. Either the oxide or the adsorbed species may act as the chromophore and generate the charge transfer process between its excited state and the ground state of the other component.

1.9.2 Metal-Organic Interactions in Aquatic Systems

A cycle of reactions involving humic substances and iron was found to act as an oxygen sink in natural waters (Miles and Brezonik 1981). Oxygen consumption in illuminated humic waters increased linearly with added $FeCl_3$, but only to a minor extent in dark controls. Negligible oxygen consumption was observed in solutions without humic material and a linear relationship was observed between O_2 consumption and humic concentration. Oxygen consumption increased non-linearly with increasing light intensity and also increased with increasing pH. The non-linear nature of this relationship was put down to secondary reactions becoming rate limiting at higher light intensities. The suggested mechanism for this system consisted of oxidation of free Fe(II) and Fe(II) complexes by oxygen, to Fe(III) complexes (any free Fe(III) produced is complexed strongly by humic material). In the dark, slow reduction of the Fe(III)-humic complex by humic matter produces an Fe(II) complex, but this process occurs more rapidly in the light. A ligand to metal charge transfer reaction is involved and CO_2 and a variety of organic products are produced. Dissociation of the complex replaces the Fe(II) in solution resulting in a catalytic cycle. The importance of the carboxylic functional groups was demonstrated through the methylation of these groups, resulting in a 50 % decrease in photochemical oxygen consumption. The proposed organic degradation reaction was:

$$RCOOH + \tfrac{1}{2} O_2 \rightarrow ROH + CO_2 \qquad \text{Equation 1.5}$$

Further experiments with model compounds found that aliphatic carboxylic acids and amino acids underwent Fe catalysed photodegradation, but not all organic acids tested reacted, possibly as a result of not complexing with the iron.

The photochemical interaction between an organic acid (citrate) and lepidocrocite (γ-FeOOH) was investigated with a view to understanding the effect on oxide dissolution (Waite and Morel 1984a). The changes to the citrate were not examined, however, it was found that dissolution of the oxide occurred through a photoreductive process that was related to the concentration of surface-bound citrate, most likely through direct excitation of the charge-transfer bonds at the surface. Solution-phase complexes between citrate and Fe(II) and Fe(III) can form following the dissolution processes, leading to photoreactions in the metal-organic complexes as well. In the presence of oxygen there appeared to be a decrease in reactivity of the surface groups as the reaction proceeded, particularly at neutral-basic pH. An additional study examined the effect of natural dissolved organic matter on the dissolution of colloidal iron oxides (Waite and Morel 1984b). The photoreduction of lepidocrocite increased 4-fold on addition of freshwater fulvic acids at pH 4.0, but at pH 6.5 the addition of fulvic acid increased the photoreduction from below detection to similar levels to the organic-free solution at pH 4. The irradiation of fulvic acids produces H_2O_2 and the rate of production at pH 8.2 is 4-5 times higher than at pH 4.0. The presence of excess H_2O_2 increases the rate of Fe(II) oxidation, and the effect is more pronounced at higher pH. The oxidation involves Fenton's reaction:

$$H_2O_2 + Fe^{2+} \rightarrow Fe^{3+} + HO^- + HO^\cdot \qquad \text{Equation 1.6}$$

$$HO^\cdot + Fe^{2+} \rightarrow Fe^{3+} + HO^- \qquad \text{Equation 1.7}$$

The photo-induced dissolution of amorphous colloidal iron oxides in the absence of organic matter was much greater than for the γ-FeOOH. The most likely mechanism for this reaction is that surface-bound hydroxylated ferric species photoreact to produce Fe(II), which is a strongly pH dependent reaction; significant dissolution is only expected at acidic pH. The greater rate of reaction in the colloidal oxide is most likely due to the increased surface area. A study using goethite and ethylene glycol (as a model compound for polysaccharides and glycoproteins) found that at a pH of 6.5, light in the wavelength range of 300-400 nm caused photochemical degradation of the organic adsorbant (Cunningham et al. 1985). The products were consistent with a

mechanism involving electron transfer from ethylene glycol adsorbed to the surface of the oxide to an Fe(III) atom, generating Fe(II) and a radical cation which underwent further reactions with O_2 and the oxide to produce formaldehyde, glycolaldehyde and an additional Fe(II). Photochemical dissolution of haematite (α-Fe_2O_3) in the presence of α-mercaptocarboxylic acids (used here as a simple model for proteins) has also been found (Waite et al. 1986), most likely through adsorption and electron transfer via the S atom. Photochemical dissolution of maghemite (γ-Fe_2O_3) and degradation of EDTA has also been observed, with the accompanying generation of formaldehyde (Litter and Blesa 1988). In this case it was concluded that light absorption generated an electron-hole pair in the solid, which was followed by charge transfer in the surface complexes. A comparative photoelectrochemical study of six iron oxide polymorphs showed substantial differences occurred in the photoreactivity (Leland and Bard 1987). The study of α- and γ-Fe_2O_3 and α-, β-, γ-, and δ-FeOOH found large variations (about 2 orders of magnitude) in the rate of photocatalytic decomposition of oxalate and sulfite in the presence of the different oxides, but there was no correlation to the hydrodynamic diameter, band gap or surface area of the colloids. The differences were attributed to variations in the electronic and chemical structures. Variations were also observed the reactivity of each oxide towards the reductants.

A daily variation in the concentration of Fe(II) has been observed in acidic streams (Madsen et al. 1986, McKnight et al. 1988), indicating that photochemical processes involving iron are of sufficient magnitude to affect iron cycling in the environment. The concentration of dissolved Fe(II) increased after sunrise, and the concentration of Fe(II) was more variable during the day, indicating a photoreductive process. The species most likely to be involved were dissolved Fe(III) species or colloidal hydrous iron oxides. UV sensitive humic-Fe complexes have also been detected in an acid bog lake (Cotner and Heath 1990). A diurnal variation in Fe(II) concentrations was observed in an acid lake (Sulzberger et al. 1990), and the cause was found to be the photochemical reductive dissolution of amorphous iron(III)hydroxide accompanied by oxidation and precipitation of Fe(II). The process was sensitive to oxalate addition, suggesting the organic matter was involved in the photo-dissolution reactions. Photochemical reactions in seawater were found to increase the lability of particulate iron at pH 8 (Wells and Mayer 1991, Wells et al. 1991). Both ferrihydrite and goethite were affected in this way. The pre-irradiation of seawater with UV light

eliminated the process, indicating a reliance on organic chromophores (Wells et al. 1991). Pronounced diurnal variations in the concentration of Fe(II) have also recently been reported in eutrophic and oligotrophic lakes (Emmenegger et al. 2001).

Studies have been conducted with model compounds to gain a better understanding of the photochemical interactions between organic matter and iron. The photochemical dissolution of haematite was examined in the presence of oxalate and a multistep mechnism was proposed (Siffert and Sulzberger 1991). The process involves bidentate surface complex formation, photoinduced electron transfer from the oxalate to the iron (to generate a surface Fe(II)) dissociation and decarboxylation to produce CO_2 and $CO_2^{\cdot-}$ (which then reduces a second surface Fe(III)) and finally detachment of the surface Fe(II). In the presence of O_2 however, adsorbed molecular oxygen may reoxidize the surface Fe(II) to regenerate the surface. In this case haematite can act as a catalyst for the oxidation of oxalate.

The photo-Fenton reaction between photochemically produced Fe(II) and H_2O_2 in aqueous solutions has also been studied (Zepp et al. 1992). The $HO^{\cdot}$ radical was found to be involved in the photo-Fenton reaction. Fe^{2+} and its oxalate, citrate and phosphate complexes were found to react with H_2O_2 to produce $HO^{\cdot}$ in aqueous solutions between pH 3 and 8. The Fe^{2+} and its complexes were formed through photoreactions of the corresponding Fe^{3+} complexes and light accelerated the Fenton reaction. Fulvic acid scavenges $HO^{\cdot}$ and its addition reduced the concentration of $HO^{\cdot}$. The results however indicated that either the formation of unreactive Fe^{2+} complexes did not occur or that complexes did form and reacted with the H_2O_2 to form $OH^{\cdot}$. Another study of reactions involving Fe-citrate complexes and peroxide lead to a proposed mechanism for the formation of H_2O_2 beginning with the single-electron reduction of molecular oxygen to form $HO_2^{\cdot}/O_2^{\cdot-}$ (Zuo and Hoigné 1992). The disproportionation of $HO_2^{\cdot}/O_2^{\cdot-}$ forms H_2O_2 and O_2. Metal ions can interact with the $HO_2^{\cdot}/O_2^{\cdot-}$, for example Fe:

$$HO_2^{\cdot}/O_2^{\cdot-} + Fe(II) \xrightarrow{H^+} H_2O_2 + Fe(III) \qquad \text{Equation 1.8}$$

$$HO_2^{\cdot}/O_2^{\cdot-} + Fe(III) \xrightarrow{H^+} O_2 + Fe(II) \qquad \text{Equation 1.9}$$

In the acidic pH range reaction 1.10 is very slow. $HO_2^{\cdot}/O_2^{\cdot-}$ can also be formed through reaction of O_2 with photo-excited organic molecules or with free electrons resulting from photo-ionization of organics. It may also be formed when photoreduction of a

complexed metal occurs, producing an organic radical which may then react with O_2. In a solution of iron and oxalate under nitrogen, it was found that no peroxide was produced by irradiation and the amount of oxalate decomposed matched the amount of iron reduced. This indicates that iron is only catalytic in these systems when oxygen is present and that the production of peroxide requires dissolved oxygen. H_2O_2 production was also a linear function of sunlight irradiation time, Fe(III) concentration, and oxalate concentration. Excess oxalate is believed to retard the decay of transient intermediates. The rate of H_2O_2 production above pH 4 decreased with increasing pH. At higher pH $O_2^{\cdot-}$ dominates over $HO_2^{\cdot}$ and reaction 4 is the dominant pathway. In summary, a reaction cycle proceeds involving: direct photolysis of the Fe(III)-oxlato complexes, reaction of the organic radical photoproducts with O_2 to form $HO_2^{\cdot}/O_2^{\cdot-}$ and hence H_2O_2, followed by reaction of these oxidants with Fe^{2+} to re-form Fe(III) and its complexes.

Photochemical reactions of Fe(III)-polycarboxylates (oxalate, malonate and citrate) were found to produce Fe(II), $HO_2^{\cdot}/O_2^{\cdot-}$, H_2O_2 and $^{\cdot}OH$ (Faust and Zepp 1993). The polycarboxylate radical formed when sunlight induces the reduction of the Fe(III) by the ligand may react in one of four ways: Back reaction with the Fe(II), react with O_2 to form $HO_2^{\cdot}/O_2^{\cdot-}$, reduction of another Fe(III) complex or decarboxylation (to form a carbon-centred radical which is also reactive with O_2 and Fe(III)). Radical reaction with O_2 can produce a variety of products including carboxy radicals and carboxylic acids in addition to the reactive species mentioned above. The quantum yields were observed to vary depending on the Fe(III) speciation in the solution, which was in turn dependent upon the pH. The Fe(III)-polycarboxylates studied were found to have half lives of minutes in sunlight, indicating that photochemical reactions are an important sink for these compounds. The photoreduction of iron oxyhydroxide particles is affected by pH, the wavelength of the light, the nature of the organic matter and the characteristics of the particle (Pehkonen et al. 1993). Formate reduced Fe(III) at a greater rate then acetate did but butyrate was less effective. The difference in rate between acetate and butyrate can be explained by steric hindrance; butyrate blocks more of the surface sites. This indicates that the rate of surface complexation may be rate limiting. The oxide structure also affected the rate of reaction with the rate increasing in the order: goethite, haematite, lepidocrocite and then amorphous $Fe(OH)_3$, but the difference was not due to the differences in surface hydroxy groups. Reactivity with H_2O_2 followed a similar pattern. A semiconductor mechanism was involved in the reaction between H_2O_2 and

the lepidocrocite. Another study also noted changes in reactivity of iron hydroxide particles with increasing crystallinity (Hrncir and McKnight 1998). Freshly formed particles were more readily reduced and affected to a greater extent by the presence of fulvic acids than aged particles, which had increased in crystallinity.

A detailed study of the photochemistry of iron(III)-carboxylic acid complexes (Abrahamson et al. 1994), confirmed that a 2:1 Fe:acid stoichiometry is involved in the oxidation of the acid:

$$2Fe^{3+} + (RCH(OH)COO^{-}) \rightarrow 2Fe^{2+} + H^{+} + RCHO + CO_2 \quad \text{Equation 1.10}$$

The quantum yields for the reactions varied with the nature of the carboxylate and with pH. The pH dependence was thought to be due to the formation of dimers, which were more photoactive than the corresponding monomer. In a comparison of the relative reactivity of three different oxides towards photooxidation of oxalate (Sulzberger and Laubscher 1995), a 1:1 stoichiometry was observed between the formation of Fe(II) from lepidocrocite and the oxidation of oxalate. Appreciable levels of Fe(II) were not produced when oxalate was photodegraded on haematite or goethite. The 2:1 stoichiometry previously reported was observed for all three under deaerated conditions. The removal of oxygen also decreased the rate of oxalate oxidation in haematite and goethite systems, but not the lepidocrocite system. The results indicate that in the most thermodynamically stable oxides reoxidation of surface Fe(II) outcompetes dissolution. The increased solubility of lepidocrocite was also thought to explain the effect of deaeration. In the more stable systems the removal of O_2 is thought to remove the source of $HO^{\cdot}$, but in the lepidocrocite system dissolved Fe(II) will scavenge $HO^{\cdot}$ and there will not be substantial reaction between $HO^{\cdot}$ and oxalate in the aerated systems either.

The effect of fulvic acid on Fenton's reactions in the absence of light (Equations 1.6, 1.7) was found to be pH dependent (Voelker and Sulzberger 1996). At pH 3 the effect was negligible but at pH 5 the degradation of H_2O_2 was accelerated by addition of fulvic acid: a result consistent with a pH dependent complexation of Fe(II) by fulvic acid to form a complex that is more reactive than aqueous Fe(II). Fulvic acid was oxidized through scavenging of $HO^{\cdot}$ radicals. Fulvic acid also reduced Fe(III) in the dark, very rapidly initially and then more slowly as competition between reducing and non-reducing binding sites became important. A reaction scheme was later proposed (Voelker et al. 1997) to explain the interaction between Fe, light and dissolved organics

(see Figure 1.2). The complex system of reactions results in little being known about the organic products, for example, it is unknown whether oxidation of fulvic acid in the presence of iron leads to the same products as oxidation in the absence of iron.

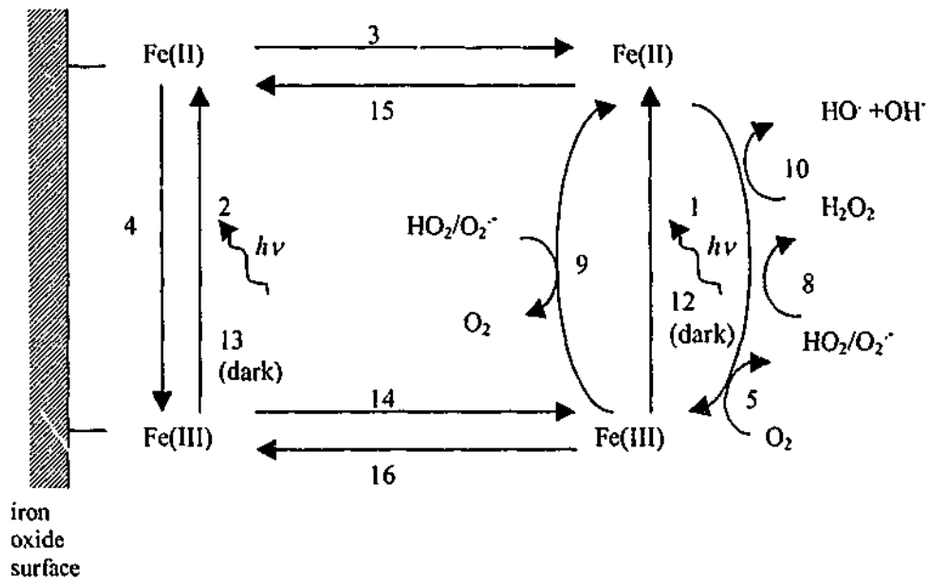

6. $DOM + O_2 \xrightarrow{h\nu} DOM_{ox} + HO_2/O_2^{\cdot-}$

7. $2\ HO_2/O_2^{\cdot-} \longrightarrow H_2O_2 + O_2$

11. $DOM + HO^{\cdot} \longrightarrow DOM_{ox} + HO_2/O_2^{\cdot-}$

Figure 1.2. Summary of possible reactions between iron particles and dissolved organic matter in surface waters (Voelker et al. 1997): (1) photo-reduction of dissolved Fe(III) by DOM, (2) photo-reduction of surface Fe(III) by DOM, (3) dissolution of surface Fe(II), (4) re-oxidation of surface Fe(II), (5) Fe(II) oxidation by O_2, (6) $HO_2/O_2^{\cdot-}$ photoproduction and oxidation of DOM, (7) bimolecular dismutation of $HO_2/O_2^{\cdot-}$, (8) Fe(II) oxidation by $HO_2/O_2^{\cdot-}$, (9) Fe(III) reduction by $HO_2/O_2^{\cdot-}$, (10), Fe(II) oxidation by H_2O_2, (11) regeneration of $HO_2/O_2^{\cdot-}$ from $HO^{\cdot}$ with oxidation of DOM, (12) Fe(III) dark reduction by DOM, (13) dark reduction of surface Fe(III) by DOM, (14) non-reductive dissolution of Fe(III) oxide, (15) sorption of dissolved Fe(II), (16) Fe(III) adsorption/ precipitation.

Fulvic acid solutions have been found to produce $HO^{\cdot}$ under aerobic and anaerobic conditions when irradiated (Vaughan and Blough 1998). Fenton's reactions contributed ~50% of the $HO^{\cdot}$ production and direct photolysis of the DOM is most likely to be responsible for the majority of the remainder. Fluoride ions have been used to inactivate the Fe(III) in a solution of dissolved organic matter, leading to reduced

production of CO, ammonia, organic acids and DIC (Gao and Zepp 1998). The production of DIC was no longer pH dependent when reactive iron was absent from the solution. The results indicate that iron plays an important catalytic role in the photooxidation of DOM, but the production of DIC, CO and NH_4^+ still occurred at significant rates in the absence of available iron. Photobleaching was not affected by the absence of iron.

It is possible that a transient ferryl complex is also acting as an oxidant in the photo-Fenton reactions (Pignatello et al. 1999). This complex may be formed when Fe(II) or Fe(III) ions with organic ligands are oxidized, producing Fe=O, where the oxidation state of Fe is +IV or +V. These reactions may also produce $HO^{\cdot}$ but the significance of the reactions in natural waters is unknown. The production of $HO^{\cdot}$ radicals in the dark has been found in humic acids loaded with either iron or copper (Paciolla et al. 1999). The presence of $Fe{=}O_2^{2+}$ was also proposed for the iron systems in the absence of H_2O_2. The copper loaded acids were more reactive than the iron loaded acids, but iron is more abundant in natural systems.

A small number of more recent studies have examined the changes to the natural dissolved organic matter following photochemical reactions in the presence of iron. A humic acid was derived from peat soil using a process which included NaOH extraction and freeze drying (which may have substantially altered the characteristics of the organic matter) and was irradiated in the presence of H_2O_2 and Fe(III) (Fukushima et al. 2001). Artificial irradiation for five hours in this photo-Fenton process mineralised 20% of the humic acid and the remaining organic matter was of reduced average molecular weight. In the absence of Fe(III) there was no significant reduction in TOC. Changes to the absorption spectra suggested that unsaturated compounds may have been degraded in the photo-Fenton system, but not in the humic acid/peroxide system. No peak shifts were observed in the EEM spectrum of the humic acid, but inner-filtering corrections had not been applied to the data. Relative fluorescence intensities increased with irradiation, perhaps due to changes in molecular size or molecular rigidity. Ether and epoxide functional groups were formed during the reactions and observed using FTIR. The photochemical degradation of Fe(III)-siderophore complexes was also studied (Barbeau et al. 2001). Siderophores are iron(III) ligands produced by bacteria to assist with Fe acquisition. In this study aquachelins (a class of siderophore) were used. These compounds contain a fatty-acid tail and a peptide headgroup and binds to Fe(III)

via two hydroxamate groups and a β-hydroxyaspartate residue. Photolysis resulted in the oxidative cleavage of the molecules at the β-hydroxyaspartate residue. A hydrophilic peptide portion (without the β-hydroxyaspartate residue) and a more hydrophobic fatty acid product were formed following a ligand to metal charge transfer via the β-hydroxyaspartate.

Photochemical interactions between organic matter and iron (as ions, complexes or oxides) clearly have the potential to influence the cycling of important elements within aquatic ecosystems. The interactions have been shown to affect the speciation of iron in natural waters, and through the degradation of organic matter, the cycling of other elements such as carbon, oxygen, nitrogen and phosphorus may also be affected.

1.10 Directions for this research

The photochemical reactions of dissolved organic matter are obviously complex and variable. In some cases exposing DOM to sunlight has been shown to decrease the average molecular weight, whereas other studies have shown the potential for increases. Similarly, both increases and decreases in bioavailability were found after photochemical reactions and a large number of interactive effects with other components of the water column have been reported. Extensive work remains to be done for the changes in the chemistry of aquatic ecosystems induced by sunlight to be properly understood. In particular, the effect of interactions with metals on the nature of the organic photoproducts and the resulting changes in bioavailability of the compounds have been neglected.

This work examines the photochemical degradation of dissolved organic matter from billabongs and leachates derived from the leaves of *Eucalyptus camaldulensis* (an important plant in the River Murray floodplain. Degradation was examined both in the presence and absence of iron oxides. The influence of the iron oxides on the rate and products of the organic photodegradation will be discussed and the influence of these reactions on the metabolism of dissolved organic matter by bacteria will be examined. In Chapter 2 studies on the photodegradation of dissolved organic matter derived from billabong water and leaf leachate during irradiation with artificial light sources will be discussed. Chapter 3 examines the effect of iron oxides on the photodegradation of dissolved organic matter with artificial light sources and Chapter 4 extends the research

to examine the role of sunlight and iron oxide on the degradation of dissolved organic matter during sunlight exposure. The environmental significance and major conclusions of this work will be discussed further in Chapter 6.

1.11 References

Abrahamson, H. B., A. B. Rezvani, and J. G. Brushmiller. 1994. Photochemical and spectroscopic studies of complexes of iron(III) with citric acid and other carboxylic acids. Inorg. Chim. Acta **226**:117-127.

Amador, J. A., M. Alexander, and R. G. Zika. 1989. Sequential photochemical and microbial degradation of organic molecules bound to humic acid. Appl. Environ. Microbiol. **55**:2843-2849.

Amon, R. M. W., and R. Benner. 1996. Photochemical and microbial consumption of dissolved organic carbon and dissolved oxygen in the Amazon River system. Geochim. Cosmochim. Acta **60**:1783-1792.

Andrews, S. S., S. Caron, and O. C. Zafiriou. 2000. Photochemical oxygen consumption in marine waters: A major sink for coloured dissolved organic matter? Limnol. Oceanogr. **45**:267-277.

Anesio, A. M., and W. Granéli. 2003. Increased photoreactivity of DOC by acidification: Implications for the carbon cycle in humic lakes. Limnol. Oceanogr. **48**:735-744.

Anesio, A. M., J. Theil-Nielsen, and W. Granéli. 2000. Bacterial growth on photochemically transformed leachates from aquatic and terrestrial primary producers. Microb Ecol **40**:200-208.

Arakaki, T., T. Miyake, T. Hirakawa, and H. Sakugawa. 1999. pH dependent photoformation of hydroxyl radical and absorbance of aqueous-phase N(III) (HNO_2 and NO_2^-). Environ. Sci. Technol. **33**:2561-2565.

Ashcroft, N. W., and N. D. Mermin. 1976. Solid State Physics. Saunders College Publishing, Fort Worth.

Baldwin, D., J. Howitt, and M. Edwards. 2001. Blackwater Event. Austasia Aquaculture **15**:21.

Bano, N., M. A. Moran, and R. E. Hodson. 1998. Photochemical formation of labile organic matter from two components of dissolved organic carbon in a freshwater wetland. Aquat. Microb. Ecol. **16**:95-102.

Barbeau, K., E. L. Rue, K. W. Bruland, and A. Butler. 2001. Photochemical cycling of iron in the surface ocean mediated by microbial iron(III)-binding ligands. Nature **413**:409-413.

Benner, R., and B. Biddanda. 1998. Photochemical transformations of surface and deep marine dissolved organic matter: Effects on bacterial growth. Limnol. Oceanogr. **43**:1373-1378.

Bertilsson, S., and B. Allard. 1996. Sequential photochemical and microbial degradation of refractory dissolved organic matter in a humic freshwater system. Arch. Hydrobiol. Spec. Issues Advanc. Limnol. **48**:133-141.

Bertilsson, S., and S. Bergh. 1999. Photochemical reactivity of XAD-4 and XAD-8 adsorbable dissolved organic compounds from humic waters. Chemosphere **39**:2289-2300.

Bertilsson, S., R. Stepanauskas, R. Cuadros-Hansson, W. Granéli, J. Wikner, and L. Tranvik. 1999. Photochemically induced changes in bioavailable carbon and nitrogen pools in a boreal watershed. Aquat. Microb. Ecol. **19**:47-56.

Bertilsson, S., and L. J. Tranvik. 1998. Photochemically produced carboxylic acids as substrates for freshwater bacterioplankton. Limnol. Oceanogr. **43**:885-895.

Bertilsson, S., and L. J. Tranvik. 2000. Photochemical transformation of dissolved organic matter in lakes. Limnol. Oceanogr. **45**:753-762.

Blough, N. V., and R. G. Zepp. 1995. Reactive oxygen species in natural waters. Pages 280-333 *in* C. S. Foote, J. S. Valentine, A. Greenberg, and J. F. Liebman, editors. Active Oxygen in Chemistry. Blackie Academic and Professional, London.

Boavida, M.-J., and R. G. Wetzel. 1998. Inhibition of phosphatase activity by dissolved humic substances and hydrolytic reactivation by natural ultraviolet light. Freshwater Biol. **40**:285-293.

Bushaw, K. L., R. G. Zepp, M. A. Tarr, D. Schulz-Jander, R. A. Bourbonniere, R. E. Hodson, W. L. Miller, D. A. Bronk, and M. A. Moran. 1996. Photochemical release of biologically available nitrogen from aquatic dissolved organic matter. Nature **381**:404-407.

Canonica, S., U. Jans, K. Stemmler, and J. Hoigné. 1995. Transformation kinetics of phenols in water: Photosensitization by dissolved natural organic material and aromatic ketones. Environ. Sci. Technol. **29**:1822-1831.

Choudhry, G. G. 1984. Humic Substances-Structural, Photophysical, Photochemical and Free Radical Aspects and Interactions with Environmental Chemicals. Gordon and Breach Science Publishers, New York.

Clark, C. D., J. Jimenez-Morias, G. Jones, II, E. Zanardi-Lamardo, C. A. Moore, and R. G. Zika. 2002. A time-resolved fluorescence study of dissolved organic matter in a riverine to marine transition zone. Mar. Chem. **78**:121-135.

Coble, P. G. 1996. Characterization of marine and terrestrial DOM in seawater using excitation-emission matrix spectroscopy. Mar. Chem. **51**:325-346.

Conrad, R., M. Aragano, and W. Seiler. 1983. Production and consumption of carbon monoxide in a eutrophic lake. Limnol. Oceanogr. **28**:42-49.

Cooper, W. J., R. G. Zika, R. G. Petasne, and A. M. Fisher. 1989. Sunlight-induced photochemistry of humic substances in natural waters: major reactive species. Pages 333-362 *in* I. H. Suffet and P. MacCarthy, editors. Aquatic Humic Substances: influence on fate and treatment of pollutants. American Chemical Society, Washington, DC.

Cooper, W. J., R. G. Zika, R. G. Petasne, and J. M. C. Plane. 1988. Photochemical formation of H_2O_2 in natural waters exposed to sunlight. Environ. Sci. Technol. **22**:1156-1160.

Cotner, J. B., and R. T. Heath. 1990. Iron redox effects on photosensitive phosphorus release from dissolved humic materials. Limnol. Oceanogr. **35**:1175-1181.

Cunningham, K. M., M. C. Goldberg, and E. R. Weiner. 1985. The aqueous photolysis of ethylene glycol adsorbed on goethite. Photochem. Photobiol. **41**:409-416.

Dahlen, J., S. Bertilsson, and C. Pettersson. 1996. Effects of UV-A irradiation on dissolved organic matter in humic surface waters. Environ Int **22**:501-506.

De Haan, H. 1993. Solar UV-light penetration and photodegradation of humic substances in peaty lake water. Limnol. Oceanogr. **38**:1072-1076.

Eisberg, R., and R. Resnick. 1985. Quantum Physics of Atoms, Molecules, Solids, Nuclei, and Particles, Second edition. John Wiley &Sons, New York.

Emmenegger, L., R. Schönenberger, L. Sigg, and B. Sulzberger. 2001. Light-induced redox cycling of iron in circumneutral lakes. Limnol. Oceanogr. **46**:49-61.

Farjalla, V. F., A. M. Anesio, S. Bertilsson, and W. Granéli. 2001. Photochemical reactivity of aquatic macrophyte leachates: abiotic transformations and bacterial response. Aquat. Microb. Ecol. **24**:187-195.

Faust, B. C., and J. Hoigné. 1987. Sensitized photooxidation of phenols by fulvic acid and in natural waters. Environ. Sci. Technol. **21**:957-964.

Faust, B. C., and R. G. Zepp. 1993. Photochemistry of aqueous iron(III)-polycarboxylate complexes: Roles in the chemistry of atmospheric and surface waters. Environ. Sci. Technol. **27**:2517-2522.

Fischer, A. M., J. S. Winterle, and T. Mill. 1987. Primary photochemical processes in photolysis mediated by humic substances. Pages 141-156 *in* R. G. Zika and W. J. Cooper, editors. Photochemistry of Environmental Aquatic Systems. American Chemical Society, Washington, DC.

Francko, D. A. 1986. Epilimnetic phosphorus cycling: influence of humic materials and iron on coexisting major mechanisms. Can. J. Fish. Aquat. Sci **43**:302-310.

Francko, D. A., and R. T. Heath. 1982. UV-sensitive complex phosphorus: Association with dissolved humic material and iron in a bog lake. Limnol. Oceanogr. **27**:564-569.

Fukushima, M., K. Tatsumi, and S. Nagao. 2001. Degradation characteristics of humic acid during photo-Fenton processes. Environ. Sci. Technol. **35**:3683-3690.

Gao, H., and R. G. Zepp. 1998. Factors influencing photoreactions of dissolved organic matter in a coastal river of the southeastern United States. Environ. Sci. Technol **32**:2940-2946.

Geller, A. 1986. Comparison of mechanisms enhancing biodegradability of refractory lake water constituents. Limnol. Oceanogr. **31**:755-764.

Gibson, J. A. E., W. F. Vincent, and R. Pienitz. 2001. Hydrologic control and diurnal photobleaching of CDOM in a subarctic lake. Arch. Hydrobiol. **152**:143-159.

Goldstone, J. V., M. J. Pullin, S. Bertilsson, and B. M. Voelker. 2002. Reactions of hydroxyl radical with humic substances: bleaching, mineralization and production of bioavailable carbon substrates. Environ. Sci. Technol **36**:364-372.

Granéli, W., M. Lindell, and L. Tranvik. 1996. Photo-oxidative production of dissolved inorganic carbon in lakes of different humic content. Limnol. Oceanogr. **41**:698-706.

Hoigné, J., B. C. Faust, W. R. Haag, F. E. J. Scully, and R. G. Zepp. 1989. Aquatic humic substances as sources and sinks of photochemically produced transient reactants. Pages 363-381 *in* I. H. Suffet and P. MacCarthy, editors. Aquatic Humic Substances: Influence on Fate and Treatment of Pollutants. American Chemical Society, Washington.

Hrncir, D. C., and D. McKnight. 1998. Variation in photoreactivity of iron hydroxides taken from an acidic mountain stream. Environ. Sci. Technol. **32**:2137-2141.

Kieber, D. J., J. McDaniel, and K. Mopper. 1989. Photochemical source of biological substrates in sea water: implications for carbon cycling. Nature **341**:637-639.

Kieber, D. J., and K. Mopper. 1987. Photochemical formation of glyoxylic and pyruvic acids in seawater. Mar. Chem. **21**:135-149.

Kieber, R. J., L. H. Hydro, and P. J. Seaton. 1997. Photooxidation of triglycerides and fatty acids in seawater: Implication toward the formation of marine humic substances. Limnol. Oceanogr. **42**:1454-1462.

Kieber, R. J., A. Li, and P. J. Seaton. 1999. Production of nitrite from the photodegradation of dissolved organic matter in natural waters. Environ. Sci. Technol. **33**:993-998.

Kieber, R. J., X. Zhou, and K. Mopper. 1990. Formation of carbonyl compounds from UV-induced photodegradation of humic substances in natural waters: Fate of riverine carbon in the sea. Limnol. Oceanogr. **35**:1503-1515.

Koopmans, D. J., and D. A. Bronk. 2002. Photochemical production of dissolved inorganic nitrogen and primary amines from dissolved organic nitrogen in waters of two estuaries and adjacent surficial groundwaters. Aquat. Microb. Ecol. **26**:295-304.

Laane, R. W. P. M., W. W. C. Gieskes, G. W. Kraay, and A. Eversdijk. 1985. Oxygen consumption from natural waters by photo-oxidizing processes. Neth. J. Sea Res **19**:125-128.

Langford, C. H., and J. H. Carey. 1987. Photocatalysis by inorganic components of natural water systems. Pages 225-239 *in* Photochemistry of Environmental Aquatic Systems. American Chemical Society.

Laurion, I., M. Ventura, J. Catalan, R. Psenner, and R. Sommaruga. 2000. Attenuation of ultraviolet radiation in mountain lakes: Factors controlling the among- and within- lake variability. Limnol. Oceanogr. **45**:1274-1288.

Lean, D. 1998. Attenuation of solar radiation in humic waters. Pages 109-124 *in* D. O. Hessen and L. J. Tranvik, editors. Aquatic Humic Substances: Ecology and Biogeochemistry. Springer, Berlin.

Leland, J., and A. J. Bard. 1987. Photochemistry of colloidal semiconducting iron oxide polymorphs. J. Phys. Chem. **91**:5076-5083.

Lindell, M. J., H. W. Granéli, and S. Bertilsson. 2000. Seasonal photoreactivity of dissolved organic matter from lakes with contrasting humic content. Can. J. Fish. Aquat. Sci **57**:875-885.

Lindell, M. J., W. Graneli, and L. J. Tranvik. 1995. Enhanced bacterial growth in response to photochemical transformation of dissolved organic matter. Limnol. Oceanogr. **40**:195-199.

Lindell, M. J., and H. Rai. 1994. Photochemical oxygen consumption in humic waters. Ergeb. Limnol. **43**:145-155.

Litter, M. I., and M. A. Blesa. 1988. Photodissolution of iron oxides: I. Maghemite in EDTA solutions. J. Colloid Interface Sci. **125**:679-687.

Madsen, E. L., M. D. Morgan, and R. E. Good. 1986. Simultaneous photoreduction and microbial oxidation of iron in a stream in the New Jersey Pinelands. Limnol. Oceanogr. **31**:832-838.

Marhaba, T. F., D. Van, and R. L. Lippincott. 2000. Rapid identification of dissolved organic matter fractions in water by spectral fluorescent signatures. Wat. Res. **34**:3543-3550.

McKnight, D. M., and G. R. Aiken. 1998. Sources and age of aquatic humus. Pages 9-39 *in* D. O. Hessen and L. J. Tranvik, editors. Aquatic Humic Substances: Ecology and Biogeochemistry. Springer, Berlin.

McKnight, D. M., E. W. Boyer, P. K. Westerhoff, P. T. Doran, K. Thomas, and D. T. Andersen. 2001. Spectrofluorometric characterization of dissolved organic matter for indication of precursor organic material and aromaticity. Limnol. Oceanogr. **46**:38-48.

McKnight, D. M., B. A. Kimball, and K. E. Bencala. 1988. Iron photoreduction and oxidation in an acidic mountain stream. Science **240**:637-640.

Miles, C. J., and P. L. Brezonik. 1981. Oxygen consumption in humic colored waters by a photochemical ferrous-ferric catalytic cycle. Environ. Sci. Technol **15**:1089-1095.

Miller, W. L., and M. A. Moran. 1997. Interaction of photochemical and microbial processes in the degradation of refractory dissolved organic matter from a coastal marine environment. Limnol. Oceanogr. **42**:1317-1324.

Miller, W. L., and R. G. Zepp. 1995. Photochemical production of dissolved inorganic carbon from terrestrial organic matter: Significance to the oceanic organic carbon cycle. Geophys. Res. Lett. **22**:417-420.

Mobed, J. J., S. L. Hemmingsen, J. L. Autry, and L. B. McGown. 1996. Fluorescence characterization of IHSS humic substances: total luminescence spectra with absorbance correction. Environ. Sci. Technol **30**:3061-3065.

Momzikoff, A., R. Santus, and M. Giraud. 1983. A study of the photosensitizing properties of seawater. Mar. Chem. **12**:1-14.

Moore, W. J. 1983. Basic Physical Chemistry. Prentice-Hall International, London.

Mopper, K., and W. L. Stahovec. 1986. Sources and sinks of low molecular weight organic carbonyl compounds in seawater. Mar. Chem. **19**:305-321.

Mopper, K., and X. Zhou. 1990. Hydroxyl radical photoproduction in the sea and its potential impact on marine processes. Science **250**:661-664.

Mopper, K., X. Zhou, R. J. Kieber, D. J. Kieber, R. J. Sikorski, and R. D. Jones. 1991. Photochemical degradation of dissolved organic carbon and its impact on the oceanic carbon cycle. Nature **353**:60-62.

Moran, M. A., W. M. J. Sheldon, and R. G. Zepp. 2000. Carbon loss and optical property changes during long-term photochemical and biological degradation of esturine dissolved organic matter. Limnol. Oceanogr. **45**:1254-1264.

Moran, M. A., and R. G. Zepp. 1997. Role of photoreactions in the formation of biologically labile compounds from dissolved organic matter. Limnol. Oceanogr. **42**:1307-1316.

Morel, F. M. M., and J. G. Hering. 1993. Principles and Applications of Aquatic Chemistry. John Wiley and Sons, INC, New York.

Naganuma, T., I. Fukai, Y. Murakami, T. Nakane, and S. Sukizaki. 2000. Effect of ultraviolet radiation on the bioavailability of marine diatom-derived low-molecular-weight dissolved organic matter. Aquatic Ecosystem Health and Management **3**:163-166.

Obernosterer, I., and G. J. Herndl. 2000. Differences in the optical and biological reactivity of the humic and nonhumic dissolved organic carbon component in two contrasting coastal marine environments. Limnol. Oceanogr. **45**:1120-1129.

Obernosterer, I., B. Reitner, and G. J. Herndl. 1999. Contrasting effects of solar radiation on dissolved organic matter and its bioavailability to marine bacterioplankton. Limnol. Oceanogr. **44**:1645-1654.

Obernosterer, I., P. Ruardji, and G. J. Herndl. 2001a. Spatial and diurnal dynamics of dissolved organic matter (DOM) fluorescence and H_2O_2 and the photochemical oxygen demand of surface water DOM across the subtropical Atlantic Ocean. Limnol. Oceanogr. **46**:632-643.

Obernosterer, I., R. Sempéré, and G. J. Herndl. 2001b. Ultraviolet radiation induces reversal of the bioavailability of DOM to marine bacterioplankton. Aquat. Microb. Ecol. **24**:61-68.

Ohno, T. 2002. Fluorescence inner-filtering correction for determination of the humification index of dissolved organic matter. Environ. Sci. Technol. **36**:742-746.

Opsahl, S., and R. Benner. 1998. Photochemical reactivity of dissolved lignin in river and ocean waters. Limnol. Oceanogr. **43**:1297-1304.

Osburn, C. L., H. E. Zagarese, D. P. Morris, B. R. Hargreaves, and W. E. Cravero. 2001. Calculation of spectral weighting functions for the solar photobleaching of chromophoric dissolved organic matter in temperate lakes. Limnol. Oceanogr. **46**:1455-1467.

Paciolla, M. D., G. Davies, and S. A. Jansen. 1999. Generation of hydroxyl radicals from metal-loaded humic acids. Environ. Sci. Technol. **33**:1814-1818.

Pehkonen, S. O., R. Siefert, Y. Erel, S. Webb, and M. R. Hoffmann. 1993. Photoreduction of iron oxyhydroxides in the presence of important atmospheric organic compounds. Environ. Sci. Technol. **27**:2056-2062.

Pignatello, J. J., D. Liu, and P. Huston. 1999. Evidence for an additional oxidant in the photoassisted Fenton reaction. Environ. Sci. Technol. **33**:1832-1839.

Reche, I., M. L. Pace, and J. J. Cole. 1998. Interactions of photobleaching and inorganic nutrients in determining bacterial growth on colored dissolved organic carbon. Microb Ecol **36**:270-280.

Reche, I., M. L. Pace, and J. J. Cole. 1999. Relationship of trophic and chemical conditions to photobleaching of dissolved organic matter in lake ecosystems. Biogeochemistry **44**:259-280.

Reitner, B., G. J. Herndl, and A. Herzig. 1997. Role of ultraviolet-B radiation on photochemical and microbial oxygen consumption in a humic-rich shallow lake. Limnol. Oceanogr. **42**:950-960.

Salonen, K., and A. Vähätalo. 1994. Photochemical mineralisation of dissolved organic matter in lake Skjervatjern. Environ Int **20**:307-312.

Schmitt-Kopplin, P., N. Hertkorn, H.-R. Schulten, and A. Kettrup. 1998. Structural changes in a dissolved soil humic acid during photochemical degradation processes under O_2 and N_2 atmosphere. Environ. Sci. Technol. **32**:2531-2541.

Siffert, C., and B. Sulzberger. 1991. Light-induced dissolution of hematite in the presence of oxalate: a case study. Langmuir **7**:1627-1634.

Skoog, D. A., and J. J. Leary. 1992. Principles of Instrumental Analysis, Fourth edition. Saunders College Publishing, Fort Worth.

Stumm, W. 1992. Chemistry of the Solid-Water Interface: Processes at the Mineral-Water and Particle-Water Interface in Natural Systems. Wiley-Interscience, New York.

Sulzberger, B., and H. Laubscher. 1995. Reactivity of various types of iron(III) (hydr)oxides towards light-induced dissolution. Mar. Chem. **50**:103-115.

Sulzberger, B., J. L. Schnoor, R. Giovanoli, J. G. Hering, and J. Zobrist. 1990. Biogeochemistry of iron in an acidic lake. Aquat. Sci. **52**:56-74.

Tarr, M. A., W. Wang, T. S. Bianchi, and E. Engelhaupt. 2001. Mechanisms of ammonia and amino acid photoproduction from aquatic humic and colloidal matter. Water Res. **35**:3688-3696.

Tranvik, L., and S. Kokalj. 1998. Decreased biodegradability of algal DOC due to interactive effects of UV radiation and humic matter. Aquat. Microb. Ecol. **14**:301-307.

Vähätalo, A. V., M. Salkinoja-Salonen, P. Taalas, and K. Salonen. 2000. Spectrum of the quantum yield for photochemical mineralization of dissolved organic carbon in a humic lake. Limnol. Oceanogr. **45**:664-676.

Valentine, R. L., and R. G. Zepp. 1993. Formation of carbon monoxide from the photodegradation of terrestrial dissolved organic carbon in natural waters. Environ. Sci. Technol. **27**:409-412.

Vaughan, P. P., and N. V. Blough. 1998. Photochemical formation of hydroxyl radical by constituents of natural waters. Environ. Sci. Technol. **32**:2947-2953.

Voelker, B. M., F. M. M. Morel, and B. Sulzberger. 1997. Iron redox cycling in surface waters: Effects of humic substances and light. Environ. Sci. Technol. **31**:1004-1011.

Voelker, B. M., and B. Sulzberger. 1996. Effects of fulvic acid on Fe(II) oxidation by hydrogen peroxide. Environ. Sci. Technol. **30**:1106-1114.

Waite, T. D., and F. M. M. Morel. 1984a. Photoreductive dissolution of colloidal iron oxide: Effect of citrate. J. Colloid Interface Sci. **102**:121-137.

Waite, T. D., and F. M. M. Morel. 1984b. Photoreductive dissolution of colloidal iron oxides in natural waters. Environ. Sci. Technol. **18**:860-868.

Waite, T. D., A. Torikov, and J. D. Smith. 1986. Photoassisted dissolution of colloidal iron oxides by thiol-containing compounds. Journal of Colloidal and interface science. **112**:412-419.

Wang, W., M. A. Tarr, T. S. Bianchi, and E. Engelhaupt. 2000. Ammonium photoproduction from aquatic humic and colloidal matter. Aquatic Geochemistry **6**:275-292.

Wells, M. L., and L. M. Mayer. 1991. The photoconversion of colloidal iron oxyhydroxides in seawater. Deep-Sea Res **38**:1379-1395.

Wells, M. L., L. M. Mayer, O. F. X. Donard, M. M. de Souza Sierra, and S. G. Ackelson. 1991. The photolysis of colloidal iron in the oceans. Nature **353**:248-250.

Wetzel, R. G., P. G. Hatcher, and T. S. Bianchi. 1995. Natural photolysis by ultraviolet irradiance of recalcitrant dissolved organic matter to simple substrates for rapid bacterial metabolism. Limnol. Oceanogr. **40**:1369-1380.

Whitehead, R. F., S. de Mora, S. Demers, M. Gosselin, P. Monfort, and B. Mostajir. 2000. Interactions of ultraviolet-B radiation, mixing, and biological activity on photobleaching of natural chromophoric dissolved organic matter: A mesocosm study. Limnol. Oceanogr. **45**:278-291.

Wiegner, T. N., and S. P. Seitzinger. 2001. Photochemical and microbial degradation of external dissolved organic matter inputs to rivers. Aquat. Microb. Ecol. **24**:27-40.

Williamson, C. E., D. P. Morris, M. L. Pace, and O. G. Olson. 1999. Dissolved organic carbon and nutrients as regulators of lake ecosystems: Resurrection of a more integrated paradigm. Limnol. Oceanogr. **44**:795-803.

Wolfbauer, G., A. M. Bond, G. B. Deacon, J. Howitt, D. MacFarlane, and L. Spiccia. 2001. Dependence of the voltammetric oxidation of the photovoltaic sensitizer $[(^{n}H_3\text{-tctpy})Ru^{II}(NCS)_3]^-$ on the electrode material, solvent, and isomeric purity. J. Electrochem. Soc. **148**:E97-E104.

Wolff, C. J. M., M. T. H. Halmans, and H. B. van der Heijde. 1981. The formation of singlet oxygen in surface waters. Chemosphere **10**:59-62.

Zafiriou, O. C., J. Joussot-Dubien, R. G. Zepp, and R. G. Zika. 1984. Photochemistry of natural waters. Environ. Sci. Technol. **18**:358A-371A.

Zepp, R. G., A. M. Braun, J. Hoigné, and J. A. Leenheer. 1987a. Photoproduction of hydrated electrons from natural organic solutes in aquatic environments. Environ. Sci. Technol. **21**:485-490.

Zepp, R. G., B. C. Faust, and J. Hoigné. 1992. Hydroxyl radical formation in aqueous reactions (pH 3-8) of iron(II) with hydrogen peroxide: The Photo-Fenton Reaction. Environ. Sci. Technol. **26**:313-319.

Zepp, R. G., J. Hoigné, and H. Bader. 1987b. Nitrate-induced photooxidation of trace organic chemicals in water. Environ. Sci. Technol. **21**:443-450.

Zepp, R. G., P. F. Schlotzhauer, and R. M. Sink. 1985. Photosensitized transformations involving electronic energy transfer in natural waters: role of humic substances. Environ. Sci. Technol. **19**:74-81.

Zepp, R. G., N. L. Wolfe, G. L. Baughman, and R. C. Hollis. 1977. Singlet oxygen in natural waters. Nature **267**:421-423.

Zhou, X., and K. Mopper. 1997. Photochemical production of low-molecular-weight carbonyl compounds in seawater and surface microlayer and their air-sea exchange. Mar. Chem. **56**:201-213.

Ziegler, S., and R. Benner. 2000. Effects of solar radiation on dissolved organic matter cycling in a subtropical seagrass meadow. Limnol. Oceanogr. **45**:257-266.

Zuo, Y., and J. Hoigné. 1992. Formation of hydrogen peroxide and depletion of oxalic acid in atmospheric water by photolysis of iron(III)-oxalato complexes. Environ. Sci. Technol. **26**:1014-1022.

Zuo, Y., and R. D. Jones. 1997. Photochemistry of natural dissolved organic matter in lake and wetland waters-production of carbon monoxide. Water Res. **31**:850-858.

2 Photodegradation of Dissolved Organic Matter

2.1 Introduction

Studies on the photochemistry of dissolved organic matter (DOM) have shown variable effects depending upon the source of the starting material. Many studies have described photodegradation of the dissolved organic matter, predominantly the complex humic and fulvic components (Kieber et al. 1990, De Haan 1993, Bano et al. 1998, Bertilsson and Tranvik 2000). However, it has also been shown that photochemical reactions can initiate processes that lead to the formation of humic substances from unsaturated triglycerides and fatty acids (Kieber et al. 1997). A diversity of reactions is to be expected as a result of the complex mixture of organic molecules which make up the dissolved organic matter. Exposing dissolved organic matter to sunlight can result in reactions through a number of mechanisms. The three major reactions of photoexcited humic substances occur: energy transfer from the excited DOM to another molecule, photoinduced electron transfer to another molecule, and photoincorporation of a molecule into the humic structure (Cooper et al. 1989). In addition, a number of photogenerated reactive species are described, including: singlet oxygen, organoperoxy radicals, hydroxyl radicals, superoxide, hydrogen peroxide, hydrated electrons and other transients. Given the mixture of mechanisms and reactive products possible, it is likely that organic matter from differing sources will undergo different degradation processes, depending on the prevailing conditions.

The photochemistry of dissolved organic matter in Australian inland waters and specifically that derived from Eucalyptus species, has not been well studied. This chapter describes studies undertaken on dissolved organic matter sourced from filter-sterilized billabong water samples, and dissolved organic matter derived from the leaves of the River red gum (*Eucalyptus camaldulensis*). River red gum is the dominant tree species on the River Murray floodplain in south-eastern Australia (Smith and Smith 1990). Leachates from the leaves may account for a large proportion of the recalcitrant DOM found in floodplain lakes and re-entering the river following flood pulses (Baldwin 1999, O'Connell

et al. 2000). Therefore, DOM derived from redgum leaves should behave in a similar manner to the allochthonous DOM inputs to many of the local waterbodies.

Dissolved organic matter sourced from billabong water samples and leachate was found to undergo oxidative photodegradation when exposed to artificial UV and visible light. Photodegradation reactions were followed using a range of techniques, which included measuring the production of carbon dioxide and consumption of oxygen in sealed reaction vessels, changes to total organic carbon content and changes to the absorbance of whole and fractionated water samples. The results illustrate a number of important features of the photodegradation reactions:

- The rate of photodegradation was found to vary between water samples, supporting the hypothesis that changes to the nature of the mixture can affect the photoreactions.
- Leachate from the *E. camaldulensis* leaves was found to be highly photoreactive.
- Substantial oxygen consumption was measured and the relationship between oxygen consumed and carbon dioxide produced altered over the course of the experiments, suggesting that the addition of oxygen to the dissolved organic matter occurs in the early stages of the degradation process.

2.2 Methods

2.2.1 Preliminary Experiments

Water was collected from Norman's Lagoon (36°15' S, 146°55'E), at Doctor's Point near Albury, NSW, Australia on the morning of May 13, 1999. Norman's Lagoon (Figure 2.1) is a small permanent billabong (oxbow lake) fed predominantly by surface water from rainfall and the Murray River (during periods of high flow) (Mitchell 2002). Norman's Billabong has an overstorey of river red gum (*Eucalyptus camaldulensis*) with the presence of some *Juncus* and a number of aquatic plant species, including: *Eleocharis, Myriophyllum, Brasenia* and *Azolla* (Mitchell 2002). Water samples were taken in 10 L Nalgene Carboys that had been soaked in 5% HCl solution, then rinsed in reverse osmosis (RO)-purified water and ultra pure water (Milli-Q), before finally being rinsed with

billabong water immediately before sampling. The water samples were returned immediately to the laboratory and filtered through a 355 μm mesh sieve. The water sample was then filtered through Advantec GC50 filters, followed by filter-sterilisation. This process involved filtering the water into five 2L autoclaved Schott bottles, through sterile 0.2μm mesh polycarbonate filters (Whatman) fitted in an autoclaved filtration unit. Filter sterilization was conducted in a laminar flow cabinet with samples kept at 4 °C, in the dark while not actually being filtered. In total two weeks of preparation passed between sampling and commencement of irradiation due to the slow filtration step. All glassware was acid washed and rinsed with RO and Milli-Q water.

One of the 2L bottles was used as an initial control for analysis by weak-anion exchange chromatography, two were wrapped in aluminium foil as dark controls and two were exposed to light (Phillips 430W Son Agro Lamp) for 13 days. The experiment was set up in a constant temperature room set to 24°C with a fan circulating air around the bottles. At the end of the irradiation period one of the dark controls and one of the light exposed samples had 20 mL of billabong water (pre-filtered with 35 μm gauze) added to introduce a natural bacterial assembly and were returned to the constant temperature room for an additional 13 days. Samples were then stored at 4°C until analysis.

Changes to the dissolved organic matter were measured qualitatively using weak-anion exchange chromatography using a protocol similar to that described by (Baldwin 1999). The 2L sample was loaded onto the column (23 x 2.6 cm DEAE-Sepharose, Pharmacia Biotech) with a peristaltic pump at a rate of 2 mL/min. Elution of the adsorbed material took place in four steps. The first involved a gradient of 0-0.33 M NaCl over 1.5L at a flow rate of 2 mL/min and 15.2 mL fractions were automatically collected using a Gradifract sampler, with the first 120 mL (column volume) discarded. The second step involved a gradient of 0.33-0.66 M NaCl over 1.5L at a flow rate of 3 ml/min and 15.8 mL fractions were collected. The third involved a gradient of 0.66-3M NaCl over 1L with 15 mL fractions collected. The final elution step involved a concentration gradient of 0-0.5 M NaOH, over 1.62L with the first 120 mL discarded and then 15.8 mL fractions collected. An elution spectrum was prepared by measuring the absorbance of each fraction at 250 nm using a Varian Carey 1E UV-vis spectrophotometer. Absorbance was measured over a 1 cm path-length and graphed against sample number.

Figure 2.1 Norman's Lagoon, looking south-east from the sampling site.

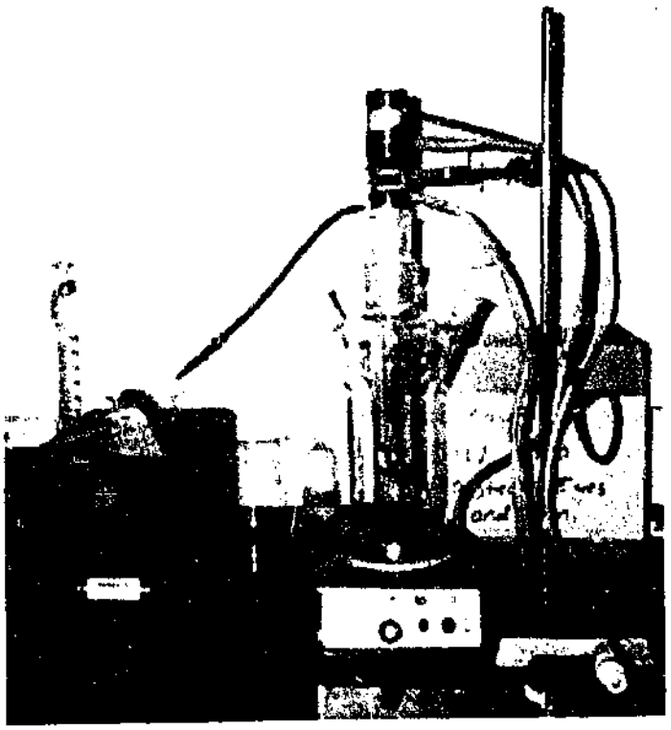

Figure 2.2 The Hanovia photochemical reactor.

2.2.2 *Billabong Water Experiments*

2.2.2.1 Photochemical Degradation of Billabong Water-Summer Samples

Water samples were collected at 7.45 am daily between the 14th and 19th of January 2000 at Norman's Lagoon, and returned immediately to the laboratory for filtering. The samples in this experiment were used for quantitative analysis and rapid filtration was required to minimise changes to the organic matter during the period of sample preparation. A new sample preparation method was developed. Water samples were poured through 35 μm gauze to remove large particles and then were pumped through a Millipore tangential flow filtration (TFF) system, fitted with six 0.2 μm plates. Eluent from the TFF was then filter-sterilized under vacuum through 0.2 μm pore sized, pre-sterilized Millipore Stericap filters. The final filtration was carried out in a laminar flow cabinet (pre-sterilized with UV light), using autoclaved, acid-washed glassware, and all open vessels were kept under a flame hood (Bunsen burner flame) to reduce the risk of bacteria falling into the sample. Filtration of 2 L of water took approximately 2 hours. Trial water samples (1 drop), were added to sterile 10 mL nutrient broths and incubated for one week. In two samples no bacteria were observed and a third sample had become cloudy only at the end of the week, indicating that this method was very effective at removing bacteria. In contrast, retentate from the TFF step grew to dense cultures after two days.

On each day 700 mL of the filter-sterilized water was aseptically transferred into a 920 mL acid-washed, UV-sterilized photochemical reactor (Hanovia, 1 L Photochemical Reactor, 125 W)*. Another 900 mL was kept in a 1 L sterile Schott Bottle, wrapped in foil and stored at 20 °C. The photochemical reactor consisted of a glass, three-necked flask with a quartz insert in the centre neck (Figure 2.2). The quartz insert housed the cooling system and UV-visible lamp. A temperature probe fitted to a Suba-seal stopper was inserted in one of the side necks and the other was stoppered with a Suba-seal stopper for gas samples to be removed. This apparatus was connected to a thermostatted, circulating

*This lamp was used for all the experiments reported in this chapter except for the preliminary experiment. Unfortunately, this lamp was broken by the couriers when sent for spectral characterisation, and hence detailed spectral data is not available. An older Hanovia lamp of similar design was obtained and characterised, but the output power was not as great. The spectral data of the second lamp is given in Appendix 3.

water bath, to give a reaction temperature of 20 °C. The photochemical reactor was continuously stirred using a Teflon-coated magnetic stirrer bar, and the dark control was placed on a shaker table and incubated at 20 °C. After scaling, the reactor was left to stabilise for 30 minutes (with stirring), before the zero-time headspace gas sample was taken and the lamp switched on. The first four days of the experiments involved irradiation, and for the last two days the lamp was left off to obtain dark "control" gas measurements.

Headspace gas samples (2 mL) were taken hourly and analysed for CO_2, CO and O_2 using a Varian Star 3400 gas chromatograph fitted with an Altech CTR 1 column and a thermal conductivity detector. Gas samples were taken with a sterile syringe and needle, which was immediately placed in a rubber stopper and stored underwater until injection into the gas chromatograph. It was not practical to take multiple gas measurements at each sampling time, as low pressures would have resulted by the end of the experiment. Having only one photochemical reactor, it was necessary to use the repeat experiments in the place of replicate measurements. The gas chromatograph was calibrated using a mixed standard (Scotty II, mix 234) and was deemed calibrated when three consecutive injections gave results within 1% of the standard value for CO_2 and O_2. The calibration was checked daily and repeated as required. Headspace carbon dioxide results were used to calculate total carbon dioxide produced using the spreadsheet in Appendix 4. The equations were based on Henry's Law and incorporated equilibrium and acidity constants to account for the speciation of dissolved inorganic carbon (Stumm and Morgan 1981). Oxygen calculations (Sander 1999) were similarly carried out using the spreadsheet in Appendix 5. A Varian Carey 1E UV-vis spectrophotometer was used to measure the absorbance spectrum of water samples before and after the irradiation.

2.2.2.2 Photochemical Degradation of Billabong Water-Autumn Samples

Water samples were collected from Norman's Lagoon at 8am on the 21, 22, 25, 26, 29 and 30th of March 2000. Every second sample was put in the photoreactor, but not irradiated, to provide the dark controls for gas measurements. The water samples were filter sterilized and light or dark experiments were conducted using the method described in 2.2.2.1. Measurements of pH were made both before and after irradiation, using a Hanna

RS232 pH meter with a Schott Geale N6180 pH probe. It was not possible to measure pH throughout the experiment, as it was impossible to remove liquid samples from the reactor while the time-course experiment was being conducted and it was not possible to build a pH meter into the reactor. Samples for Total Organic Carbon measurements were taken and frozen. The TOC analysis however, could not be undertaken as the samples were affected by a freezer failure. Gas analysis and absorbance measurements were carried out as described previously.

2.2.3 Leachate Experiments

To ensure reproducibility, all DOM solutions used in these experiments were prepared on a daily basis from a single combined batch of leaves from the river redgum, *Eucalyptus camaldulensis*. Leaf material was collected at forest sites on the Murray River at Albury, Barmah and Hattah between December 1998 and September 1999, dried at 65 °C overnight and stored dry until use in July 2000. A sample of dried leaf (390 g) was chopped and then ground to a coarse powder using a sample mill and stored in a polypropylene screw-top jar. The leachate was prepared in ultrapure (Milli Q) water by adding 0.1 g ground leaf L^{-1}. This mixture was shaken in the dark at 20 °C for one hour, and then filtered through a Whatman GF/C filter. The leachate was then filter-sterilized by filtration using 0.2 μm Millipore Stericap™ filters in a sterile laminar flow cabinet. Leachate was collected in 1 L autoclaved Schott bottles. This method produced a leachate with an average DOC content of 14 mg C L^{-1}, which is within the range of values found in freshwater ecosystems.

The irradiation experiments were carried out using the protocols and equipment described in Section 2.2.2.1, with the exception that reaction length and sampling times were varied. The leachate was used unbuffered at its natural pH of 5.3 and was monitored at the beginning and end of each experiment using a Hanna pH 211 microprocessor pH meter. Samples for TOC analysis were taken at the beginning and end of the experiments, preserved with 100 μL of conc. phosphoric acid and stored frozen in pre-fired glass bottles with Teflon lined caps. These TOC samples were then analysed at the Murray-Darling Freshwater Research Centre using an O-I-Analytical 1010 Total Organic Carbon Analyser.

2.3 *Results and Discussion*

2.3.1 Preliminary Experiments

Noticeable fading of the yellow colour of the irradiated water at the end of the 13-day irradiation period, compared to that of the dark controls, suggested that photochemical degradation of the organic material had occurred in this experiment. Figure 2.3(a) shows the elution spectra produced for the initial control sample, and Figure 2.3(b) gives a comparison of the light-exposed and dark-control samples. Bacteria were found in the samples, but were present in all samples so differences in the elution spectrum could still be interpreted as photochemical effects. It seems that the peaks in the middle range of the elution spectrum of the initial sample represent compounds that are available for bacterial metabolism or are otherwise readily degraded, and these compounds were not present in the same concentrations in subsequent samples. Comparing these results with Figure 2.3(b), it can be seen that the dark control was very similar to the initial material in its general shape and the key features were well matched in elution volume (NaOH region not collected). There was however, an increase in early eluting material (around tube number 12). This peak was also present in one of the light exposed samples. Adding a small volume of water introduced bacteria to these samples, but did not result in significant changes to the carbon content. It seems likely that the additional peak is a result of additional bacterial metabolites produced during the incubation period.

There are three dominant peaks in the 20-80 tube number range, and the two light-exposed samples have these peaks shifted towards earlier elution times compared to the initial samples and the dark control. The DEAE-Sepharose gel is cross-linked agarose with $-O\text{-}CH_2CH_3\text{-}N^+(C_2H_5)_2H$ surface groups and separates the organic material based on negative charge, so a forward shift in elution time may be the result of the loss of some negative charge on the molecules, as would occur if some acidic functional groups were lost during light exposure.

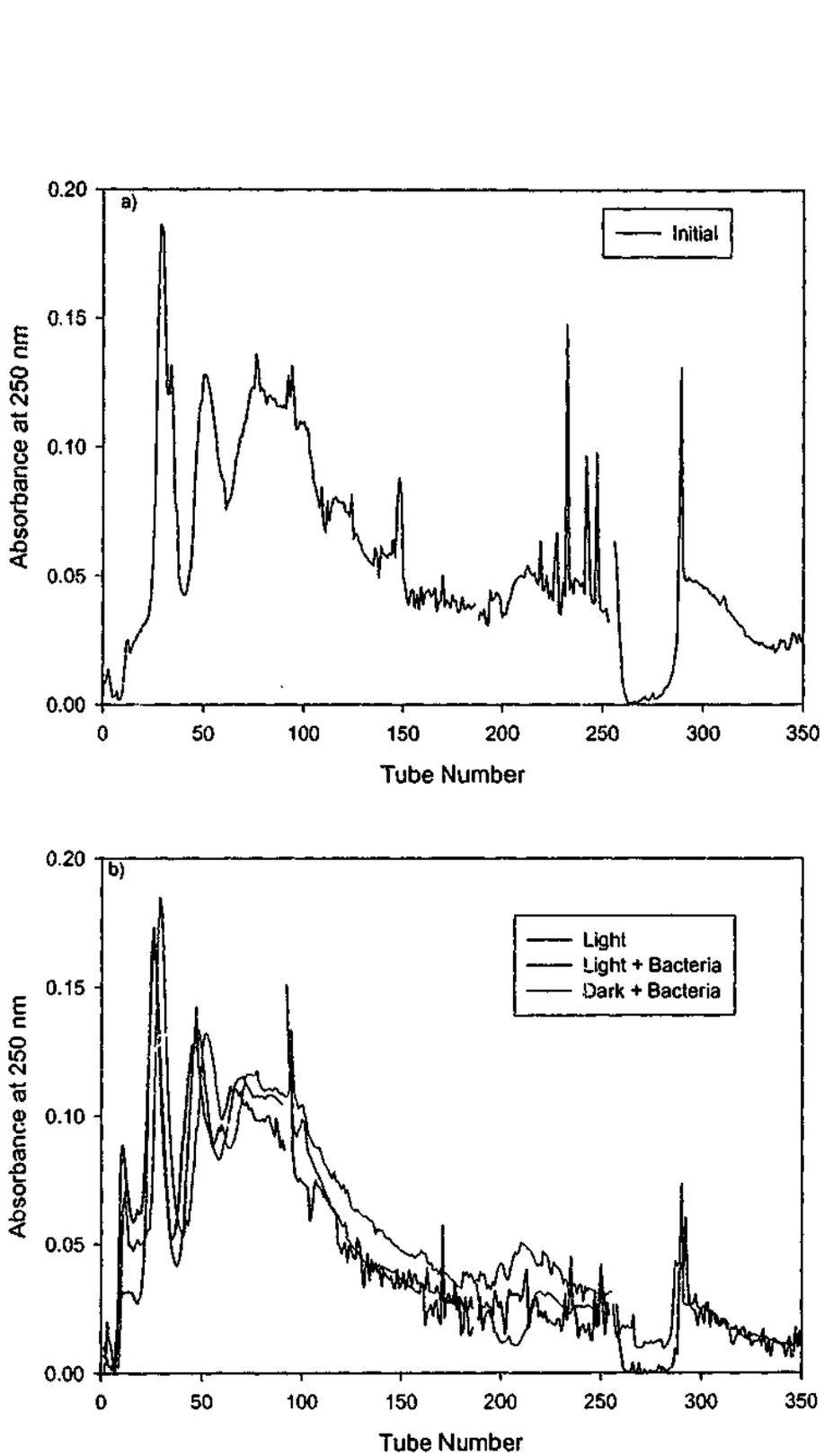

Figure 2.3 Elution spectra of billabong water samples at the beginning of the experiment (a) and after the irradiation experiment (b). Samples marked + Bacteria had a small quantity of unsterilized billabong water added after the irradiation and were incubated in the dark for 13 days.

2.3.2 Billabong Water Experiments

2.3.2.1 Photochemical Degradation of Billabong Water-Summer Samples

Photochemical generation of carbon dioxide measured in all light-exposed samples demonstrated that dissolved organic matter sampled from Norman's Lagoon in mid summer was photochemically active (Figure 2.4). As only one photochemical reactor was available, irradiation of water samples taken on consecutive days takes the place of replicate measurements. Some variability between samples was expected, but this was accepted as indicative of environmental conditions. Samples from the 14th to the 17th, inclusive, are light exposed treatments, and the samples from the 18th and 19th were used as dark controls. Values plotted are the total net CO_2 production. A first order rate equation of the form:

$$y=a*(1-\exp(-b*x)) \qquad \text{Equation 2.1}$$

where y and x represent total CO_2 and duration of irradiation respectively and a and b are constants could be fitted to each of the data sets with good correlation obtained (Table 2.1). The constant a represents the maximum y value of the curve and b indicates a rate of reaction.

Table 2.1 Constants generated for first order rate equations for carbon dioxide production from billabong water samples

Sample Date	Constant (a) (mol)	Std Error (a) (mol)	Rate (b) (h^{-1})	Std Error (b) (h^{-1})	R^2
14/01/00	0.0007	0.0001	0.144	0.033	0.994
15/01/00	0.0005	0.0000	0.310	0.048	0.990
16/01/00	0.0006	0.0001	0.314	0.082	0.973
17/01/00	0.0010	0.0005	0.16	0.11	0.928
18/01/00	0.2	4190	0.0000	0.64	0.327
19/01/00	0.0001	0.0001	0.48	0.60	0.553

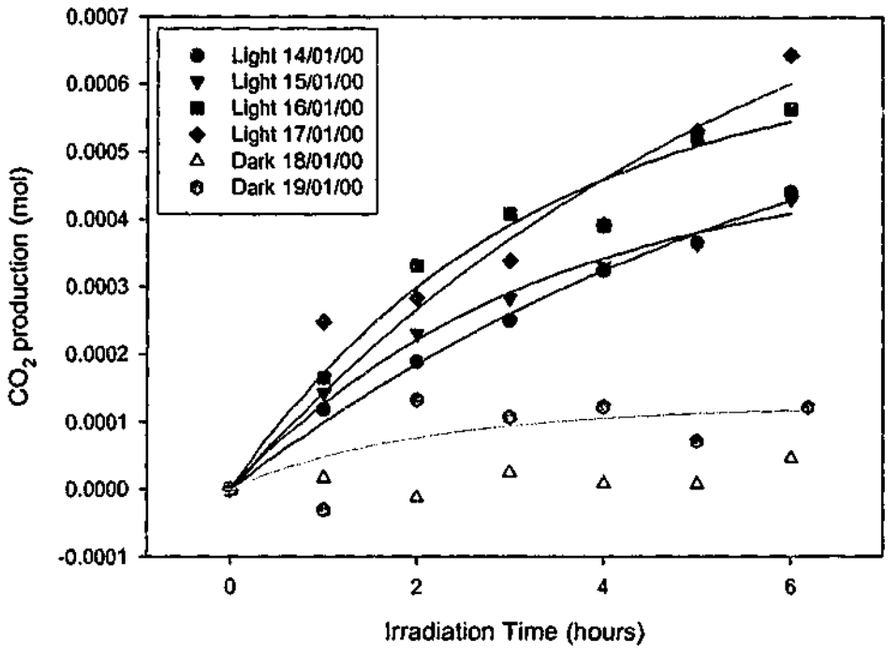

Figure 2.4 Photochemical production of CO_2 from billabong water- summer. Solid lines represent first order rate equation fits for each data set.

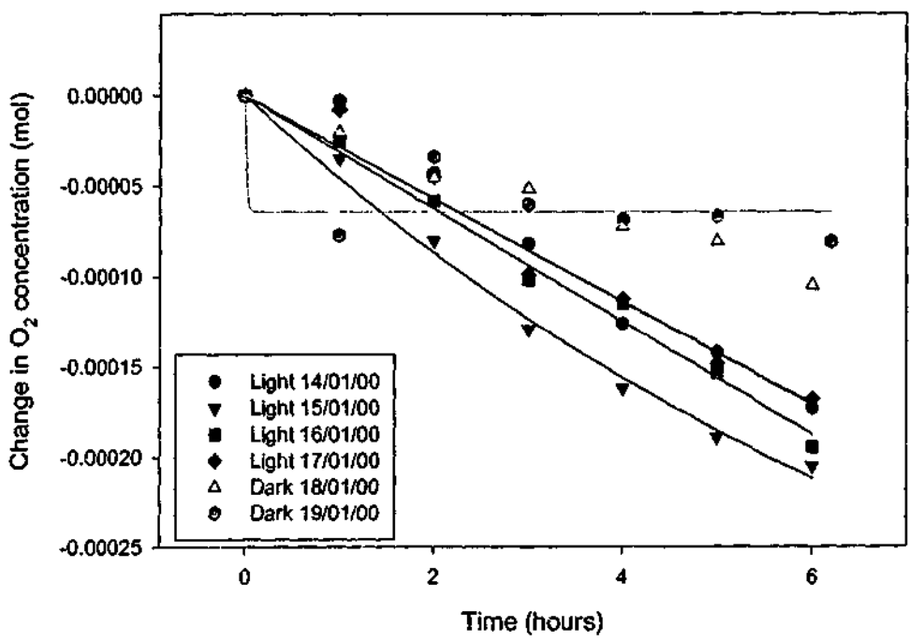

Figure 2.5 Photochemical consumption of O_2 from billabong water- summer. Solid lines indicate first order rate equation fits to the data.

Light-exposed samples had a much greater rate of carbon dioxide generation than the dark controls, suggesting a photochemical mechanism. The light induced carbon dioxide production fits very well to a first order rate equation ($R^2 > 0.92$), however, the dark controls do not fit well to a first order rate equation ($R^2 < 0.6$). This suggests that the low levels of carbon dioxide production in the dark control samples is not a result of the same mechanism as the production of carbon dioxide in the light exposed samples.

There was some daily variability in the photoreactivity, with the later samples proving to be the most reactive. The water on the 16th (a more reactive sample) was more turbid at the time of sampling than the previous samples had been. Data obtained from the Australian Bureau of Meteorology indicated that this was not the result of rain or wind events. It is possible that an internal mixing process (such as ebullition from the sediments or disturbance by wildlife) caused the increased turbidity. This may have introduced organic matter of greater photochemical reactivity into the water column from the sediments. The organic matter content of the filtered sample (measured as absorbance at 250 nm) was still within the range of the earlier samples, which indicates that the change in rate was a response to changing nature of the organic matter rather than a change in concentration. Measurement of pH was not possible during the irradiation (water sampling would generate pressure problems in the photoreactor) thus, for the total CO_2 calculations it was necessary to assume constant pH throughout the experiments. The initial pH of the samples was in the range 6.7-7.0 and as the pKa of carbonic acid is 6.3 (Stumm and Morgan 1981), fluctuations in the pH in this region may also influence the calculated total inorganic carbon concentration. However, given the magnitude of the difference between the light exposed carbon dioxide concentration and the dark controls, photochemical carbon dioxide generation did occur.

Light-exposed samples were subject to significant photobleaching (Table 2.2). After six hours of irradiation in the photochemical reactor, the absorbance of the samples at 250 nm was between 13 % and 24% of the absorbance measured in the starting material. In the dark controls, however, the absorbance at 250 nm was between 96 % and 105 % of the initial absorbance. These results indicate that the majority of the coloured dissolved organic matter in the billabong water samples was photolabile.

Table 2.2 Initial and final absorbance at 250 nm (A_{250}) in billabong water samples

Date	Initial A_{250}	Final A_{250} (light)	Final A_{250} (Dark)
14/01/00	0.174	0.023	0.169
15/01/00	0.155	0.026	0.162
16/01/00	0.164	0.021	0.162
17/01/00	0.161	0.039	0.154
18/01/00	0.159	NA	0.162
19/01/00	0.164	NA	0.161

The consumption of oxygen during irradiation was much greater in the light-exposed samples than in the dark controls (Figure 2.5). Some oxygen consumption occurred in the dark control experiments in the photochemical reactor and may reflect either some oxidative "dark" reactions were occurring or low-level bacterial respiration. First order rate equations were also fit to the oxygen consumption data (Table 2.3). The first-order fit was less appropriate for these results than the carbon-dioxide results (as indicated by the size of the error relative to the predicted value), suggesting that the reactions are not following the same path.

Table 2.3 Constants generated for first order rate equations describing the photochemical consumption of O_2 in summer samples of billabong water

Sample Date	Constant (a) (mol)	Std Error (a) (mol)	Rate (b) (h^{-1})	Std Error (b) (h^{-1})	R^2
14/01/00	-1.81	10456	0.00	0.09	0.96
15/01/00	-0.0004	0.0001	0.11	0.04	0.99
16/01/00	-1.31	2186	0.00	0.4	0.99
17/01/00	-1.43	5475	0.00	0.08	0.97
18/01/00	-0.0003	0.0002	0.073	0.05	0.98
19/01/00	-0.0001	0.0000	69	832	0.72

Figure 2.6 illustrates the relationship between oxygen consumption and carbon dioxide production for each of the experiments conducted in the photochemical reactor. The dark control samples did not show a strong relationship between oxygen consumption and carbon dioxide production. The relationship between oxygen consumption and carbon dioxide production in the light-exposed samples varied between water samples, but could

be approximated with a linear regression (r^2 values between 0.87 and 0.96). For the 14/01/00 sample, 0.44 ± 0.04 (1 standard error) moles of O_2 were consumed per mole of CO_2 produced, and on 15/01/00, 0.53 ± 0.05 moles of O_2 per mole of CO_2 were consumed. However, for the 16/01/00 sample, following the water disturbance, there was more of a lag in O_2 consumption relative to CO_2 production, and 0.34 ± 0.05 moles of O_2 were consumed for each mole of CO_2 produced. Similarly, the 17/01/00 sample had a lag in O_2 consumption and the trend v s 0.30 ± 0.05 moles of O_2 consumed to each mole of CO_2 produced.

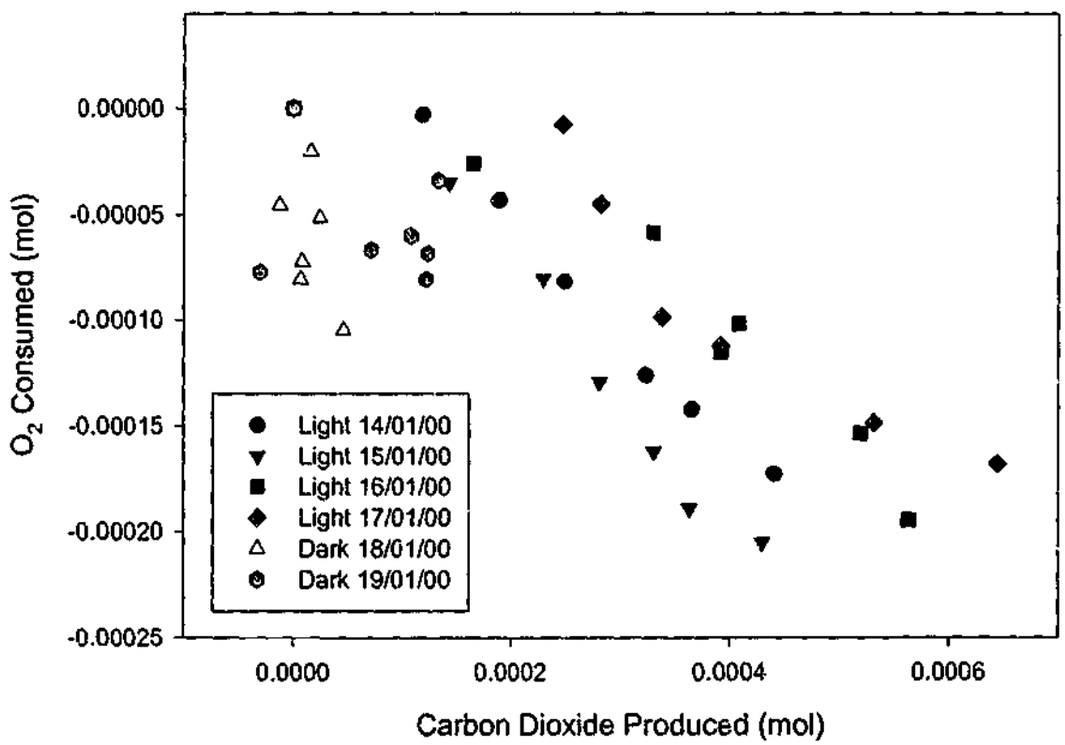

Figure 2.6 The correlation between CO_2 production and O_2 consumption in the summer billabong water irradiation experiment.

These results suggest that the most highly oxygenated compounds in the dissolved organic matter were the first to photodegrade to CO_2, with atmospheric oxygen becoming important when the oxygen poor organic compounds begin to degrade. The results of this experiment suggest that the role of molecular oxygen in the photochemical reactions can be

variable. The initially slow rate of oxygen uptake relative to carbon dioxide production in the 16/01/00 and 17/01/00 samples, after the mixing event, suggests that the organic matter in these samples is initially capable of undergoing direct photochemical degradation to generate a carbon dioxide molecule. As the reactions proceed the reactions depend more heavily on dissolved oxygen species, indicating an increasing importance of oxygen radicals in the degradation process.

Increasing levels of carbon monoxide were observed in the photochemical reactor in the light-exposed samples. The amount of carbon monoxide was unquantifiable as it was very close to the limit of detection of the gas chromatograph and also eluted in a region prone to interference by moisture retained on the column from the previous sample, but there did appear to be an increasing trend in the peak area of the unaffected samples.

2.3.2.2 Photochemical Degradation of Billabong Water-Autumn Samples

These experiments were carried out to measure photoreactivity of DOM present in samples taken from Norman's Lagoon during autumn. The results verify the photochemical reactivity of dissolved organic matter from Norman's Billabong and indicate that photochemically reactive components are not depleted over the summer period. As in the previous experiment, inability to measure pH during the experiment meant that pH was measured at the start and finish of each experiment. The CO_2 calculations were again undertaken with the assumption that the pH remained constant at the starting pH (7.2-7.4). Some measurements tended to fluctuate, leading to increased uncertainty. For example, the initial pH measurement for the water sample used on the 25th of March 2000 was 6.9, the dark control measured 7.3 and the light-exposed 7.1. All other experiments showed a trend for the dark control pH to stay approximately the same as the initial sample and light-exposed samples to be a lower pH. A possible reason for this discrepancy was that the initial pH measurement was incorrect. Assuming this was the case, a value of 7.3 was used in the calculations, consistent with the dark controls and initial measurements of the other water samples. Again, in this pH region, small fluctuations in the pH measurements lead to major changes in the total calculated inorganic carbon. There was an apparent trend for small reductions in pH in the light-exposed samples.

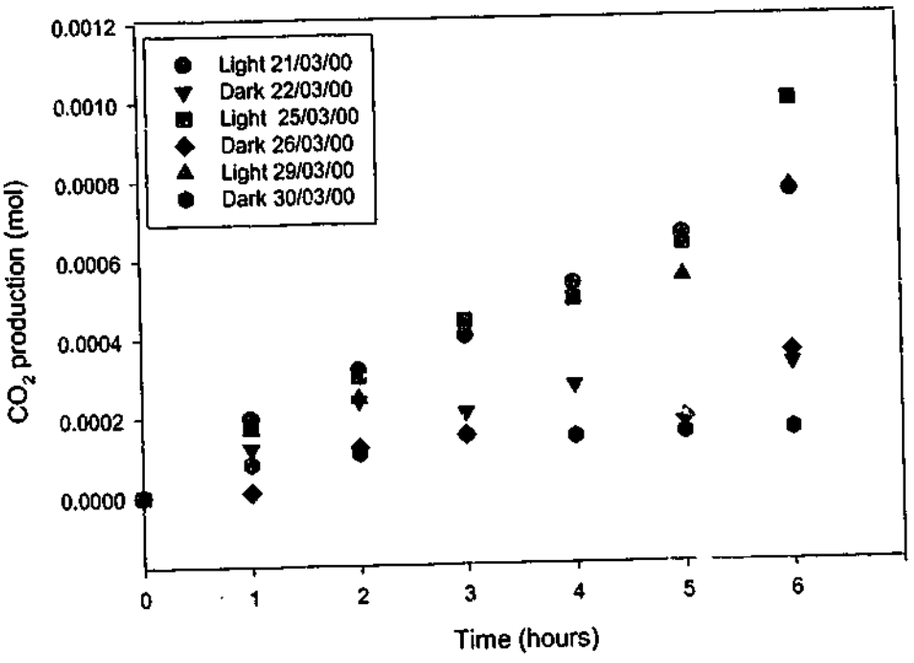

Figure 2.7 Photochemical production of CO_2 from billabong water- autumn.

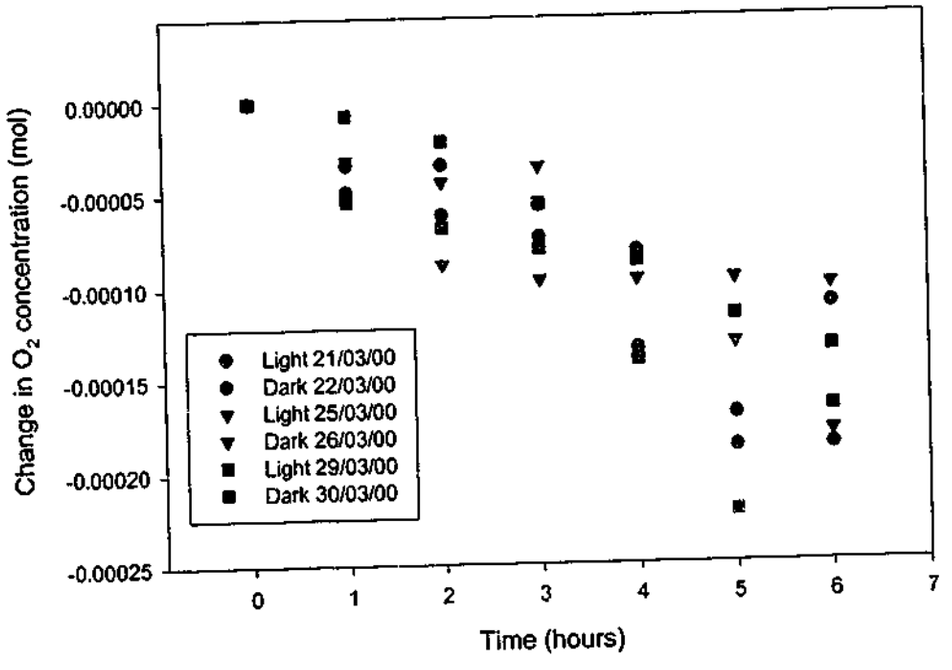

Figure 2.8 Photochemical consumption of O_2 from billabong water-autumn

Photochemical carbon dioxide production occurred in all the light-exposed samples and the rates across the different samples were similar (Figure 2.7). The scatter in the data prevents a first order rate equation being fit to the data, and the rate would be subject to change if the reduction in sample pH over time could be taken into account. Given that the same assumptions were made when calculating the CO_2 production in this and the previous experiment, it is interesting to note that the summer experiment showed an apparent decline in the rate of CO_2 production towards the end of the experiment, while no decline was apparent in the autumn experiment. More CO_2 was generated in the autumn experiments than the summer experiments, perhaps indicating differences in the reactivity of the organic matter or that the later samples were more prone to direct photomineralisation, rather than photochemical modification of the macromolecules.

The summer experiment had a higher initial absorbance at 250 nm than this experiment, suggesting either a higher DOC content, or that the DOC sampled in the autumn had been partially photobleached by sunlight. The changes in absorbance of the samples are given in Table 2.4. Following six hours of irradiation in a photochemical reactor, 18-28% of the initial absorbance at 250 nm (A_{250}) remains, and 18-35% of the absorbance at 360 nm (A_{360}). The dark controls remained unchanged, with 98-100% of the absorbance at 250 nm remaining, and 97-104% of the absorbance at 360 nm remaining. The ratio of absorbance at 360 to 250 nm remained essentially unchanged (0.13 - 0.19, vs 0.14 - 0.15). This suggests that the photobleaching was relatively uniform across the spectrum. As the absorbance continued to diminish with increasing wavelength, it was not practical to monitor photobleaching at longer wavelengths.

As in the January experiments, it is evident that most of the coloured dissolved organic matter in these water samples was susceptible to degradation under this light regime, although the reactions had not come to completion after six hours of irradiation. The final A_{250} results for light exposed treatments in both the summer (average 0.027) and autumn experiments (0.025) are very similar, despite the higher initial absorbance of the summer samples. This could indicate that a fraction of the coloured dissolved organic matter is resistant to photobleaching, or that bleaching occurred more rapidly in the summer experiment. Slower photobleaching of the autumn DOM could be expected if the most readily photobleached DOM had already undergone additional fading in the field,

compared to the earlier sampling time. Norman's Lagoon has extensive macrophyte growth in and around it, and so despite negligible rainfall in the intervening months, DOM input into the billabong may have occurred. These results highlight the fact that the photochemical reactivity of dissolved organic matter in aquatic environments will vary considerably not only with source but also with time.

Table 2.4 Changes in absorbance at 250 nm (A_{250}) and 360 nm (A_{360}) of billabong water samples: March 2000. Cells marked NA indicate samples used for dark treatments in the photochemical reactor, for which there was no light-exposed equivalent.

Sample	Initial A_{250}	Light A_{250}	Dark A_{250}	Initial A_{360}	Light A_{360}	Dark A_{360}
21/3/00	0.124	0.035	0.123	0.019	0.007	0.019
22/3/00	0.117	NA	0.116	0.017	NA	0.017
25/3/00	0.105	0.02	0.103	0.015	0.003	0.015
26/3/00	0.111	NA	0.111	0.016	NA	0.016
29/3/00	0.113	0.020	0.113	0.016	0.003	0.016
30/3/00	0.113	NA	0.113	0.016	NA	0.016

The photochemical degradation of the dissolved organic matter from these billabong water samples was again accompanied by the consumption of oxygen (Figure 2.8). As a result of the considerable scatter in these data, a first order rate equation was not fit to the results, however, the light-exposed samples (pink symbols) decreased in O_2 concentration more than the dark controls (blue symbols). The total consumption of oxygen in these experiments was similar to the total consumption of oxygen in the summer experiment.

Figure 2.9 illustrates the relationship between O_2 consumption and CO_2 production in these experiments. The total molar consumption of O_2 is approximately a quarter of the molar production of CO_2 in the light-exposed samples. Fitting linear regressions to the data produces reasonable fits (r^2 = 0.76-0.96). The first and last experiments had relationships that were essentially the same (0.27 ± 0.03 and 0.26 ± 0.06 moles of O_2 per mole of CO_2 respectively), while the middle experiment had a somewhat lower relative oxygen consumption (0.17 ± 0.02).

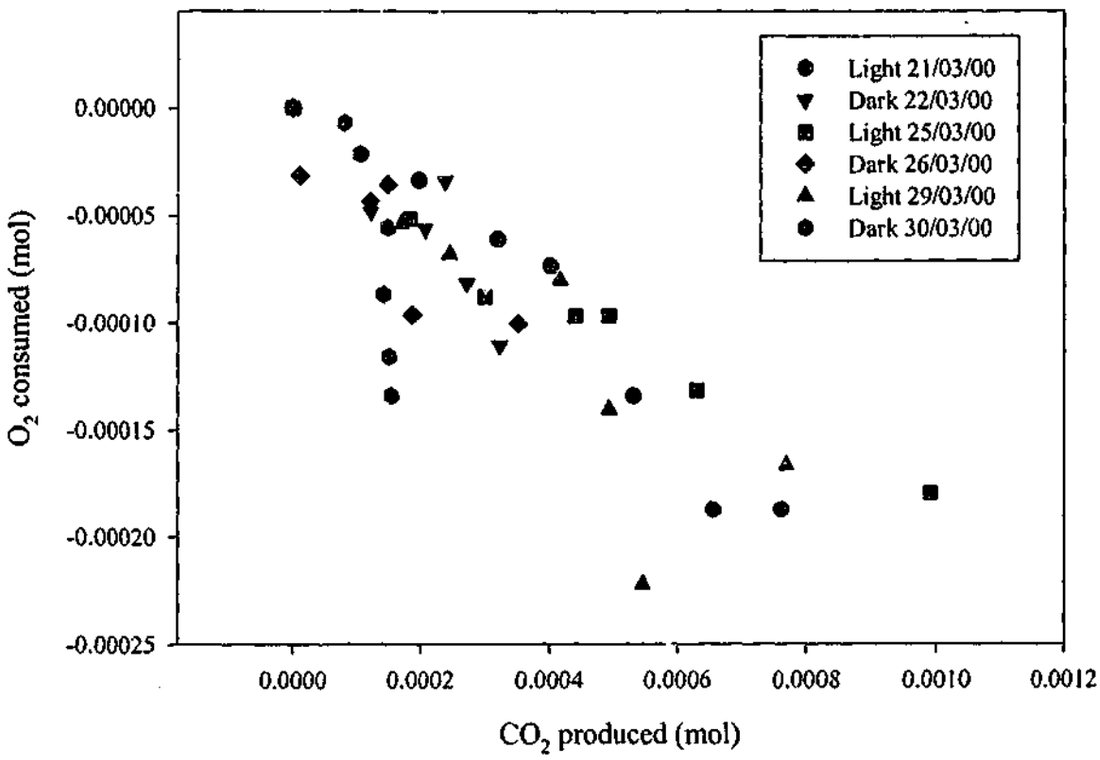

Figure 2.9 Correlations between photochemical CO_2 production and O_2 consumption in autumn billabong water samples.

As was the case for the summer experiment, trace levels of carbon monoxide were detected (but not quantified) in the light-exposed samples, with an apparent trend towards increasing concentration with time.

2.3.3 Leachate Experiments

Leaching experiments to obtain DOC from red gum leaves showed that over 80% of the DOC (measured as absorbance at 250 nm) that leached from the powdered leaf material in a 70-hour period actually entered the solution within the first hour (data not shown). Leaching for 70 hours gave time for bacteria and fungi to grow in the leachate, affecting the reproducibility of leachate composition. Hence, it was decided that a one-hour leaching period was the most practical, as leaching for additional time did not greatly increase the concentration of DOC.

These experiments were run with variable reaction times to maximise the data that could be obtained. The number of gas samples taken from the photoreactor was limited to ensure that the pressure change remained below 10%. For some experiments the gas samples were clustered in the first eight hours to measure initial rates of reaction, and in other experiments the initial measurements were spread further apart and the irradiation was continued to give an indication of when the reactions came to completion.

Unbuffered leachate was used in these photochemical experiments, at the natural pH of 5.2 ± 0.1 (1 s.d., n = 8). The light-exposed samples decreased in pH over the course of the reaction. However, at this end of the pH scale, small changes in pH have negligible effects on the total amount of inorganic carbon in solution, as the dominant species is dissolved CO_2 (Stumm and Morgan 1981). For this reason, calculations were performed assuming the pH remained constant as no data on the rate of pH change was available. The final pH for dark control samples was also 5.2 ± 0.1 (n = 8) and the final pH in light exposed samples was 4.4 ± 0.4 (n = 7).

The photochemical production of carbon dioxide from leaf leachate in the photochemical reactor is illustrated in Figure 2.10. The light-exposed samples had highly reproducible photogeneration of carbon dioxide, while the dark control did not generate carbon dioxide. The longer experiments (greater than 70 hours of irradiation) were the only ones to generate sensible constants with realistic error values when Equation 2.1 was fitted to the data (see Table 2.5). This is likely to be a result of the long reactions approaching completion, whereas the short reactions were ended while the rate of reaction was still quite rapid and the rate of CO_2 production is near linear. A close inspection of the carbon dioxide generation data also indicates that there is a lag in the initial carbon dioxide generation (the rate of reaction is slower for the first two hours), suggesting more than one mechanism involved in the reactions. The first mechanism appears to dominate for only the first 2-3 hours, and then the remainder of the experiment is dominated by the second mechanism. Fitting first order rate equations to the longer experiments gives reasonable results as the first few hours are less significant to the overall result. However, in the shorter experiments, the lag is sufficient to invalidate the regression (i.e. an exponential rise to a maximum is not a suitable model for the data).

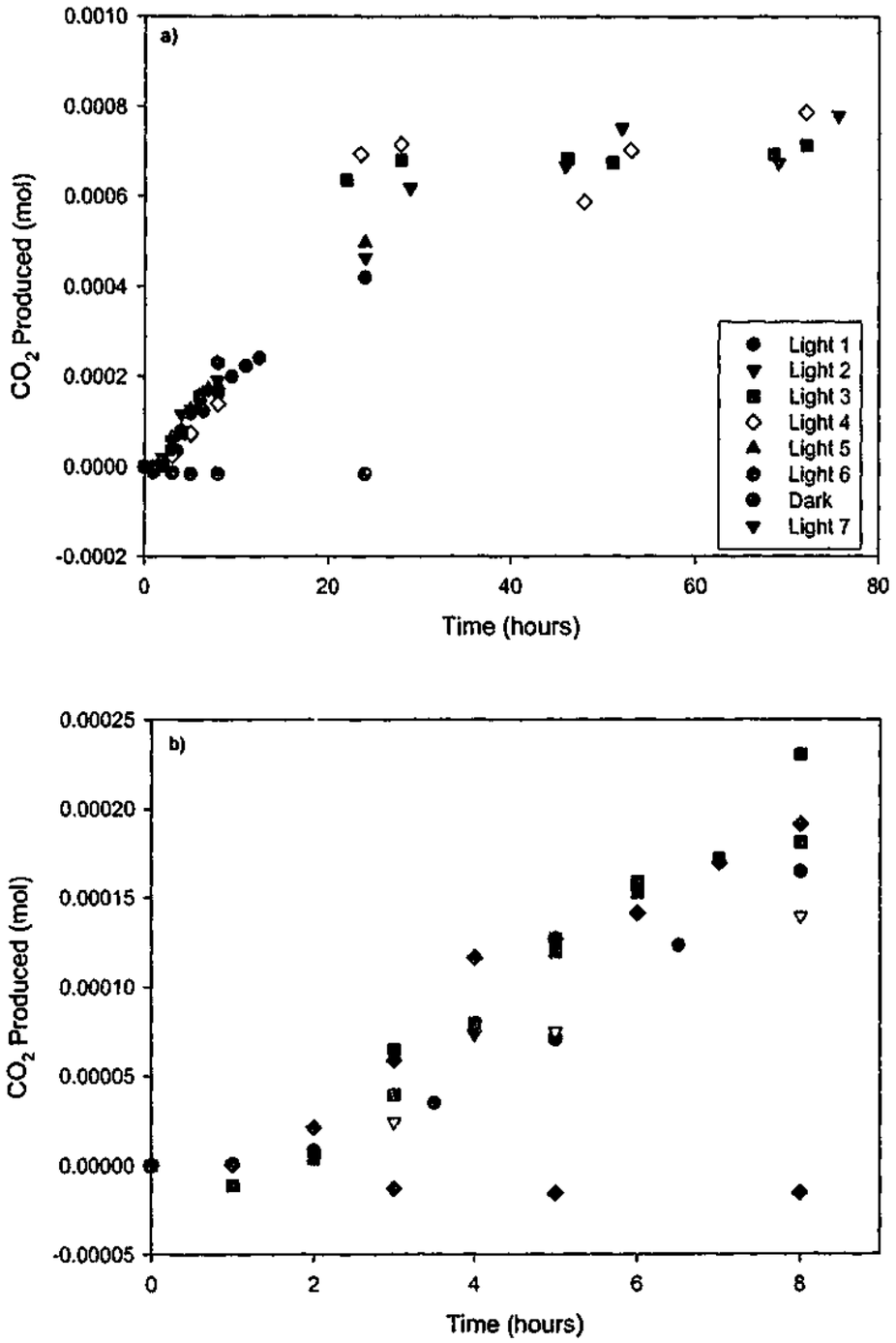

Figure 2.10 Photochemical production of CO_2 from irradiated red gum leaf leachate. Part a) shows the results over the full irradiation times, while part b) is an enlargement of the results over the first nine hours, enabling the initial lag to be examined.

Table 2.5 Constants for first order rate equation fits to photochemical CO_2 production from leachate. Figures in parentheses indicate duration of the experiment.

Sample (hours)	Constant (a) (mol)	Std Error (a) (mol)	Rate (b) (h^{-1})	Std Error (b) (h^{-1})	R^2
Light 1 (24)	3	5010	0.00	0.01	0.975
Light 2 (75.5)	0.0008	0.0001	0.040	0.009	0.970
Light 3 (72)	0.0007	0.0000	0.08	0.02	0.969
Light 4 (72)	0.0008	0.0001	0.05	0.02	0.907
Light 5 (24)	2	2353	0.0000	0.009	0.988
Light 6 (8)	2	17307	0.0000	0.115	0.883
Dark (24)	-0.0000	0.0000	0.55	0.05	0.998
Light 7 (8)	2	9806	0.0000	0.06	0.955

Total organic carbon concentrations also changed during the experiments (Table 2.6). The initial leachate contained around 14 mg/L dissolved organic carbon. It appears that after 70 hours almost all (ca. 90%) of the DOC was degraded. After this time the carbon dioxide production had plateaued, suggesting that a small proportion (ca. 10%) of the organic matter is resistant to photochemical degradation, even under the high-intensity lighting used in these experiments.

Table 2.6 A comparison between changes to total organic carbon and the production of CO_2 in leachate irradiation experiments. Figures in parentheses indicate the duration of each experiment. $\Delta CO_2/\Delta TOC$ is the ratio of CO_2 produced per litre of leachate to the change in TOC concentration.

Sample (hours)	Initial TOC (mg C L^{-1})	Final TOC Light (mg C L^{-1})	Final TOC Dark (mg C L^{-1})	CO_2 Production (mg C L^{-1})	$\Delta CO_2/\Delta TOC$
Light 1 (24)	13.2	12.9	16.2	7.2	24
Light 2 (75.5)	14.3	2.8	15	13.4	1.2
Light 3 (72)	13.6	1.6	13.8	12.2	1.0
Light 4 (72)	14.2	0.72	14.1	13.5	1.0
Light 5 (24)	15.1	21.9	14.7	8.5	-1.3
Light 6 (8)	12.7	9.5	14.6	4.0	1.2
Dark (24)	13.8	Na	14.3	-0.3	0.5
Light 7 (8)	14.6	12.9	16.6	3.3	1.9

The changes to absorbance measured at 250 nm suggest that the remaining fraction of dissolved organic matter is resistant to photodegradataion as a result of very low absorbance (Table 2.7). Even after eight hours of irradiation there is less than 5% of the original absorbance remaining in the light-exposed samples, and after 70 hours this falls to a fraction of a percent. It is likely therefore, that the organic material remaining after irradiation in a photochemical reactor consisted of non-light absorbing molecules, including organic molecules with simpler bonding structure (i.e. without complicated systems of aromatic and conjugated bonds) that do no absorb the visible and UV wavelengths longer than 250 nm. This simpler organic matter is likely to be readily available for bacterial degradation.

Table 2.7 Changes to the absorbance at 250 nm of leachate, including the remaining absorbance expressed as a percentage of the initial absorbance. Numbers in parentheses indicate experiment duration.

Sample (hours)	Initial A_{250}	Final A_{250} Light	Final A_{250} Dark	Light % Initial	Dark % Initial
Light 1 (24)	0.483	0.005	0.506	1.0	105
Light 2 (75.5)	0.476	0.003	0.504	0.6	106
Light 3 (72)	0.456	0.002	0.483	0.4	106
Light 4 (72)	0.446	0.000	0.475	0	107
Light 5 (24)	0.459	0.001	0.477	0.2	104
Light 6 (8)	0.466	0.017	0.440	3.6	94
Dark (24)	0.536	-	0.468	-	87
Light 7 (8)	0.497	0.023	0.477	4.6	96

The photochemical consumption of oxygen in the leachate irradiation experiments is shown in Figure 2.11. Given that each set of points represents a repeat experiment rather than a replicate sample, the results are remarkably reproducible and indicate that the gas analysis is reasonably precise and that minimal variation in the amount of DOC leached from the leaves and the strength of irradiation occurs. First order rate equations were fitted to each set of data (Table 2.8). Two of the regressions did not generate sensible coefficients, despite the good R^2 values. These particular samples were amongst those that had a similar problem with the CO_2 data. However, some of the experiments in which the CO_2 data did not give a good fit to a first order rate equation had oxygen results that gave

good fits. This may be a result of there being no apparent lag in the oxygen consumption. There may be two types of reactions occurring, both consuming oxygen but only one readily generating carbon dioxide.

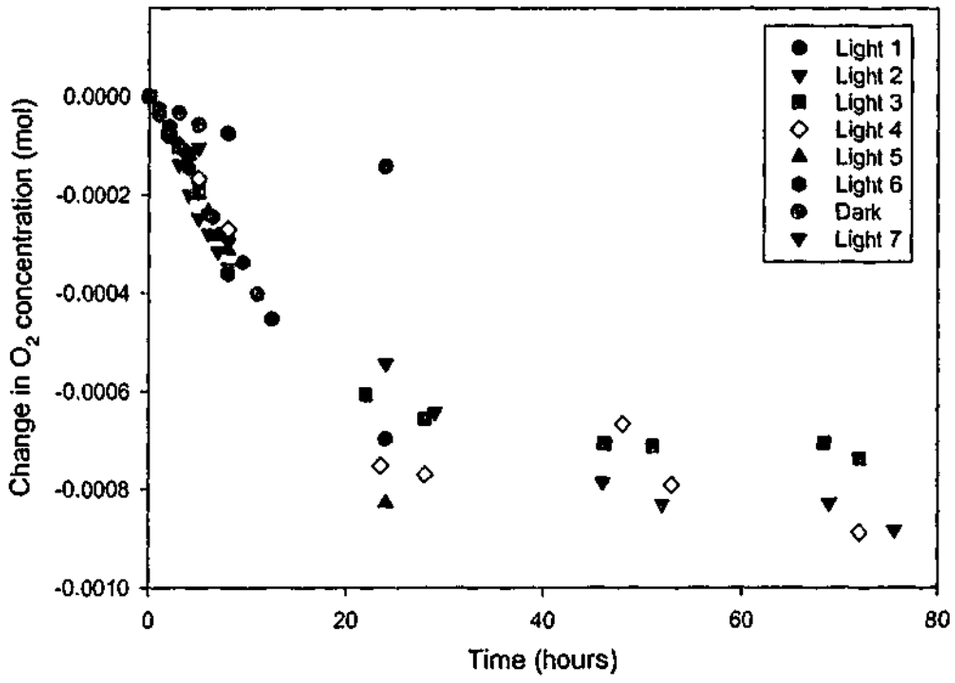

Figure 2.11 Photochemical O_2 consumption during irradiation of leaf leachate.

Carbon dioxide generation and oxygen consumption were highly correlated (Figure 2.12), with linear regressions fitted to each light-exposed data set giving very good approximations of the relationship ($R^2 > 0.98$). The gradient of the regressions varies between experiments. This can be easily seen in Figure 2.12, where some of the data points cluster quite closely to the $y = -x$ line, while other experiments deviated substantially from this line. The apparent reason for the changes to the gradients is the time over which the irradiation was conducted. The data points at the end of the longer experiments tend to weight the regression towards a 1:1 ratio (mol/mol) of O_2 consumed to CO_2 produced, however the early data indicates a ratio between 1.5 and 2.

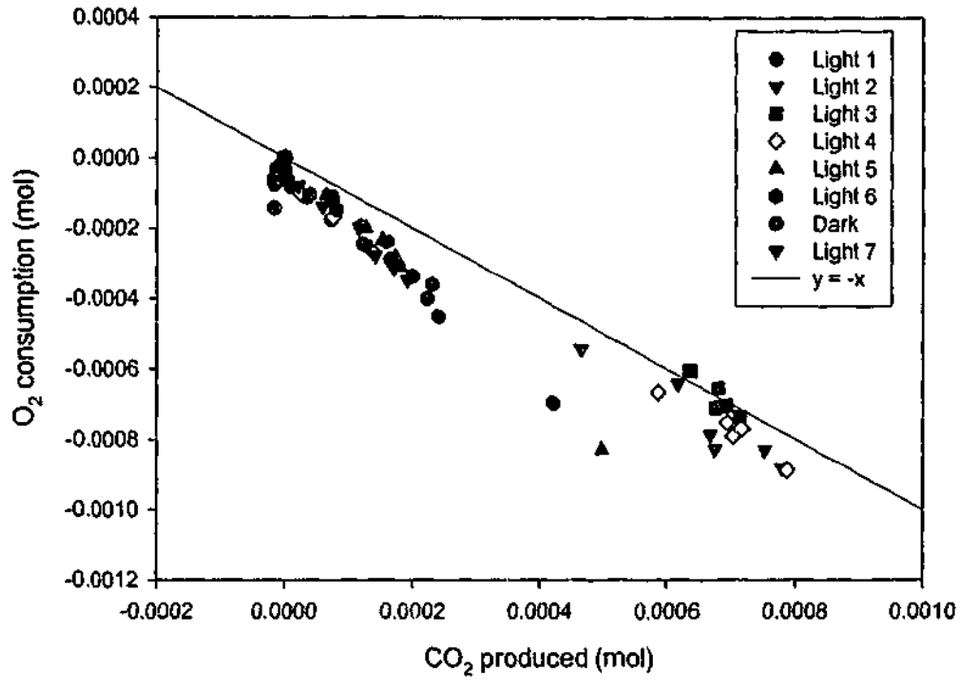

Figure 2.12 Correlations between photochemical CO_2 production and O_2 consumption. The red line indicates the trend that would be observed if O_2 consumption equalled CO_2 production.

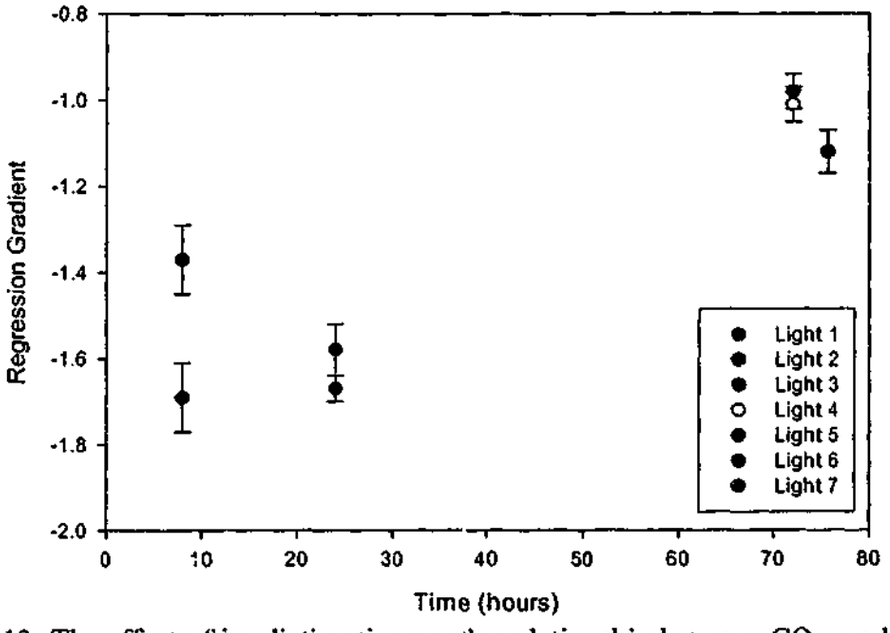

Figure 2.13 The effect of irradiation time on the relationship between CO_2 production and O_2 consumption.

The relationship between gradient and length of irradiation is illustrated in Figure 2.13; the dark control was omitted as a linear relationship was not observed with these data. The data suggest that the early part of the reactions resulted in photoproduction of carbon dioxide with a simultaneous increase in the oxygen content of the remaining DOC, and as the experiment progresses the more oxygenated organic matter is converted to CO_2, leading to an overall trend towards one molecule of oxygen consumed for each molecule of CO_2 produced. Clearly, the relationship between photochemical consumption of oxygen and photogeneration of carbon dioxide will depend on the initial oxygen to carbon ratio of the dissolved organic matter and the degree of degradation that occurs in the experiments.

Table 2.8 Constants for First Order Rate Equations Describing the Photochemical Consumption of O_2 in Leachate Experiments

Sample	Constant (a) (mol)	Std Error (a) (mol)	Rate (b) (h^{-1})	Std Error (b) (h^{-1})	R^2
Light 1	-0.0014	0.0002	0.030	0.004	0.996
Light 2	-0.00094	0.00004	0.037	0.004	0.992
Light 3	-0.00074	0.00002	0.070	0.009	0.990
Light 4	-0.00084	0.00006	0.062	0.015	0.952
Light 5	-4	3778	0.00001	0.007	0.992
Light 6	-3	13260	0.00001	0.05	0.974
Dark	-0.00017	0.00001	0.079	0.006	0.998
Light 7	-0.0016	0.0012	0.03	0.02	0.993

Carbon monoxide was detected at trace levels in these experiments, generally not appearing until after four hours of irradiation and with an apparently increasing trend over time.

The experiments in this chapter, taken together, suggest a quite variable relationship between photochemical oxygen consumption and the production of CO_2. A study of the photochemical degradation of a soil humic acid in the presence and absence of oxygen (Schmitt-Kopplin et al. 1998) found that under an oxygen atmosphere the molar O/C ratio of the humic acid increased from 0.61 to 0.97. The production of carboxylic groups was confirmed by a variety of techniques and was accompanied by a decrease in solution pH.

The authors also found that under a nitrogen atmosphere, photochemical reactions lead to a reduction in the average molecular weight of the humic acid (but to a lesser extent than in the oxygenated samples), but the solution pH did not fall significantly.

These results support the hypothesis that the high initial ratio of O_2 consumed to CO_2 produced is a result of photochemical reactions that incorporate oxygen into the DOM dominating in the early stages of the reaction. The observed decrease in pH in these experiments suggests that carboxylate functional groups are being generated in the DOC. The significant reduction in the absorbance of the samples indicates that aromatic structures and conjugated double bonds (the functional groups likely to be responsible for absorption of UV and visible light) present in the leachate were photodegraded. As these structures are highly absorbing, it is probable that these reactions are responsible for the early consumption of oxygen thorough generation of reactive oxygen species (See Section 1.6, Reaction Scheme 1.1) followed by reaction of these transients with the organic matter. Carbon dioxide, carbon monoxide and small organic acids can be produced from further photodegradation of organic material containing carbonyl groups (Schmitt-Kopplin et al. 1998). A number of potential mechanisms were offered for organic matter with the general formula $R_1(C=O)AR_2$, where A is either O or NH. Photochemical bond cleavage can lead to a variety of products, depending on the exact nature of the starting substituents, and oxygen radicals can also interact with molecules of this type. Decarboxylation may for example, proceed via a radical intermediate following hydrogen abstraction from an organic acid, in a similar fashion to the Hunsdiecker reaction (McMurry 1992):

$$RCOOH \rightarrow RCOO^{\cdot} \rightarrow R^{\cdot} + CO_2 \qquad \text{Equation 2.2}$$

The delay in CO_2 production in the leachate experiments may be the result of the leachate containing insufficient carbonyl groups for decarboxylation reactions to occur at a significant rate in the starting material. This delay was not observed in the billabong water samples. This was probably a result of the contribution of humic materials, which are known to contain a high proportion of carboxylic acid groups (Morel and Hering 1993).

All the experiments examining the photodegradation of dissolved organic matter, whether from leachate or natural water samples, illustrate the importance of oxygen to the photochemical degradation of dissolved organic matter, most likely through the action of oxygen radicals. The photochemical reactions possible between dissolved organic matter

and oxygen are complex and a range of mechanisms can coexist (see Section 1.6). Despite the variety of products possible, a large proportion of the oxygen consumed in these reactions can be accounted for by carbon dioxide generation, however the significant lag in CO_2 production suggests that the photochemical formation of carbonyl compounds such as carboxylic acids is an important step in the photochemical degradation of dissolved organic matter.

2.4 Conclusions

The dissolved organic matter found in Norman's Lagoon was readily photodegraded by UV and visible light and produced carbon dioxide (and carbon monoxide) as gaseous products, with simultaneous consumption of oxygen. Leachate from River red gum leaves can be an important component of the DOC input into aquatic ecosystems associated with the Murray River, especially at times of flooding. This material is highly photoreactive and almost all of the coloured material was photodegraded in these experiments. The varying relationship between oxygen consumed and carbon dioxide produced suggests that the role of gaseous oxygen depends on the nature of the organic material. These results also indicate the importance of considering photochemical mechanisms when considering the turnover of both carbon and oxygen in aquatic environments, particularly in situations of high carbon loading, where the absorbance of the water is quite high.

2.5 References

Baldwin, D. S. 1999. Dissolved organic matter and phosphorus leached from fresh and 'terrestrially' aged river red gum leaves: implications for assessing river-floodplain interactions. Freshwater Biol. **41**:675-685.

Bano, N., M. A. Moran, and R. E. Hodson. 1998. Photochemical formation of labile organic matter from two components of dissolved organic carbon in a freshwater wetland. Aquat. Microb. Ecol. **16**:95-102.

Bertilsson, S., and L. J. Tranvik. 2000. Photochemical transformation of dissolved organic matter in lakes. Limnol. Oceanogr. **45**:753-762.

Cooper, W. J., R. G. Zika, R. G. Petasne, and A. M. Fisher. 1989. Sunlight-induced photochemistry of humic substances in natural waters: major reactive species. Pages 333-362 *in* I. H. Suffet and P. MacCarthy, editors. Aquatic Humic Substances:

influence on fate and treatment of pollutants. American Chemical Society, Washington, DC.

De Haan, H. 1993. Solar UV-light penetration and photodegradation of humic substances in peaty lake water. Limnol. Oceanogr. **38**:1072-1076.

Kieber, R. J., L. H. Hydro, and P. J. Seaton. 1997. Photooxidation of triglycerides and fatty acids in seawater: Implication toward the formation of marine humic substances. Limnol. Oceanogr. **42**:1454-1462.

Kieber, R. J., X. Zhou, and K. Mopper. 1990. Formation of carbonyl compounds from UV-induced photodegradation of humic substances in natural waters: Fate of riverine carbon in the sea. Limnol. Oceanogr. **35**:1503-1515.

McMurry, J. 1992. Organic Chemistry, 3rd edition. Brooks/Cole, Pacific Grove, California.

Mitchell, A. M. 2002. Anaerobic nutrient cycles in freshwater sediments. PhD. Charles Sturt University, Wagga Wagga.

Morel, F. M. M., and J. G. Hering. 1993. Principles and Applications of Aquatic Chemistry. John Wiley and Sons, INC, New York.

O'Connell, M., D. S. Baldwin, A. I. Robertson, and G. Rees. 2000. Release and bioavailability of dissolved organic matter from floodplain litter: influence of origin and oxygen levels. Freshwater Biol. **45**:333-342.

Sander, R. 1999. Compilation of Henry's Law constants for inorganic and organic species of potential importance in environmental chemistry. *http://www.mpch-mainz.mpg.de/~sander/res/henry.html April 8, 1999*

Schmitt-Kopplin, P., N. Hertkorn, H.-R. Schulten, and A. Kettrup. 1998. Structural changes in a dissolved soil humic acid during photochemical degradation processes under O_2 and N_2 atmosphere. Environ. Sci. Technol. **32**:2531-2541.

Smith, P., and J. Smith. 1990. *in* N. Mackay and D. Eastburn, editors. The Murray. Murray Darling Basin Commission, Canberra.

Stumm, W., and J. J. Morgan. 1981. Aquatic Chemistry: An Introduction Emphasizing Chemical Equilibria in Natural Waters, 2nd edition. John Wiley and Sons, New York.

3 Photochemical Degradation of Dissolved Organic Matter in the Presence of Iron Oxide

3.1 Introduction

The photochemical degradation of dissolved organic matter in freshwater ecosystems has the potential to have a significant impact on the cycling of both carbon and oxygen in these systems. Most of the studies on these processes reported in the literature discuss work conducted on filtered solutions. The filtration of natural water samples is necessary so that photochemical changes to the DOM can be separated from microbial influences. Other methods of sterilization are unsuitable as they have the potential to alter the dissolved organic matter substantially, for example, autoclaving exposes the organic matter to high temperatures and may initiate a wide range of thermal reactions that change the nature of the DOM. However, as a result of removing the particles in the water, the experiments exclude the influence of reactive surfaces and photochemically active minerals.

Amongst the range of environmentally significant particles, iron oxides, hydroxides and oxyhydroxides (collectively referred to as iron oxides throughout this thesis) are widespread in the natural environment and are important in many environmental processes (Schwertmann and Cornell 1991). They are known to sorb a wide range of organic compounds and can be photochemically active (Feng and Nansheng 2000). Iron oxides such as goethite are positively charged in solution over a wide range of pHs; adsorption of natural organic matter will be assisted by electrostatic attraction between the oxides and negatively charged functional groups such as acids and phenols (Gu et al. 1994, Spark et al. 1997, Evanko and Dzombak 1998). Furthermore, the adsorption can lead to the formation of surface complexes between the iron atoms and carboxyl and hydroxyl functional groups, leading to poorly reversible adsorption (Gu et al. 1994). As discussed in Chapter 1, iron-organic complexes can be photochemically active, and so the adsorption of organic matter on the surface of iron oxides may lead to significant influences on the photochemical degradation of dissolved organic matter.

This chapter examines the effect of iron oxides on the photochemical degradation of dissolved organic matter. It will be shown that the photochemical interactions in aged systems- represented by billabong water samples and goethite- are

not the same as those found in systems containing fresh iron oxide and organic matter. Goethite, a relatively stable oxide, was found to suppress photochemical degradation of the dissolved organic matter, whereas amorphous iron oxide was found to significantly increase the rate of photochemical degradation of dissolved organic matter in the leachate from the leaves of River Redgums. The influence of oxide aging on its photoreactivity was evident from the changing reaction rates of oxide on storage.

3.2 Methods

3.2.1 Irradiation of Billabong Water in the Presence of Goethite

Preliminary experiments to investigate the effects of iron oxides on the photochemical degradation of dissolved organic matter were conducted in conjunction with the autumn billabong-water degradation experiments (Chapter 2). The preparation of water samples and sample analysis for pH, CO_2 and O_2 was carried out as described in Section 2.2.2.2. Water samples on the second, fourth and sixth days of the experiment were used as dark treatments for gas measurements (placed in the photochemical reactor without the lamp switched on). For all days involving light-exposed treatments a corresponding dark control was kept in a 1 L Schott bottle and analysed using all techniques except headspace gas analysis. These experiments were subject to the same pH measurement difficulties as those outlined in Section 2.3.2.2, and all calculations were performed assuming that the pH remained constant at the initial level measured for each sample.

The iron oxide used in these experiments was a sample of goethite which had previously been prepared using published methods (Schwertmann and Cornell 1991). This was ground to a fine powder using a mortar and pestle. Goethite (556 mg) was weighed into a polypropylene screw-capped tube and surface sterilized by washing with ethanol. The ethanol was evaporated from the goethite by leaving the container open below a bunsen burner flame, in a laminar flow cabinet. The oxide was dry and free-flowing after two days. A slurry was prepared by adding 20 mL of autoclaved ultrapure (Milli-Q) water to this oxide. One millilitre of this slurry was added to 700 mL of billabong water to give an approximate iron concentration of 25 mg/L in light-exposed and dark control samples, with additional dark controls prepared without oxide. Three additional experiments were conducted with 0.2 mL of slurry added to the water samples to give 5 mg Fe/L.

Absorbance measurements were made on water samples at the end of the experiment (see Section 2.2.2.2), however, samples with added iron oxide were filtered prior to final absorbance measurements being made. Approximately 5 mL of sample was drawn into a syringe, a 0.45 μm syringe filter was placed on the tip and the sample expelled to rinse the filter. Another 3-5 mL was then passed through the filter and collected directly in the quartz cuvette used for absorbance measurements. A new filter was used for each sample.

3.2.2 Irradiation of Leachate in the Presence of Amorphous Iron Oxide

Further experiments to investigate the photochemical interactions between dissolved organic matter and iron oxide were conducted using leachate and amorphous iron oxide as a model system for fresh inputs of both oxide and organic matter into an ecosystem. Leachate from *Eucalyptus camaldulensis* leaves was prepared using the method detailed in Chapter 2.2.3.

Four batches of amorphous Fe(III) oxide were prepared using a method modified from the literature (Lovley and Phillips 1986). Bacterial contamination of oxides was minimised by conducting the synthesis in a sterilized laminar flow cabinet, using autoclaved glassware and autoclaved Milli-Q water to make up the solutions. Batches of iron oxide were prepared from 0.4 M $FeCl_3$ solutions and a number of different preparative approaches were used.

Batch 1: The first batch was prepared by gradual manual addition of 100 mL of NaOH (~1M) to the stirred iron chloride solution and then a pH probe (rinsed with ethanol and then autoclaved ultrapure water) was placed in the solution. Further NaOH was added dropwise to give a final pH of 6.86. The resulting oxide slurry was collected by centrifugation at 8700 x g for 10 minutes. The supernatant was discarded and the oxide in each tube washed in 20 mL of sterile ultrapure water and centrifuged (5 min). This was repeated a further four times to give a final conductivity in the rinsing water of 100 μS cm^{-1}, indicating that most of the NaCl had been removed. The iron oxide was stored as slurry in 200 mL of water at 4 °C.

Batch 2: Preparation of the second batch of oxide differed from the first only in the rate of initial hydroxide addition; the first 100 mL of NaOH was added to the stirred solution as a single dose and then the pH was brought to 6.86 by dropwise addition of additional NaOH.

Batch 3 and Batch 4: The third and fourth batches of oxide were prepared using a slower, and more controlled method of NaOH addition. The first 90 mL of sodium hydroxide was added using a peristaltic pump at a rate of 2 mL min^{-1}, then a pH probe was introduced to the vessel and further NaOH was added dropwise until the required pH was obtained.

The irradiation experiments were conducted in a similar manner to those described in Section 2.2.3 with some modifications. Iron oxide slurry was added to 700 mL of leachate in each experiment. The volume of slurry varied between batches due to differences in oxide concentration, but in each case was calculated so that the oxide addition was equivalent to 6 mg (dry weight) of oxide. Oxide concentrations were calculated by pipetting 2x350 µL of slurry into each of six weighed glass bottles, evaporating to dryness in a drying oven (approximately 80 °C), and re-weighing the bottles to calculate oxide mass. All glassware used for iron oxide, including the photochemical reactor, was washed with hot water, rinsed with a small quantity of concentrated HCl, and then left to soak overnight in 5% HCl solution to prevent iron being carried over into the next experiment.

Qualitative tests for Fe(II) were carried out at the completion of some experiments by addition of a few drops of the leachate mixture to 2 mL of ferrozine solution (1 g/L) in 50 mM HEPES buffer (N-2-hyroxyethylpiperazine-N-2-ethanesulfonic acid) (Lovley and Phillips 1986). The presence of Fe(II) was indicated by the development of a purple colour.

Initial absorbance measurements were made on leachate without added iron oxide and final measurements were made on both unfiltered and filtered samples. The absorbance at both 250 nm and 360 nm was measured for each sample in a 1 cm quartz cuvette, against an ultrapure water blank. Filtration was carried out using 0.45µm syringe filters as described in Section 3.2.1.

3.3 Results and Discussion

3.3.1 Irradiation of Billabong Water in the Presence of Goethite

Irradiating billabong water in the presence of goethite gives an indication of the effect of iron oxides on the photochemistry of organic matter in a system that has not had recent fresh input of either the oxide or organic matter.

The photochemical production of carbon dioxide is illustrated in Figure 3.1. As expected, the production of CO_2 is greater in the light-exposed samples than in the dark controls, with the exception of a single replicate of the dark experiment that had unexpectedly high CO_2 production. There is a considerable amount of variability in these results. There are several possible explanations for the variability. The water sample used for each experiment was collected on the morning of the experiment, leaving the potential that changes to the dissolved organic matter could have occurred over the period that these experiments were conducted. Comparison with Figure 2.7, which represents experiments conducted on intervening days in the absence of iron oxides, indicates slightly smaller variability in the absence of oxide (range at 6h: 2.3 x 10^{-4} mols CO_2 -no oxide samples; 2.8 x 10^{-4} mols CO_2 - 5 mg oxide samples, 3.8 x 10^{-4} mols CO_2 - 25 mg oxide samples). However, the results confirm that the potential for photochemical carbon dioxide production does vary between water samples. Fluctuations in pH may also have influenced the variability. As mentioned previously, the calculations for converting headspace CO_2 to total CO_2 are pH dependent but it was necessary to assume constant pH to undertake the calculations. The average initial pH in the water samples was 7.4 ± 0.1 (1 s.d., n=9) and the average final pH for dark controls without added iron oxide was 7.2 ± 0.2 (n=9). In samples with the higher oxide concentration the final pH in light-exposed samples was 7.0 ± 0.1 (n=3), and in the dark controls it was 7.1 ± 0.1 (n=6). When the lower concentrations of iron oxide were used the final pH was measured at 7.0 ± 0.1 (n=3) and 7.2 ± 0.1 (n=3) for light-exposed samples and dark controls, respectiveiy.

Within these constraints, it appears that the overall effect of adding goethite particles to the billabong water during irradiation is to suppress the photochemical production of carbon dioxide compared to samples without added goethite (represented by the solid line in Figure 3.1). The higher rate of carbon dioxide production in the first

two samples (one light-exposed, one dark control), was unusual and may indicate some sample contamination.

Samples for absorbance measurements were filtered prior to measurement to minimise scattering and absorption due to the presence of added oxide. The absorbance of filtered samples is given in Table 3.1. The absorbance changes varied between treatments. The samples from experiments with 25 mg Fe/L have A_{250} (the absorbance reading at 250 nm) values that are on average 37% (range 31-40%) of the absorbance of the sample prior to irradiation. The A_{360} (absorbance at 360 nm) values for these experiments average 35 % (range 25-40%) of the initial after six hours of irradiation. Where the oxide concentration was reduced, the A_{250} was 28% (range 24-30%) of the initial value and the A_{360} was 24% (range 17-30%) of the initial. The higher oxide concentration reduced the amount of photodegradation observed in the samples compared to the results obtained with oxide-free billabong water. In oxide-free samples, the A_{250} was 22% of the initial (range 18-28%) and the A_{360} was 25% of the initial (range 18-35%) (ref. Table 2.4). The experiments with 5 mg/L Fe had results more similar to the samples without added oxide, indicating a dose-dependent relationship between oxide loading and the suppression of photodegradation. As discussed in Chapter 1, several authors have observed that preferential photobleaching at longer wavelengths is indicative of decreasing average molecular weight (De Haan 1993, Schmitt-Kopplin et al. 1998, Bertilsson and Bergh 1999). No substantial change to the ratios were observed at the two wavelengths measured here, suggesting that the reactions did not lead to preferential degradation of the larger molecules, but were more uniformly distributed across the range of molecular weights.

The absorbance changes were much smaller in the dark controls. For samples without added oxide the A_{250} was 99% (range 91-102%) of the initial, and the A_{360} was 99% (range 96-108%) of the initial. Where oxide was added at 25 mg Fe/L the A_{250} was 94% (range 91-100%) of initial and the A_{360} was 95% (range 85-102%) of initial. At the lower loading of oxide, A_{250} and A_{360} values were 89% (range 85-93%) and 99% (range 92-105%) of the initial values respectively. Dark reactions clearly did not significantly alter the absorbance of these samples.

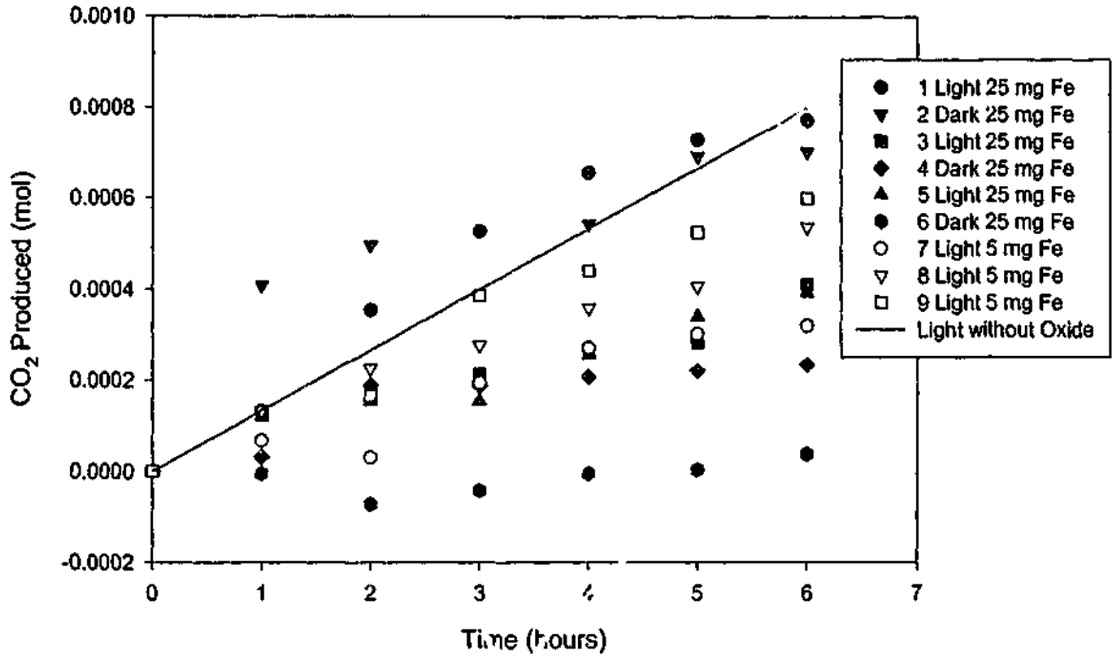

Figure 3.1 Photochemical production of carbon dioxide from billabong water samples with added goethite. The line represents the average photoproduction of CO_2 in samples without oxide (see Figure 2.7).

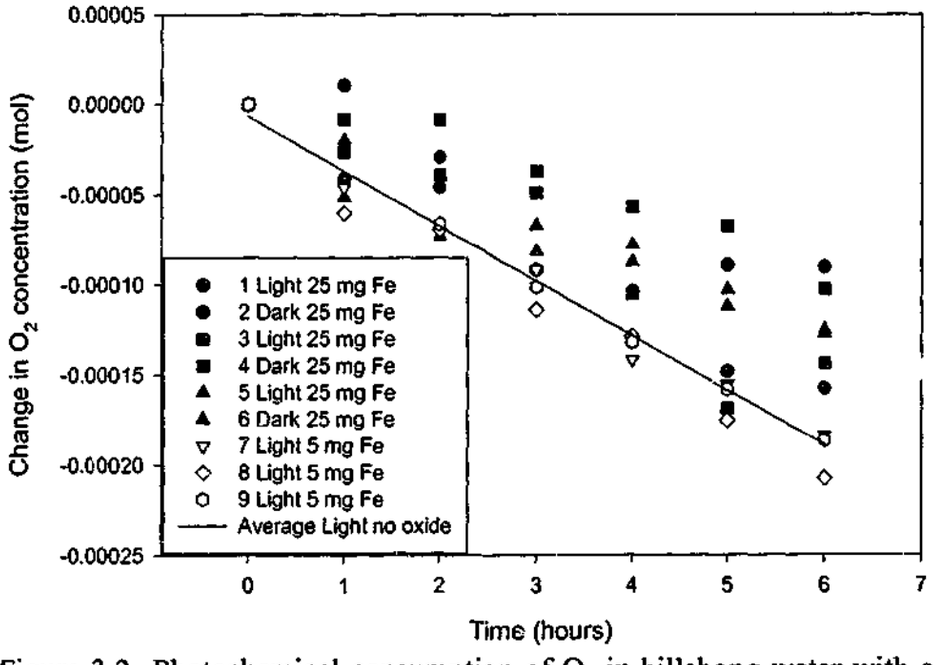

Figure 3.2 Photochemical consumption of O_2 in billabong water with added goethite. The line represents the average results for light-exposed samples without goethite (Figure 2.8).

Table 3.1 Absorbance measurements at the beginning and end of irradiation experiments at 250 nm and 360nm (1 cm path length). Initial measurements made before addition of oxide, final measurements were made on filtered (0.45 μm) solutions. 25 Fe indicates samples with oxide equivalent to 25 mg Fe/L, 5 Fe indicates those samples with 5 mg of Fe/L, av indicates an average value. *Data from Table 2.4

Sample	Initial A_{250}	Final A_{250} Light	Final A_{250} Dark (Fe)	Final A_{250} Dark (no Fe)	Initial A_{360}	Final A_{360} Light	Final A_{360} Dark (Fe)	Final A_{360} Dark (no Fe)
1 (25 Fe)	0.117	0.036	0.109	0.106	0.017	0.004	0.017	0.016
2 (25 Fe)	0.113	-	0.102	0.109	0.016	-	0.014	0.016
3 (25 Fe)	0.113	0.044	0.103	0.110	0.016	0.007	0.016	0.016
4 (25 Fe)	0.112	-	0.107	0.113	0.016	-	0.016	0.016
5 (25 Fe)	0.121	0.049	0.113	0.123	0.019	0.007	0.016	0.019
6 (25 Fe)	0.114	-	0.114	0.113	0.016	-	0.015	0.016
7 (5 Fe)	0.111	0.033	0.103	0.112	0.015	0.005	0.015	0.015
8 (5 Fe)	0.116	0.028	0.099	0.117	0.018	0.003	0.016	0.016
9 (5 Fe)	0.109	0.033	0.098	0.111	0.015	0.004	0.016	0.016
av (25 Fe)	0.115	0.043	0.108	0.112	0.017	0.006	0.016	0.017
av (5 Fe)	0.112	0.031	0.100	0.113	0.016	0.004	0.016	0.016
av (no Fe)*	0.114	0.025	-	0.113	0.017	0.004	-	0.017

The fraction of the dissolved organic carbon that adsorbed to the surface of the goethite particles was minor. Adsorbed material would be removed with the particles during filtration and this would have been reflected in differences between absorbance readings for the two dark controls. However, the filtered dark-control samples have very similar absorbances at both wavelengths, regardless of treatment. The reported values of the point of zero charge (PZC) for goethite are variable but lie within the region of 7-9.5 (Filius et al. 2000, Varadachari et al. 2000, Villalobos and Leckie 2000). It is possible that these experiments were conducted very near to the PZC of the goethite and that this minimised the interactions between the particles and the organic matter. Adsorption of organic matter onto the surface of goethite still occurs at pHs near the PZC (Filius et al. 2000, Zhou et al. 2001), but the former also note a shift from inner-sphere coordination to outer-sphere interactions as the pH is increased. The shift in coordination arises as a result of the changing surface charge on the goethite. At low pH, the positively-charged goethite can react with deprotonated carboxylic acid groups, whereas at high pH the goethite surface has a negative charge and interaction with uncharged phenolic groups is more likely. The total adsorption of DOM was found to be strongly pH dependent, with the maximum levels of adsorption at lower pH, and diminished, but still measurable adsorption at the maximum pH of 10.6 (Filius et al.

2000). It is likely that the natural organic matter in these experiments was adsorbed to a minor extent and that, being at a pH near the PZC of goethite, the adsorption may have involved weak outer-sphere coordination which may not have facilitated photochemical interactions between the organic matter and the goethite surface.

Photochemical consumption of oxygen in these experiments was also affected by the added goethite, although to a lesser extent than the carbon dioxide production. At the lower goethite concentration the photochemical consumption of O_2 is not substantially different to the average observed in the absence of iron oxide, but at the higher loadings less oxygen is consumed in the system (Figure 3.2).

The addition of goethite to these samples resulted in suppression of the photobleaching, CO_2 production and O_2 consumption compared to previous experiments without goethite additions. It is likely that the suppression is due to a shading effect, where the particles themselves both absorb and scatter light, and reduce the light available to initiate photochemical reactions in the organic matter. These experiments indicate that under some circumstances, particularly in aged systems, the removal of particles from water samples may result in an overestimate of the potential for photodegradation of the dissolved organic matter. Experiments with particles removed will not take into account light scattering and absorption by the particles in the system. As these experiments have demonstrated, the suppression depends on the concentration of oxide particles in the samples. It was not possible to determine the nature of the relationship between suppression of the photochemical reactions and the concentration of goethite in the system. The relationship may be non-linear and experiments at further oxide concentrations would be required to quantify it (a consistent source of DOM would be required to undertake these experiments).

3.3.2 Irradiation of Leachate in the Presence of Amorphous Iron Oxide

The photochemical degradation of dissolved organic matter in the presence of iron oxide proved to be quite different in experiments using fresh amorphous oxide and leaf leachate, compared with the goethite/billabong water experiments described in the previous section. The addition of amorphous iron oxide to the leaf leachate influenced the photochemical degradation of the organic matter, increasing the rate of reaction in most instances. The rate of reaction was variable between batches of oxide and also changed within individual batches of oxide over time. Both the effect of the iron oxide

on the photochemical reactions and the effect of oxide aging on the reactions are discussed.

The photochemical production of carbon dioxide (Figure 3.3) illustrates the effect of amorphous oxide on the degradation reactions. The variable nature of the results is particularly evident in Figure 3.3b, where the first few hours of the reactions are detailed. The very low carbon dioxide production in the dark controls indicates that both the leachate and the oxide were free of significant bacterial contamination (bacterial respiration would have generated CO_2 in the dark controls). The curve plotted with this data represents an average first order rate equation for all the data obtained for experiments with leachate in the absence of oxide (R^2 = 0.95) and is included to facilitate comparison (see Section 2.3.3).

The photochemical reactions in the presence and absence of oxide appear to approach the same end point, but at substantially different rates. Many of the oxide-catalysed reactions approached this end point after only 8 hours of irradiation, while the uncatalysed reactions required at least 24 hours of irradiation for the CO_2 levels to plateau. These experiments were of variable length, some designed with long reaction times and widely spaced sampling to examine the end-points of the reactions, others run for shorter periods with more frequent sampling to examine the initial rates of reaction. First order rate equations were fit to each set of experimental results from light-exposed treatments, as for the results in Chapter 2. The two hour time lag in the observed production of carbon dioxide affected the fits to the shorter experiments to an extent that the coefficients generated by Sigma Plot® for experiments shorter than 24 hours were nonsensical (standard errors many orders of magnitude greater than the coefficients). One of the 24-hour experiments was also affected in this way. This indicated that the first order approximation for the reactions was only appropriate where the carbon dioxide production had plateaued and that in the shorter experiments, the initial points that deviated from this behaviour had sufficient weighting to affect the fit.

An alternate method of rate analysis was therefore employed. A maximum rate of reaction (v_{max}) was defined as the gradient of the graph at the most rapid part of the reaction. This was obtained for each experiment by taking the carbon dioxide production values between two and eight hours of irradiation and fitting a linear equation to them (Table 3.2). Where the production had plateaued before eight hours or irradiation, the last point was removed so that it did not unduly influence the v_{max} value.

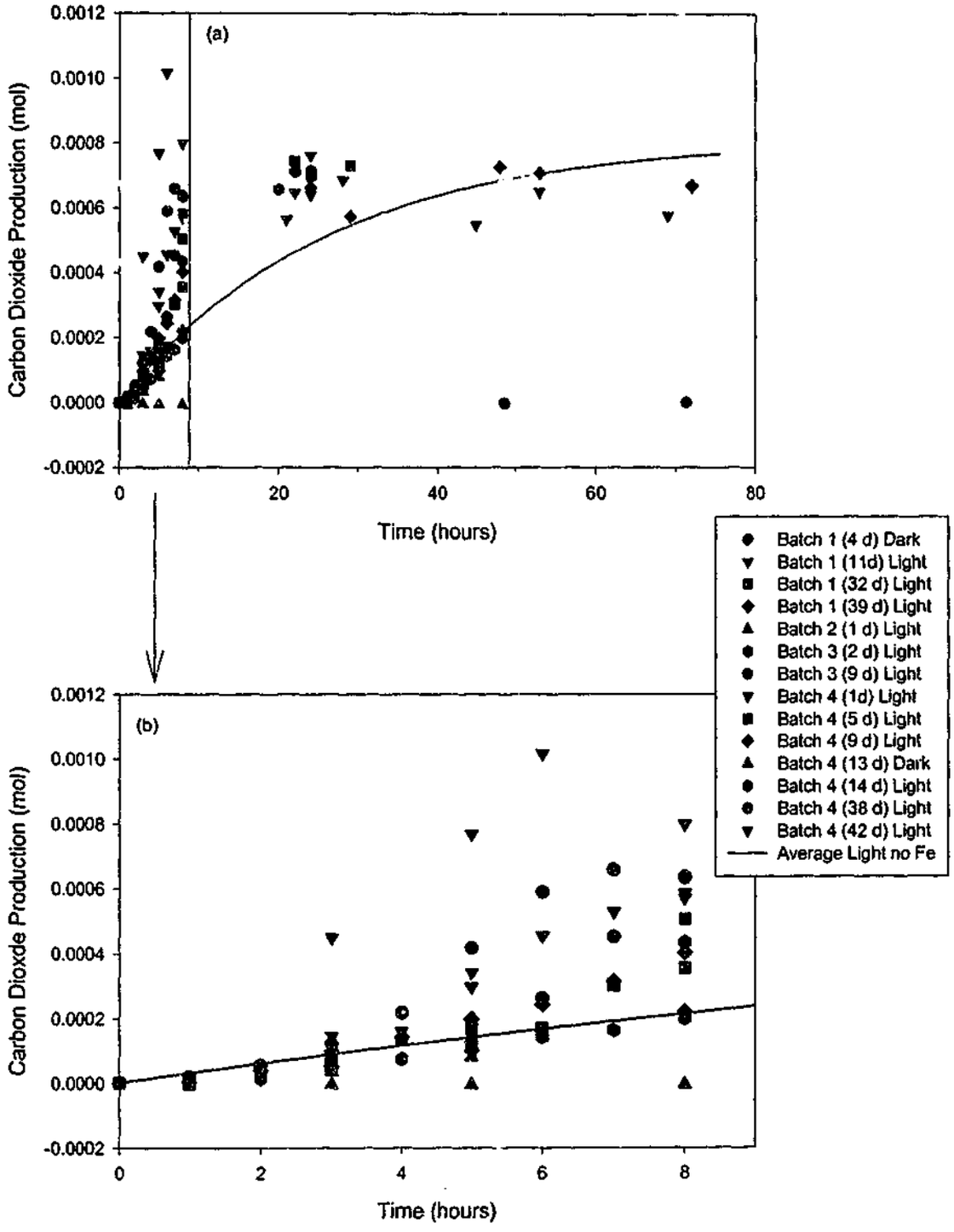

Figure 3.3 The photochemical production of carbon dioxide from leachate of Redgum leaves with added amorphous iron oxide. (a) Data for the full lengths of the experiments. Solid line indicates average fit to data without added oxide (Figure 2.10). (b) Results for the first eight hours of the reactions.

Table 3.2 Maximum rate of reaction (v_{max}) for each experiment.

Oxide batch includes data on light conditions in ( ). Oxide age represents number of days since synthesis and No. points indicates the number of CO_2 measurements used to calculate the v_{max} value for each experiment.

Oxide Batch	Oxide Age (d)	No. points	v_{max} (mol/h) $x10^{-5}$	Std Error $x10^{-5}$	R^2
1 (Light)	11	3	8.4	0.6	0.995
1 (Light)	32	3	9.1	1.6	0.970
1 (Light)	39	3	3.5	0.4	0.984
2 (Light)	1	3	3.4	0.5	0.978
3 (Light)	2	3	8	2	0.939
3 (Light)	9	5	12	2	0.907
4 (Light)*	1	2	16	-	1
4 (Light)	5	7	5.1	0.6	0.942
4 (Light)	9	7	5.8	0.3	0.988
4 (Dark)	13	3	-0.03	0.01	0.770
4 (Light)	14	7	3.11	0.07	0.997
4 (Light)	38	6	13	1	0.973
4 (Light)	42	7	10.0	0.7	0.975
No Oxide (av)	-	28	2.9	0.2	0.854

* This rate had to be calculated with 2 points as the third point was clearly incorrect (higher than all subsequent points), and the rate had plateaued by the 8th hour. Data is not available for boxes marked with (-) due to insufficient data points in the region specified.

The v_{max} values show that the presence of iron oxide has the potential to substantially increase the rate of photodegradation of the dissolved organic matter; the fastest of the rates being almost an order of magnitude greater than the average rate observed in the absence of oxide. The presence of the two-hour lag in CO_2 generation (note the change in rate of reaction after 2 hours in Figure 3.3b), is similar to that found in the experiments without iron oxide (Section 2.3.3). This indicates that the effect of the iron oxide on the initial oxygen-consuming reactions is minimal. Thus, once the carbon dioxide generating mechanism begins to dominate, the presence of iron oxide increases the rate of reaction.

The other notable feature of the results in Table 3.2 is the large degree of variation in the v_{max} values between batches of oxide. For example, the second batch of oxide, prepared with rapid initial addition of hydroxide to the ferric chloride solution, had a reactivity that was barely above that of the leachate in the absence of oxide. The rapid addition of hydroxide resulted in a brief period of localised high pH in the reaction mixture that influenced the formation of the oxide. The formation of a 2-line ferrihydrite from a ferrous nitrate solution by addition of KOH has been described

(Schwertmann and Cornell 1991), however, it was noted that the pH of precipitation must not exceed 8 or conversion to goethite and hematite may occur. In addition, these authors found storage in water also encouraged this conversion. It seems likely that the rapid addition of the NaOH in the production of oxide batch 2 encouraged the generation of more crystalline material than was produced in the other three batches and decreased the reactivity.

The effect of iron oxide aging in suspension was examined by using the fourth batch of oxide in a series of experiments over several weeks. Figure 3.4 illustrates the effect of storage time on the v_{max} of the reactions, which indicates the ability of the oxide to catalyse the photochemical reactions. With oxide aging times up to 14 days, the reaction rate declined quite significantly, but after 38 days the rate appeared to increase again.

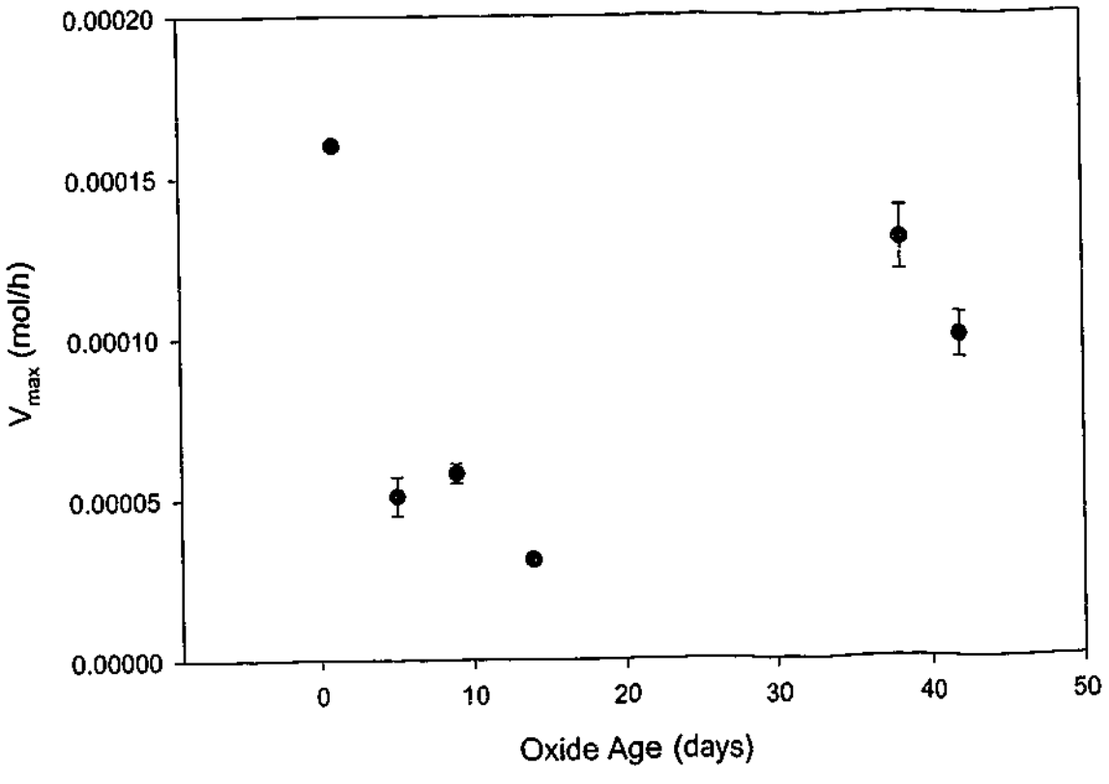

Figure 3.4 The effect of oxide age on the v_{max} of the reaction. Error bars indicate one standard error (see Table 3.2)

The initial decrease in reactivity may be explained if the amorphous iron oxide transforms into more crystalline (and less reactive) material during storage as an aqueous slurry. However, this would not explain the increase in reactivity observed at the end of the experiment. The most likely explanation for this observation is that slow bacterial growth in the slurry altered the surface of the oxide and restored some of the initial reactivity. It is feasible that bacterial growth occurred, given the long time that passed (24 days) between the fourth experiment and the two following experiments in which the increase in reactivity was observed. Although every effort was made to prepare the iron oxide under sterile conditions, it seems this was not completely successful. It was assumed that the ferric chloride and sodium hydroxide solids were sterile because of the extreme pH of each compound ($FeCl_3$ < 2, NaOH > 12). In addition, since the oxide slurry was handled on multiple occasions during the washing steps and during removal of sample for each experiment, it is possible that low-level bacterial contamination was introduced, possibly at the 14-day point in the experiment. A sample of the oxide slurry was examined for bacterial contamination at the end of this experiment. Acridine orange staining and epifluorescence microscopy showed that the slurry was contaminated with bacteria after the final experiment had been conducted. The numbers were very low, but not quantified due to difficulties conducting counts using slides with high particle concentrations. The negligible change in carbon dioxide concentration in the dark control experiments indicates that this contamination either was not present in the slurry at that time (immediately prior to the lowest rate being observed in) or was of no consequence on the timescale of these experiments.

The Total Organic Carbon (TOC) results (Table 3.3) indicate that the initial concentration of organic carbon in the leachate is quite reproducible and is consistent with the samples studied without added iron oxide (Table 2.7). The first experiment using oxide batch 4 was conducted the day after the oxide was prepared; only 3% of the carbon remained after 24 hours of irradiation in the photochemical reactor. In the associated dark control with added oxide, 92% of the TOC remained and in the absence of both light and oxide essentially none of the TOC was removed (TOC was 102% of the initial value at the end of the experiment).

In the experiments that followed, such high levels of organic matter degradation were not observed in the light-exposed samples, presumably because of changes in time of irradiation and oxide reactivity. As the reactivity of the oxide decreased, the

reactions take longer to approach completion, and this was reflected by the higher end-point TOC concentration. The carbon dioxide production data indicated an increase in reactivity of the oxide after 38 days of storage compared to the reduced reactivity of the oxide when it was 14 days old. This is supported by the higher proportion of TOC degraded in the last two experiments compared to the one conducted after the oxide had been stored for 14 days, all of which were 24 hour experiments.

Table 3.3 Total Organic Carbon data for samples of leachate irradiated in the presence of iron oxide, dark controls with iron oxide and dark controls without added oxide. Total CO_2 refers to results for the samples in the photochemical reactor, and corresponds to the light-exposed samples in all but experiments with Batch 1(4) and 4(13).

Oxide Batch	Oxide Age (days)	Duration (hours)	Initial TOC (mg C/L)	Final TOC Light (mg C/L)	Final TOC Dark Fe (mg C/L)	Final TOC Dark (mg C/L)	Total CO_2 Produced (mg C/L)	$\Delta CO_2/\Delta TOC$
1	4	71.3	14.5	-	9.8 (filt)	-	0.009	1.8×10^{-3}
1	11	72	12.3	1.8	12.4	15.5	11.42	1.09
1	32	29	14.4	-	-	-	12.54	-
1	39	72	14.8	1.8	13.8	14.5	11.48	0.88
2	1	8	14.3	-	-	-	3.47	-
3	2	8	14.5	7.2	15.5	14.1	7.43	1.02
3	9	8	13.6	6.1	14.2	15.3	10.90	1.45
4	1	24	15.0	0.4	13.8	15.3	13.05	0.89
4	5	8	13.9	6.3	14.8	13.2	6.07	0.80
4	9	8	14.3	6.2	13.8	12.8	6.89	0.85
4	13	8	13.7	-	15.0	-	-0.42	0.32
4	14	24	13.7	4.6	14.7	12.2	12.25	1.35
4	38	24	15.2	2.4	16.9	14.9	11.91	0.93
4	42	24	14.0	2.7	14.0	13.6	10.98	0.97

The results from two dark control experiments (Batch 1, four days old and Batch 4, 13 days old) are also included in Table 3.3 (experiments in which the photochemical reactor was wrapped in foil and the lamp left off so that carbon dioxide production in the dark could be established). In the first of these experiments, the TOC sample was filtered immediately after removal from the photochemical reactor and the reduced concentration reflects the adsorption of DOM to the oxide particles. The adsorption of DOM to the oxide surface was quite obvious from the colour change in the dark control samples. All leachate samples had a very pale yellow colour in the absence of oxide, which became cloudier and darker yellow once oxide was added. On storage in the dark

for several hours the colour of the mixture changed to cloudy black (see Figure 3.5). This black colour was associated with the suspended particulate matter, since it was retained on a 0.45 μm filter, leaving a clear solution. Addition of hydrochloric or phosphoric acid to the mixture returned the black particles to their original colour, suggesting that the adsorption of organic matter was reversible, although the extent of this reversibility was not quantified. Irradiation in the photochemical reactor prevented this dark colour from forming, and in the most reactive mixtures the sample actually appeared clear yellow at the end of the experiment. Filtration through a 0.45 μm nylon filter removed the yellow colour from the solution. This suggested that the photochemical reactions removed the DOM from the oxide surface. Following these reactions, light-exposed samples also tested positive for Fe^{2+}, whereas dark controls did not produce any visible purple colour in the ferrozine test. The changes to the "cloudiness" of the samples may also indicate that the particle size of the oxide was changed. The second dark control listed in Table 3.3 (Batch 4, 13 days old) was not filtered prior to TOC analysis and did not show a decrease in the organic carbon concentration.

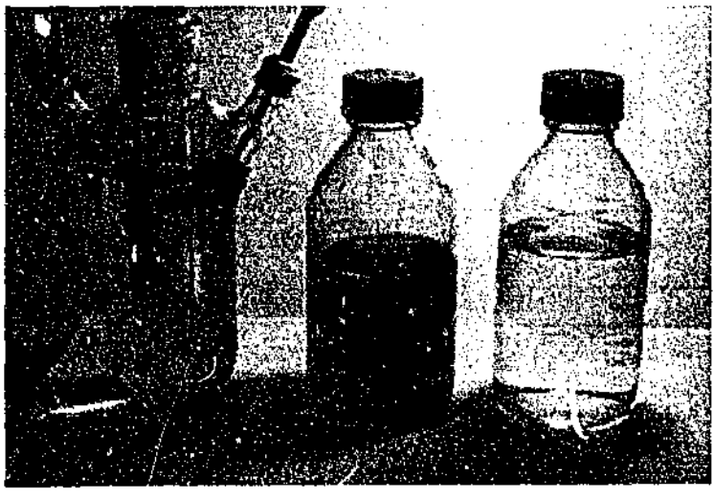

Figure 3.5 The changing colours of leachate with added amorphous iron oxide. Strong yellow colour with low turbidity after irradiation (left), darkened, cloudy colour when stored in the dark (centre) and oxide added to pure water (right)

The average molar ratio of carbon dioxide produced to total organic carbon lost in light-exposed treatments was 1.0 ± 0.2, indicating a quite good agreement between the two techniques, and suggesting that the carbon losses to the wall of the reaction

vessel and from the seals are minimal. Given the low carbon concentration in the leachate, and particularly in the irradiated samples it is easy for trace levels of contamination in the TOC samples to have a significant effect on the measured concentration. This is the likely explanation for some of the dark controls having higher carbon concentrations than the initial sample.

Measuring the absorbance of the samples after the addition of amorphous iron oxide posed some difficulty because of adsorption of organic matter to the surface of the particles. Initial measurements were made on leachate samples before iron oxide was added, and final measurements were made on unfiltered samples (Table 3.4.). Filtering of samples (0.45 μm nylon syringe filter) proved unsuitable due to retention of DOM by the filter. Taking into account that the initial samples contained no iron oxide, but the light-exposed treatment and one of the dark controls did, it is clear that considerable photobleaching did occur.

Table 3.4 Absorbance at 250nm of unfiltered leachate. Absorbances are averages of n repeat measurements and presented as mean (standard deviation).

Sample	Initial		Final Light with oxide		Final Dark with oxide		Final Dark no oxide	
	A_{250}	n	A_{250}	n	A_{250}	n	A_{250}	n
1(4)	0.470 (0.003)	4	-	0	-	0	-	0
1(11)	0.4771 (0.0007)	3	0.269 (0.004)	2	0.481 (0.002)	2	0.489 (0.002)	2
1(32)	0.468 (0.002)	3	-	0	-	0	-	0
1(39)	0.449 (0.002)	3	0.1651 (0.0001)	2	0.481 (0.002)	2	0.482 (0.002)	2
2(1)	0.446 (0.002)	3	-	0	-	0	-	0
3(2)	0.467 (0.003)	3	0.088 (0.003)	2	0.523 (0.005)	2	0.442 (0.007)	2
3(9)	0.480 (0.002)	3	0.150 (0.003)	3	0.546 (0.001)	3	0.459 (0.004)	3
4(1)	0.475 (0.001)	3	0.219 (0.002)	3	0.527 (0.002)	3	0.4621 (0.0008)	3
4(5)	0.477 (0.002)	3	0.082 (0.002)	3	0.550 (0.002)	3	0.452 (0.002)	3
4(9)	0.463 (0.001)	3	0.162 (0.001)	3	0.551 (0.002)	3	0.434 (0.002)	3
4(13)	0.462 (0.002)	3	-	-	0.563 (0.002)	3	-	-
4(14)	0.473 (0.001)	3	0.183 (0.001)	3	0.590 (0.002)	3	0.457 (0.002)	3
4(38)	0.505 (0.002)	3	0.286 (0.002)	3	0.630 (0.003)	3	0.515 (0.002)	3
4(42)	0.481 (0.002)	3	0.272 (0.001)	3	0.654 (0.002)	3	0.463 (0.004)	3

The pH of the leachate was measured only at the beginning and end of each experiment as sufficient liquid could not be removed from the photochemical reactor during the course of the experiments to allow measurement of pH. The pH was found to decrease in the irradiated samples by an average of 0.4 pH units (Table 3.5). This

compares with an average decrease in the corresponding irradiated experiments without added iron oxide of 0.8 pH units (Table 3.5 and Section 2.3.3). A reduction in sample pH on irradiation was also observed in a study of the photoreactions of the coloured dissolved organic matter in the Satilla River (Gao and Zepp 1998), and the authors interpreted this as indicating the formation of acidic photoproducts such as carboxylic acids.

Table 3.5 Initial and final pH values for each of the oxide addition experiment and the average results for experiments without added iron oxide.

Sample	Initial	Final (Light)	Final (Dark, Oxide)	Final (Dark, No Oxide)
1(4)	5.3		4.5	
1 (11)	5.4	4.8	5.3	5.3
1 (32)	4.9	-	-	-
1 (39)	5.2	5.0	5.2	5.3
2 (1)	5.0	-	-	-
3 (2)	4.9	4.3	4.9	4.8
3 (9)	5.2	4.5	4.9	5
4 (1)	-	4.2	5.0	5.0
4 (5)	4.9	5.1	4.9	4.6
4 (9)	5.1	4.7	5.1	5.1
4 (13)	5.0		4.2	
4 (14)	5.0	4.6	5.1	5.0
4 (38)	5.3	4.7	5.3	5.3
4 (42)	-	4.6	4.9	5.0
Average	5.1 ± 0.2	4.7 ± 0.3	4.9 ± 0.3	5.0 ± 0.2
No Oxide (av)	5.2 ± 0.1	4.4 ± 0.4	-	5.2 ± 0.1

The photochemical consumption of oxygen is presented in Figure 3.6. The solid line in Fig 3.6 represents an average fit to the data obtained from the photochemical consumption of oxygen in the absence of iron oxide (Section 2.3.3). The graph clearly shows that the addition of oxide influences the rate of the consumption of oxygen to the same extent as it influences the rate of carbon dioxide production. Most of the experiments showed increased rates of O_2 consumption when iron oxide was added. The effects of oxide aging are again evident in the O_2 consumption rates. An increase in the photochemical consumption of oxygen in humic systems on addition of iron (as dissolved Fe^{3+}) has been reported previously (Miles and Brezonik 1981), however, that study did not specifically look at iron oxides.

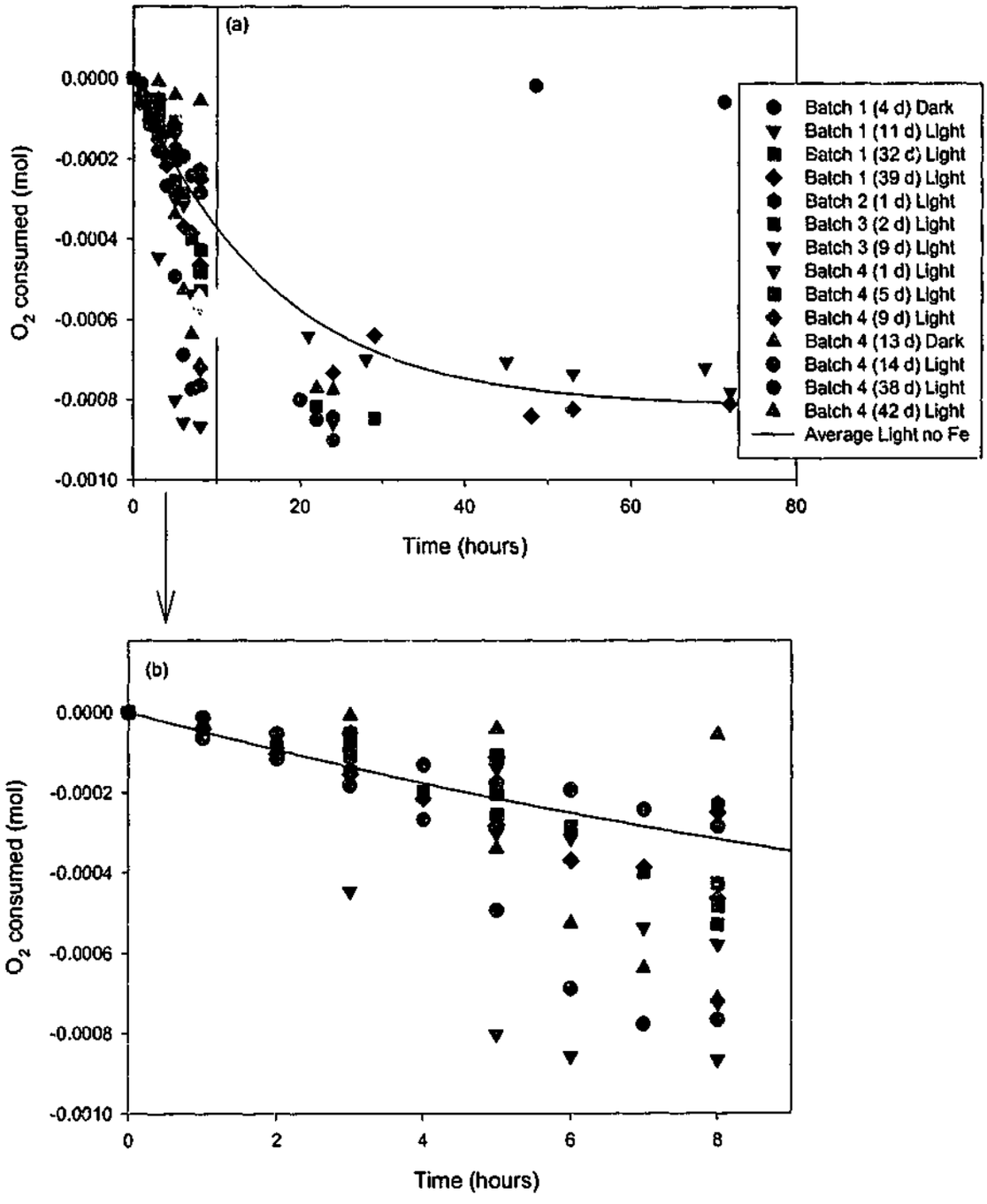

Figure 3.6 Photochemical oxygen consumption in leachate samples with added iron oxide. (a) Results over the entire duration of the experiments. (b) Focus on the first eight hours. The solid line represents an average fit to all the data obtained in the absence of iron oxide (see Figure 2.11)

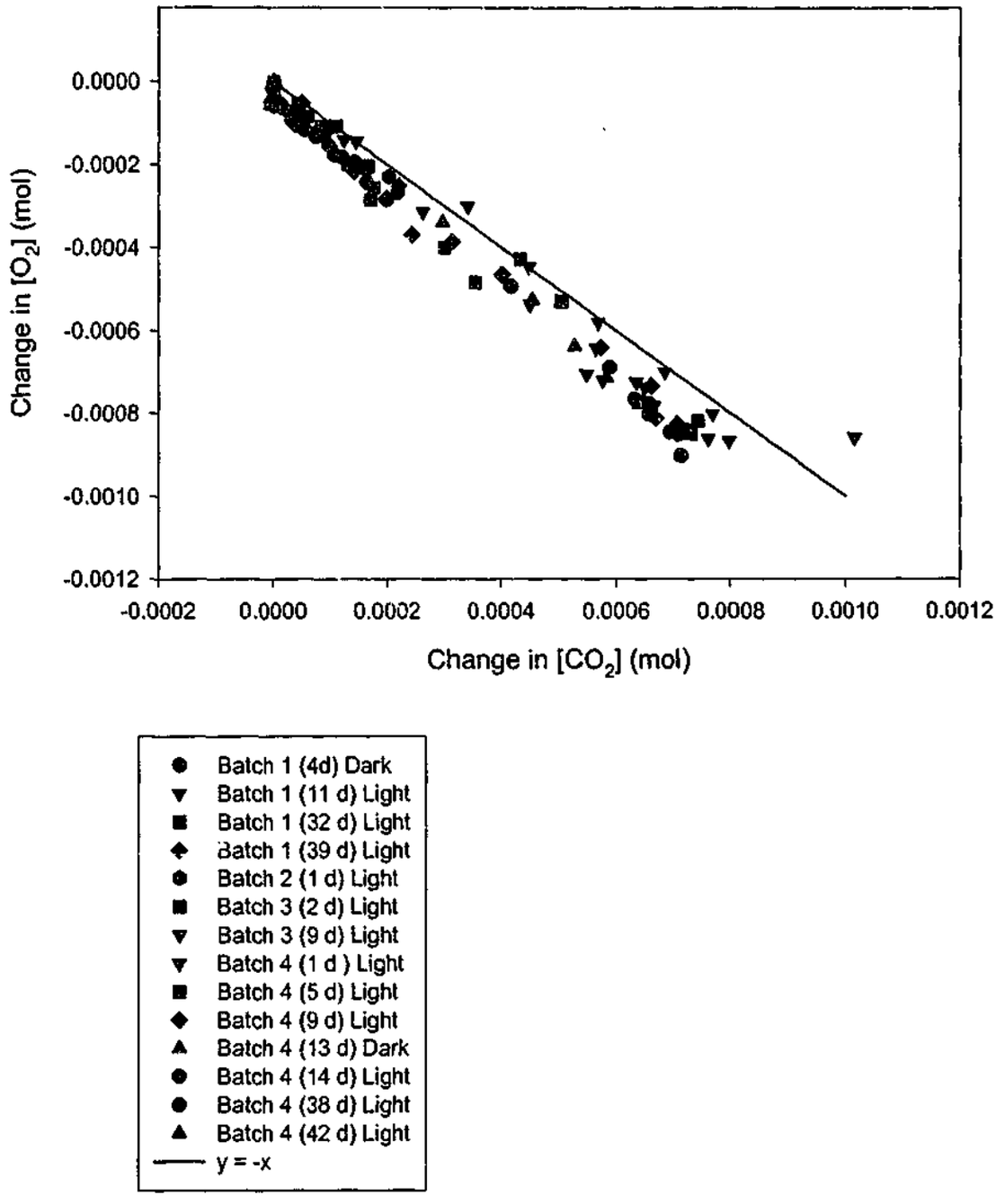

Figure 3.7 Correlation between O_2 consumption and CO_2 production for leachate irradiated in the presence of amorphous iron oxide. The line represents the relationship which would be observed if one mole of CO_2 was produced for each mole of O_2 consumed.

Figure 3.7 shows the correlation between the production of CO_2 and the consumption of O_2 for each of the irradiated experiments where iron oxide was present. The relationship is reasonably uniform across all experiments, giving a mean value of 1.1 ± 0.1 (range 0.95-1.27) moles of O_2 consumed for each mole of CO_2 produced. This value is double that reported by Miles and Brezonik (1981) who found 0.5 mol of O_2 were consumed for each mole of CO_2 produced from DOM derived from highly coloured lake water. A possible reason for these differences is that the composition of the organic matter differed between the two studies.

The initial lag in CO_2 production compared to O_2 consumption, discussed in Chapter 2, is still present, but does not have as large an effect on the overall gradient in the experiments where iron oxide was added. This is most likely because the experiments are closer to completion due to the longer running times or iron oxide catalysis (the higher rate of reaction bringing the reactions to completion more quickly). The fact that the lag persists, and is approximately the same with and without iron oxide, suggests that the initial processes that are responsible for the consumption of oxygen are not catalysed by the presence of oxide. Re-examination of Figure 3.3b indicates that the different rates of reaction really only becoming evident from the third hour onwards.

3.3.3 Mechanisms

A number of mechanisms may be involved in the increase in reaction rate in the leachate/amorphous oxide experiments. In the dark controls, it appears that adsorption of DOM onto the particle surface occurred, changing the colour of the mixture to black. As neither of the starting materials had this dark colour, it is suggestive of the creation of iron-organic complexes. As discussed in Appendix 1, the interactions between molecular orbitals on the organic ligands and the *d* orbitals on the iron atoms can alter both the energy levels of the *d* orbitals and the energy of the organic bonds (Oxtoby and Nachtrieb 1990). As a result of these interactions, the complexes may absorb light over a greater region of the visible spectrum than the uncomplexed DOM, increasing the proportion of incoming photons with the potential to induce chemical reactions.

The adsorption of organic matter by iron oxides has been widely reported in the literature. A diverse range of oxides have been studied, including: ferrihydrite (Bartoli et al. 1992, Edwards et al. 1996), haematite (Murphy et al. 1990, Gu et al. 1994) and goethite (Spark et al. 1997, Evanko and Dzombak 1998, Filius et al. 2000). A

comparative study of the adsorption of humic substances by goethite, haematite and an amorphous Fe-gel (Tipping 1981), indicated the adsorption isotherms showed a reasonably good fit to the Langmuir isotherm. The extent of adsorption diminished with increasing pH, due to decreases in both the number of adsorption sites ($Fe\text{-}OH_2^+$ and Fe-OH) and the affinity between the oxide surface and the humic acids (increase in $Fe\text{-}O^-$ groups leads to electrostatic repulsion). The results were consistent with a ligand-exchange mechanism for humic acid adsorption. Amorphous iron oxides appear to have a particularly high affinity for humic substances (derived from a catechol-glycine system) and organic carbon adsorption was also found to increase the concentration of soluble $Fe(OH)_2^+$ and $Fe(OH)^{2+}$ (Bartoli et al. 1992). The authors suggested that adsorption was predominantly electrostatic. Another study utilising amorphous iron oxide (Edwards et al. 1996) found that the carboxylic acid component of natural organic matter was important in the adsorption process. In particular, very strong acids (those deprotonated at pH 3) were preferentially adsorbed, and their adsorption was accompanied by adsorption of weak acids (deprotonate between pH 8 and 11), possibly indicating a paired-acid group in the molecules. A mechanism for the fast adsorption of carboxylic acids onto iron oxide (haematite) has been proposed (Gu et al. 1994), and involves the collapse of organic molecules onto the oxide surface to maximise the number of points of interaction between the molecule and the oxide surface. Electrostatic interactions were eliminated as the major adsorption mechanism and a ligand exchange mechanism was supported by FTIR evidence of bond formation between oxide surfaces and COO^- and OH functional groups (Gu et al. 1994). Thus, it is likely that substantial adsorption of organic matter onto the amorphous iron oxide occurred mainly via the acid groups on the DOM.

The photochemical experiments reported in this thesis also generated Fe(II), and this suggests two features of the mechanism. First, the complexation of organic matter to Fe(III) may alter the quantum yield for photochemical reactions relative to non-destructive processes such as fluorescence. The fluorescence of DOM is quenched by complexation to metals (McKnight et al. 2001). When an incoming photon is absorbed, electron transfer between the organic matter and the iron could provide an irreversible pathway for organic matter oxidation (Equation 3.1), and reduce the likelihood of non-reactive energy loss (through processes such as relaxation and fluorescence) (Langford and Carey 1987).

$$Fe(III)\text{-}DOM + h\nu \rightarrow Fe(II)^{\cdots}DOM_{ox} \rightarrow Fe(II) + DOM_{ox} \qquad \text{Equation 3.1}$$

The other effect this reaction may have on the system is related to the solubilities of Fe(III) and Fe(II). As Fe(II) is more soluble than Fe(III), some dissolution of Fe(II) into the solution will occur, exposing new surface on the oxide particle. The dissolved Fe(II) could then be oxidized back to Fe(III) and form new particles, or complexes with organic matter may form. As the reaction progresses, the particle size can decrease as a result of the dissolution and re-precipitation processes, and new reactive surfaces are continually being re-formed (Wells and Mayer 1991, Waite and Szymczak 1993).

The results of the experiments containing leachate and amorphous iron oxide support the two-mechanism hypothesis proposed in Chapter 2. A lag in the production of CO_2 relative to the consumption of O_2 again persists for the first two hours, followed by a relationship that is close to 1 mole of O_2 consumed for each mole of CO_2 produced. Again, this observation suggests that in the first few hours the reaction is dominated by reactions which consume O_2 without producing CO_2, possibly through the generation of reactive oxygen species, such as singlet oxygen or hydroxyl radicals, which react with the DOM to increase the concentration of carbonyl and carboxyl groups in the organic molecules (See Section 1.6, particularly Reaction Scheme 1.1). The drop in solution pH on irradiation supports the theory that an increased number of acidic groups were present. These acidic groups would need to be in a non-volatile form as the solution pH did not increase when solutions were left open to equilibrate with the air. Different equipment would be required to determine the timing of this pH change relative to the lag in CO_2 production. It was the second phase of the reaction that was most affected by the presence of iron oxide. As discussed above, the maximum rate of reaction occurred in the period between two and eight hours after the irradiation commenced (following the lag); the rate at this phase was affected by the presence of oxide, as well as by the age of the oxide.

The decarboxylation of acid groups (Equation 2.2) can be influenced by iron oxide through the complexation of iron by the carboxyl groups. Photo-electron transfer from an acid group to a complexed iron centre, resulting in CO_2 generation, has been reported for model compounds including oxalic acid, formic acid, citric acid and malate (Zuo and Hoigné 1992, Abrahamson et al. 1994). In addition, a number of studies have observed the production of Fe(II) from oxides such as goethite, haematite, maghemite and lepidocrocite (Waite and Morel 1984, Cunningham et al. 1985, Litter and Blesa

1988, Siffert and Sulzberger 1991, Sulzberger and Laubscher 1995) following irradiation in the presence of similar model compounds. A mechanism for the interaction between surface bound Fe(III) and a carboxylate group attached to a molecule of DOM is given in Reaction Scheme 3.1 (adapted from Siffert and Sulzberger, 1991).

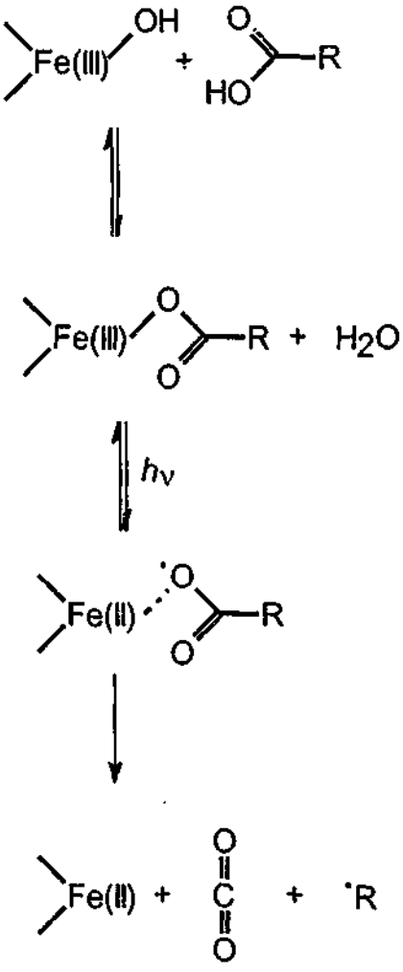

Reaction Scheme 3.1 A proposed mechanism for the photochemical interaction between DOM and iron oxide surfaces via carboxylate adsorption.

The increased rate of CO_2 generation arises from the movement of an electron from the carboxyl oxygen to the metal. Depending on the structure of the oxide, this can be thought of either as a Ligand-to-Metal-Charge-Transfer (LMCT) reaction, or as the injection of an electron into the conduction band of a semi-conducting oxide (Langford and Carey 1987). The loss of an electron to the metal leads to electron rearrangement within the organic ligand, breaking both the metal-oxygen bond and the C-R bond, to produce carbon dioxide and an organic radical. The organic radical

produced can react with dissolved O_2 to generate a peroxy radical, which will then undergo further reactions. Oxygen is also consumed by surface or dissolved Fe(II), regenerating Fe(III), however at the pH of these experiments this conversion was not complete (Fe(II) was detected at the end of the reactions). All of these reactions may be occurring with either surface or free iron atoms, and it is likely that both exist in the reaction mixture (refer to Figure 1.2) (Voelker et al. 1997).

The varying reactivity of the oxide samples is an important feature of these photochemical reactions. Comparing the goethite experiments with those using amorphous iron oxides, it is apparent that aged oxide systems may behave quite differently to those with inputs of newly-formed oxide. In these experiments the catalytic effects of the amorphous iron oxide samples diminished with age and were affected by sample preparation. Other authors have also reported that the reactivity of metal oxides may be affected by oxide aging and surface properties (Schwertmann and Cornell 1991, Hrncir and McKnight 1998, Larsen and Postma 2001). A decrease in the photoreactivity of iron oxides with aging in an acidic freshwater environment has been observed (Hrncir and McKnight 1998). The authors suggested that these changes were associated with an observed increase in the oxide crystallinity, and perhaps also with increased hydrolyzation of the surface. The rate of reductive dissolution of iron oxides has also been found to vary with crystal structure (Larsen and Postma 2001). Comparing three ferrihydrite samples, they found that 2-line ferrihydrites were more reactive than a 6-line ferrihydrite. Differences in reactivity (measured as rate of reductive dissolution in the presence of ascorbic acid) between batches prepared by apparently identical methods were also observed. Lepiocrocite and goethite were both less reactive than the ferrihydrites. Photo-induced increases in iron oxide reactivity have been observed, in addition to decreases in reactivity when the oxide was stored in solution in the dark (Wells and Mayer 1991). A study comparing the photo-dissolution of haematite, goethite and lepidocrocite in the presence of oxalate (Sulzberger and Laubscher 1995) concluded that the more thermodynamically stable oxides are more resistant to light-induced dissolution. Another study (Leland and Bard 1987) concluded that the differences in photoreactivity between iron oxides were the result of differences in electronic and structural properties. It is likely that the difference in oxide reactivity observed in the experiments reported in this chapter were the result of changes to the oxide crystallinity and that either the more crystalline oxides were less favourable for

electron-transfer reactions or that the reduced tendency to release Fe(II) into solution resulted in the loss of reactive surface as the reactions progressed. It may be possible to differentiate between these mechanisms using a model compound with the iron oxide, and measuring both organic matter loss and Fe(II) production continually during the irradiation. If the reduced reactivity was the result of a lower rate of electron-transfer reactions, the rate of reaction would be consistently slow, whereas loss of surface active sites may be indicated by a decreasing rate of reaction with time. However, these mechanisms would be difficult to separate using natural organic matter as slow initial rate of reaction could disguise these differences.

3.4 Conclusions

The interactions between dissolved organic matter and iron oxides may be influenced by a number of factors, potentially many more than have been examined in this work. The difference observed between experiments using billabong water and goethite, and those using leachate and fresh amorphous iron oxide may have resulted from differences in oxide reactivity, the characteristics of the dissolved organic matter, pH, degree of organic adsorption to the particle surface or other mechanisms. Certainly the degree of organic matter adsorption differed greatly between the experiments with more adsorption occurring in samples with amorphous iron oxide. The goethite appeared to adsorb little of the DOM. The ageing experiments with the fresh iron oxide also indicated that the age the iron oxide could have a large effect on the rate of photodegradation of the organic matter, possibly due to changes in oxide reactivity.

The experiments reported here that the photochemical degradation of dissolved natural organic matter may be influenced positively or negatively by the presence of iron oxide particles. Goethite decreased the rate of photodegradation of DOM sourced from a billabong, most likely due to the absorption of light by the oxide and scattering effects reducing the available light for initiating reactions in the dissolved organic matter. In contrast, reactive amorphous iron oxide increased the rate of carbon dioxide production (and hence DOM degradation) by up to an order of magnitude.

Ultraviolet irradiation of DOM may be of considerable environmental importance in waterbodies with high DOM and a source of fresh iron oxide. Fe(II) can be produced from amorphous iron oxyhydroxide (hydrous iron oxide) by microbes under anoxic conditions (Lovley and Phillips 1986), and when this dissolved Fe(II)

diffuses upwards into the oxic zone of a stratified waterbody iron oxyhydroxides can be produced at the interface (Davison and De Vitre 1992). In shallow lakes and billabongs (oxbow lagoons), where an anoxic layer forms within the photic zone in summer months, fresh iron oxides may form which can then catalyse DOM photodegradation and further increase O_2 consumption. This process may also be important at zones of mixing between aerobic and anaerobic water; for example, at the onset of flooding, when anoxic billabong waters with high DOM may be mixed with oxygenated river water and will be discussed further in Chapter 6.

3.5 References

Abrahamson, H. B., A. B. Rezvani, and J. G. Brushmiller. 1994. Photochemical and spectroscopic studies of complexes of iron(III) with citric acid and other carboxylic acids. Inorg. Chim. Acta **226**:117-127.

Bartoli, F., R. Philippy, J. M. Portal, and B. Gerard. 1992. Poorly ordered hydrous Fe oxides, colloidal dispersion and soil aggregation. I. Effect of humic macromolecules on surface and colloidal properties of Fe (III) polycations. Journal of Soil Science **43**:47-58.

Bertilsson, S., and S. Bergh. 1999. Photochemical reactivity of XAD-4 and XAD-8 adsorbable dissolved organic compounds from humic waters. Chemosphere **39**:2289-2300.

Cunningham, K. M., M. C. Goldberg, and E. R. Weiner. 1985. The aqueous photolysis of ethylene glycol adsorbed on goethite. Photochem. Photobiol. **41**:409-416.

Davison, W., and R. De Vitre. 1992. Iron particles in freshwater. Pages 315-355 *in* J. Buffle and H. P. van Leeuwen, editors. Environmental Particles. Lewis Publishers INC, Boca Raton Ann Arbor London Tokyo.

De Haan, H. 1993. Solar UV-light penetration and photodegradation of humic substances in peaty lake water. Limnol. Oceanogr. **38**:1072-1076.

Edwards, M., M. M. Benjamin, and J. N. Ryan. 1996. Role of organic acidity in sorption of natural organic matter (NOM) to oxide surfaces. Colloids and Surfaces A: Physicochemical and Engineering Aspects **107**:297-307.

Evanko, C. R., and D. A. Dzombak. 1998. Influence of structural features on sorption of NOM-analogue organic acids to goethite. Environ. Sci. Technol. **32**:2846-2855.

Feng, W., and D. Nansheng. 2000. Photochemistry of hydrolytic iron (III) species and photoinduced degradation of organic compounds. A minireview. Chemosphere **41**:1137-1147.

Filius, J. D., D. G. Lumsdon, J. C. L. Meeussen, T. Hiemstra, and W. H. Van Riemsduk. 2000. Adsorption of fulvic acid on goethite. Geochim. Cosmochim. Acta **64**:51-60.

Gao, H., and R. G. Zepp. 1998. Factors influencing photoreactions of dissolved organic matter in a coastal river of the southeastern United States. Environ. Sci. Technol **32**:2940-2946.

Gu, B., J. Schmitt, Z. Chen, L. Liang, and J. F. McCarthy. 1994. Adsorption and desorption of natural organic matter on iron oxide: mechanisms and models. Environ. Sci. Technol **28**:38-46.

Hrncir, D. C., and D. McKnight. 1998. Variation in photoreactivity of iron hydroxides taken from an acidic mountain stream. Environ. Sci. Technol. **32**:2137-2141.

Langford, C. H., and J. H. Carey. 1987. Photocatalysis by inorganic components of natural water systems. Pages 225-239 *in* Photochemistry of Environmental Aquatic Systems. American Chemical Society.

Larsen, O., and D. Postma. 2001. Kinetics of reductive bulk dissolution of lepidocrocite, ferrihydrite, and goethite. Geochim. Cosmochim. Acta **65**:1367-1379.

Leland, J., and A. J. Bard. 1987. Photochemistry of colloidal semiconducting iron oxide polymorphs. J. Phys. Chem. **91**:5076-5083.

Litter, M. I., and M. A. Blesa. 1988. Photodissolution of iron oxides: I. Maghemite in EDTA solutions. J. Colloid Interface Sci. **125**:679-687.

Lovley, D. R., and E. J. P. Phillips. 1986. Organic matter mineralization with reduction of ferric iron in anaerobic sediments. Appl. Environ. Microbiol. **51**:683-689.

McKnight, D. M., E. W. Boyer, P. K. Westerhoff, P. T. Doran, K. Thomas, and D. T. Andersen. 2001. Spectrofluorometric characterization of dissolved organic matter for indication of precursor organic material and aromaticity. Limnol. Oceanogr. **46**:38-48.

Miles, C. J., and P. L. Brezonik. 1981. Oxygen consumption in humic colored waters by a photochemical ferrous-ferric catalytic cycle. Environ. Sci. Technol **15**:1089-1095.

Murphy, E. M., J. M. Zachara, and S. C. Smith. 1990. Influence of mineral-bound humic substances on the sorption of hydrophobic organic compounds. Environ. Sci. Technol. **24**:1507-1516.

Oxtoby, D. W., and N. H. Nachtrieb. 1990. Principles of Modern Chemistry. Saunders College Publishing, Fort Worth.

Schmitt-Kopplin, P., N. Hertkorn, H.-R. Schulten, and A. Kettrup. 1998. Structural changes in a dissolved soil humic acid during photochemical degradation processes under O_2 and N_2 atmosphere. Environ. Sci. Technol. **32**:2531-2541.

Schwertmann, U., and R. M. Cornell. 1991. Iron Oxides in the Laboratory: Preparation and Characterization. VCH, Weinheim.

Siffert, C., and B. Sulzberger. 1991. Light-induced dissolution of hematite in the presence of oxalate: a case study. Langmuir **7**:1627-1634.

Spark, K. M., J. D. Wells, and B. B. Johnson. 1997. Characteristics of the sorption of humic acid by soil minerals. Australian Journal of Soil Research **35**:103-112.

Sulzberger, B., and H. Laubscher. 1995. Reactivity of various types of iron(III) (hydr)oxides towards light-induced dissolution. Mar. Chem. **50**:103-115.

Tipping, E. 1981. The adsorption of aquatic humic substances by iron oxides. Geochim. Cosmochim. Acta **45**:191-199.

Varadachari, C., T. Chattopadhyay, and K. Ghosh. 2000. The crystallo-chemistry of oxide-humus complexes. Australian Journal of Soil Research **38**:789-806.

Villalobos, M., and J. O. Leckie. 2000. Carbonate adsorption on goethite under closed and open CO_2 conditions. Geochim. Cosmochim. Acta **62**:3787-3802.

Voelker, B. M., F. M. M. Morel, and B. Sulzberger. 1997. Iron redox cycling in surface waters: Effects of humic substances and light. Environ. Sci. Technol. **31**:1004-1011.

Waite, T. D., and F. M. M. Morel. 1984. Photoreductive dissolution of colloidal iron oxide: Effect of citrate. J. Colloid Interface Sci. **102**:121-137.

Waite, T. D., and R. Szymczak. 1993. Particulate iron formation dynamics in surface waters of the eastern Caribbean. Journal of Geophysical Research **98**:2371-2383.

Wells, M. L., and L. M. Mayer. 1991. The photoconversion of colloidal iron oxyhydroxides in seawater. Deep-Sea Res **38**:1379-1395.

Zhou, Q., P. A. Maurice, and S. E. Cabaniss. 2001. Size fractionation upon adsorption of fulvic acid on goethite: Equilibrium and kinetic studies. Geochim. Cosmochim. Acta **65**:803-812.

Zuo, Y., and J. Hoigné. 1992. Formation of hydrogen peroxide and depletion of oxalic acid in atmospheric water by photolysis of iron(III)-oxalato complexes. Environ. Sci. Technol. **26**:1014-1022.

4 Photochemical Reactions of Dissolved Organic Matter in Sunlight.

4.1 Introduction

The experiments discussed in the previous chapters have established that mechanisms exist for iron oxides to influence the photochemical degradation of dissolved organic matter. All of the previous experiments were conducted with artificial sources of light and so do not give an indication of the significance of these reactions in the natural environment. This chapter describes experiments conducted with both billabong water and River Red Gum leaf leachate in quartz tubes, using sunlight as the source of light energy. The photochemical reactions were followed using gas chromatography, absorbance and TOC measurements, as for previous experiments, with the addition of three-dimensional fluorescence spectroscopy and High Performance Liquid Chromatography techniques to enable further characterisation of the organic matter remaining in solution.

These experiments demonstrate that photochemical degradation of dissolved organic matter can occur under natural irradiation conditions, but on a slower timescale than was observed in the photochemical reactor. These changes produce not only gaseous products, but also result in the production of low molecular weight organic acids and reduce the aromatic nature of the remaining dissolved organic matter.

4.2 Methods

4.2.1 Preliminary Quartz Tube Experiment-Air Cooling

An experiment was conducted to test the effectiveness of quartz tubes laid out in the sun for photochemical experiments using leachate. Twelve quartz tubes (1m long, 13mm inner diameter) were acid washed (5% HCl) for two days, rinsed and air-dried. The tubes were sterilized prior to use by UV irradiation for 30 minutes in a laminar flow cabinet. Two litres of leachate were prepared and filter-sterilized according to the methods described in Section 2.2.3. One end of each tube was stoppered using an ultrapure silicon stopper (Cole-Parmer) which had been acid washed and autoclaved. Seventy millilitres of leachate were poured into each tube, using an autoclaved measuring cylinder. The open end of the tube remained within the laminar flow cabinet until it could be stoppered. An additional non-sterile tube was also prepared for zero-

time gas measurements and to use for temperature monitoring over the course of the experiment.

A roof area was chosen as the site for the initial experiments and a rack was constructed so that the tubes could lie horizontally. The tubes were placed on the rack at 12.30 pm on September 18, 2001 and measurement of light intensity (using an Odyssey Photosynthetic Irradiance Sensor) commenced at 12.40 pm. One of the twelve sterile tubes was wrapped in aluminium foil to act as a dark control.

Tubes were removed for gas sampling and then opened for other analyses. The sampling regime was as follows: 1 sample after 3 hours, 5 hours, 24 hours, 47 hours, 72 hours, 144 hours, 216 hours, 336 hours and then three light exposed samples and the dark control after 410 hours. Note, hours refer to time since beginning of experiment, not hours of light exposure. The water temperature of the non-sterile sample was measured at the same time as each tube was removed using a Cole-Parmer Thermistor Thermometer (Model 8202-20).

For each of the removed tubes, 2 mL of headspace gas was sampled for gas analysis (using the method described in section 2.2.2) after vigorous shaking. The position of the liquid and stoppers were marked on the tube before the stoppers were removed (markings were used to measure ratio of headspace to liquid as the internal diameter of the tubes varied slightly, affecting the overall capacity of the tube). Calculation of the total amount of gas produced or consumed was carried out as described in Appendix 4 (CO_2) and Appendix 5 (O_2). Liquid samples were then taken for organic acid analysis, fluorescence, absorbance and pH measurements.

In this experiment, organic acids were analysed using two methods to identify which would be the most useful in full-scale experiments. The *HPLC method* involved injection of 50 µL of sample into a Waters HPLC fitted with a U6K Injection port, an Aminex HPX-87H organic acid column and a 450 variable wavelength detector set at 210 nm. The mobile phase used for the experiments was 0.005M H_2SO_4 at a flow rate of 0.6 mL/min and a column temperature of 40°C. Data was collected using a plotter. The *gas chromatograph method* involved injection of 5 µL of sample into a Varian CP 3380 gas chromatograph fitted with an Alltech Econocap EC1000 column and a flame ionisation detector. The mobile phase was N_2 (2 mL/ min). The samples for HPLC and GC analysis were acidified prior to injection by adding 0.025 ml of 1M H_2SO_4 to 2.425 mL of sample, to ensure all organic acids were protonated. Samples were centrifuged

(13000 rpm) to prevent the injection of particles into the instruments. Samples for organic acid analysis were injected into the instruments as soon as possible after sampling.

Samples for fluorescence measurements were acidified to a pH of 2 with HCl to minimise binding to any metals that may have been present in the sample. The absorbance of both acidified and unmodified samples was measured. Fluorescence scans were made on the acidified samples by scanning the excitation wavelength from 200 nm to 400 nm in 10 nm steps, and measuring the emission intensity every 2 nm between 200 nm and 550 nm for each excitation wavelength. The resulting data was exported to Excel and corrected using the absorbance data for acidified samples before it was graphed. This technique and the data corrections are explained in detail in Appendix 2, but briefly, in strongly coloured samples, absorbance of the emitted light can lead to a concentration dependent shift in the peak locations (known as the inner-filtering effect). The corrections are based on the assumption that the detector measures fluorescence at the centre of the cell, and corrects for absorbance of light between the light source and the centre of the cell then from this point to the detector. Fluorescence measurements were made on a Hitachi f-4500 fluorescence spectrophotometer.

4.2.2 Preliminary Quartz Tube Experiment-Billabong Cooling

This experiment was designed to test the suitability of using a natural billabong as the site for irradiation experiments. A batch of amorphous iron oxide was prepared using the method described for batches 3 and 4 in Section 3.2.2. Following washing and slurry preparation, 2 x 350 μL of slurry (350 μL was the approximate volume required for most batches) was pipetted into each of six pre-dried, weighed glass bottles and these were placed in a drying oven (approximate temperature 80 °C). These were dried while tube and leachate preparation was carried out, and then re-weighed to establish the mass of oxide per mL of slurry and enable calculation of required volume of slurry in the leachate to give the equivalent concentration to the 6mg/700 mL which had been used in photochemical reactor experiments.

Four litres of *Eucalyptus camaldulensis* leachate was prepared and sterilized using the method described in Section 2.2.3. Iron oxide was added to two 900 mL samples of leachate and the remainder was used unmodified. Forty-three quartz tubes were cleaned, sterilized and filled as described above, twenty-two contained leachate

plus oxide and twenty-one contained unmodified leachate. Ten tubes from each treatment were wrapped in aluminium foil for use as dark controls. The tubes were mounted in five polystyrene racks and stored overnight at room temperature. Each rack was constructed of two pieces of polystyrene, each with eight holes cut into it. The holes were cut with a cork borer only slightly larger in diameter than the tubes themselves. The polystyrene was cut to a size that allowed for minimum shading of the tubes while still positioning the tubes just a few millimetres below the surface of the water. The racks were floated on the surface of Ryan's Billabong (36°07' S 146°58' E) at 9.25 am the following morning, as illustrated in Figure 4.1. This billabong was chosen as it provided a large open-water area to minimise shading of the tubes and was located in a sufficiently secluded location for the equipment to be left for extended periods without interference. The purpose of suspending the tubes at the surface of the billabong was to ensure that the reactions did not occur at temperatures higher than would be environmentally significant, i.e. the billabong was acting as a heat sink only in this experiment.

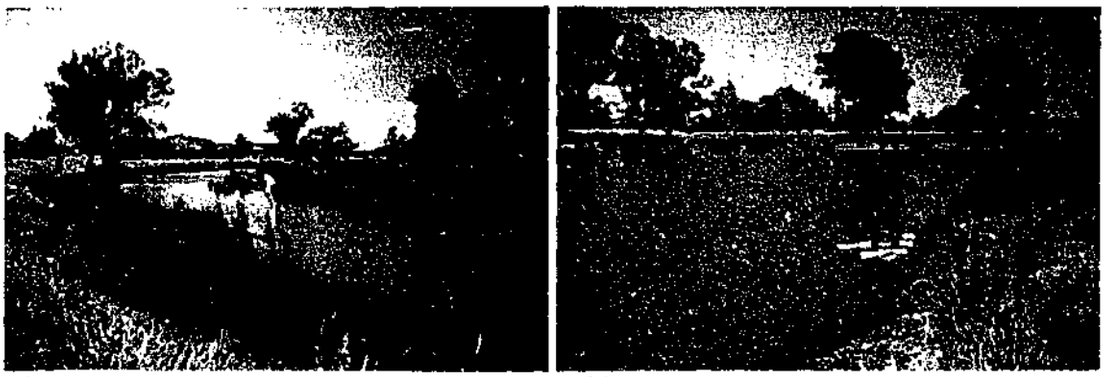

(a) (b)

Figure 4.1 Experimental set-up at Ryan's Billabong showing a) the environment to the east of the experiment and b) the environment facing west with the quartz tubes in position.

Three tubes (one leachate, two leachate plus iron oxide) were kept out of the billabong and used for zero-time measurements. One rack (consisting of two light, two dark, two light plus oxide and two dark plus oxide samples) was removed from the billabong after 1 day, another after 4 days and the experiment was ended after 7 days. On the seventh day 3 replicates from each treatment were sampled and the remainder were discarded (some had been damaged by cattle). Each of the samples was analysed using all the techniques described in 4.2.1 except the gas chromatograph organic acid

analysis. HPLC data were collected with a DAPA data collection card and software. Light levels were recorded using an Odyssey Photosynthetic Irradiance Sensor.

4.2.3 Irradiation of Leachate- pool based cooling.

A wading pool (metal frame, blue plastic "canvas" type) was erected in the courtyard of the Murray Darling Freshwater Research Centre in Thurgoona, and positioned to give the maximum day-length. The pool had dimensions of 1.6 x 1.2 metres and was filled to a depth of 20 cm (maximum sustainable depth). A small garden fountain (MeBner, 1200 L/h, 120 cm fountain height) was installed in the centre of the pool (as shown in Figure 4.2) to improve water circulation and allow for some evaporative cooling. This was done to compensate for the smaller body of water used in this experiment compared to the billabong experiment and to prevent overheating of the tubes. Trials indicated that this system did not exceed a water temperature of 30.5 °C over a weekend where the maximum air temperature reached 40.8 °C. This is within the range observed for local billabongs (Boon et al. 1990). A floating ball-style valve was added to the system to maintain the water level and the attached hose covered with shade cloth to minimise solar heating of the water in the hose (which was also kept to the minimum possible length).

The sample preparation was the same as in Section 4.2.2 with the exception that:

* Five litres of leachate was prepared

* UV sterilization of tubes was conducted for 1 hour

* Forty tubes were prepared: four for initial measurements (measured 30 minutes after sealing), and nine each of leachate (unwrapped), leachate (wrapped), leachate plus oxide (unwrapped) and leachate plus oxide (wrapped). New polystyrene floats were made, each with four tubes (one of each treatment).

Analysis of samples was as described in Section 4.2.2. Water temperature was recorded hourly during the experiment using a TPS WP-82 logger. A Odyssey Photosynthetic Irradiance Sensor was used to record light levels at 5 minute intervals. Three tubes from each treatment were removed after 2 days, 1 week and 2 weeks.

4.2.4 Irradiation of Billabong water- pool based cooling.

Seven litres of water was collected from Norman's Lagoon at 9:30am on March 6 2002 and transported to the laboratory in a 10 L acid-washed carboy. The water was filtered through 35 μm gauze then GFF filters before filter-sterilization using the method described in 2.2.2.1. This water was then stored overnight at 4°C.

The following morning a fresh batch of iron oxide was prepared using the method described for batches 3 and 4 in Section 3.2.2. The tube preparation, treatments and sample analyses were as described in 4.2.3, with the exception that this experiment was only conducted for 1 week, with samples removed after 2 days and 7 days. The tubes were placed in the pool at 9 pm on the day they were filled. Twenty millilitre samples were also preserved with 100 μL concentrated phosphoric acid and frozen for Total Organic Carbon analysis.

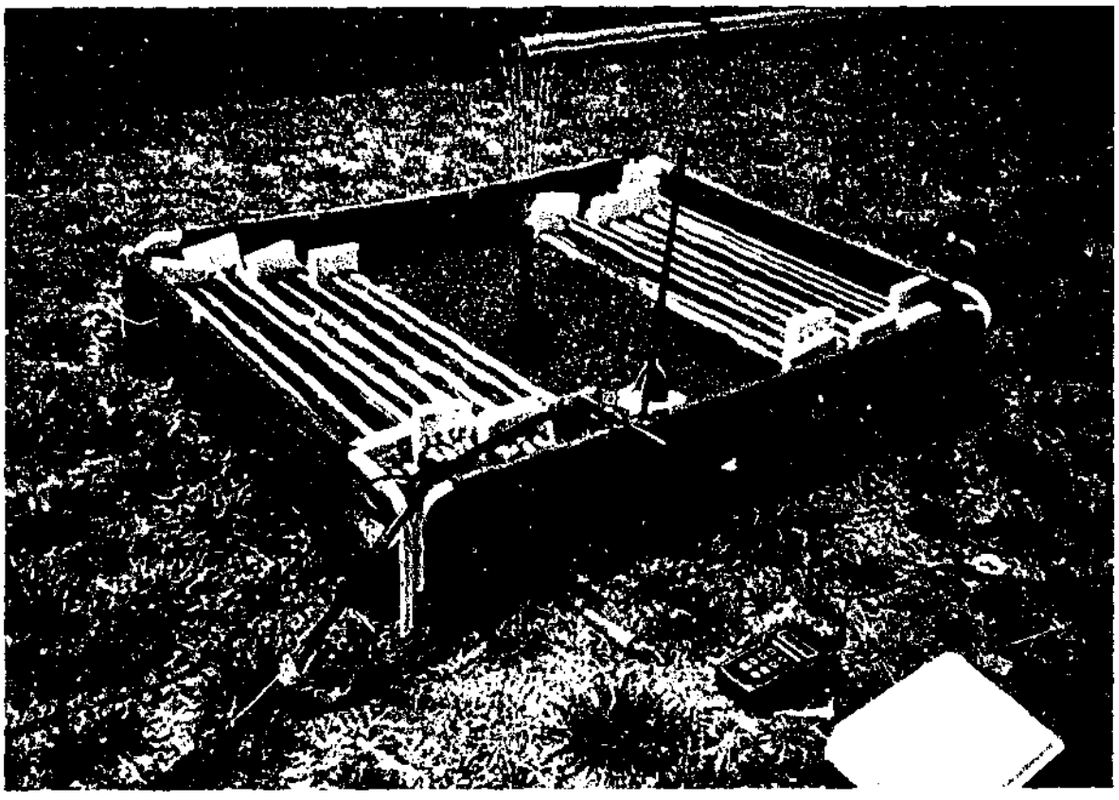

Figure 4.2 Quartz tubes in position in the wading pool.

4.3 Results and Discussion

4.3.1 Preliminary Quartz Tube Experiment-Air cooling

This experiment and the billabong experiment which follows were designed to examine a range of conditions and investigate the use of some additional analytical techniques. This experiment demonstrated that quartz tubes were appropriate as reaction vessels, and sunlight irradiation could induce measurable photochemical degradation of the dissolved organic matter on a practical time-scale. Photochemical degradation of the leachate was observed over a matter of days. The irradiation was reasonably consistent due to clear spring weather (Figure 4.3) but was not equivalent to full sunlight for the entire day due to partial shading by a nearby glasshouse in the early morning.

The carbon dioxide produced in each of the tubes exhibited an increasing trend with time (Figure 4.4). The single dark control also had an elevated CO_2 concentration, but this was less than in the light exposed tubes. It appeared that substantial generation of CO_2 occurred in the light-exposed samples over a matter of two weeks, but further replicates and controls are required before the significance of the results can be determined. Traces of carbon monoxide were also observed in light-exposed samples after two days and the quantity did appear to increase over the course of the experiment, as occurred with lamp irradiations. Quantification of CO was not possible with the available equipment due to poor signal to noise ratios and difficulties resolving the standard peak. No carbon monoxide was observed in the dark control sample.

The absorbance of the leachate was measured as a scan at each of the sampling times, and the results, expressed as absorbance at three selected wavelengths, are illustrated in Figure 4.5. The trend indicates that the photobleaching occurred throughout the experiment. At the end of the experiment, the average absorbance for the three light exposed samples was 70%, 55% and 47% of the initial at 200 nm, 250 nm and 300 nm respectively. In terms of the absorbance spectrum of the leachate, this indicates an increasing ratio of absorbance at short wavelengths to long wavelengths in the 300-200nm region as photodegradation proceeds. This preferential bleaching at the longer wavelengths has previously been interpreted as a reduction in the average molecular weight (Schmitt-Kopplin et al. 1998, Bertilsson and Bergh 1999).

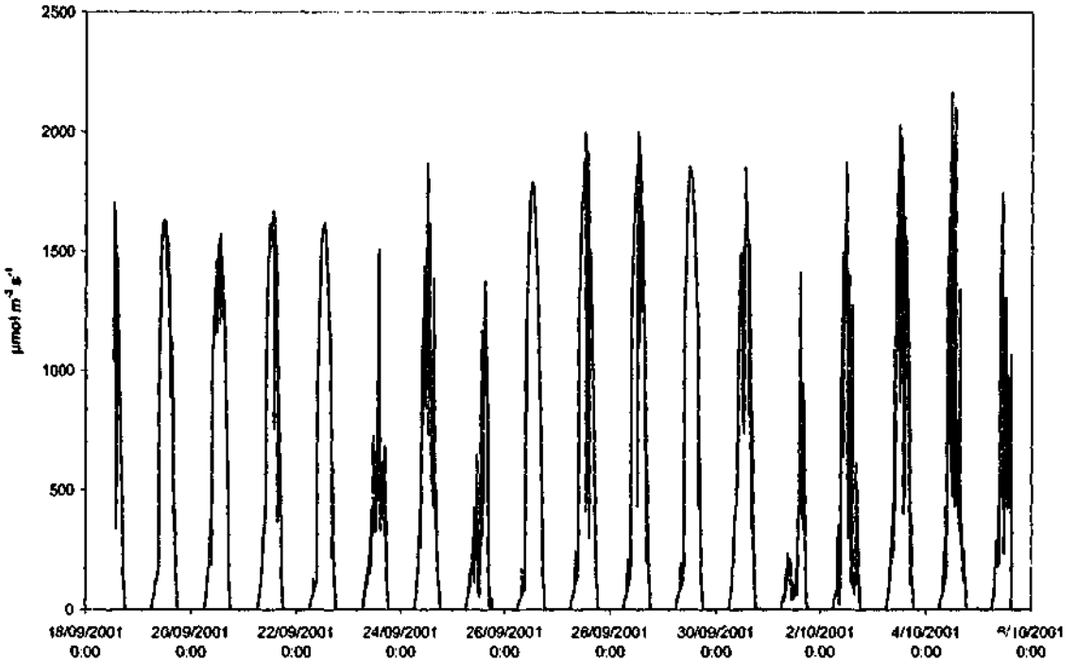

Figure 4.3 Light data for the period of the preliminary experiment with air cooling.

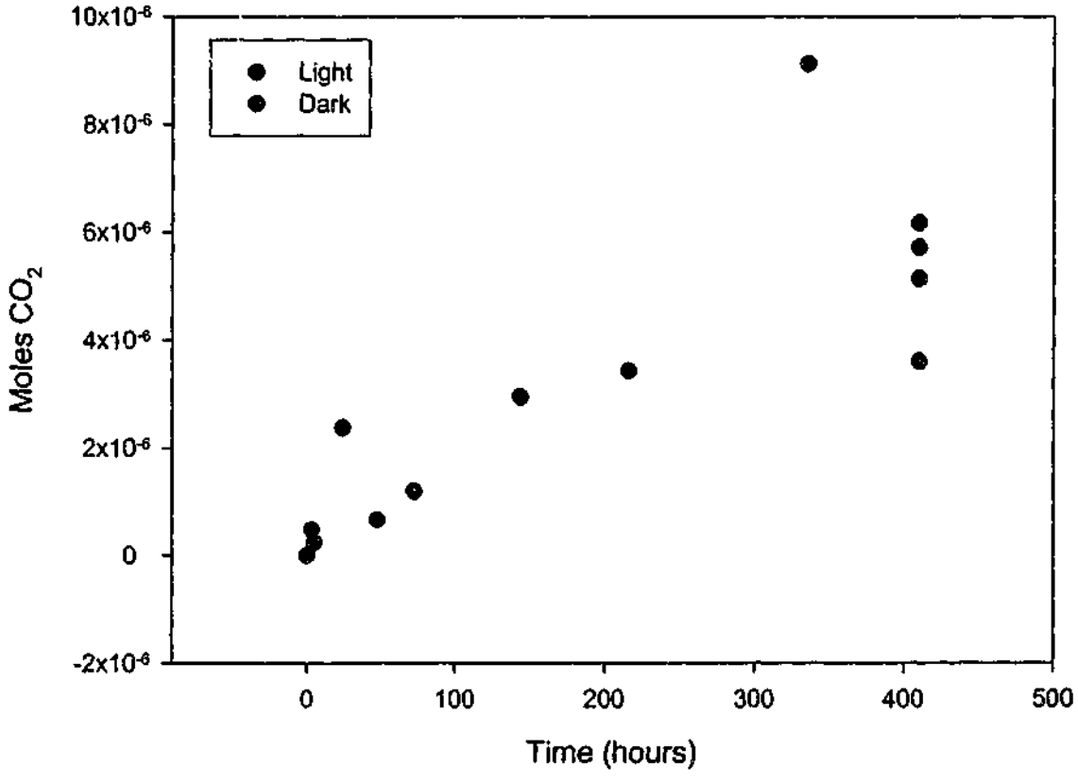

Figure 4.4 Carbon dioxide production in the air-cooled preliminary experiment.

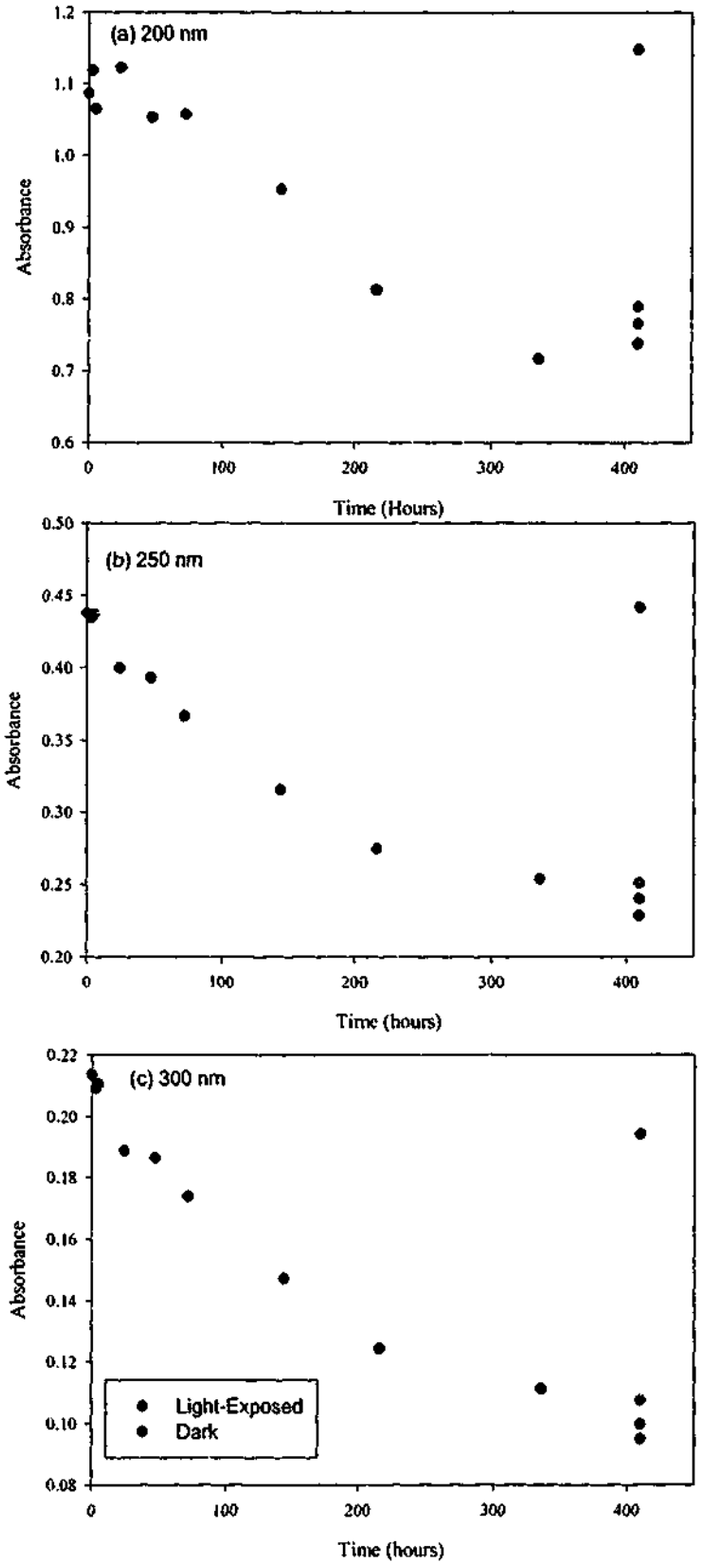

Figure 4.5 Changes to the absorbance of the leachate at (a) 200 nm, (b) 250 nm and (c) 300 nm over the course of the air-cooled preliminary experiment.

Meaningful oxygen consumption data was not obtained in this experiment, even after correction for differing tube volumes (data not shown). The data contained a large amount of scatter; a result of attempting to measure very small reductions in the comparatively high atmospheric concentration of oxygen. As most sampling times had only a single replicate it was not appropriate to attempt to interpret this data.

The pH of the leachate declined over the course of the experiment (Figure 4.6). The rate of decline was quite rapid during the early part of the reaction, but was much slower towards the end of the experiment. The general shape of the pH vs time curve suggests that the decrease in pH occurs more rapidly than the generation of CO_2 (c.f. Figure 4.4). This is in agreement with the mechanism proposed on Chapter 2, whereby the initial photochemical reactions tend to result in the uptake of oxygen by the dissolved organic matter molecules, increasing the number of acidic functional groups (amongst others).

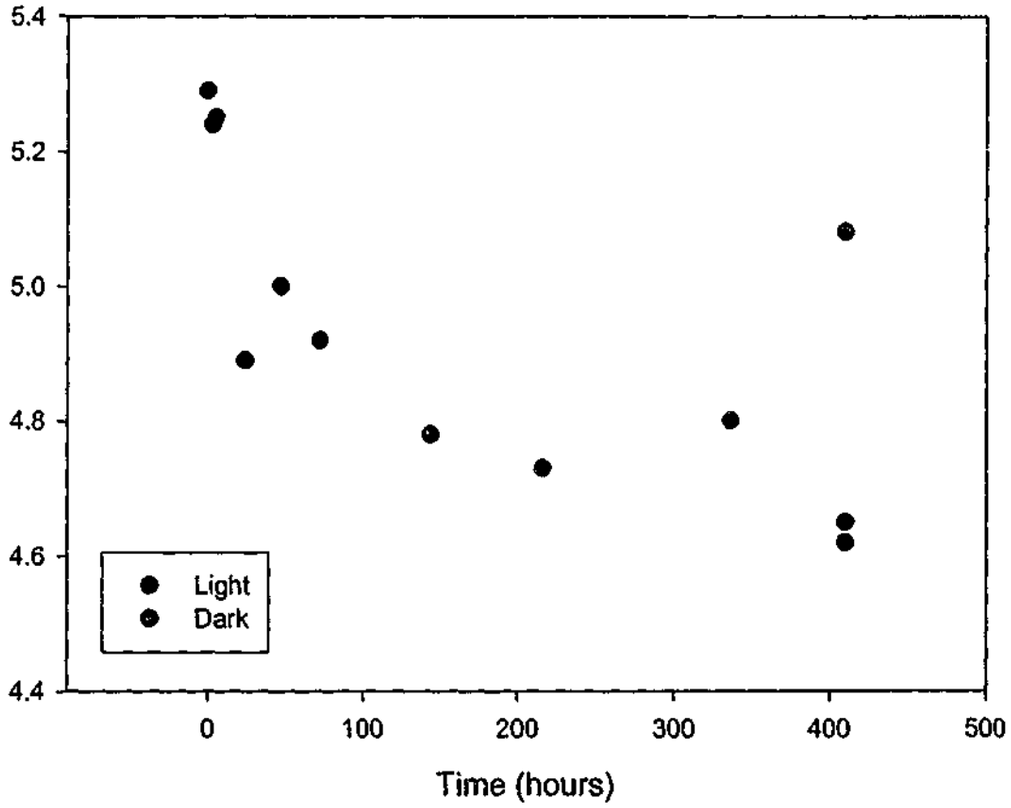

Figure 4.6 Change in sample pH over the course of the air-cooled preliminary experiment.

The generation of small organic acids was examined using both gas chromatography and high performance liquid chromatography. The gas chromatography technique proved to be of insufficient sensitivity to be of value for these experiments, but better results were obtained using HPLC (Table 4.1).

Table 4.1 Peak Area for HPLC analysis of leachate samples. Areas given were calculated using peak height x width at half height (measured in cm from printouts).

Peak No	Elution Time	0 h	3 h	5 h	24 h	47 h	72 h	144 h	216 h	336 h	410 h	410 h	410 h	410 h#
1	6.9	*	*	*	*	*	*	*	*	*	*	*	*	*
2	8.8							s	s	s		s	s	
3	10.2	s	s	s	s	0.49	0.45	0.6	0.96	0.48	0.56	0.35	0.6	s
4	11.6										0.4	0.36		
5	13.4	1.2	1.2	1.2	1.14	1.2	0.95	1.05	0.96	0.81	0.72	0.96	0.72	0.54
6	15.9	0.5	0.3	0.4	0.28		0.28		0.2		0.16	0.24	0.24	0.65
7	16.6							0.36	0.45		0.36	0.35	0.45	
8	18.5										0.24	0.9		
9	20			0.9							0.2			
10	20.8						0.32				0.18	0.48	0.65	0.9
11	29	2.53	2.64	2.76	2.86	3.6	2.47	0.72	0.9	0.75	0.6	0.4	0.72	2.6
12	30.3	s	s	s	0.7	0.6	s			0.4	0.6	0.5	0.36	s
13	33.7	1.08	1.54	1.26	1.61	0.72	0.9	0.55	0.9	1.08	1	1.5	1.19	1.05
14	40.5												0.6	
15	50											2.25		

* represent the unretained material (these peaks were offscale). Those marked with an s were shoulder peaks and areas could not be estimated. # signifies the dark control. Unmarked boxes indicate the peak did not appear in those samples.

The organic acid analysis of these preliminary experiments suggest that the peaks initially present diminish in size over time (e.g. peak 6), and that additional peaks appear with time (e.g. peak 7), indicating the production of new low-molecular-weight organic molecules (possibly organic acids). Only one of the additional peaks found at the end of the experiment (410 h) was present in the dark control, suggesting a photochemical mechanism. No attempt was made to identify the new compounds in this experiment.

The degradation of the organic matter was also observed using 3-D fluorescence spectra (also known as Excitation/Emission Matrices) as shown in Figure 4.7. The spectra contain a large amount of spectroscopic data about the DOM mixture. The x-axis represents emitted wavelengths and the y-axis represents excitation wavelengths. Corrected fluorescence intensity is indicated by the colour of the contours, with red representing very low fluorescence and blue indicating fluorescence peaks. The

diagonal bars represent reflectance bands and are of no diagnostic value. Sections parallel to the x-axis represent emission spectra and sections parallel to the y-axis represent excitation spectra, with the excitation spectra representing the absorbance of all the fluorescent compounds in the sample (Coble 1996). The peaks in these spectra represent the combination of excitation and emission wavelengths that give the maximum fluorescence intensity, and changes to the location of these peaks was used as an indication of changes to the fluorescence (and hence structural) properties of the bulk DOM. In this experiment the fluorescence spectrum did not alter substantially over the course of the experiment. The initial spectrum is characterised by the presence of two peaks (Em 305 nm, Ex 280 nm and Em 305 nm, Ex 240 nm), both covering relatively small regions of the spectrum. The spectrum of the leachate is concentrated at the high-energy end of the spectrum and suggests a dominance of small or simple aromatic molecules as a more complex conjugated or aromatic system is required to produce features in the lower energy region of the spectrum (Coble 1996). At the end of the experiment the key features of the spectra in both the dark control and light-exposed sample are in the same region. The intensity of the spectrum has increased slightly in the dark control and the peaks overlap more. In the light- exposed sample there is an increased dominance of the lower peak, but the bulk characteristics of the leachate have not changed substantially in either sample.

This experiment demonstrated that photochemical degradation of leaf leachate could be observed in samples irradiated by natural sunlight, over the period of only a couple of weeks. In particular, this experiment provided data that could not be obtained in any of the previous experiments- time course studies of photochemical carbon dioxide production, pH changes and loss of absorbance. The absorbance bleaching and CO_2 production followed similar, reasonably steady patterns, but the decline in pH in light-exposed samples was quite rapid initially and then levelled off. The results were consistent with the mechanism proposed in Chapter 2, which involved early formation of acidic functional groups through incorporation of oxygen into the DOM, followed by decarboxylation reactions to produce CO_2. The results also indicated that minor changes in the fluorescence spectra and organic acid profiles of the leachate were occurring.

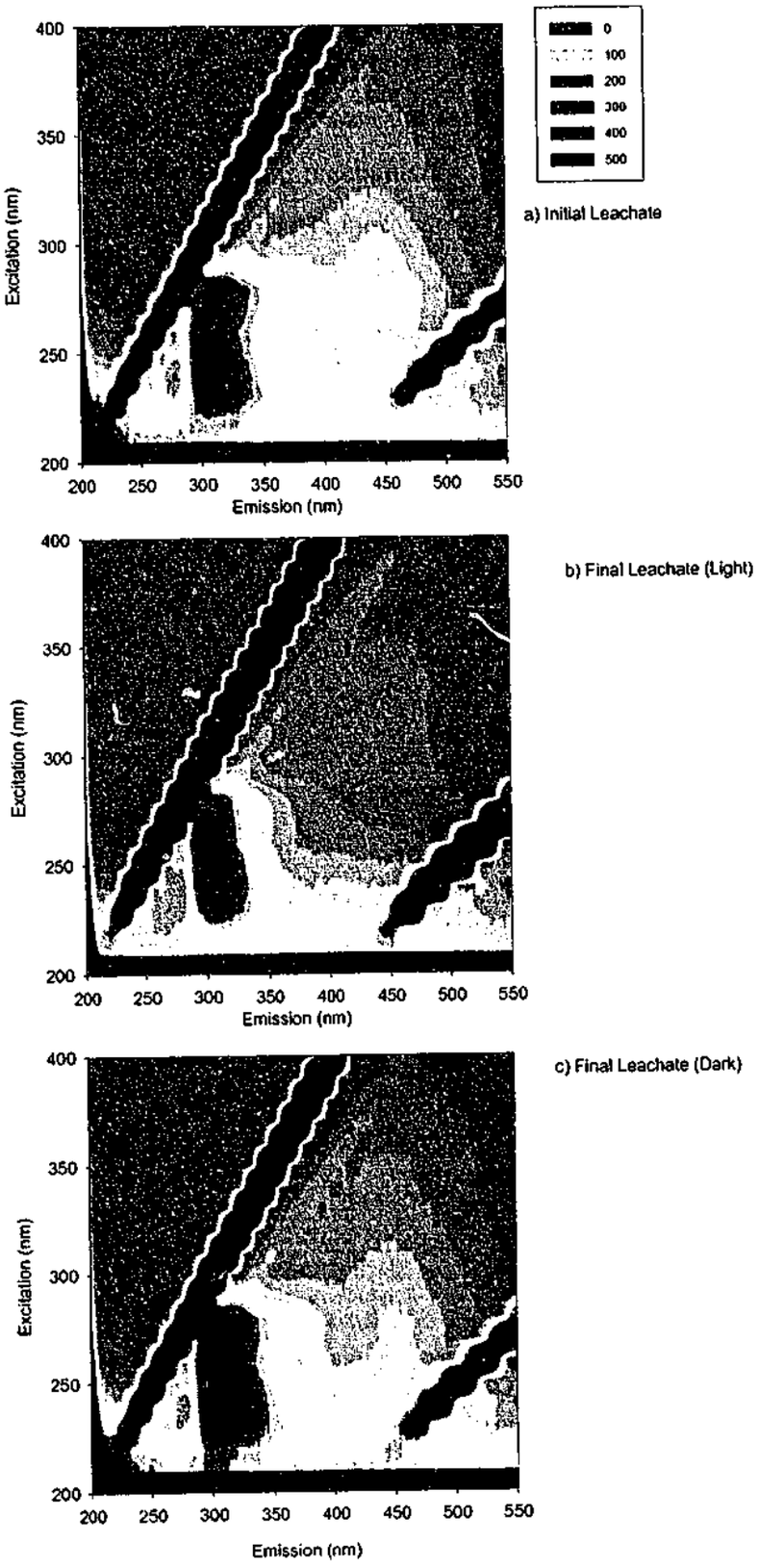

Figure 4.7 Three-dimensional fluorescence spectra of the leachate at the beginning (a) and end (b,c) of the preliminary experiment. Contour colours indicate fluorescence intensity.

4.3.2 Preliminary Quartz Tube Experiment-Billabong Cooling

This experiment was designed to expand the preliminary experiment described above to a more natural situation and assess the suitability of using a billabong as an irradiation environment and a cooling mechanism. The experiment incorporated both light-exposed and control (foil wrapped) tubes, with and without added iron oxide. The intention was that the temperature and light conditions would approximate early summer environmental conditions through suspending the tubes at the surface of a billabong. As illustrated in Figure 4.1, the initial billabong conditions were suitable for this type of experiment; however, a bloom of cyanobacteria had influenced the light environment of the tubes within one week of placement in the billabong (Figure 4.8). The light data in Figure 4.9 is therefore indicative of the light incident on the surface of the billabong over this period, but not necessarily indicative of the light environment within the tubes, especially in the later part of the experiment.

Figure 4.8 Quartz tubes following removal from the billabong environment, showing coating of algae and other material.

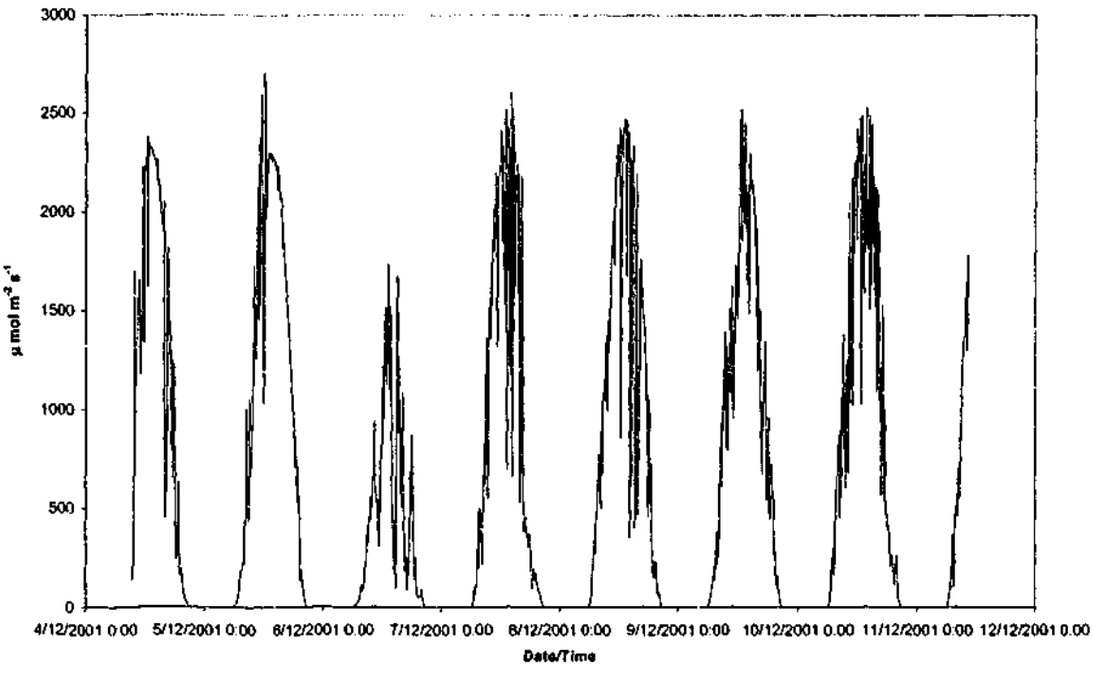

Figure 4.9 Incident light intensity during the period of the experiment at Ryan's Billabong.

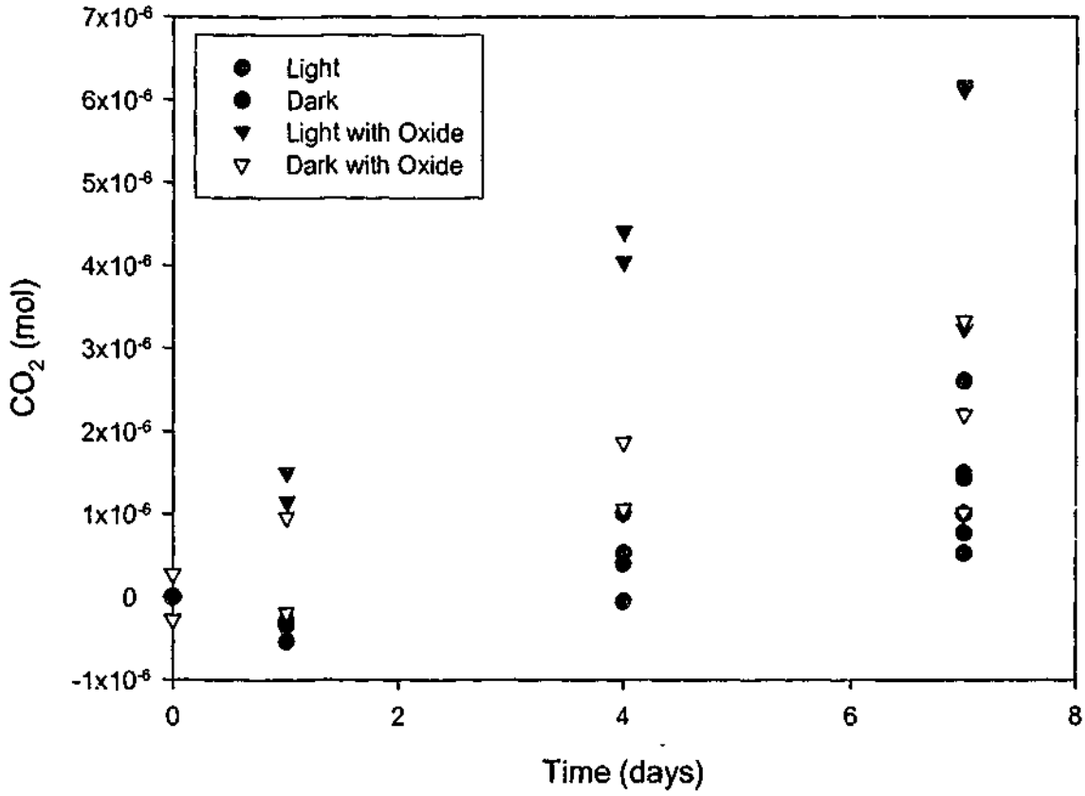

Figure 4.10 Carbon dioxide produced during leachate irradiation at Ryan's Billabong.

Photochemical production of carbon dioxide was evident in the light-exposed samples containing amorphous iron oxide (Figure 4.10). The sample without added iron oxide was not distinguished from the dark controls; all of these treatments showed some increase in carbon dioxide concentrations in the tubes. These results indicate that the photochemical interactions between dissolved organic matter and amorphous iron oxide, as discussed in Chapter 3, are also significant under natural lighting conditions. In this experiment, the photocatalytic reaction between iron oxide and dissolved organic matter increased the rate of photochemical CO_2 production to an observable level under conditions that did not generate substantial levels of CO_2 without catalysis.

The change in absorbance in this experiment did not follow such a clear trend as that observed in the first preliminary experiment (Figure 4.11). Examining first the absorbance at 200 nm; the absorbance in the light-exposed samples after one week was 85 (± 7)% of the initial, while the dark controls retained 99 (± 2)% of the initial absorbance at that wavelength. In the samples with added iron oxide, the absorbances in the light and dark treatments were 67 (± 7)% and 94 (± 3)% of the initial values, respectively. At 250 nm the absorbance in the light-exposed treatment was 85 (± 8)% of the initial after one week, the dark control was 104 (± 2) %, the light with added oxide treatment was 72 (± 8)% and the dark with oxide was 94 (± 5)% of the initial value. The percentage differences in the 300 nm results were not significantly different from those at 250 nm. The results indicate that the photobleaching in this experiment was reasonably uniform across these wavelengths and do not suggest a preferential bleaching at long wavelengths (presumably higher molecular weights). The end-point results, however, do not reflect the lowest absorbances measured for each treatment. For each of the wavelengths reported here, the greatest decline in absorbance occurred after one day of sunlight exposure and then stabilised or increased, depending upon the treatment. This pattern is apparent in the control tubes as well as those exposed to sunlight, and may indicate a temperature-dependent process or even an anomaly in the spectrophotometer response.

Measurement of oxygen in the tubes again did not produce significant results. This was due to the difficulties associated with measuring relatively small changes in the gas concentration, leading to large errors.

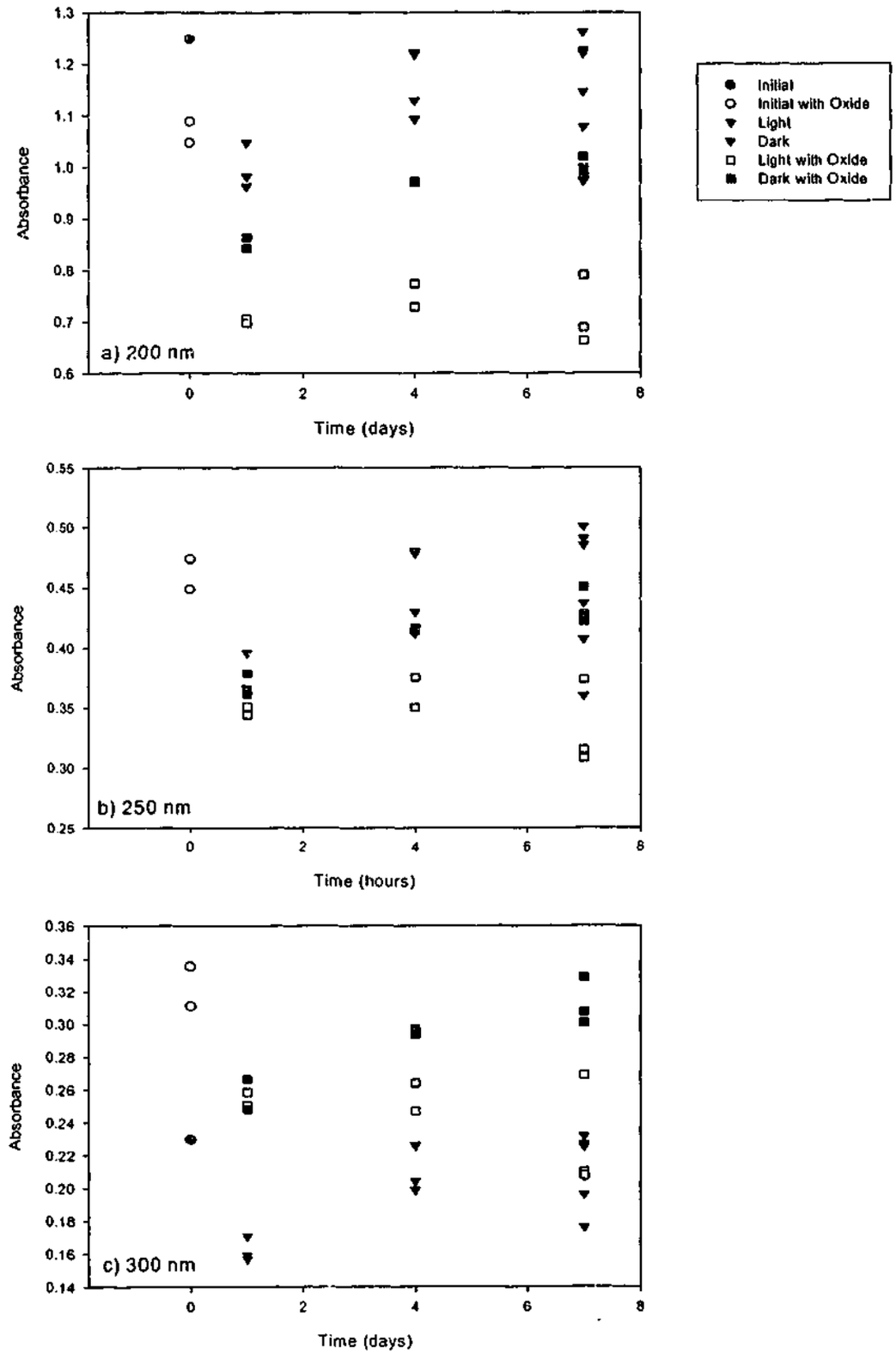

Figure 4.11 Changes to leachate absorbance at (a) 200 nm, (b) 250 nm and (c) 300 nm during irradiation in Ryan's Billabong.

The only treatment in which the final pH was significantly different to the starting pH of 5.1 (± 0.1) was the light-exposed treatment to which no iron oxide had been added. This treatment had a final pH of 4.79 (± 0.03), while the light-exposed treatment with added oxide had a final pH of 5.21 (± 0.04). This may indicate that pH reduction through the formation of organic acids is counter-balanced by the catalysed destruction of carboxylate groups in the presence of both light and iron oxide.

The HPLC analysis for organic acids did not show strong evidence for the production of organic acids. The light-exposed samples without added iron oxide had one additional unidentified peak compared to the initial chromatograms and the enhancement of another peak. Further examination of photochemical organic acid production was deferred to a later experiment (Section 4.3.3).

The 3-D fluorescence data for this experiment did not show major changes to the bulk properties of the leachate (Figure 4.12). The most notable change that occurred was the shift from two peaks (Em 305, Ex 280; Em 310, Ex 230) to one peak (Em 305, Ex 240) at the end of the experiment. This occurred in the light-exposed and control samples, both with and without iron oxide, although traces of the other peak were still present in two of the light-exposed samples. The intensity of the peaks (after correction for absorbance) indicates an intensification of the peaks compared to the initial leachate, this being much more pronounced in the dark and dark with oxide treatments, indicating a chemical aging process.

While this experiment proved that photochemical degradation of dissolved organic matter is accelerated by the presence of amorphous iron oxide under sunlight irradiation, it also indicated that the use of a billabong as the irradiation site was not appropriate for the remaining experiments, due to the influences of algae and cattle.

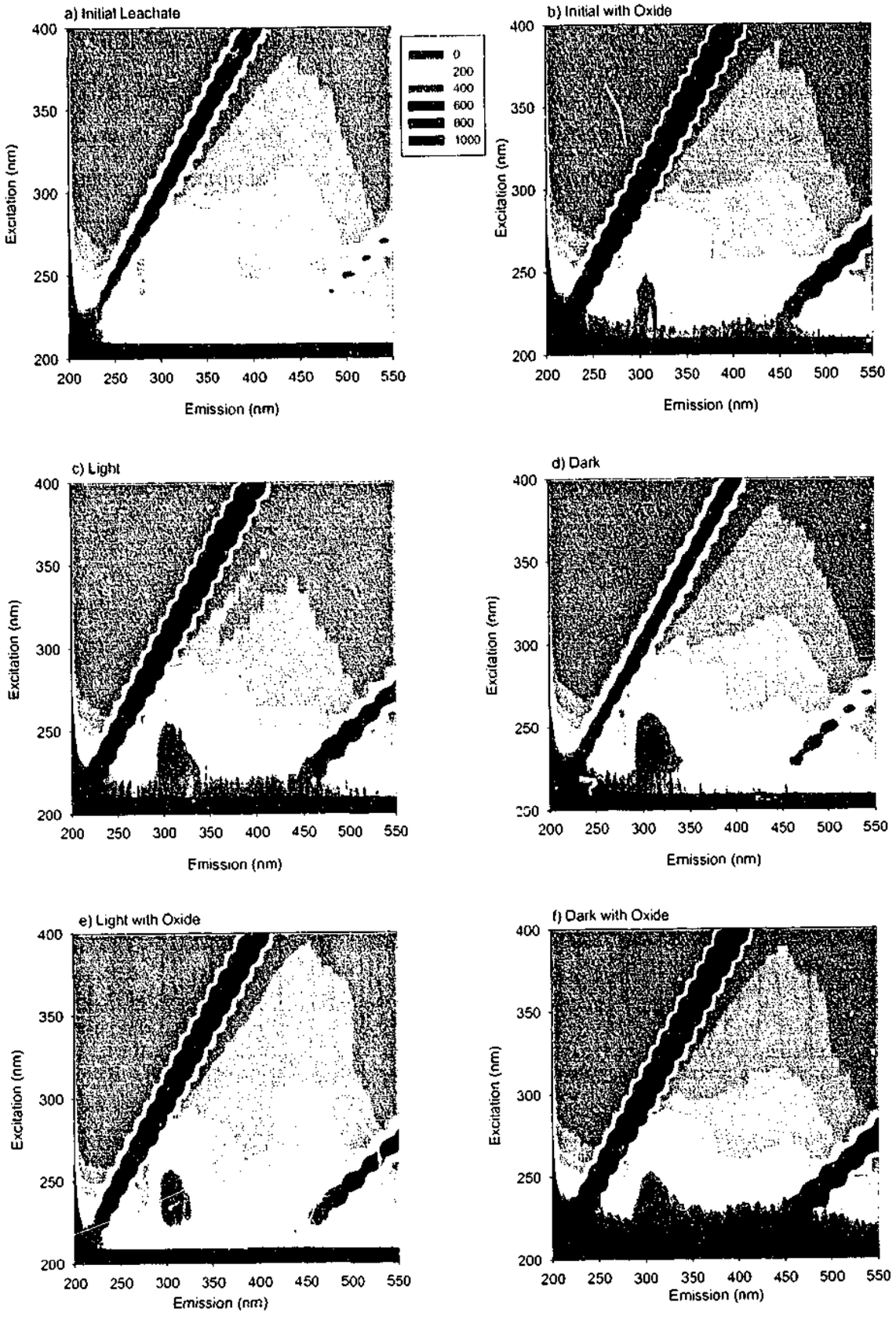

Figure 4.12 Three-dimensional fluorescence spectra of the leachate at the beginning (a,b) and end (c-f) of the irradiation at Ryan's Billabong.

Irradiation of Leachate- pool based cooling.

This experiment was designed to thoroughly examine the photochemical degradation of leachate and the role of iron oxide during sunlight irradiation, in an environment that minimised the risk of serious algal blooms interfering with the light exposure inside the tubes. Hence, the experiment was set up to use a wading pool as an artificial billabong. The positioning of the experiment was a compromise between finding a site with full sunlight exposure and locating the equipment in a location safe from damage by stock and vandals. Consequentially, some early-morning and late-afternoon sunlight was excluded from the experiment due to shading by buildings (Figure 4.13). The experiment was conducted over a fortnight of predominantly fine weather, although two days were considerably affected by cloud cover.

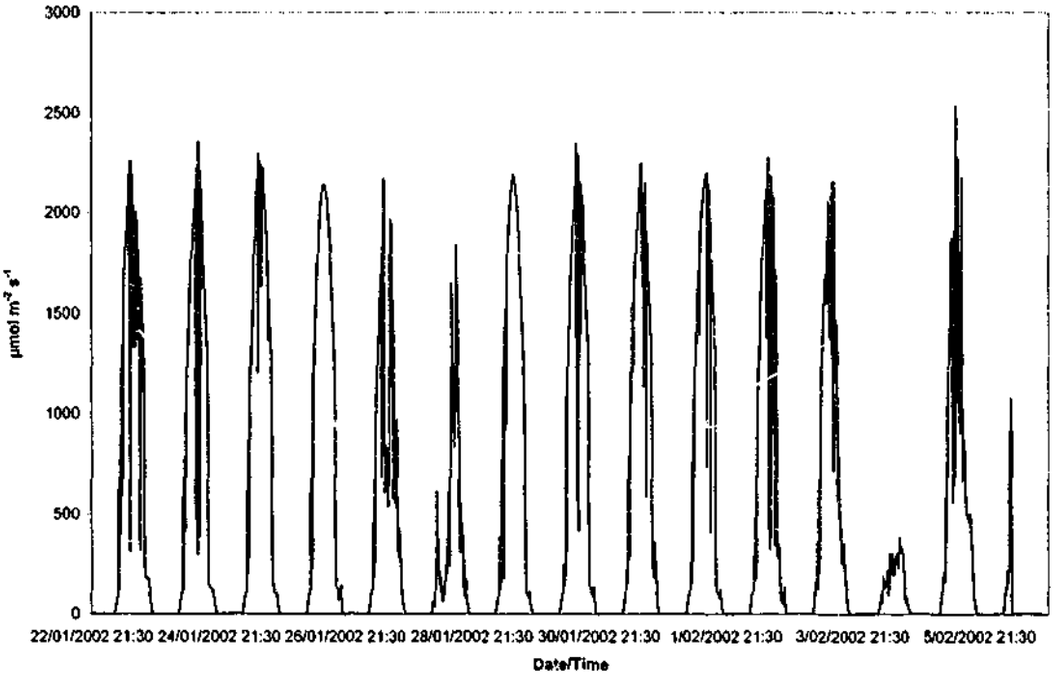

Figure 4.13 Incident light data for the period of the pool-based leachate irradiation.

Photochemical carbon dioxide production was observed in the light-exposed tubes where amorphous iron oxide was added (Figure 4.14). In the absence of iron oxide the light-exposed samples were not significantly different from the control samples at any time in the experiments. At the end of the experiment one of the light-exposed samples (without added oxide) had elevated CO_2 levels, but the other did not (the third was damaged during sampling) and as a result the range of possible results

encompasses the region occupied by the dark controls. After 14 days of sunlight exposure, the light-exposed treatment had produced 7.1 (range 4.8-9.3) x 10^{-6} moles of CO_2, the dark control had generated 4.3 (range 4.0-4.6) x 10^{-6} moles of CO_2, the dark control with oxide generated 3.3 (range 3.2-3.5) x 10^{-6} moles of CO_2 and the light-exposed with added oxide had generated 17 (range 14-18) x 10^{-6} moles of CO_2 from 70 mL of leachate.

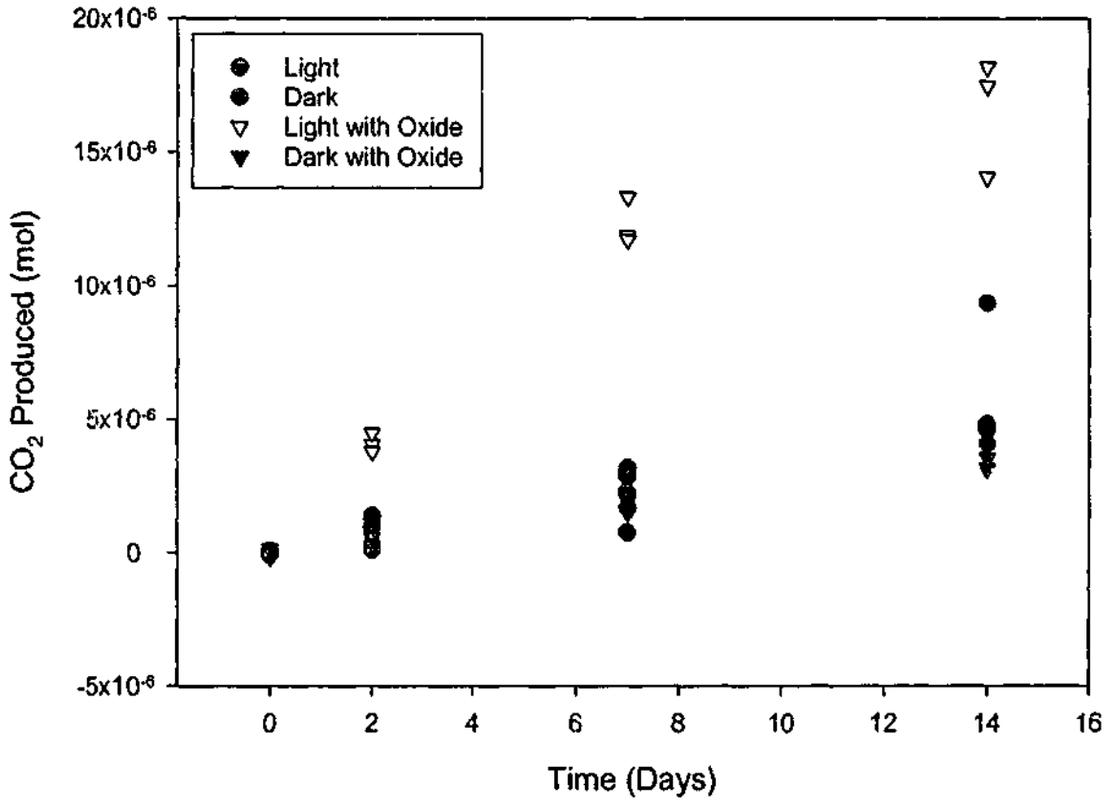

Figure 4.14 Photochemical carbon dioxide production from sunlight irradiated leachate.

The changes to the absorbance of the samples indicate definite photobleaching in the light-exposed samples in both the presence and absence of iron oxide (Figure 4.15). The dark controls remain relatively unchanged at each of the measured wavelengths while the absorbance of the light-exposed samples declines significantly at each of the wavelengths. After 14 days of sunlight exposure, photobleaching in the light-exposed treatment without added iron oxide had reduced the absorbance at 200 nm to 50 (± 2) % of the initial absorbance, while the dark controls retained 99.5 (± 0.4) % of the initial absorbance. In the samples with added iron oxide the A_{200} of the light exposed sample was 24 (± 6)% of the initial and the dark treatment retained 82.6 (±

0.6)% of the initial absorbance at that wavelength. The results at 250 nm were similar, the light-exposed sample had an A_{250} that was 48 (± 1)% of the initial, the A_{250} for the dark control was 107 (± 0.2)% of the initial, the light-with-oxide treatment was 30 (± 5)% of the initial and the dark-with-oxide treatment was 84 (± 2)% of the initial. At 300 nm, the A_{300} for the light-exposed treatment was 41.1 (± 0.8)% of the initial, the dark treatment was 97.0 (± 0.8)% of the initial, the light-with-oxide treatment was 31 (± 3)% of the initial and the corresponding dark treatment was 90 (± 3)% of the initial absorbance. As was observed in the previous experiment, the photobleaching was fairly uniform across these wavelengths and did not indicate a significant change in the ratio of low molecular weight to high molecular weight molecules.

The change to sample pH followed a similar trend to the previous experiments. The initial samples without iron oxide had a pH of 5.24, and those with added oxide had a pH of 5.2 (± 0.1). For the first week, all treatments except the light-exposed (without added oxide) remained within error of the initial measurements. In the light-exposed samples, however, the pH fell to 4.9 (± 0.2) after two days and 4.70 (± 0.03) after seven days. At the end of the experiment, samples from this treatment had an average pH of 4.66 (± 0.06), while the dark-control had a pH of 5.06 (± 0.01), the dark treatment with added oxide had a pH of 4.89 (± 0.04) and the light-exposed with added oxide had a pH of 5.18 (± 0.2). The light-exposed treatment had a pH that was significantly lower than the other treatments, suggesting the formation of carboxylate functional groups. The higher pH of the light-exposed treatment to which amorphous iron oxide had been added, coupled with the higher CO_2 production in those samples, supports the hypothesis that interactions between the oxide and the carboxylate groups catalyses the photodegradation of the carboxylates to form carbon dioxide.

The use of HPLC for organic acid analysis produced mixed results (Figure 4.16). The first graph (a) illustrates the chromatograms generated by elution of the initial leachate samples, with and without added iron oxide. The results are quite similar and show that centrifugation of the sample under acidic conditions, to settle the oxide does not remove key components of the leachate from the analysis. The broad peaks eluting at sixteen (IV) and twenty-one (V) minutes have similar elution times to formic and acetic acid, respectively. Definite identification of these and the other peaks was not possible. The second graph (b) represents the chromatograms of a selection of samples

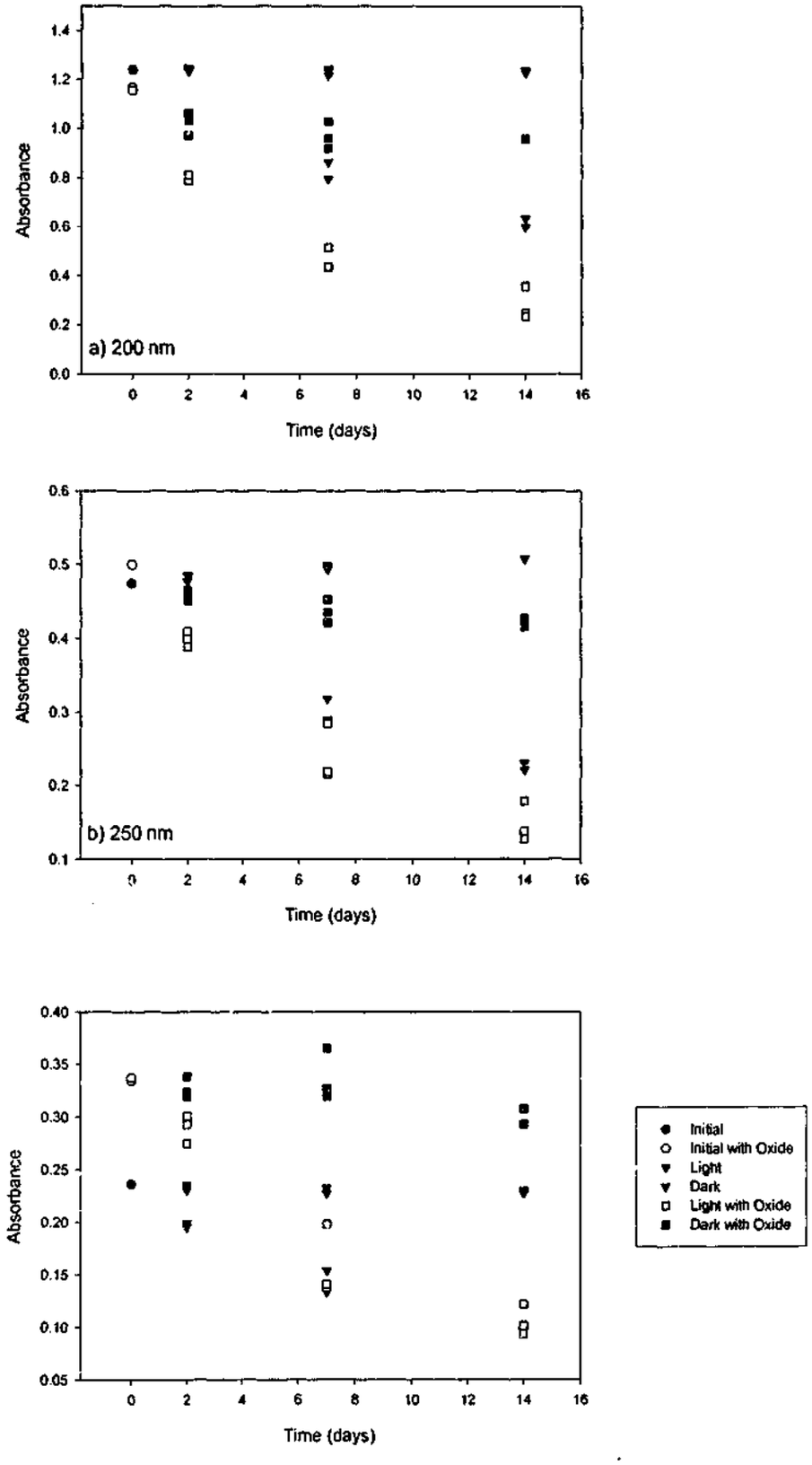

Figure 4.15 Changes to the absorbance of the leachate at (a) 200 nm, (b) 250 nm and (c) 300 nm with time during the pool-based irradiation.

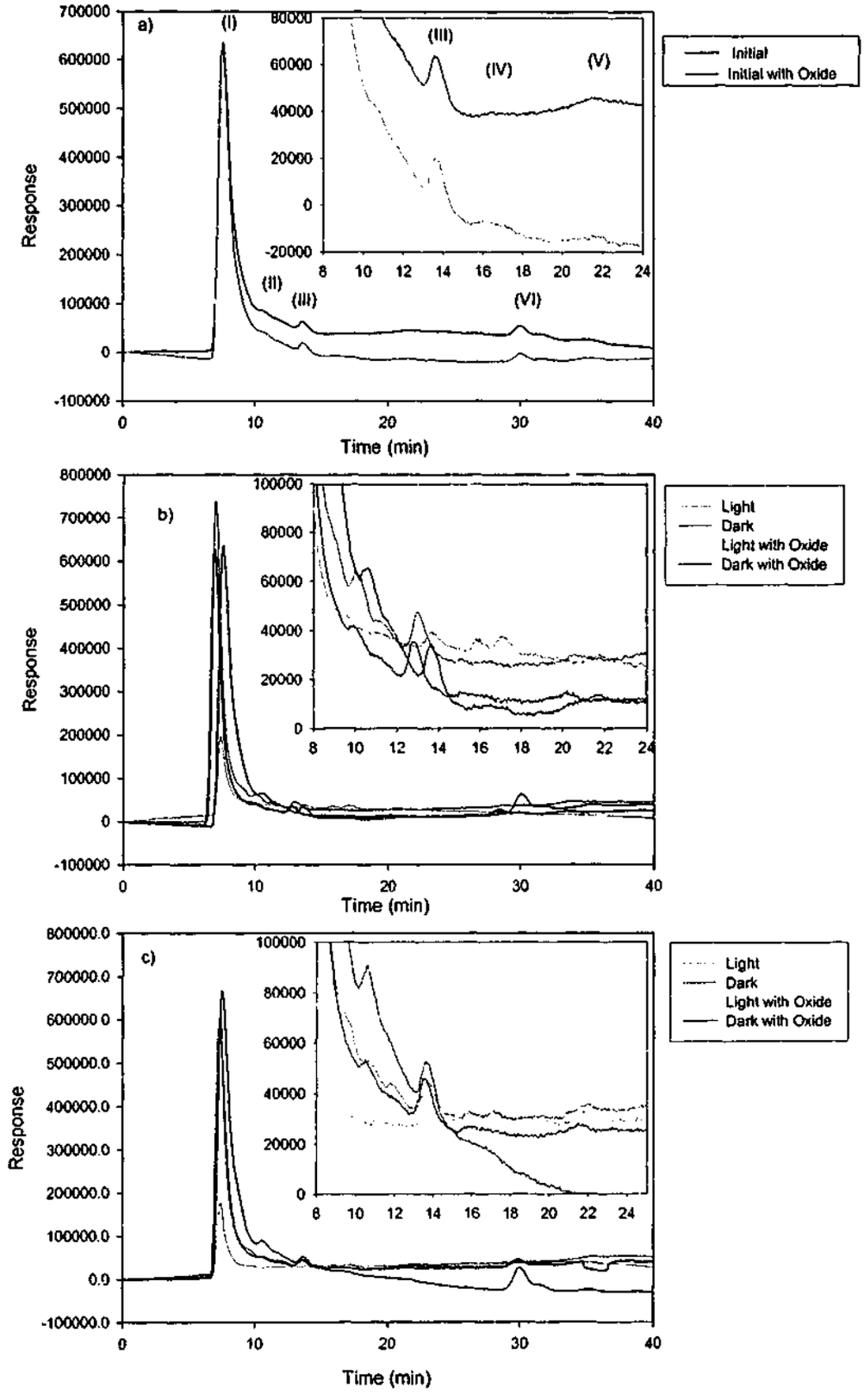

Figure 4.16 Chromatograms generated by HPLC analysis for the photochemical production of organic acids from leachate. Chromatograms are example results from initial (a), one week (b) and two week (c) samples.

after one week of sunlight exposure. The first notable feature of this graph is the dramatic reduction in peak (I), indicating a significant loss of starting material. While the two dark controls retained the basic features of the initial chromatograms (with the exception that the shoulder peak (II) is a little more pronounced, the light-exposed treatments have undergone some changes. Without additional iron oxide, the light-exposed treatment has lost peak (VI) and gained an extra shoulder at peak (II). With the addition of iron oxide the undefined band at (IV) had become two well-defined peaks (which co-elute with succinic and formic acid). After two weeks of sunlight exposure (c), these two peaks are present in both of the light-exposed treatments to the same extent. The degradation of peak (II) is complete in the light-exposed sample with added iron oxide, and has also occurred to some extent in the corresponding dark-control and the light-exposed treatment without added iron oxide. There is also slightly improved definition of peak (V) in these samples. In this final chromatogram the new peak between (II) and (III) co-elutes with citrate, (III) co-elutes with malate, the two following peaks again co-elute with succinate and formate and peak (V) co-elutes with acetate. Confirmation of the identity of the peaks would require further analysis, using different techniques, as co-elution does not necessarily provide identification. However, citrate, acetate, formate and other fatty acids have previously been observed following photodegradation of macrophyte leachate (Wetzel et al. 1995) and was thought to be a result of the oxidation of the side-chains of lignin-based macromolecules. Succinic acid has also been observed in irradiated lake water (Bertilsson and Allard 1996). Quantitative analysis of the organic acid results was not undertaken for a number of reasons: most of the chromatograms had wandering baselines or low signal-to-noise ratios, and definite identification of peaks was not possible. However, to give an indication of concentration, the peak at 17 minutes in graph (c) is of a similar size to a peak which corresponds to a concentration of 2×10^{-5} M formate. If these results are considered in comparison to the pH changes in the sample, it is clear that the decline in pH in the light-exposed sample (which was not present in the light-exposed with added iron oxide treatment) was not a result of the production of low-molecular-weight organic acids, as these were not evident in the chromatogram after a week of sunlight exposure. It is more likely that the addition of carboxylic acid groups to DOM macromolecules was responsible for the drop in pH.

The rapid destruction of the starting material in the light-exposed sample with added iron oxide is likely the reason why this pH reduction was not observed in this treatment.

The changes to the 3-D fluorescence spectra (Figure 4.17) of the samples were similar to those observed in the previous experiments, although the merging of peaks was not as pronounced in this experiment. After fourteen days, the two initial peaks were still present in the light-exposed treatment, but reduced in intensity and covering a much smaller region of the spectrum compared to both the initial sample and the dark control. This suggests the destruction of a portion of the fluorescing structures- leading to a change in intensity- without the formation of structures which fluoresce at different wavelengths. The smaller peak areas also suggest that the mixture of fluorescent structures is less diverse than in the initial samples, leading to a smaller range of possible energy level transitions that produced the fluorescence. The samples with added iron oxide that were exposed to sunlight had more significant changes in their fluorescent properties. In these samples the two peaks merge into one peak of reduced intensity and substantially reduced area. In the corresponding dark treatment the two peaks were still present, but beginning to join to form a large band. These results suggest that the presence of iron oxide catalyses not only the destruction of carboxylate groups, but also structures responsible for the fluorescence of the leachate (likely to be aromatic in nature).

This experiment demonstrated that the photochemical degradation of dissolved leachate can be an important process in the presence of sunlight. The photochemical production of CO_2 in the absence of iron oxide could not be determined conclusively, but the effect of photochemical reactions was evident in the photobleaching and pH reduction in this sample as well as the generation of small quantities of low-molecular-weight organic acids. The catalytic effect of amorphous iron oxide addition was again observed, particularly in relation to CO_2 generation and the consumption of the starting material (as observed in the HPLC analysis). It would appear that the presence of iron oxide both increases the rate of carbon dioxide production and reduces the lowering of pH relative to the light-exposed treatment without added iron oxide, supporting the theory that the interaction occurs via the carboxylate groups. The changes to the fluorescence and absorbance characteristics of the bulk DOM indicated that the photochemical reactions were also causing modification to the structure of the remaining organic matter.

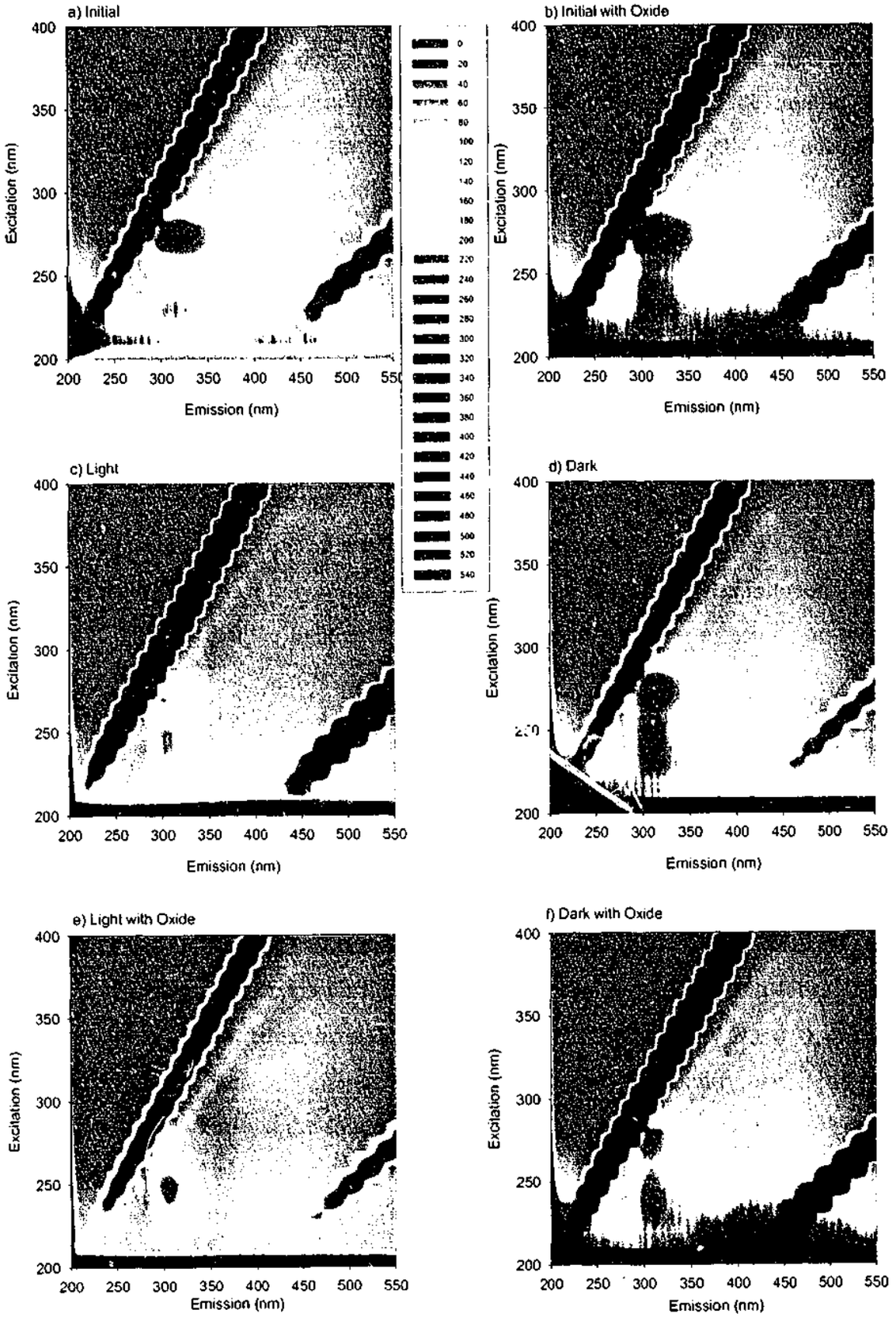

Figure 4.17 Three-dimensional fluorescence spectra of leachate from initial (a, b) and two-week (c-f) samples during the pool-based irradiation experiment.

4.3.3 Irradiation of Billabong water- pool based cooling.

This experiment was designed to examine the photodegradation of aged DOM under similar environmental conditions to those in the previous leachate experiment. This experiment was conducted for one week instead of two to ensure that an adequate number of replicates could be sampled on each occasion (breakages had resulted in a smaller number of tubes to work with). Differences between treatments became apparent within seven days in the previous experiments, so samples in this experiment were taken after two and seven days of sunlight exposure. The sunlight exposure during this experiment (Figure 4.18) was slightly lower than over the same time-frame in the previous experiment, with only one day exceeding 2000 μmol photons m^{-2} s^{-1}. The data for March 9th does not necessarily reflect the actual sunlight exposure, due to interference with the instrument. The instrument was re-set at approximately 10:20 on the tenth. The temperature profile of the pool water over this period (data not shown) indicated that the weather conditions on the 9th were the same as on the following four days, so it is likely that the light data was also consistent with that measured on those days.

Carbon dioxide production in these experiments displayed an unusual pattern (Figure 4.19). The CO_2 in each tube increased, with the largest increase being in the light-exposed samples with added iron oxide. However, the smallest increase after seven days was actually in the light-exposed treatment where no iron oxide had been added. This was not the case two days into the experiment, this treatment had actually been one of the higher CO_2 producers. Close inspection of the raw data indicated that the pH had a strong influence on the calculated increase in CO_2 in each tube. This experiment was conducted at the natural pH of the billabong water (7.2 ± 0.1), and in this region, small changes in pH cause large changes in the solubility of CO_2 in the water. A slight decrease in the solution pH in the light-exposed samples without added oxide (average final pH of 6.9 ± 0.1) reduced the calculated CO_2 results substantially, and perhaps inaccurately if the system was not in equilibrium. The pH measurements in all the experiments with billabong water were recorded to an accuracy of one decimal place, as the readings tended to fluctuate in these solutions, even after cleaning and calibration of the pH meter. The possibility of these solutions not being in equilibrium, or the pH measurements being insufficiently accurate makes further interpretation of the CO_2 results inappropriate.

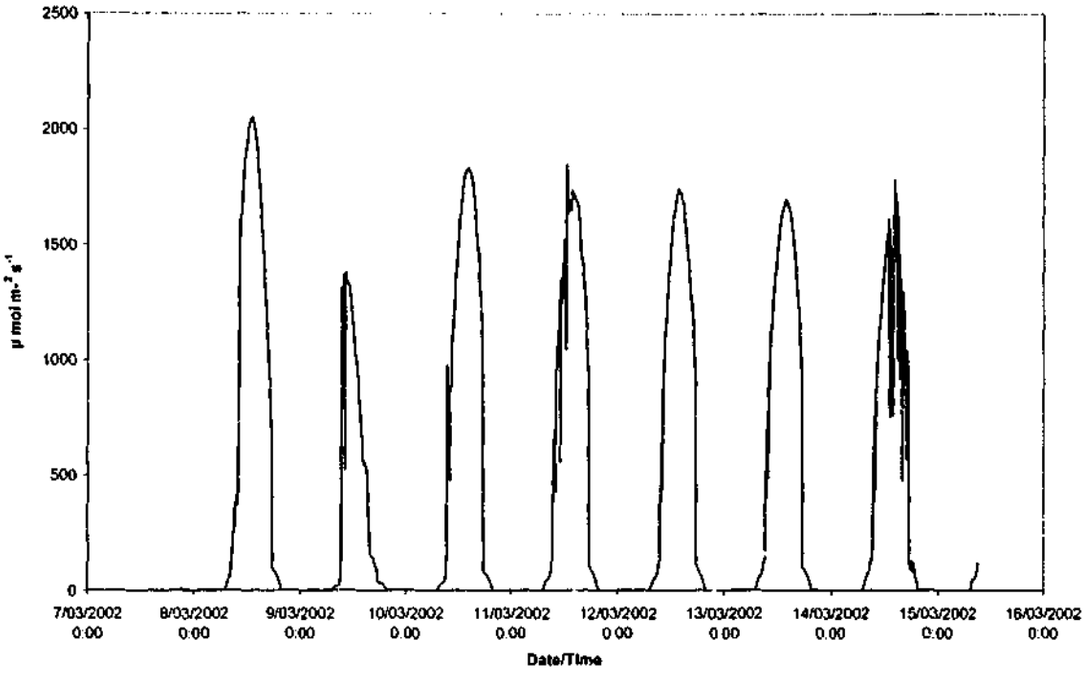

Figure 4.18 Incident light intensity during the period of the billabong water irradiation.

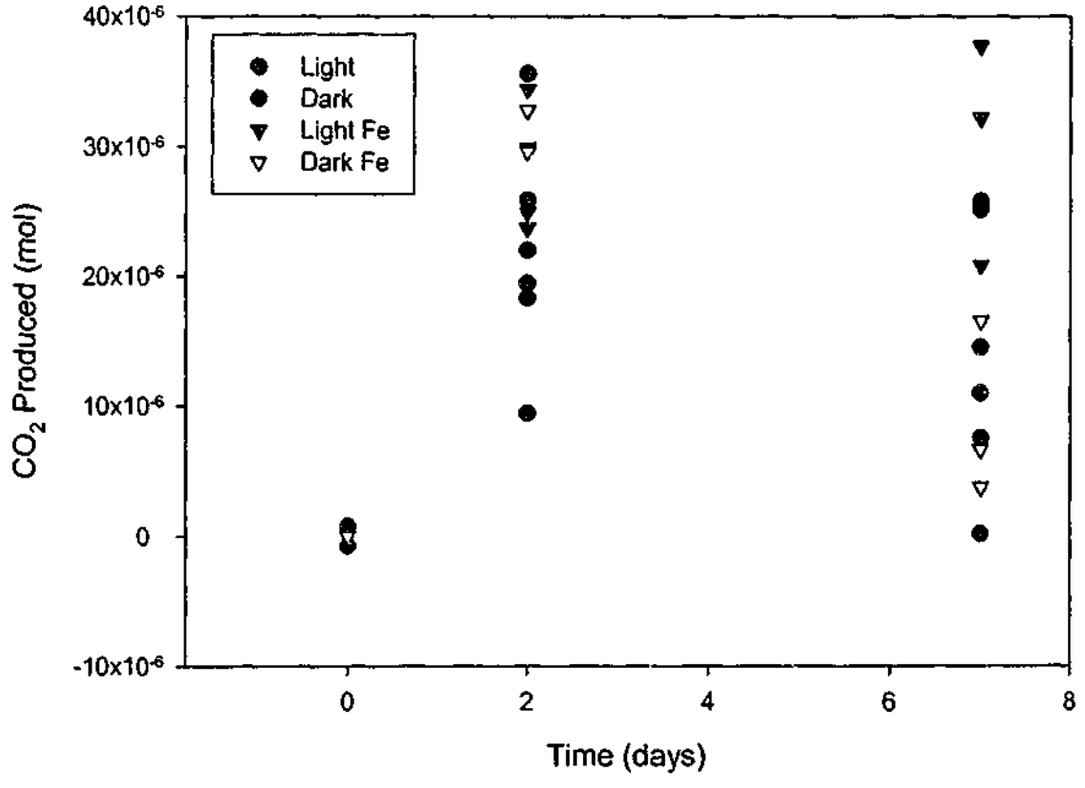

Figure 4.19 Photochemical CO_2 production during sunlight irradiation of billabong water.

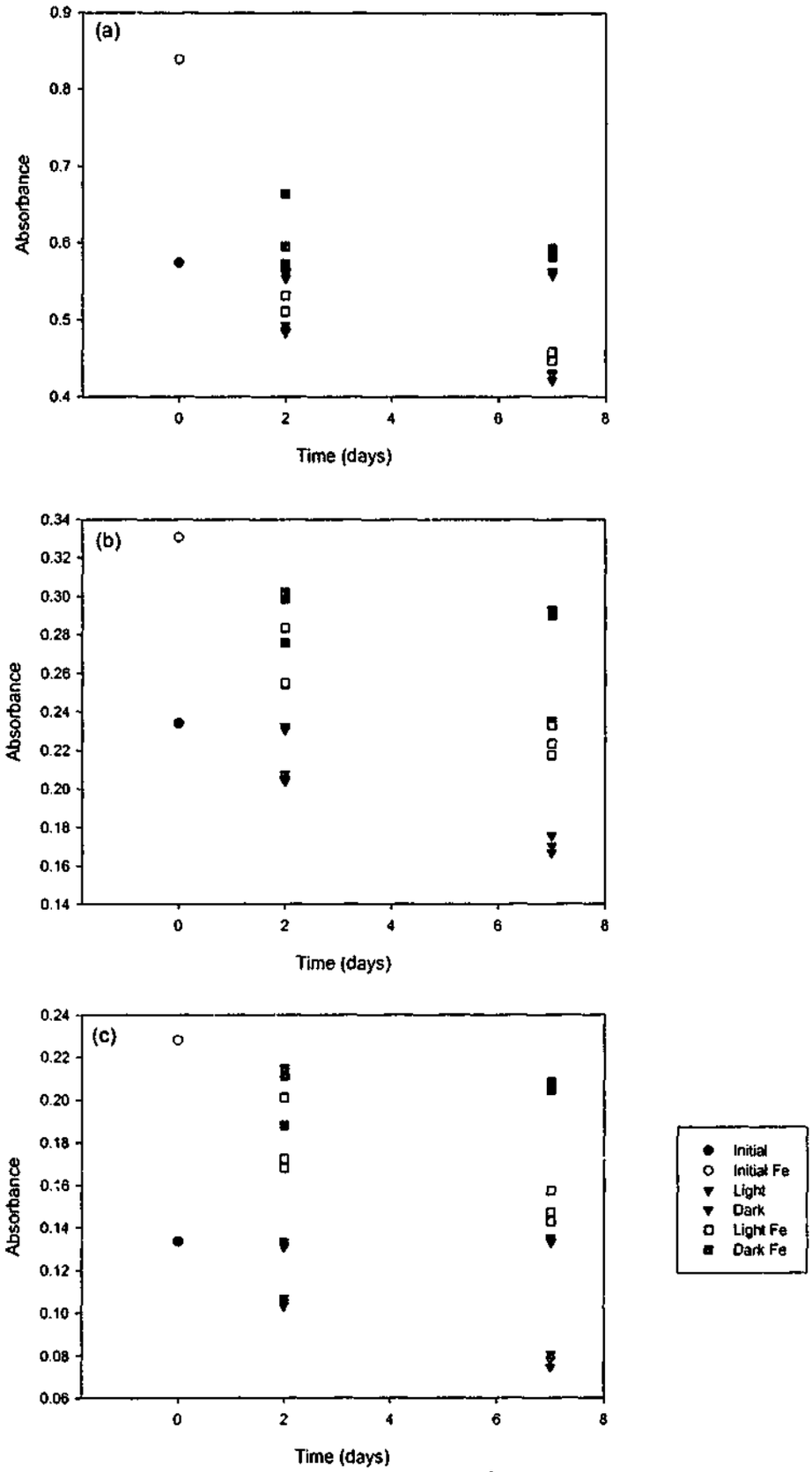

Figure 4.20 Changes to the absorbance of billabong water samples at (a) 200 nm, (b) 250 nm and (c) 300 nm during the sunlight irradiation of billabong water.

The changes to the absorbance of the samples (Figure 4.20) indicate a different trend for billabong water compared to the leachate used in the previous experiments. Photobleaching effects were evident in the light-exposed treatments (both with and without added iron oxide) after only two days. After seven days the photobleaching was quite significant at all three of the observed wavelengths. The absorbance at 200 nm had declined to 74.6 (± 0.9) % of the initial value in the light-exposed sample without added oxide, but the dark-control retained 97.8 (± 0.4) % of the initial absorbance. The decline was even larger in the light-exposed samples with added iron oxide, where the final absorbance was only 54.1 (± 0.7) % of the initial and the dark control was 70.0 (± 0.7) %. At 250 nm the samples without added oxide underwent similar levels of photobleaching, retaining 73 (± 2) % and 100.5 (± 0.4) % in the light and dark samples, respectively. In the samples with added iron oxide the loss of absorbance was slightly less: 68 (± 2) % and 88.0 (± 0.3) % for the light and dark samples, respectively. At 300 nm the photobleaching of the light-exposed sample without added iron oxide was more pronounced, with only 58 (± 2)% of the initial absorbance remaining, while the dark-control remained unchanged. This suggests that, unlike the previous experiment using leachate, there was some change in the molecular weight distribution occurring, or at least, destruction of large conjugated bond structures was occurring preferentially. In samples with added iron oxide however, the light-exposed samples underwent photobleaching to the same extent at 300 nm as at 250 nm, retaining 65 (± 3) %. The change in absorbance of the dark control was also similar to that observed at 250 nm, retaining 90.8 (± 0.9) %. A number of notable features can be observed in Figure 4.20: in samples without added iron oxide, the dark-control samples do not change their absorbance at any of the wavelengths over the period of the experiment but the light-exposed treatment has diminished absorbance at all three wavelengths. This is consistent with the theory that the changes are photochemical and that the larger conjugated systems are more prone to photochemical damage. In contrast, some reduction in absorbance was observed in the dark-control samples in the treatments with added iron oxide. This reduction in absorbance was most notable at 200 nm and may indicate a change in the overall properties of the mixture as the organic matter adsorbs to the surface of the particle, perhaps a change in the scattering. The difference between the light and dark treatments when oxide has been added gives a better indication of the photobleaching. In this case the A_{200} is 77 (± 1) % of the

control, the A_{250} is 77 (± 3) % of the control and the A_{300} is 72 (± 3) % of the control, suggesting photobleaching in this case is reasonably uniform across these wavelengths.

Table 4.2 Average Total Organic Carbon results for each treatment, at each sampling time (results are average of n samples)

Time (days)	Treatment	TOC (mg C L^{-1})	Standard Deviation	n
0	Initial	9.2	-	1
0	Initial + Fe	6.8	-	1
2	Light	5.8	0.2	3
2	Dark	6.0	0.2	3
2	Light + Fe	7.1	1.2	3
2	Dark + Fe	8.9	1.6	3
7	Light	6.8	0.9	3
7	Dark	5.8	0.4	3
7	Light + Fe	6.4	0.6	3
7	Dark + Fe	6.4	-	2

The concentration of total organic carbon in the samples was quite variable (Table 4.2). Clear trends are not evident in the results, partially as a result of the relatively large standard deviation for some of the values. A number of factors may have contributed to the high standard deviations. The highest concentration of TOC found in any sample was 10.2 mgC/L, which in a 20 mL sample, only represents 0.2 mg of carbon. At these levels, contamination of the samples is quite difficult to prevent, the most likely source being the lip of the quartz tube as the samples were poured out of the tube at the end of the experiments.

Photochemical production of low-molecular weight organic acids was observed after a week of sunlight exposure (Figure 4.21). The initial chromatograms of the billabong water (a) were considerably simpler than for the leachate. The initial chromatograms consist of two peaks - the unretained material and a small peak at approximately 20.5 minutes (co-elutes with acetate). As simple organic acids are likely to be rapidly consumed in aquatic environments, the relatively featureless chromatograms are not surprising. At the end of a week, changes had occurred in all but the dark control samples without added iron oxide (b). The peak of unretained material was reduced slightly in the dark-control with added iron oxide, but it was noticeably reduced in the light-exposed treatment and substantially reduced in the light-exposed treatment to which iron oxide had been added. No new peaks were formed in

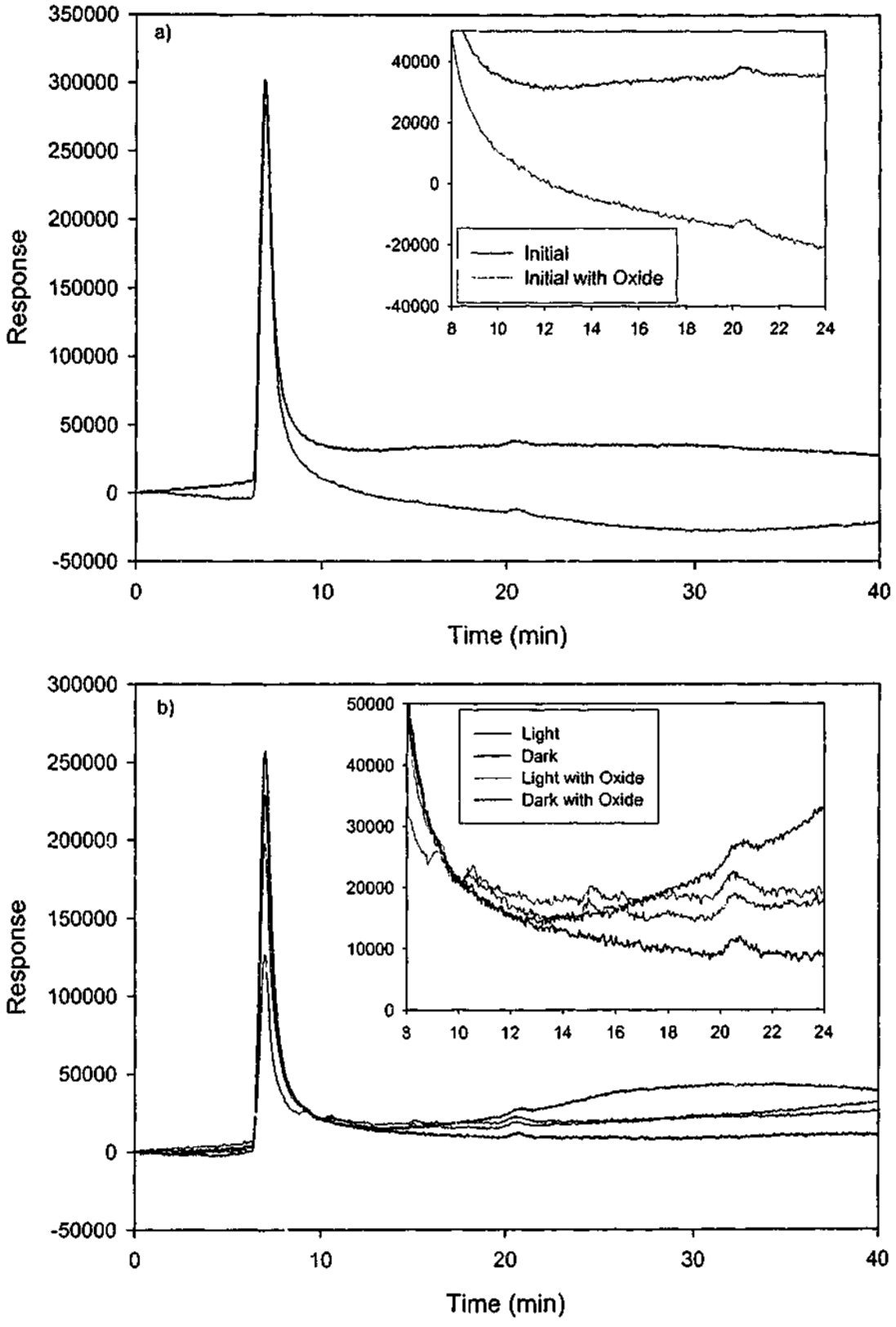

Figure 4.21 Example HPLC results for the analysis of organic acids in billabong water initially (a) and after one week (b).

either of the control treatments, but traces of peaks were observed in the two light-exposed treatments. The peaks at 10, 15 and 16 minutes co-elute with citric, succinic and formic acid respectively, and the later peak at 20.5 minutes still corresponds with the acetate peak. These peaks were close to the limit of detection, and of similar size to a peak produced by 2 x 10^{-5} M formate. An additional peak in the light-exposed treatment with added iron oxide occurs at 9 minutes and may be oxalic acid. Traces of this peak occur as a shoulder in the light-exposed treatment. Again, conclusive identification of the new compounds was not possible with the available equipment.

The use of 3-D fluorescence spectroscopy in this experiment provided valuable information on the organic matter that remained after the photochemical reactions had taken place and differences between the initial billabong water and the leaf leachate used in the previous experiment. The changes to the fluorescence of the billabong water samples suggested much more significant changes to the bulk properties of the organic matter in these samples, compared to the leachate experiments (Figure 4.22). To begin with, the initial spectrum of the billabong water (a) has broad peaks, displaced to longer emission wavelengths than the leachate samples were. Slight differences exist between the initial samples with (b) and without (a) added iron oxide, most likely due to some fluorescence quenching in molecules adsorbed to the particle surfaces. Excitation of these molecules also occurs over a wider range of wavelengths than was the case in the leachate. Two days into the experiment, changes had occurred to all of the samples, including the controls. Each graph represents one of three replicates, but replicate samples were quite similar. All four treatments contained three peaks instead of the initial two (although traces of the new peak at (Em 300, Ex 240) had been present in the initial sample to which iron oxide had been added). The peak in this region represents molecules with a much larger energy gap between the lowest excited molecular orbital and the ground state, likely to be molecules of simpler bonding arrangement. The formation of this peak in both of the control samples indicates that some changes to the organic matter were occurring through non-photochemical processes. The intensity of the peak at (Em 410, Ex 240) also increased, suggesting that fluorescence of energy absorbed in the 220-250 nm region was becoming more important. In contrast, fluorescence induced by light in the 280-350 nm range became less important in all but the control without added iron oxide. The reactions responsible for this change appear to include a photochemical mechanism and are enhanced in the presence of both light

and iron oxide. The fluorescence in this region is associated with humic fluorescence (Coble 1996) and the reduction in both peak intensity and area suggests diminished humification of the samples, leading to a simpler bonding structure. After seven days (g-j) the fluorescence spectra of the control samples without added iron oxide have diminished slightly in intensity, but the overall characteristics remain unchanged. The dark control with added iron oxide had also reduced intensity, especially in the (Em 410 nm, Ex 330 nm) peak. This peak had gone from the spectrum of the light-with-oxide treatment and almost gone from the light-without-oxide treatment. In these two treatments the peak at (Em 410 nm, Ex 240 nm) had also diminished substantially.

Over the course of the experiment, the changes in fluorescence indicated a shift from humic-like fluorescence to protein-like fluorescence in the light-exposed samples (Coble 1996). The final peaks covered a smaller area of the Emission-Excitation plane, indicating that the remaining molecules that were responsible for fluorescence were more similar to each other than in the initial samples (i.e. the energy gaps between the ground and excited states were quite similar). The broadening of peaks in the dark controls and all the treatments at the two-day sampling suggest that changes were occurring that lead to a larger variety of possible transitions (i.e. a bigger diversity of bonding arrangements). In summary, photochemical degradation leads to a fluorescent signature that indicates a reduction in large aromatic and conjugated systems and indicates a higher degree of similarity between the molecules than had been present in the initial sample. Aging of the organic matter in the dark results in a more complex mixture of structures, retaining the aromatic and conjugated signatures, but also increasing the signature of simpler systems. Aging in the presence of iron oxide also lead to a wider mix bonding arrangements, but also enhances the degradation of some of the more complex structures. The use of three-dimensional fluorescence spectroscopy has not been widespread in the field of environmental photochemistry, but these results demonstrate the potential of the technique. The fluorescence spectra provide important data on the changes brought about to the dissolved organic matter that remains in solution after the photochemical reactions have taken place. Dissolved organic matter is a complex mixture of compounds and it was impossible to completely characterise either the starting compounds or the products, but this technique provides important clues to the structural characteristics of the compounds which make up the mixture.

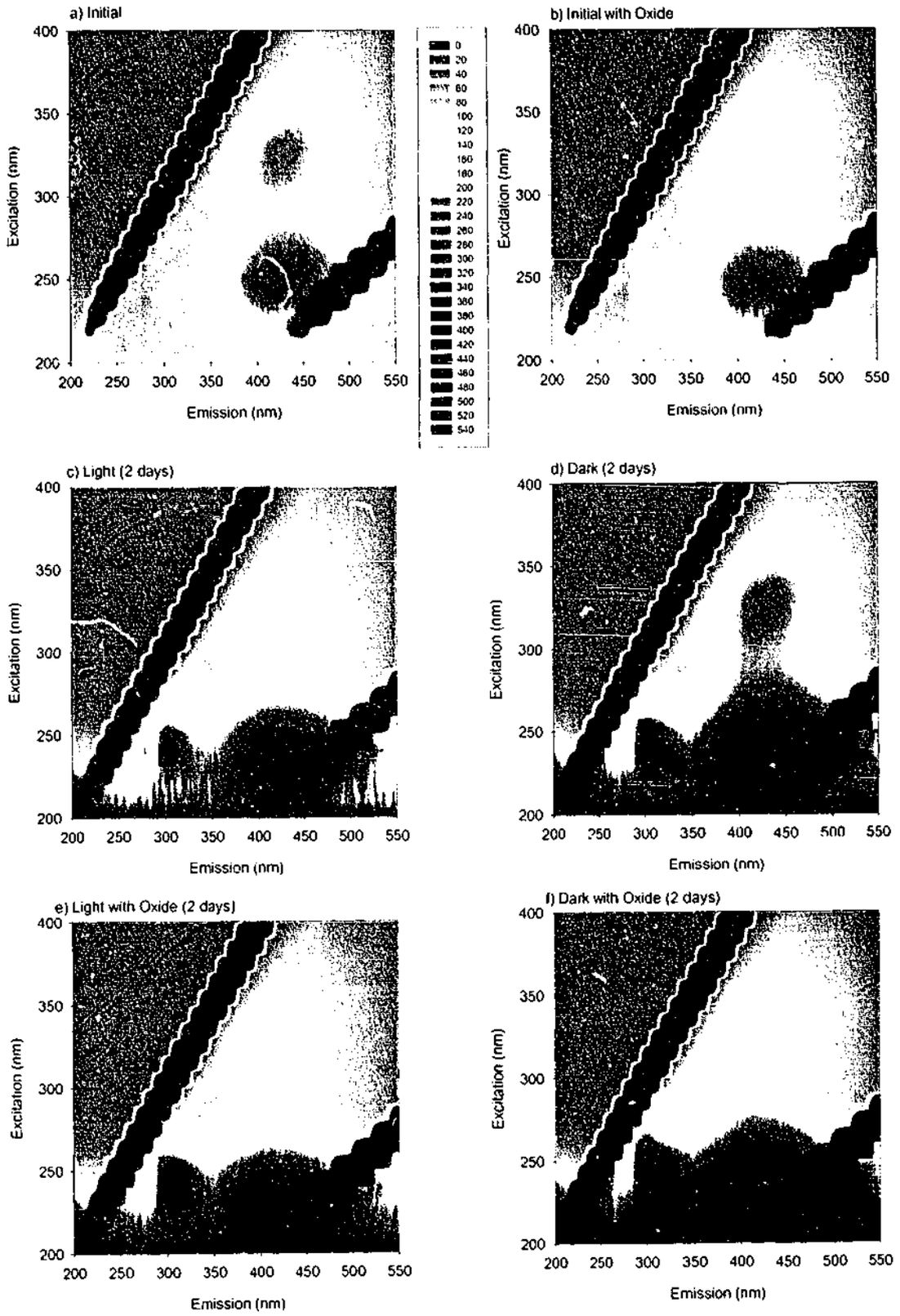

Figure 4.22 Changes to the three-dimensional fluorescence spectra of billabong water. Scans include the initial spectra (a, b), spectra two days into the experiment (c-f) and after seven days (g-j).

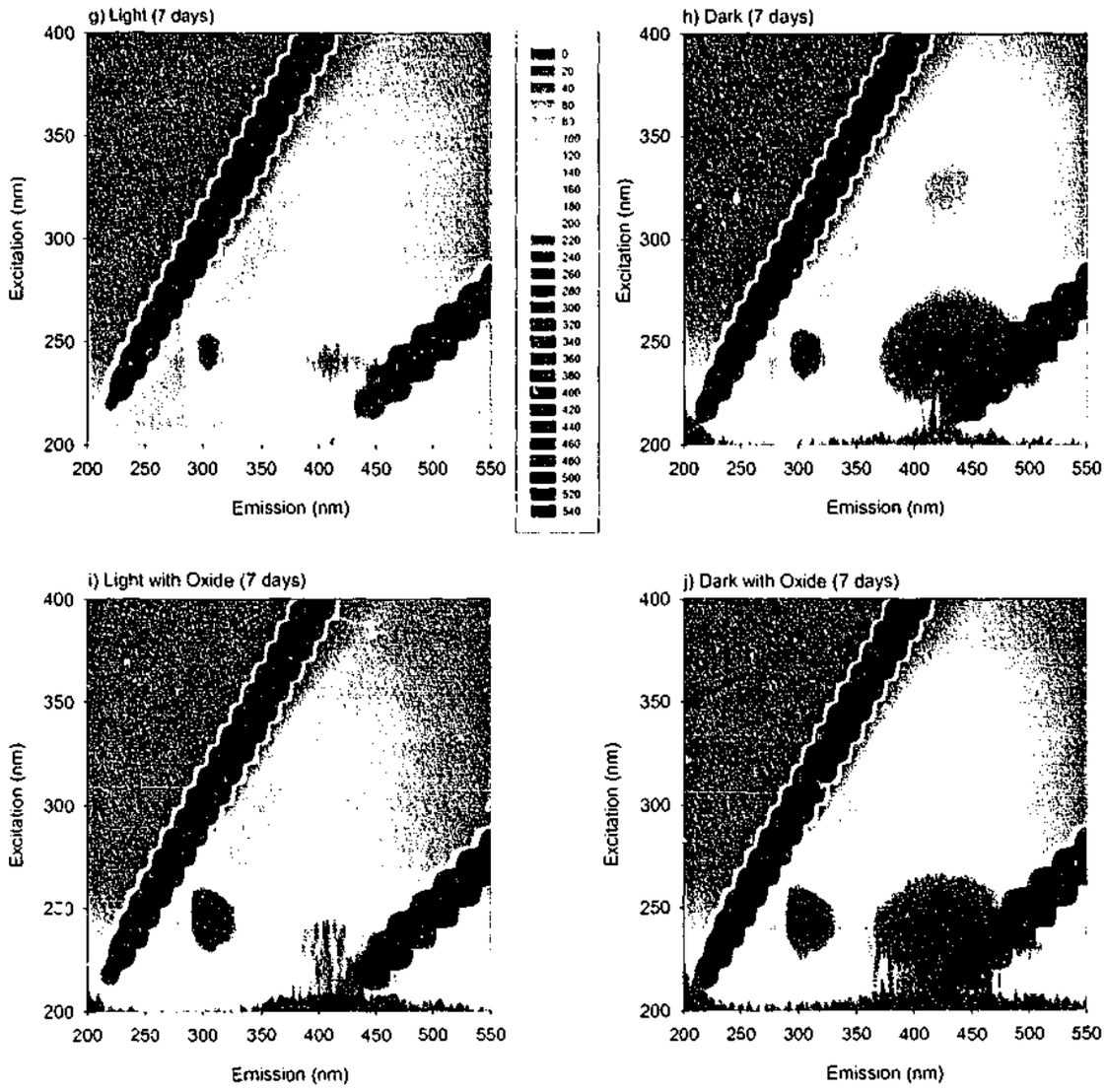

Figure 4.22 (cont.)

The photochemical degradation of billabong water was enhanced by the presence of amorphous iron oxide, and some reactions between the iron oxide and the organic matter also occurred in the dark. In a similar manner to the experiments with leachate, the iron oxide was found to increase the rate of CO_2 production and also the photobleaching and fluorescence bleaching.

4.4 Conclusions

These experiments indicate that the addition of amorphous iron oxide can increase the rate of degradation of both leachate and billabong water when irradiated with natural light. The billabong water samples are likely to contain a mixture of fresh and aged dissolved organic matter and showed considerable capacity to be modified. The modifications to the organic matter that remained in solution differed according to the source of the organic matter. The use of 3-D fluorescence spectroscopy has suggested that the humic component of the billabong DOM was particularly susceptible to photochemical degradation. A peak shift from emission maxima in the 420-450 nm region to the 300-350 nm region, observed in the billabong water samples, is indicative of a shift from a humic-like system to an aromatic protein-like system (Coble 1996), also implying that the leachate fluorescence is in the protein-like region. The bleaching of both leachate and billabong water suggests that environmental photochemical reactions are capable of destroying aromatic compounds. So, in addition to the evidence for photochemical oxygen consumption and carbon dioxide production described in previous chapters, this work suggests that photochemical production of low molecular weight compounds (likely to be organic acids) and destruction of conjugated and aromatic molecules occurs in environmental reactions.

4.5 References

Bertilsson, S., and B. Allard. 1996. Sequential photochemical and microbial degradation of refractory dissolved organic matter in a humic freshwater system. Arch. Hydrobiol. Spec. Issues Advanc. Limnol. **48**:133-141.

Bertilsson, S., and S. Bergh. 1999. Photochemical reactivity of XAD-4 and XAD-8 adsorbable dissolved organic compounds from humic waters. Chemosphere **39**:2289-2300.

Boon, P., J. Frankenberg, T. Hillman, R. Oliver, and R. Shiel. 1990. Billabongs. Pages 183-200 *in* N. Mackay and D. Eastburn, editors. The Murray. Murray Darling Basin Commission, Canberra.

Coble, P. G. 1996. Characterization of marine and terrestrial DOM in seawater using excitation-emission matrix spectroscopy. Mar. Chem. **51**:325-346.

Schmitt-Kopplin, P., N. Hertkorn, H.-R. Schulten, and A. Kettrup. 1998. Structural changes in a dissolved soil humic acid during photochemical degradation processes under O_2 and N_2 atmosphere. Environ. Sci. Technol. **32**:2531-2541.

Wetzel, R. G., P. G. Hatcher, and T. S. Bianchi. 1995. Natural photolysis by ultraviolet irradiance of recalcitrant dissolved organic matter to simple substrates for rapid bacterial metabolism. Limnol. Oceanogr. **40**:1369-1380.

5 Photochemically Induced Changes to the Bioavailability of Dissolved Organic Matter

5.1 Introduction

The work described in the previous chapters established that photochemical reactions, both in the presence and absence of iron oxides, contribute to the degradation of dissolved organic matter in aquatic solutions. The photochemical reactions result in some loss of carbon from the aquatic ecosystem system (in the form of carbon dioxide and carbon monoxide gases), but also cause modification of the remaining dissolved organic matter. The composition of the altered DOM includes low-molecular-weight organic acids and, in the case of billabong water, a substantial loss of humic-like structure, generating a mixture of more simple organic molecules. As microbes represent a major pathway for DOC to re-enter food webs, assessing the importance of photochemical reactions to the cycling of carbon in aquatic ecosystems also needs to take into account the impact of these changes on the subsequent microbial processing of the remaining dissolved organic matter.

Changes to the bioavailability of dissolved organic matter following photochemical reactions have been widely studied with highly variable results. The effects have been found to vary with the source of the organic matter and the criteria used to measure bioavailability (Anesio et al. 2000, Farjalla et al. 2001, Obernosterer et al. 2001). In some studies DOM availability increased (Lindell et al. 1995, Wetzel et al. 1995), however decreases in bioavailability have also been found (Obernosterer et al. 2001).

Given the variability in the literature reports, prediction of changes in bioavailability of DOM resulting from photochemical reactions cannot be accurately made at this time. This chapter will describe changes in DOC bioavailability associated with four of the photochemical degradation experiments described in the previous chapters. These experiments examine the effect of photochemical changes on the organic matter for billabong water and leachate in the presence and absence of added iron oxide. The effect of oxide-catalysed photochemical reactions on the bioavailability of dissolved organic matter has not been reported in the literature.

5.2 Methods

5.2.1 Preliminary Experiment

The first bioavailability experiment was an addition to the preliminary experiment described in Section 2.2.1. This experiment was predominantly intended to asses the methods of sample preparation, irradiation and the use of bacteria counts to measure changes in billabong water bioavailability. Samples were prepared as described in Section 2.2.1. In addition to the 2 L bottles of billabong water, 95 mL of filtered water was added to each of sixteen glass serum bottles (125 mL capacity) and capped with butyl rubber seals. Four additional bottles were prepared with filtered ultrapure (milli-Q) water as controls. Half of the bottles were wrapped in foil and all the bottles were irradiated alongside the 2 L bottles.

A bacterial inoculum was prepared from a fresh sample of billabong water, filtered through 35 μm gauze to remove larger particulate material. One mL of this inoculum was added to each of the ultrapure water samples and to four of the light-exposed and four of the dark-control bottles. All bottles were then incubated at 24 °C for 13 days. At the end of the incubation period 9 mL was preserved with 1 mL of formaldehyde to give a 4% (v/v) final concentration. Samples were stored at 4 °C until bacteria counts could be conducted. Absorbance measurements were also made on the remaining unfiltered liquid.

Bacterial numbers were estimated from direct counts made using epifluorescence spectroscopy. An acridine orange solution was prepared (1g/L) and 100 μL of this solution was added to 5 mL of bacterial sample in a Sartorius 25 mm filter set and left to stain for 10 minutes. The bacteria were then filtered onto a pre-blackened 0.2 μm polycarbonate filter under low vacuum. In samples where 5 mL introduced too many bacteria onto the slide, a smaller amount was used and made up to 5 mL with ultrapure water. The bacterial abundance in these samples was adjusted accordingly. Bacteria were counted at 1600 x magnification on a Zeiss microscope fitted with an Epifluorescence Condenser III RS and a Microscope Illuminator 100. As the distribution of bacteria on the slide was not uniform, seven fields of view (chosen at random) were counted from each sample to ensure that in excess of 500 bacteria were counted in the majority of samples.

5.2.2 Bioavailability of Billabong DOM- Irradiation in a Photochemical Reactor

An experiment was conducted using the irradiated and dark-control water produced during the experiment described in Section 2.2.2.1 (involving irradiation of summer billabong water samples). At the end of each of the four irradiation experiments (involving water samples from four consecutive days), bacterial cultures were prepared on the irradiated water and control water, which had been kept in a foil-wrapped bottle at 20 °C during the irradiation period. Twenty-five mL of solution was added to each sterile serum bottle, which was then sealed. On each day, three replicates of each of the following eight treatments were prepared:

- Light-exposed
- Light-exposed + P + N
- Light-exposed + bacteria
- Light-exposed + bacteria + P + N
- Dark-control
- Dark-control + P + N
- Dark-control + bacteria
- Dark-control + bacteria + P + N

Phosphorus and nitrogen were added as a sterile nutrient solution to give a final concentration of 9.5 mM NH_4^+ and 3.5 mM PO_4^{3-}. The bacterial inoculum was prepared by collecting the retentate from the 0.2 μm tangential flow filtration treatment of the initial water sample. The retentate was filtered through a Whatman GFC filter to remove the larger particles and 1 mL was added to each bottle. The bottles were incubated in the dark at 24 °C for 10 days, after which gas samples were removed and analysed using gas chromatography (method as described in 2.2.2.1) and 1 mL of 25% glutaraldehyde was added to the liquid to preserve the bacteria for bacterial counts (as described in 5.2.1).

5.2.3 Bioavailability of Leachate- Sunlight Irradiation

Bacterial cultures were prepared on leachate from the quartz tube irradiation experiment described in Section 4.2.3. A culture was prepared from each of the sampled quartz tubes after seven days or fourteen days of irradiation. These samples consisted of sunlight-irradiated leachate with and without amorphous iron oxide, and the

corresponding dark-control samples. Twenty-five mL of each sample was measured using a 50 mL autoclaved measuring cylinder and transferred into a sterile serum bottle. Nitrogen and phosphorus were added to give a final concentration of 9.5 mM NH_4^+ and 3.5 mM PO_4^{3-}. The pH was adjusted to 7 by addition of NaOH.

As these samples were to be prepared on different days, an inoculum was prepared in advance for use in all the cultures. A more concentrated leachate than normal was prepared by addition of 1 g of the powdered leaf material in 1 L of ultrapure (Milli-Q) water and left to leach for one hour. The extract was filtered (Whatman GFF), NH_4Cl was added to give a final concentration of 9.5 mM and the pH adjusted to 7.5. The extract was inoculated with 10 mL of GFF filtered water from Norman's Lagoon and incubated in the dark for seven days. The resulting culture was collected by centrifugation at 8700 x g. The bacterial pellet was resuspended in a total of 10 mL of 5 mM NaH_2PO_4 (pH of 7), and then divided between five 2 mL Eppendorf tubes. A bacterial pellet was collected in each tube by centrifugation at 13 000 rpm for 2 minutes. The liquid was removed and the pellets were frozen in their tubes until use (within 3 weeks). Immediately before use the pellet was thawed and resuspended in 2 mL of 9.5 mM NH_4Cl, 3.5 mM NaH_2PO_4. A 2 mL syringe was used to add 0.1 mL of inoculum to each culture. The experimental cultures were capped and incubated at 25 °C for nine days. The gas samples were taken and bacteria preserved for counts as described above. Bacteria were counted at a magnification of 1200 x on a Zeiss Axioskup 2 with a HBO 100 lamp.

5.2.4 Bioavailability of Billabong DOM- Sunlight Irradiation

This experiment was set up as described in 5.2.3, using the same frozen bacterial inoculum and water taken from each quartz tube at the end of the experiment described in Section 4.2.4.

5.3 Results and Discussion

5.3.1 Preliminary Experiment

A comparison of the absorbance at both 250 nm and 400 nm in each of the treatments provides evidence for photobleaching. In the treatments without added bacteria, the light-exposed samples had an absorbance at 250 nm (A_{250}) of 0.181 (± 0.004) and an absorbance at 400 nm (A_{400}) of 0.028 (± 0.001), while the dark-control treatment had an average A_{250} of 0.205 (± 0.005) and an A_{400} of 0.03ɔ ˎ. 0.002). In other words, the light controls retained 88 (± 3) % and 85 (± 6) % of the absorbance in the dark controls at 250 and 400 nm respectively.

In the treatments to which bacteria had been added after the irradiation, the light-exposed samples had an A_{250} of 0.171 (± 0.004) and an A_{400} of 0.0271 (± 0.0003) while the dark-control had an A_{250} of 0.199 (± 0.003) and an A_{400} of 0.031 (± 0.001). In this case the light-exposed treatment retained 86 (± 2) % and 87 (± 3) % of the A_{250} and A_{400} found in the dark-controls, respectively. In these experiments the addition of bacteria after irradiation produced no statistical difference in the bleaching of the light-exposed samples relative to the dark controls. The addition of the inoculum to the Milli-Q water samples resulted in an A_{250} of 0.016 (± 0.003) and an A_{400} of 0.0050 (± 0.0001) after the incubation period. This indicates that while the inoculum made only a 1% difference to the volume of the sample, the change in absorbance in the samples suggests the added organic matter constitutes approximately 10 % of the final organic matter (based on the A_{250}).

An increase in bacterial abundance was observed in the light-exposed treatment to which the billabong water inoculum had not been added (Figure 5.1). The use of bacterial counts to estimate carbon bioavailability in this experiment was affected by two factors: the addition of predators (e.g. protozoans) with the inoculum and the fact that the experimental design did not account for the possibility that other nutrients may become limiting. Each of the average values is accompanied by a wide margin of error, as would be expected for this type of experiment. The errors reflect variation in bacterial density on each individual slide, and variation between replicate samples. All the samples contained bacteria, indicating that the method of sterilization of the initial samples was not adequate, but this produced an interesting result. The treatment with the highest average bacterial concentration was the light-exposed treatment that did not

have added inoculum, indicating two features of this experiment. Despite the irradiation occurring through glass and thus reducing the exposure to UV light, the photochemical reactions increased the bioavailability of the organic matter, relative to the corresponding dark control. The higher average concentration of bacteria in this sample, relative to the light-exposed sample to which bacteria had been deliberately added, suggested that the addition of 35 μm filtered billabong water in low concentrations reduced the bacterial abundance. Examination of the water samples revealed protozoa in the inoculated samples. Some algal cells were found in samples from all treatments, but at extremely low numbers. The results from this experiment were confounded by the presence of predators, however, it is apparent that the photochemical degradation of billabong water can increase the bioavailability of the dissolved organic matter. This experiment did not determine if that increase was the result of changes to carbon, nitrogen or phosphorus bioavailability and further experiments were designed to assess the impact of photochemistry on the carbon bioavailability.

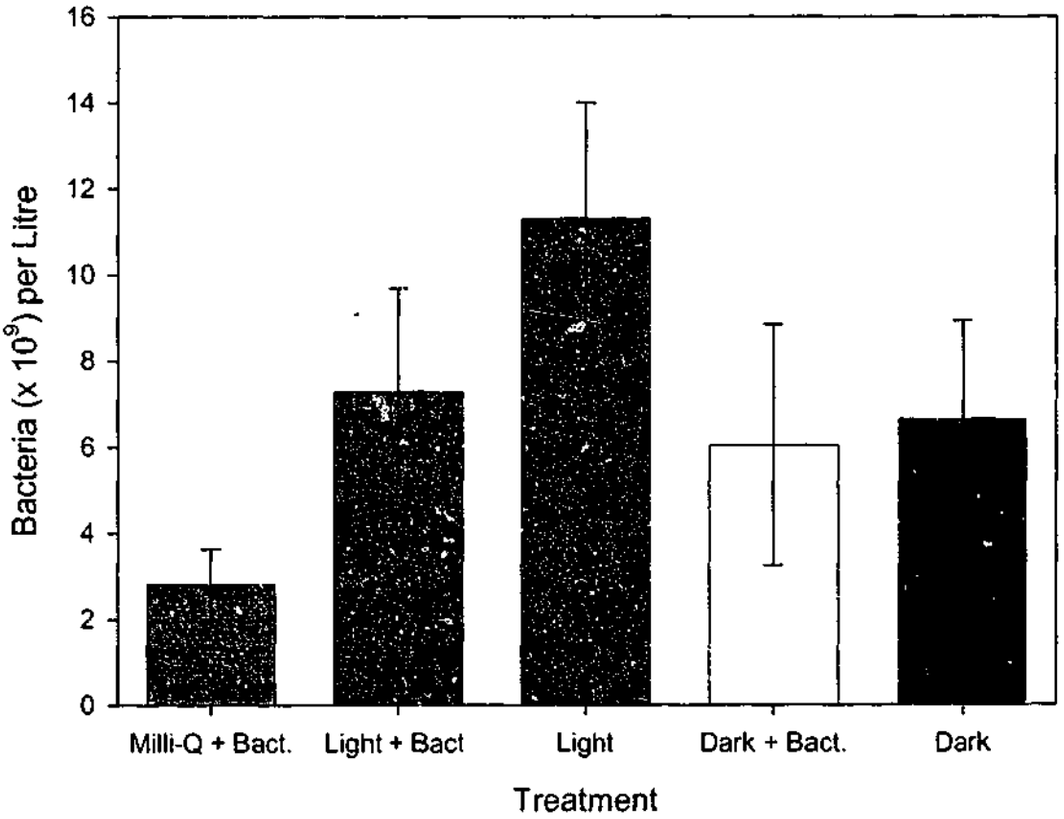

Figure 5.1 Average bacterial abundance in billabong water after irradiation experiment and incubation. Error bars indicate one standard deviation.

5.3.2 Bioavailability of Billabong DOM- Irradiation in a Photochemical Reactor

The production of CO_2 in the serum bottles suggests that photochemical degradation of the DOM increased the amount of organic carbon converted to CO_2 through bacterial respiration (Figure 5.2)*. For each of the four batches of water, the light-exposed sample with added bacteria and nutrients had the highest concentration of CO_2 in the headspace. This suggests that these waters are both carbon and nutrient limited as both modification of the organic matter and additional nutrients were required to maximise bacterial respiration. For each batch of water, the equivalent sample without added nutrients (LB) had lower levels of CO_2 in the headspace, but more CO_2 had been produced than in the corresponding dark control without added nutrients (DB). For each pair of treatments with and without added nutrients, the sample to which additional nutrients were added always had increased CO_2 concentrations, suggesting that each water sample was initially either N or P limited. Comparing the samples without added nutrients, we find that three of the treatments were equivalent to each other and did not vary between the water samples. The increased CO_2 in the light-exposed treatment with added bacteria suggests that the light exposure increased the bioavailability of the carbon to the bacteria, and also partially overcame the nutrient limitation. Comparing the samples with added nutrients, a similar pattern is observed, with the addition of a slight increase in CO_2 production in the dark-control with added bacteria.

These results then suggest that exposing billabong water to light has the potential to increase the bioavailability of the carbon, and also the bioavailability of nitrogen and/or phosphorus. Once the nutrient limitation is removed, the natural variability in carbon availability, photochemical reactivity or bacterial community also becomes apparent through the differences between water samples in the LBN treatment.

---

* To facilitate comparison between treatments, carbon dioxide concentration is expressed as percentage in the headspace rather than moles of CO_2, as the numbers are more easily visualised. The gas samples were taken to confirm the systems did not become anoxic (no sample reported in this chapter became anoxic) and to make comparisons between treatments, hence conversion from gas percentages to moles of CO_2 was not necessary. Comparison between experiments is confounded by other factors, including variable concentrations of DOM, different sources of organic matter and the introduction a natural assembly of bacteria, which can be expected to vary between samples. Throughout this chapter, quantitative comparisons for both CO_2 results and bacteria counts will be made within experiments only, but only the relative changes between treatments can be compared across experiments.

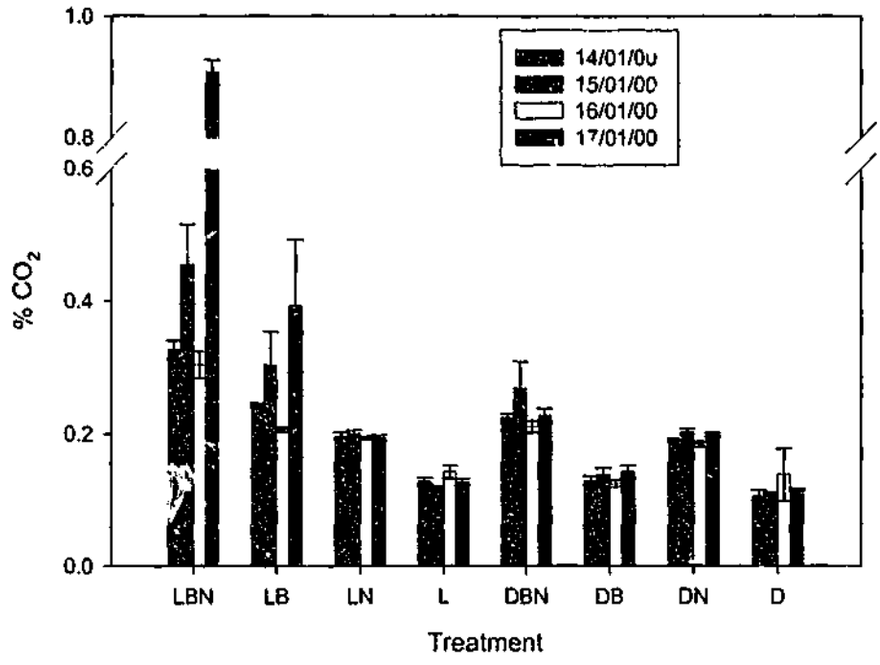

Figure 5.2 Carbon dioxide in the headspace of bacteria cultures. Variables included light (L), dark (D), added bacteria (B) and added nutrients (N). Results are average of three cultures and error bars indicate one standard deviation.

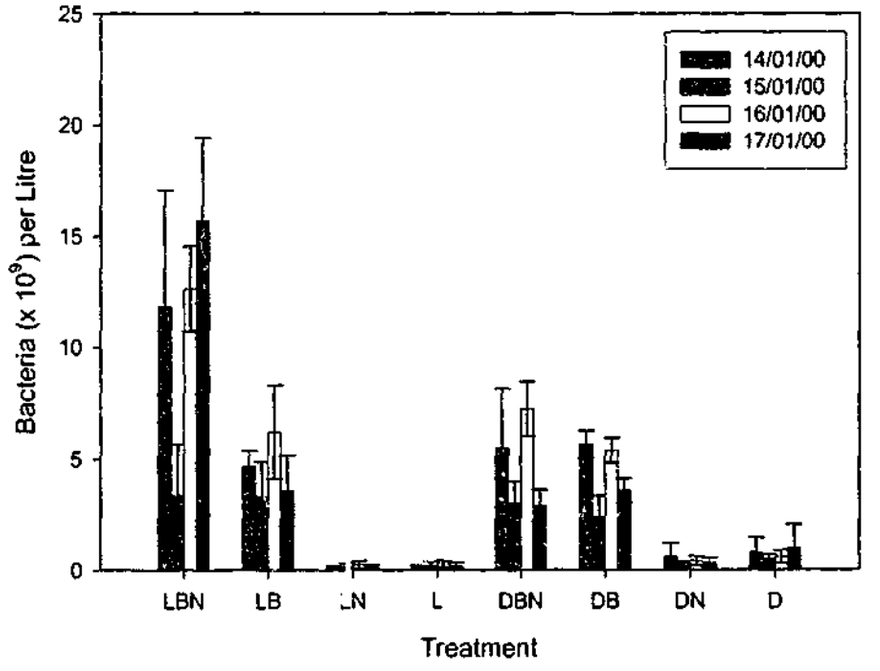

Figure 5.3 Bacterial abundance in cultures prepared on billabong water after various pre-treatments: Light (L), dark (D), nutrient addition (N) and inoculation with bacteria (B). Average values calculated from three cultures, plus or minus one standard deviation.

The CO_2 production indicates that bacterial respiration occurred, however, this may not reflect the amount of organic carbon converted to bacterial biomass. As a result, the CO_2 production and increase in bacterial numbers (Figure 5.3) need to be considered together. Bacteria numbers remained relatively low in the samples without added inoculum (within the range of 1-8 x 10^8 cells/L). The highest numbers were found in the light-exposed samples with added nutrients and bacteria (in the order of 1-1.5 x 10^{10} cells/L for most of the samples). Two of these samples had lower bacteria numbers than would be expected from the CO_2 results (samples from 15/01/00 and 17/01/00). Protozoa were present in these samples, which presumably reduced the bacterial numbers. However, overall the bacterial counts support the CO_2 results: that the starting material is both nutrient and organic carbon limited and the photochemical degradation of the DOM increases the bioavailability of the carbon. Added nutrients were required for the bacteria in this system to take advantage of the increased organic carbon availability.

5.3.3 Bioavailability of Leachate- Sunlight Irradiation

The production of CO_2 in cultures growing on leachate suggested that sunlight irradiation for seven days and fourteen days did not lead to an apparent difference in the amount of organic carbon lost from the aquatic mixture via bacterial respiration (Figure 5.4). Seven days into the experiment, three of the treatments were within one standard deviation (s.d.) of each other and the other generated only slightly less CO_2. Fourteen days into the experiment the samples were all within one s.d. of each other. The bacterial counts produced similar results to the CO_2 production - all the treatments were within one s.d. of each other (Figure 5.5). As discussed in Section 4.3.3, photochemical degradation of the light-exposed leachate had been observed, including substantial photobleaching, and both photobleaching and CO_2 photoproduction had been catalysed in the presence of amorphous iron oxide. Traces of low-molecular-weight organic acids were also detected. It appears, however, that these photochemical changes had no measurable effect on the bioavailability of the leachate, perhaps indicating that the leachate had relatively high initial bioavailability. The bacterial abundance in all of the leachate samples was similar in magnitude to that found in the light-exposed billabong water samples in the two previous experiments, supporting the theory that the organic matter was largely bioavailable prior to irradiation.

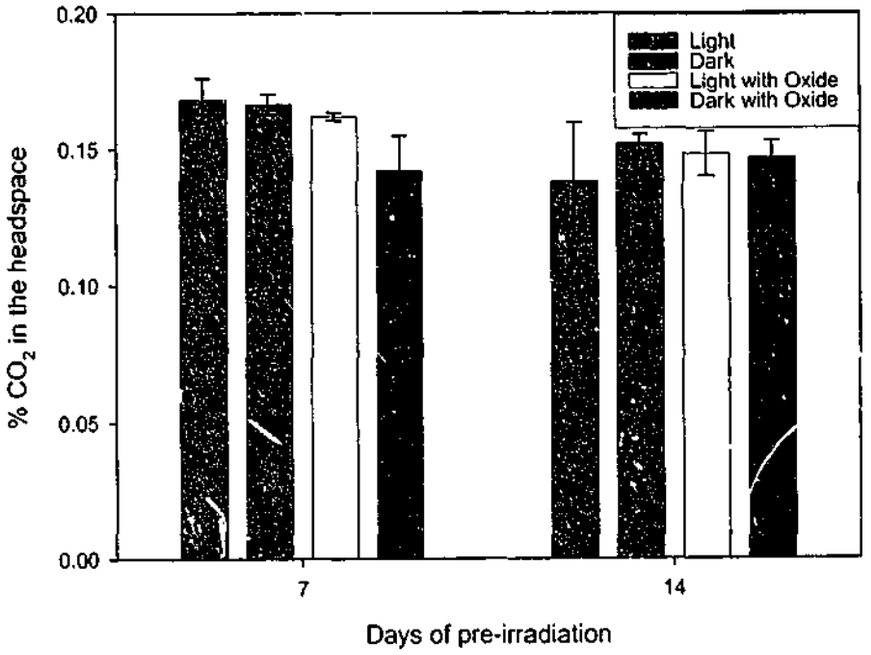

Figure 5.4 Headspace CO_2 in bacterial cultures growing on leachate prepared after either seven or fourteen days of the sunlight-irradiation experiment. Error bars indicate one standard deviation.

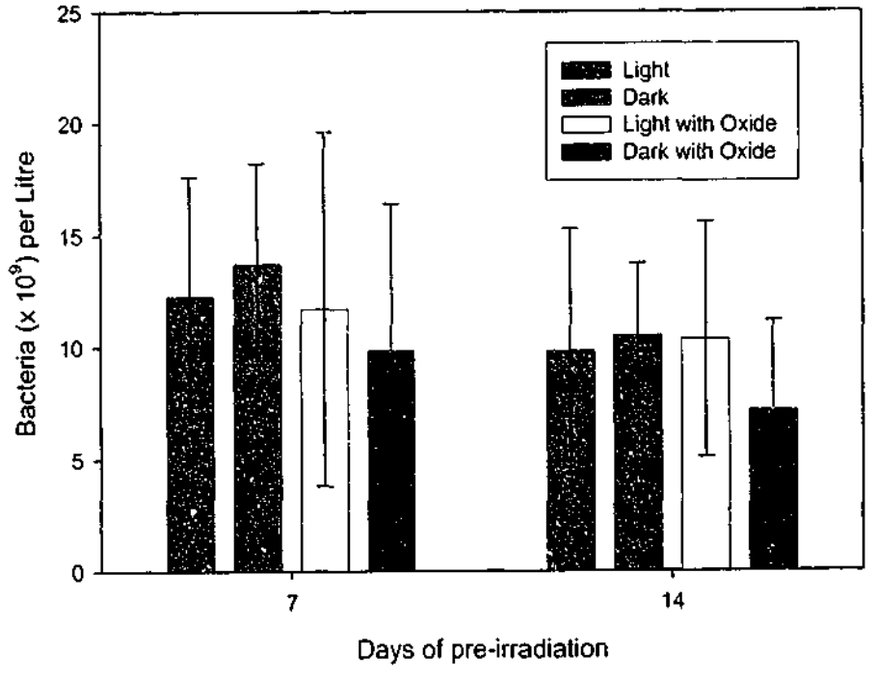

Figure 5.5 Bacterial abundance in cultures prepared on leachate from the sunlight-irradiation experiment. Errors indicate one standard deviation.

5.3.4 Bioavailability of Billabong DOM- Sunlight Irradiation

Both the carbon dioxide production and the bacterial abundance in this experiment suggest that photochemical reactions increased the bioavailability of the dissolved organic matter, and that this increase was greater in the samples which had been irradiated in the presence of iron oxide. The production of CO_2 (Figure 5.6) indicated that bacteria respired slightly more of the organic matter as CO_2 in the light-exposed sample compared to the dark-control. The same pattern occurred in the samples with added iron oxide, but each of these had slightly higher averages than the corresponding samples without iron oxide.

The bacterial abundance (Figure 5.7) followed the same pattern as the CO_2 production, however, these results were accompanied by much greater errors than the CO_2 results. The bacterial abundance in all treatments was high compared to other billabong water experiments, indicating higher initial bioavailability. This complicates the assessment of changes to bioavailability as the increase is small relative to the total. The errors associated with these results would make it impossible to interpret the bacterial abundance in isolation, but the similarity to the CO_2 results suggests that the pattern is real

Taken together, these results suggest that the photochemical degradation of billabong water under sunlight can increase the subsequent bacterial metabolism of the dissolved organic matter, leading to increased biomass and also an increase in the amount of CO_2 emitted from the aquatic ecosystem through bacterial respiration. The three-dimensional fluorescence spectra of the billabong water at the beginning and end of the photochemical phase of this experiment (ref. Section 4.3.4) indicated that the irradiation of the DOM resulted in a loss of the humic-like character of the water, and a reduction in the overall fluorescence signal. Some loss of the humic character was also observed in the dark-control with added iron oxide, potentially explaining the slight increase in the bioavailability of the DOM in those samples. As discussed in Chapter 4, the fluorescence characteristics of the billabong water became more like the leachate as it degraded, i.e. the bulk characteristics of the organic matter became less complex and less aromatic. The bulk characteristics of the leachate were initially less complex than the billabong water, and this may be the reason why there were no apparent differences between the bioavailability of the treatments in this experiment, despite the observed photochemical degradation and production of trace quantities of organic acids.

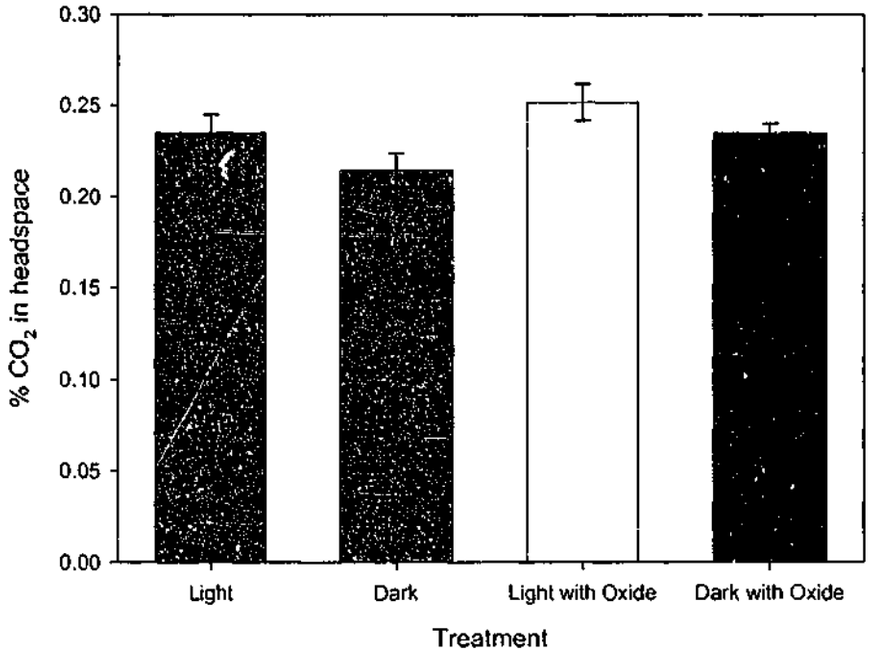

Figure 5.6 Headspace gas concentration in cultures prepared on billabong water after the sunlight irradiation experiment. Errors indicate one standard deviation.

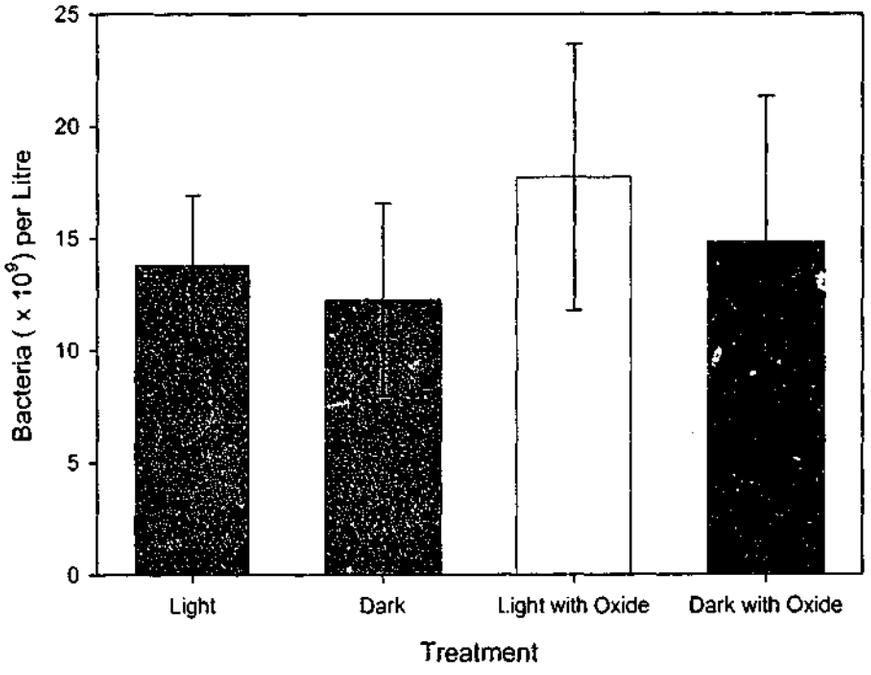

Figure 5.7 Bacterial abundance in cultures prepared on billabong water after the sunlight irradiation experiment. Errors indicate one standard deviation.

In each of the experiments in which the effect of photochemical reactions on the bioavailability of billabong-derived dissolved organic matter was examined, the results indicated that photodegradation increased the bioavailability of the dissolved organic matter. The source of light and its UV component varied between experiments, but in each case the changes brought about in the organic matter increased the bacterial population which it could support, and in the two experiments in which gas production was measured, the amount of CO_2 respired by the bacteria was also increased. The measured effect of the photochemical reactions may be greater if data was available to examine the bacterial respiration and growth per mg of carbon, as in the light-exposed samples some carbon has been lost through photochemical CO_2 production in the first phase of the experiments. The catalytic effect of amorphous iron oxide on the photodegradation of the billabong water was also evident in the change to carbon bioavailability, but no effect was observed in the leachate experiment. The data suggest that the stimulation in bacterial production and respiration brought about by photochemical reactions of the initial DOM are the result of a reduction in the complexity and humic nature of the organic matter, and not exclusively from the production of low-molecular-weight organic acids.

Increases in bioavailability have often been attributed to the production of low-molecular-weight photoproducts (Kieber et al. 1989, Moran and Zepp 1997, Goldstone et al. 2002), however, a study of photochemical enhancement of dissolved organic matter in seawater (Obernosterer and Herndl 2000), also observed stimulation of bacterial activity correlated to changes in optical properties, suggesting a reduction in humification. In that study the relative response of the humic and non-humic fractions to photochemical degradation varied depending on the source of the samples. No increase in bioavailability was observed in the non-humic fraction of samples dominated by terrestrially-derived organic matter. Another study of coastal marine DOM (Miller and Moran 1997) found that alternating cycles of photochemical and microbial degradation lead to more complete degradation than microbial activity alone. The authors also observed that the production of low-molecular-weight photoproducts was insufficient to account for the increased microbial activity and concluded that modification of higher molecular weight molecules was also contributing to increased bioavailability.

Other studies have suggested that in freshwater ecosystems, the humic fraction is less bioavailable than the non-humic fraction (Moran and Hodson 1990, Tranvik 1990). In contrast to the above results, photochemical production of carboxylic acids in humic lakes has been found to exceed the microbial utilization of the acids and they could serve as major bacterioplankton substrates (Bertilsson and Tranvik 1998). These and other studies indicate the contrasting results which can be obtained when attempting to understand the effect of photochemical reactions on organic matter bioavailability and the carbon cycle in general. The experiments reported in this thesis suggest that both organic acid production and photodegradation of the humic structure of the organic matter play a role in enhancing the biodegradability of organic matter derived from billabong water. If the production of organic acids was entirely responsible for enhanced bacterial activity, then the light-exposed samples of leachate should have been more bioavailable than the dark-control samples. In the last billabong water experiment the two light-exposed treatments would have had similar increases in bioavailability and the dark-controls would have been similar to each other. This was not the case; in this experiment the changes to bioavailability were more closely correlated to the changes in fluorescence (and hence humic content) than to the production of organic acids.

5.4 Conclusions

Photochemical degradation of dissolved organic matter was found to increase the bioavailability of billabong DOM, especially when the initial bioavailability was low. The photoproduction of low-molecular-weight organic acids does not adequately account for changes to the bioavailability of dissolved organic matter. In samples of aged organic matter derived from billabong water, exposure to sunlight consistently enhanced the bioavailability of the carbon, and the effect was increased by the presence of amorphous iron oxide during the irradiation. No enhancement was observed after the irradiation of leachate, possibly due to its high initial bioavailability. It was concluded that the effect of photochemical degradation on the bioavailability of dissolved organic matter depended on the source of the initial material, with irradiation of more humic material resulting in increased bioavailability through the degradation of the complex, aromatic structure and the production of low-molecular-weight organic acids. The presence of amorphous iron oxide may contribute to this reaction, particularly through the degradation of humic material.

5.5 References

Anesio, A. M., J. Theil-Nielsen, and W. Granéli. 2000. Bacterial growth on photochemically transformed leachates from aquatic and terrestrial primary producers. Microb Ecol **40**:200-208.

Bertilsson, S., and L. J. Tranvik. 1998. Photochemically produced carboxylic acids as substrates for freshwater bacterioplankton. Limnol. Oceanogr. **43**:885-895.

Farjalla, V. F., A. M. Anesio, S. Bertilsson, and W. Granéli. 2001. Photochemical reactivity of aquatic macrophyte leachates: abiotic transformations and bacterial response. Aquat. Microb. Ecol. **24**:187-195.

Goldstone, J. V., M. J. Pullin, S. Bertilsson, and B. M. Voelker. 2002. Reactions of hydroxyl radical with humic substances: bleaching, mineralization and production of bioavailable carbon substrates. Environ. Sci. Technol **36**:364-372.

Kieber, D. J., J. McDaniel, and K. Mopper. 1989. Photochemical source of biological substrates in sea water: implications for carbon cycling. Nature **341**:637-639.

Lindell, M. J., W. Graneli, and L. J. Tranvik. 1995. Enhanced bacterial growth in response to photochemical transformation of dissolved organic matter. Limnol. Oceanogr. **40**:195-199.

Miller, W. L., and M. A. Moran. 1997. Interaction of photochemical and microbial processes in the degradation of refractory dissolved organic matter from a coastal marine environment. Limnol. Oceanogr. **42**:1317-1324.

Moran, M. A., and R. E. Hodson. 1990. Bacterial production on humic and nonhumic components of dissolved organic carbon. Limnol. Oceanogr. **35**:1744-1756.

Moran, M. A., and R. G. Zepp. 1997. Role of photoreactions in the formation of biologically labile compounds from dissolved organic matter. Limnol. Oceanogr. **42**:1307-1316.

Obernosterer, I., and G. J. Herndl. 2000. Differences in the optical and biological reactivity of the humic and nonhumic dissolved organic carbon component in two contrasting coastal marine environments. Limnol. Oceanogr. **45**:1120-1129.

Obernosterer, I., R. Sempéré, and G. J. Herndl. 2001. Ultraviolet radiation induces reversal of the bioavailability of DOM to marine bacterioplankton. Aquat. Microb. Ecol. **24**:61-68.

Tranvik, L. J. 1990. Bacterioplankton growth on fractions of dissolved organic carbon of different molecular weights from humic and clear waters. Appl. Environ. Microbiol. **56**:1672-1677.

Wetzel, R. G., P. G. Hatcher, and T. S. Bianchi. 1995. Natural photolysis by ultraviolet irradiance of recalcitrant dissolved organic matter to simple substrates for rapid bacterial metabolism. Limnol. Oceanogr. **40**:1369-1380.

6 Photochemical Degradation of Dissolved Organic Matter in the Environment

6.1 This Study

The overall aim of this thesis was to examine the importance of photochemical degradation in the cycling of organic carbon within aquatic ecosystems. In particular, the effect of suspended particles on the photochemical processes is not well understood and to address this matter, the effect of suspended iron oxides on the photochemistry of dissolved organic matter was examined. Amorphous iron oxide was found to significantly accelerate the photochemical degradation of dissolved organic matter, with rate increases of almost an order of magnitude observed in some instances. However, aged iron oxides did not enhance the rate of transformation, and in the case of goethite, a reduction in the rate of reaction occurred. Iron is an important component of many aquatic ecosystems. For example, iron makes up 3% by weight of the sediment at Norman's Lagoon (Mitchell 2002) and is generally found in the water column of the River Murray near Albury at concentrations ranging between 0.5 – 10 mg/L (pers. com. Dr Darren Baldwin, Murray Darling Freshwater Research Centre, Albury). As a result of the abundance of iron in the natural environment, photochemical interactions between iron oxides and organic matter may be significant in a range of aquatic ecosystems. Photochemical reactions influence the carbon cycle in the aquatic environment through direct transformation of the organic matter and subsequent changes to carbon bioavailability - leading to flow-on effects through the food web.

The work reported in this thesis has shown that dissolved organic matter derived from billabong water and *Eucalyptus camaldulensis* leaf leachate is susceptible to photochemical degradation under both artificial and natural radiation. The conclusions of this research are summarised here and the environmental relevance of the research are then discussed.

In Chapter 2 it was confirmed that the photodegradation of dissolved organic matter, using artificial sources of UV and visible light, produced carbon dioxide and traces of carbon monoxide as gaseous products, with simultaneous consumption of oxygen. Of particular interest was the varying relationship between oxygen consumed and carbon dioxide produced, which suggested that the role of gaseous oxygen

depended on the nature of the organic material. The relationship between O_2 consumption and CO_2 production varied between samples of billabong water, and also varied over time in the leachate derived from Red Gum leaves. For billabong water samples, substantially more CO_2 was produced than O_2 was consumed (on a molar basis), with a delay in the consumption of O_2 noted for some summer samples. With leachate samples the trend was quite different, involving the initial consumption of O_2 and a delay in CO_2 production, but longer reaction times tending towards a 1:1 molar ratio of O_2 consumed for CO_2 produced. The difference may be a result of the uptake of oxygen into the dissolved organic matter through processes involving reactive oxygen intermediates such as singlet oxygen, hydroxy and peroxy radicals (Blough and Zepp 1995) with variable uptake depending on the initial composition of the organic matter.

These results highlight the importance of assessing both the consumption of O_2 and the production of CO_2 when measuring photochemical processes in aquatic environments. While some studies have noted variable rates of O_2 consumption between samples (Reitner et al. 1997), or changing DIC production with different O_2 levels (Gao and Zepp 1998), very few studies of the photolysis of DOM have simultaneously measured O_2 consumption and CO_2 production. A ratio of 1.11-1.14 (CO_2:O_2) was inferred from DOC loss after irradiation of water from the Amazon River system (Amon and Benner 1996), a relationship of approximately two moles of CO_2 produced for each mole of O_2 consumed was observed in lake water (Miles and Brezonik 1981) and the average rates (over four hours) of O_2 consumption and CO_2 production in Satilla River water were found to be approximately the same (Gao and Zepp 1998). This group of studies however, did not involve sufficient data points to indicate a changing relationship with time of irradiation. Another study (Andrews et al. 2000), used measured rates of CO production and O_2 consumption, and a literature value for the CO/CO_2 ratio to estimate the ratio of $-O_2/CO_2$ as 1.1. The results described in this thesis indicate that methods of estimating either CO_2 production from O_2 consumption, or vice versa, are not appropriate as they fail to take into account the variable nature of this relationship, both within and between samples.

The role of iron oxides in the photochemical degradation of dissolved organic matter was found to be complex and depended strongly on the age and structure of the iron oxide (Chapter 3). Experiments using leachate and fresh amorphous iron oxyhydroxide showed that the iron oxide could increase the maximum rate of reaction

by almost an order of magnitude. The relationship between O_2 consumption and CO_2 production were similar in the presence and absence of iron oxide. The results were consistent with a mechanism by which the iron oxide accelerated the rate of CO_2 production through coordination between oxygen atoms in the DOM and surface or dissolved Fe(III) atoms. This mechanism could involve a lag phase through delays in the production of functional groups containing oxygen atoms in the organic matter (e.g. –COOH, or –OH).

Amorphous iron oxide, stored as a slurry in water, undergoes an aging process which diminishes the photochemical interaction between leachate DOM and the oxide. The aging process is likely to result in the formation of goethite or haematite (Schwertmann and Cornell 1991). Goethite was found to suppress the rate of photochemical degradation of billabong DOM, the extent of the suppression being dependent on the concentration of goethite particles. A number of potential factors may have been involved, including reduced oxide reactivity (photochemical and/or surface adsorption) combined with increased light absorption and scattering by the oxide.

Amorphous iron oxide also increased the rate of photochemical degradation of both leachate and billabong DOM under natural sunlight irradiation. Small quantities of low-molecular-weight products were detected, these most likely being organic acids (Chapter 4). The fluorescence signatures of the leachate and the billabong water indicated a number of important features of the DOM and the reactions. The aromatic content of the leachate was concentrated in the "protein-like" region of the spectrum, wheras the billabong water had a strongly "humic-like" signature (Coble 1996). The photochemical degradation of the billabong water caused the fluorescence spectra to become more like that of the leachate, indicating a reduction in the humic content, and potentially, an increase in the bioavailability of the remaining organic matter through a simplification of the molecular structure of the DOM. The bioavailability experiments (Chapter 5), did suggest that an increase in the bioavailability of the carbon can arise from irradiation of billabong water, increasing both the number of bacteria present in cultures and bacterial CO_2 production. The effect was more noticeable in samples which had been irradiated with artificial light sources, because either the reactions had progressed further or additional UV light had influenced the reactions.

6.2 Environmental Significance

The photochemical degradation of dissolved organic matter will affect the cycling of organic matter in aquatic ecosystems in a number of ways. Direct photochemical production of CO_2 and CO may lead to removal of carbon from the aquatic environment, particularly in shallow turbulent systems that facilitate gas transfer to the surrounding atmosphere. Some of the photochemically produced gases however, could be reclaimed within the system through photosynthetic uptake of the CO_2 or microbial consumption of the CO (Badr and Probert 1995). The importance of the gas transfer processes will depend on the saturation of the gases in the system and the rate of loss. In some systems the additional CO_2 may be important for autotrophs, but in many the additional CO_2 will be negligible relative to input from the atmosphere. The importance of the CO_2 will be driven by factors such as water depth, turbulence and in-flows to the system. Changes to the bioavailability of the organic matter may also affect ecosystem function, through stimulation of microbial growth and respiration following photochemical degradation of previously recalcitrant organic matter. Concurrent with both of these processes will be an increase in the consumption of oxygen within the system. In the case of flooding, where high levels of fresh leachate enter the system, photochemical oxygen consumption could exceed the rate of photochemical CO_2 production. This process, in association with the high levels of microbial respiration that result from both the input of fresh material and the photochemical production of low-molecular-weight and simplified bacterial substrates, can lead to situations of low oxygen concentrations in the water. The reduction in oxygen concentration is likely to reduce the rate of photochemical DOM degradation in all but the upper layers of the water body (where gas transfer from the atmosphere is capable of replenishing O_2 supplies). Photochemical reactions of dissolved organic matter will be particularly important in systems with high DOC input, very humic waters, organic matter with low initial bioavailability and in floodwaters with large well illuminated and shallow areas.

Photochemical interactions between dissolved organic matter and amorphous iron oxides will be important under a number of environmental conditions. Iron is the most abundant transition metal in these systems and under conditions of high oxygen concentration and neutral pH, will form a variety of oxides. As described earlier, different oxides can have quite different effects on the photochemical degradation of

DOM, so the importance of the processes will vary between systems. The formation of amorphous iron oxides will most likely occur in environments that that have a source of dissolved Fe(II), mixing with oxygenated waters with a pH in the range of approximately 5-7. Iron oxide formation takes place at diffusion-controlled rates near the oxycline in stratified waterbodies (Perret et al. 2000), and will also occur during the inundation of anoxic waterbodies with oxygenated water (e.g. flooding of anoxic billabongs), the mixing or overturn of stratified waterbodies or the release of water from the base of deep dams. As some of these conditions will also correspond to times of high organic carbon loading (e.g. flooding) there are times when the photochemical interactions between DOM and iron oxides will make significant contributions to the transformation of the organic matter and the depletion of dissolved oxygen. The processes may be of importance in the "blackwater" events that occasionally occur during floodplain inundation (Baldwin et al. 2001). Furthermore, the heating that is also associated with the absorption of light by strongly coloured DOC solutions will also act to reduce mixing between surface and deeper waters if the system is non-turbulent.

In contrast to the accelerated degradation that can be expected where dissolved organic matter is exposed to sources of fresh amorphous iron oxide, inputs of aged iron oxide such as goethite could potentially decrease the rate of photochemical DOM degradation. Amorphous iron oxide was found to decrease in reactivity as it aged, while goethite actually decreased the rate of billabong water degradation. Goethite is a common iron oxide in the environment, and can be expected to be a component of soil inputs into aquatic ecosystems through erosion processes (Schwertmann and Cornell 1991). It is therefore expected that the effect of iron oxides on the photochemical processes in an aquatic ecosystem will depend on the source of the oxides, freshly-formed oxides being most likely in waters which have recently been anoxic or in contact with anoxic water and aged oxides being more likely in fast-flowing water.

While the photochemical reactions between dissolved organic matter and iron oxides have the potential to be catalytic in terms of the oxide, the re-formation of the oxide material may be prevented by a number of mechanisms. The dissolution of surface iron species may lead to complexation of iron by dissolved organic matter, preventing re-deposition on the oxide surface. This has the potential to change the bioavailability of the iron species in solution and hence influence the growth of algae, generating flow on effects for the aquatic food web (Wells and Mayer 1991). As

discussed in Chapter 1, the cycling of nitrogen and phosphorus may also be affected by the photochemical degradation of dissolved organic matter and dissolved organic-iron-P complexes.

6.3 Directions for Future Research

This work has highlighted the potential importance of photochemical degradation reactions, particularly including interactions with amorphous iron oxides, to the functioning of aquatic ecosystems. However, many questions remain to be answered before the effect of suspended particulate matter on the photochemical reactions of dissolved organic matter can be thoroughly understood. While iron oxides are an important fraction of the particles that exist in aquatic environments, a diverse range of other particles also exist in these environments and have the potential to interact in the photochemical processes. To assess the full impact of turbidity on photochemical processes in the environment, it will be necessary to examine the role of other abundant natural particles. Manganese oxides may also have a catalytic role in these processes, and transition metal coatings on other particles (e.g. organic detritus, silicates or clays) may also function in a similar way. The role of clay particles in photochemical reactions in aquatic environments has not been fully addressed, but is of interest due to the ability of clays to sorb organic matter and other substances and some evidence exists that synthetic clays can be involved in photodegradation of model compounds (Liu et al. 1994). Understanding the balance between the relative importance of the catalytic role of particles and potential shading effects will require further examination of the effect of particle loading and mineral phase on the system. It also remains to be established whether the thickness of the organic coatings on the particles has an effect on the photochemical activity of the particle.

Further fieldwork to measure the importance of photochemical and photocatalytic degradation of dissolved organic matter in natural environments is required to address a number of water management questions arising from this work:

- what is the extent of the photochemical changes to bioavailability of the organic matter in the environment?
- what are the low-molecular-weight products?
- what is the impact of the process on the Fe, N and P cycles?

- can it be established whether photochemistry can influence the proportion of bacterial to algal processing of nutrients in an ecosystem?

Overall, the question remaining is: does increased turbidity change the chemistry of the system to favour high water quality or poor water quality? In the past, for the most part, the role of photochemistry has been overlooked when considering river and wetland management in Australia. It is now time that the role of light and turbidity are given due consideration, both as water quality modifiers and as important ecosystem factors.

6.4 References

Amon, R. M. W., and R. Benner. 1996. Photochemical and microbial consumption of dissolved organic carbon and dissolved oxygen in the Amazon River system. Geochim. Cosmochim. Acta **60**:1783-1792.

Andrews, S. S., S. Caron, and O. C. Zafiriou. 2000. Photochemical oxygen consumption in marine waters: A major sink for coloured dissolved organic matter? Limnol. Oceanogr. **45**:267-277.

Badr, O., and S. D. Probert. 1995. Sinks and environmental impacts for atmospheric carbon monoxide. Applied Energy **50**:339-372.

Baldwin, D., J. Howitt, and M. Edwards. 2001. Blackwater Event. Austasia Aquaculture **15**:21.

Blough, N. V., and R. G. Zepp. 1995. Reactive oxygen species in natural waters. Pages 280-333 *in* C. S. Foote, J. S. Valentine, A. Greenberg, and J. F. Liebman, editors. Active Oxygen in Chemistry. Blackie Academic and Professional, London.

Coble, P. G. 1996. Characterization of marine and terrestrial DOM in seawater using excitation-emission matrix spectroscopy. Mar. Chem. **51**:325-346.

Gao, H., and R. G. Zepp. 1998. Factors influencing photoreactions of dissolved organic matter in a coastal river of the southeastern United States. Environ. Sci. Technol **32**:2940-2946.

Liu, X., K.-K. Lu, and J. K. Thomas. 1994. Photoinduced reactions on clay and model systems. Pages 187-193 *in* G. R. Helz, R. G. Zepp, and D. G. Crosby, editors. Aquatic and Surface Photochemistry. Lewis, Boca Raton.

Miles, C. J., and P. L. Brezonik. 1981. Oxygen consumption in humic colored waters by a photochemical ferrous-ferric catalytic cycle. Environ. Sci. Technol **15**:1089-1095.

Mitchell, A. M. 2002. Anaerobic nutrient cycles in freshwater sediments. PhD. Charles Sturt University, Wagga Wagga.

Perret, D., J.-F. Gaillard, J. Dominik, and O. Atteia. 2000. The diversity of natural hydrous iron oxides. Environ. Sci. Technol. **34**:3540-3546.

Reitner, B., G. J. Herndl, and A. Herzig. 1997. Role of ultraviolet-B radiation on photochemical and microbial oxygen consumption in a humic-rich shallow lake. Limnol. Oceanogr. **42**:950-960.

Schwertmann, U., and R. M. Cornell. 1991. Iron Oxides in the Laboratory: Preparation and Characterization. VCH, Weinheim.

Wells, M. L., and L. M. Mayer. 1991. Variations in the chemical lability of iron in esturine, coastal and shelfwaters and its implications for phytoplankton. Mar. Chem. **32**:195-210.

Appendix 1

Atomic and Molecular Structure and Bonding

A1.1 Theory

An understanding of photochemical concepts relies on knowledge of the theory of atomic and molecular electronic structure. A very brief overview is given here to facilitate explanation of the interactions between light, organic matter and particles.

Quantum mechanics uses the Schroedinger theory to describe atoms in terms of a nucleus with associated electrons confined to quantised energy levels. Each of these energy levels is associated with a probability density function that describes the region around the nucleus in which the electron is likely to be located, known as an orbital (Eisberg and Resnick 1985). These orbitals are described in terms of three quantum numbers: n, the principal quantum number; l, the azimuthal quantum number; and m_l the magnetic quantum number. The principle quantum number specifies the total energy, and for each of the values of n, the number of orbitals with equivalent energy is determined by the other quantum numbers through the relationship:

$$\begin{aligned} n &= 1, 2, 3, \ldots \\ l &= 0, 1, 2, \ldots, n\text{-}1 \\ m_l &= -l, -l\text{+}1, \ldots, 0, \ldots, +l\text{-}1, l \end{aligned} \qquad \text{Equation A1.1}$$

Two further quantum numbers arise from the quantisation of the intrinsic angular momentum of the electron, known as spin (S). The first of these two quantum numbers, s, defines the magnitude of S, and has the fixed value of ½, while the second, m_s, defines the magnitude of S in the z direction and has values of + ½, or – ½. An important feature of quantum mechanics is the Pauli exclusion principle, which requires that in a multielectron atom there can never be more than one electron in the same quantum state, in other words, no two electrons within the atom can have all four quantum numbers n, l, m_l, and m_s be identical (s is constant and can be disregarded). The result of the relationships between the quantum numbers is that the three primary quantum numbers define the orbitals to which electrons are assigned and also the degree of degeneracy of each energy level (e.g. when n=1, l=0, m_l =0 and we have the 1s orbital, but when n=2 we can have l=0, m_l =0 to give the 2s orbital, or l= 1 and m_l = -1,

0, 1 to give the three 2p orbitals). The electrons are then paired in the orbitals with m_s + ½ or – ½ (spin up or down), to give the electronic configuration of the atom (Eisberg and Resnick 1985). An atom in the ground-state has the electrons arranged in the lowest energy orbitals. The total spin S of the atom is the sum of the m_s of the electrons in the atom, and the multiplicity of the atom is equal to 2S+1. So for an atom where all the spins are paired (antiparallel) the multiplicity is 1 and the configuration is described as a singlet state. Where two unpaired electrons are found in the atom (spins parallel) the multiplicity is three and the state is known as a triplet. Hund's rule states that the state with the highest multiplicity has the lowest energy, on other words, the electrons remain unpaired in orbitals of equivalent energy where possible (Moore 1983). The electrons in the highest occupied energy levels are known as valence electrons and are involved in chemical bonding.

Covalent bonding between atoms is often described in terms of molecular orbital theory. Molecular orbitals are constructed from linear combinations of atomic orbitals that fulfil requirements for similarity of energies and symmetry and overlap as much as possible (Hollas 1995). The combination of atomic orbitals results in the production of two molecular orbitals with energy levels displaced from the atomic energy levels by the bond energy (see Figure A1.1)

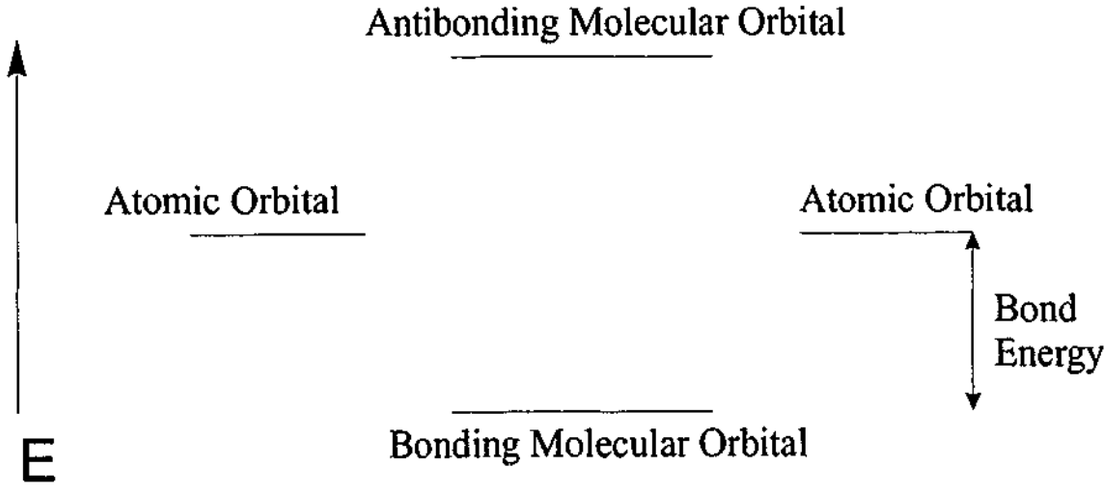

Figure A1.1 The combination of atomic orbitals to generate molecular orbitals (adapated from (Hollas 1995))

Two types of molecular orbital are most common in organic molecules. Sigma (σ) bonds are cylindrically symmetrical and are formed by head-on overlap of two atomic orbitals (such as s or p_z orbitals), while pi (π) orbitals arise from the sideways overlap of p_x and p_y orbitals. The corresponding antibonding orbitals are denoted with σ^* and π^*. The bonding character of an electron in a bonding orbital is approximately cancelled by the antibonding character of an electron in an antibonding orbital, and so the bond order can be determined by filling the molecular orbitals with electrons and then establishing the net number of filled bonding orbitals (Hollas 1995).

The interaction of transition metals with organic ligands can be described in terms of ligand field theory, which is a form of molecular orbital theory. Molecular orbitals are constructed using the ligand orbitals that point along the metal ligand bonds and the *d* orbitals of the metal atom. There are five *d* orbitals and those which are closest to the ligand orbitals are raised in energy compared to those that are further from the ligands. The splitting of the energy of the *d* orbitals can be thought of as due to the presence of the ligand electrons causing a repulsive effect for electrons in the higher energy *d* orbitals. The degree of splitting between the *d* orbitals depends on the molecular orbitals of the ligand and the extent to which these can interact with both the *d* orbitals involved in bonding, and the non-bonding *d* orbitals (through a process known as back-bonding, involving interaction with the π^* orbitals of some ligands) (Oxtoby and Nachtrieb 1990).

Of the many types of electronic structure possible in solids, the one of most interest in the field of environmental photochemistry is the semiconductor structure, which is found in crystals of elements such as silicon, and is also found in many metal oxides. The combination of atomic orbitals for crystalline solids results in a series of filled energy levels that form a near-continuous "band" separated by an energy gap from a corresponding band of unfilled energy levels (which correspond to the antibonding orbitals). The presence of the band gap has important implications for the light absorbing and conductance properties of the semiconductor (Smart and Moore 1992).

A1.2 References

Eisberg, R., and R. Resnick. 1985. Quantum Physics of Atoms, Molecules, Solids, Nuclei, and Particles, Second edition. John Wiley &Sons, New York.

Hollas, J. M. 1995. Modern Spectroscopy, 2nd edition. John Wiley & Sons, Chichester.

Moore, W. J. 1983. Basic Physical Chemistry. Prentice-Hall International, London.

Oxtoby, D. W., and N. H. Nachtrieb. 1990. Principles of Modern Chemistry. Saunders College Publishing, Fort Worth.

Smart, L., and E. Moore. 1992. Solid State Chemistry, An Introduction. Chapman & Hall, London.

Appendix 2

Fluorescence Scans: Theory, Concentration Effects and Absorbance Corrections.

A2.1. Theoretical Considerations of Molecular Fluorescence

Photoluminescence (fluorescence and phosphorescence) occurs when electrons in excited states return to the ground state and emit radiation in the process. This can occur at the same wavelength as the absorbed light which generated the excited state, or can often occur at longer wavelengths due to Stokes shift (Skoog and Leary 1992). The excitation process can produce a molecule in a variety of vibrational levels associated with the excited electronic state, but the excess vibrational energy is rapidly lost to solvent molecules with the result that emission of light from an excited state always occurs from the lowest vibrational energy level, but can return to any of the vibrational energy levels of the ground state. This vibrational relaxation process results in the emitted light being of lower energy than the excitation energy with a corresponding shift in the wavelength. Internal conversion between electronic excited states also contributes to the shift in wavelength of emission. Intersystem crossing involves a change in the spin of the electron and results in the excited state transforming from a singlet to a triplet, and energy emission from this excited state is known a phosphorescence and occurs over longer timescales (10^{-4}-10 s) (Skoog and Leary 1992). Fluorescence usually occurs as a result of a $\pi^* \rightarrow \pi$ or a $\pi^* \rightarrow$ n transition, the former being the most common. Aromatic functional groups display the most intense fluorescence but aliphatic and acyclic carbonyl structures or conjugated double bonds may also fluoresce. The fluorescence of aromatic structures is affected by the number of rings, their degree of condensation and substitution on the rings, for example halogen, carboxylic or carbonyl substituents can inhibit fluorescence (Skoog and Leary 1992). Changes in structure rigidity or solution pH may also alter the fluorescence. A large proportion of the fluorescence of humic substances has been attributed to the presence of quinone functional groups (Klapper et al. 2002), and the effect of the substituents on the fluorescence has been used to investigate the origins of the humic substances.

The 3-D fluorescence spectra of a sample of dissolved organic matter gives information on the average molecular properties of the component molecules, as a large number of compounds are present and all fluorescing materials will contribute to the measured spectrum. Changes to the peak positions can give an indication to changes to major components of the dissolved organic matter, for example, changes to the excitation spectrum indicate changes to the absorption of light by the organic matter. Changes to the emission spectra however indicate changes to the energy difference between the ground state and the first excited state, caused by alterations to the degree of conjugation in the system, number of aromatic rings, or addition or elimination of certain functional groups (Coble 1996).

A2.2 Absorbance Corrections

As discussed in Chapter 1, interpretation of peak shifts requires correction for inner-filtering in the sample or concentration changes may lead to misleading results. The fluorescence results reported in this work have all been corrected for primary and secondary inner-filtering to prevent concentration effects (Mobed et al. 1996). The corrections were as described in (McKnight et al. 2001), and the specific equations used were obtained by personal communication with Dianne McKnight and J. Robin Fulton of the University of Colorado, USA. Briefly, the corrections rely on the assumption that the spectrometer measures emitted light from a small region in the centre of the 1-cm cell, resulting in a pathlength of 0.5 cm for both the excitation and emission light. To correct for absorbance of excitation light before it reaches the region of interest, and emission light before it reaches the detector a correction factor is applied to each measured fluorescence intensity:

$$I = I_m / 10^{-0.5(A_{ex} + A_{em})} \qquad \text{Equation A2.1}$$

Where I is the corrected intensity, I_m is the measured intensity and A_{ex} and A_{em} are the measured absorbances at the excitation and emission wavelengths respectively. This correction was applied to each of the data points in the scan by the application of two macro programs in Microsoft Excel. Data was collected as described in Chapter 4. The exported data from the fluorimeter was imported into Excel and the first macro (Scan

3D) was applied. This macro was obtained from Zygmunt Lorenz of the Murray-Darling Freshwater Research Centre and edited to insert an additional page for the absorbance data to be pasted into. The two columns of absorbance data were then pasted in to the first two columns of the absorbance page and the macro Absorcorrect was applied. The first, second and sixth columns of the page 'XYZ' could then be exported to Sigma Plot for graphing and analysis.

A2.3 Impact of concentration change with and without corrections

The impact of changing concentration is illustrated by Figure A2.1, which shows the fluorescence results for a sample of leachate at two different concentrations. Examine firstly the difference between graphs a) and b) on this figure. These graphs illustrate the same data, with and without the absorbance correction being applied. Aside from the changes to the intensity of the peaks, there are also differences in the distribution of the peaks. The main peak is very similar in each graph, but the minor peak below this has the peak maximum shifted towards slightly longer excitation and emission wavelengths. The trailing fluorescence shoulder that exists to the right of these peaks is also shifted to longer wavelengths in the uncorrected example. In the diluted sample, however, the application of absorbance corrections does not alter the peak locations or the distribution of intensity. These results correspond quite well to the corrected results in the more concentrated example. These results demonstrate the purpose of the data corrections: to eliminate artefacts in peak location, brought about by changing absorption in samples of differing concentration.

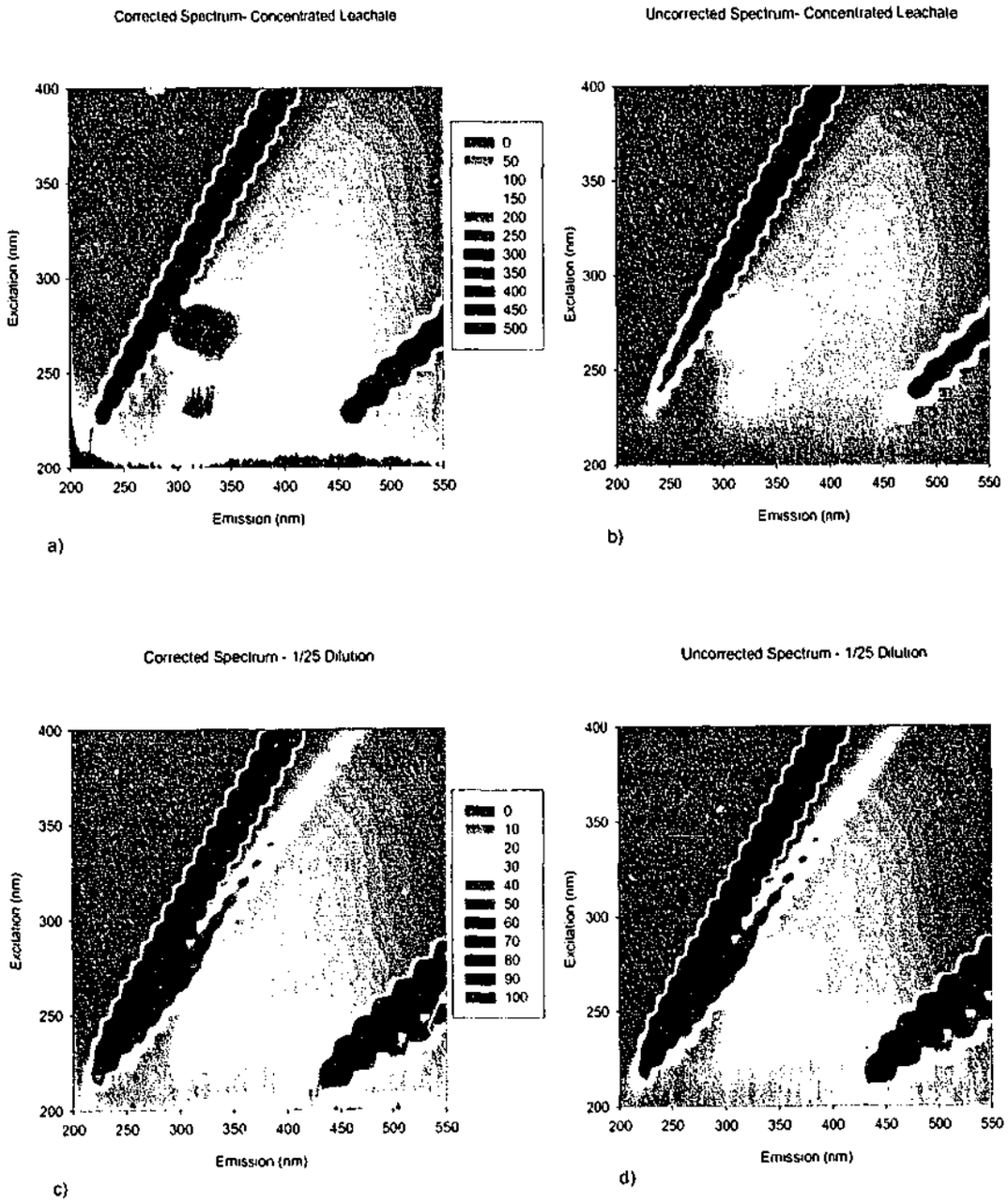

Figure A2.1 Three-dimensional fluorescence spectra for a sample of leaf leachate, showing a) The corrected spectrum of the concentrated leachate, b) the uncorrected spectrum of the concentrated leachate, c) the corrected spectrum of diluted leachate and d) the uncorrected spectrum of diluted leachate.

A2.4 Macro: Scan 3D

```
Option Explicit

Sub Scan3DConvert()
'
' Converting 3D Scan data from Hitachi F4500 Fluorometer(1 column)
' into  1. XYZ data
'       2. Matrix (Em in columns)
' Macro written by Zygmunt Lorenz and edited by Julia Howitt
'
' Keyboard Shortcut: Ctrl+s
'
Dim exstart As Integer, exend As Integer, exstep As Integer
Dim emstart As Integer, emend As Integer, emstep As Integer
Dim exn As Integer, emn As Integer, n As Integer
Dim i As Integer, j As Integer, row As Integer, ex As Integer, em As Integer

Application.ScreenUpdating = False
Sheets.Add after:=Sheets(1), Count:=3
Sheets(2).Name = "XYZ"
Sheets(3).Name = "Matrix"
Sheets(4).Name = "Absorbance"
Sheets(1).Activate

exstart = [A2]
exend = [A3]
exstep = [A4]
emstart = [A5]
emend = [A6]
emstep = [A7]
exn = (exend - exstart) / exstep + 1
emn = (emend - emstart) / emstep + 1
n = exn * emn

Sheets("XYZ").[A1:F1] = Array("Em", "Ex", "F", "Abs Em", "Abs Ex", "Corr F")
Sheets("Matrix").[A1:B1] = Array("Em", "Ex\Ex")
Sheets("Matrix").[B1].HorizontalAlignment = xlRight
em = emstart
For j = 1 To emn
   Sheets("Matrix").Cells(j + 1, 1) = em
   em = em + emstep
Next j

row = 2
ex = exstart
For i = 1 To exn
```

```
    Range(Sheets("Matrix").Cells(2, 1), Sheets("Matrix").Cells(emn + 1, 1)).Copy _
      Destination:=Sheets("XYZ").Cells(row, 1)
    Range(Sheets("XYZ").Cells(row, 2), Sheets("XYZ").Cells(row + emn - 1, 2)) = ex
    Sheets("Matrix").Cells(i + 1, 2) = ex
    Sheets("Matrix").Cells(1, i + 2) = ex
    Range(Cells(row + 9, 1), Cells(row + emn + 8, 1)).Copy _
      Destination:=Sheets("Matrix").Cells(2, i + 2)
    ex = ex + exstep
    row = row + emn
Next i
Range(Cells(11, 1), Cells(n + 10, 1)).Copy Destination:=Sheets("XYZ").Cells(2, 3)

Application.ScreenUpdating = True
End Sub
```

A2.5 Macro: Absorcorrect

```
Sub Absorbancecorrection()
'
' Absorbancecorrection Macro
' Macro written on 30/07/01 by Julia Howitt
' A Macro for absorbance corrections to fluorescence data
' To Use: Take *.f3d from fluorimeter, and run scan 3d macro.
' Paste 2 columns of data from spec onto absorbance page.
' Then run this macro.
' Note: Designed for Em steps of 2nm, Ex 10nm, abs 2nm (200-500)
'
'Keyboard Shortcut: Ctrl+t
'
'
    Rows("1:2").Select
    Selection.Delete Shift:=xlUp
    Columns("A:B").Select
    Selection.Sort Key1:=Range("A1"), Order1:=xlAscending, Header:=xlGuess, _
      OrderCustom:=1, MatchCase:=False, Orientation:=xlTopToBottom
    Range("B1:B176").Select
    Selection.Copy
    Sheets("XYZ").Select
    Range("D2:D177").Select
    ActiveSheet.Paste
    Range("D178:D353").Select
    ActiveSheet.Paste
    Range("D354:D529").Select
    ActiveSheet.Paste
    Range("D530:D705").Select
    ActiveSheet.Paste
    Range("D706:D881").Select
    ActiveSheet.Paste
```

```
Range("D882:D1057").Select
ActiveSheet.Paste
Range("D1058:D1233").Select
ActiveSheet.Paste
Range("D1234:D1409").Select
ActiveSheet.Paste
Range("D1410:D1585").Select
ActiveSheet.Paste
Range("D1586:D1761").Select
ActiveSheet.Paste
Range("D1762:D1937").Select
ActiveSheet.Paste
Range("D1938:D2113").Select
ActiveSheet.Paste
Range("D2114:D2289").Select
ActiveSheet.Paste
Range("D2290:D2465").Select
ActiveSheet.Paste
Range("D2466:D2641").Select
ActiveSheet.Paste
Range("D2642:D2817").Select
ActiveSheet.Paste
Range("D2818:D2993").Select
ActiveSheet.Paste
Range("D2994:D3169").Select
ActiveSheet.Paste
Range("D3170:D3345").Select
ActiveSheet.Paste
Range("D3346:D3521").Select
ActiveSheet.Paste
Range("D3522:D3697").Select
ActiveSheet.Paste

Range("D2").Copy
Range("E2:E177").Select
ActiveSheet.Paste
Range("D7").Copy
Range("E178:E353").Select
ActiveSheet.Paste
Range("D12").Copy
Range("E354:E529").Select
ActiveSheet.Paste
Range("D17").Copy
Range("E530:E705").Select
ActiveSheet.Paste
Range("D22").Copy
Range("E706:E881").Select
ActiveSheet.Paste
Range("D27").Copy
Range("E882:E1057").Select
```

```
ActiveSheet.Paste
Range("D32").Copy
Range("E1058:E1233").Select
ActiveSheet.Paste
Range("D37").Copy
Range("E1234:E1409").Select
ActiveSheet.Paste
Range("D42").Copy
Range("E1410:E1585").Select
ActiveSheet.Paste
Range("D47").Copy
Range("E1586:E1761").Select
ActiveSheet.Paste
Range("D52").Copy
Range("E1762:E1937").Select
ActiveSheet.Paste
Range("D57").Copy
Range("E1938:E2113").Select
ActiveSheet.Paste
Range("D62").Copy
Range("E2114:E2289").Select
ActiveSheet.Paste
Range("D67").Copy
Range("E2290:E2465").Select
ActiveSheet.Paste
Range("D72").Copy
Range("E2466:E2641").Select
ActiveSheet.Paste
Range("D77").Copy
Range("E2642:E2817").Select
ActiveSheet.Paste
Range("D82").Copy
Range("E2818:E2993").Select
ActiveSheet.Paste
Range("D87").Copy
Range("E2994:E3169").Select
ActiveSheet.Paste
Range("D92").Copy
Range("E3170:E3345").Select
ActiveSheet.Paste
Range("D97").Copy
Range("E3346:E3521").Select
ActiveSheet.Paste
Range("D102").Copy
Range("E3522:E3697").Select
ActiveSheet.Paste

Range("F2").Select
ActiveCell.FormulaR1C1 = "=RC[-3]/10^(-0.5*(RC[-2]+RC[-1]))"
Range("F2").Copy
```

```
Range("F3:F3697").Select
ActiveSheet.Paste


End Sub
```

A2.6 References

Coble, P. G. 1996. Characterization of marine and terrestrial DOM in seawater using excitation-emission matrix spectroscopy. Marine Chemistry **51**:325-346.

Klapper, L., D. M. McKnight, E. L. Blunt-Harris, K. P. Nevin, D. R. Lovley, and P. G. Hatcher. 2002. Fulvic Acid Oxidation State Detection Using Fluorescence Spectroscopy. Environmental Science and Technology **36**:3170-3175.

McKnight, D. M., E. W. Boyer, P. K. Westerhoff, P. T. Doran, K. Thomas, and D. T. Andersen. 2001. Spectrofluorometric characterization of dissolved organic matter for indication of precursor organic material and aromaticity. Limnol. Oceanogr. **46**:38-48.

Mobed, J. J., S. L. Hemmingsen, J. L. Autry, and L. B. McGown. 1996. Fluorescence characterization of IHSS humic substances: total luminescence spectra with absorbance correction. Environ. Sci. Technol **30**:3061-3065.

Skoog, D. A., and J. J. Leary. 1992. Principles of Instrumental Analysis, Fourth edition. Saunders College Publishing, Fort Worth.

Appendix 3

Spectral Characteristics of Hanovia Photochemical Reactor

The spectral characteristics for the photochemical reactor used for experiments in Chapter 2 and Chapter 3 are not available. This lamp was damaged by couriers when sent for characterisation. It is known, however, that the lamp had a maximum output in the order of 6000 μmol m^{-2} s^{-1} (measured approximately 1 cm from the most intense portion of the lamp). Spectral characteristics for an older lamp of the same brand and specifications are included to give an indication of the wavelengths emitted. This lamp was not used in any experiments described in this thesis due to relatively low light intensity and had an output of approximately 350 μmol m^{-2} s^{-1}.

Spectral characterisation was carried out by Dr Richard Morrison from the School of Chemistry, Monash University, using equipment constructed in his laboratory. The spectral peaks observed in Figure A3.1 corresponded to the peaks observed from a known mercury lamp. The intensity increases for a brief period after the lamp is switched on and a continuum of light develops under the spectral lines, as shown in Figure A3.2. This spectrum was recorded after a very brief warm-up period (less than a minute), as the light intensity shifts the signal offscale at longer times.

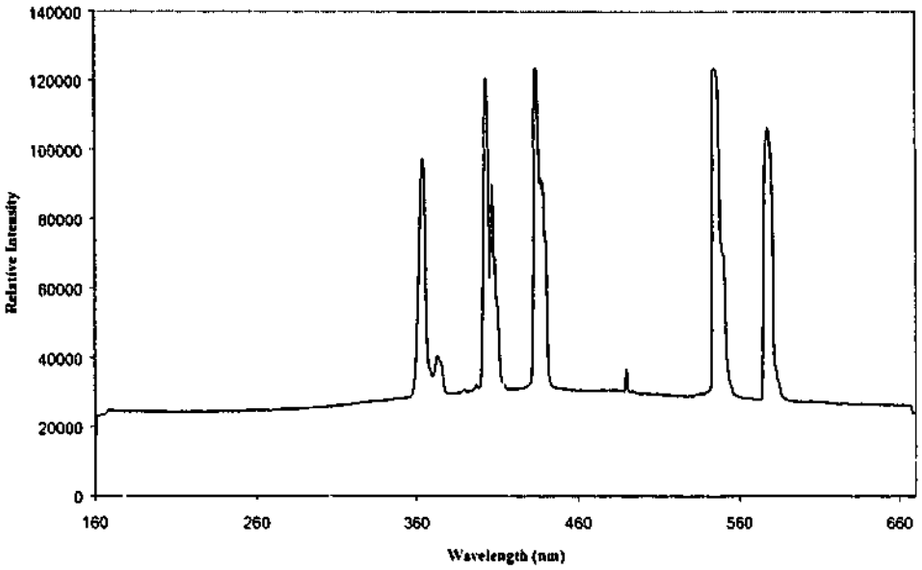

Figure A3.1 The high-energy region of the lamp spectrum, recorded immediately after turning the lamp on.

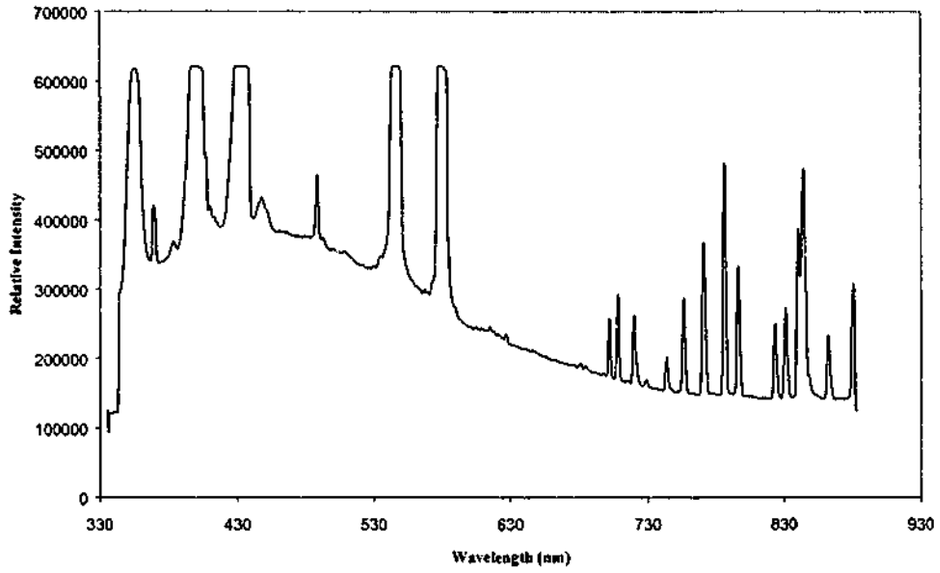

Figure A3.2 The lower-energy region of the lamp spectrum, measured shortly after starting the lamp.

Appendix 4

Conversions from headspace CO_2 to total CO_2

A4.1 Theory

The theory for the conversion of headspace carbon dioxide concentration to total carbon dioxide was based on a couple of key assumptions. Firstly, it was assumed that for all experiments, the headspace gas pressure at the time of the sealing of the vessel was one atmosphere. It was also necessary to assume that CO_2 behaves as an ideal gas in the headspace, so that the moles of CO_2 in the headspace could be calculated. The equations and constants to follow are all derived from the same reference (Stumm and Morgan 1981). The total dissolved inorganic carbon, C_T, is defined as:

$$C_T = [H_2CO_3^*] + [HCO_3^-] + [CO_3^{2-}] \qquad \text{Equation A4.1}$$

Where $H_2CO_3^*$ is the sum of dissolved carbon dioxide and carbonic acid.

C_T can be calculated from the partial pressure of CO_2, ρ_{CO_2}, using the formula:

$$C_T = \frac{1}{\alpha_0} K_H \rho_{CO_2} \qquad \text{Equation A4.2}$$

$$\frac{1}{\alpha_0} = 1 + \frac{K_1}{[H^+]} + \frac{K_1 K_2}{[H^+]^2} \qquad \text{Equation A4.3}$$

Where K_H is the Henry's law equilibrium constant for CO_2 in water, K_1 is the equilibrium constant for the formation of bicarbonate from carbonic acid, and K_2 is the equilibrium constant for the formation of carbonate from bicarbonate.

A4.2 Temperature Dependence of Equilibrium Constants

Each of the equilibrium constants in equations A4.2 and A4.3 change with the temperature of the system. Estimates for the temperature dependence of each constant were made by plotting the negative log of each constant versus temperature between 20°C and 30°C, calculated from data on pp 204-206 of (Stumm and Morgan 1981) and fitting a linear regression to each, generating the following output:

Equations in the form of y=b(1)x + b(0), where x= temp in degree Celcius.
Plot 1

Order 1

Curve 1: Temperature vs -LogKh:
Coefficients: b[0] = 1.17, b[1] = 0.012; $r^2 = 1$

Curve 2: Temperature vs -LogK1:
Coefficients: b[0] = 6.4883333333, b[1] = -5.4e-3; $r^2 = 0.9981743496$

Curve 3: Temperature vs -Log K2:
Coefficients: b[0] = 10.5495, b[1] = -8.7e-3; $r^2 = 0.9964454976$

A4.3 Corrections for the photochemical reactor and quartz tubes

The spreadsheet used for CO_2 calculations in the experiments using the photochemical reactor (Chapters 2 and 3) is given in Table A4.1. Blank columns are for entry of experiment data. Columns J and K are used to calculate the pressure in the reactor at the time of sampling and the partial pressure of CO_2 respectively, taking into account that the pressure is reduced by the removal of gas samples. Columns L, M and N are used to calculate the equilibrium constants at the sampling temperature, using the equations described above. The following two columns, combined, make use of equations A4.2 and A4.3 to calculate the concentration of inorganic carbon in the liquid. All of the remaining columns, with the exception of T, work with moles of CO_2 to derive the net production of carbon dioxide over the course of the experiment.

In a similar manner, Table A4.2 indicates the method used to calculate the CO_2 generated in the quartz tube experiments. Pressure measurements are independent of the values in the column above them as each row indicates a separate tube. The net CO_2 equation (e.g. S2-(0.00000149214 /69*F2)-(0.000000393785 /18*G2)) is equivalent to the total CO_2 in the tube (from column S) – an estimate of the initial CO_2 in the tube. The initial CO_2 is calculated from the average concentration of inorganic carbon in the liquid of the 0-time samples, (in this example 1.49214×10^{-6} moles, divided by the average volume of liquid in those samples, time the volume of liquid in the sample of interest), plus the initial CO_2 in the headspace (calculated similarly).

A4.4 Reference

Stumm, W., and J. J. Morgan. 1981. Aquatic Chemistry: An Introduction Emphasizing Chemical Equilibria in Natural Waters, Second Edition. John Wiley and Sons, New York.

Table A4.1 The spreadsheet used to calculate CO_2 production in photochemical reactor experiments

A	B	C	D	E	F	G	H	I	J	K	L	M	N	O	P	Q	R	S	T	U	V	W
Sample No.	Hours	CO_2 %	°C	Kelvins	Volume Liquid	Volume Gas	pH	[H+]	P(total)	$p_{(CO2)}$	K_H	K_1	K_2	molality	Conc Aq CO2	n(aq)	n(g)	n(total)	mg C	Removed	Cumulative n	Net CO2 produced
1				=D2+273.15	700	220		=10^(-H2)	=G2/(G2+2)	=J2*C2/100	=10^(-(1.17+0.012*D2))	=10^(-(6.4883-0.0054*D2))	=10^(-(10.5495-0.0087*D2))	=K2*L2	=O2*(1+(M2/L2)+(M2*N2/(L2*I2)))	=P2*F2/1000	=K2*(G2/1000)/(0.08205*E2)	=R2+Q2	=S2*12.01*1000	=2/220*R2	=S2+U2	=V2-V2
2				=D3+273.15	700	220		=10^(-H3)	=J2*(218/220)	=J3*C3/100	=10^(-(1.17+0.012*D3))	=10^(-(6.4883-0.0054*D3))	=10^(-(10.5495-0.0087*D3))	=K3*L3	=O3*(1+(M3/I3)+(M3*N3/(I3*I3)))	=P3*F3/1000	=K3*(G3/1000)/(0.08205*E3)	=R3+Q3	=S3*12.01*1000	=2/220*R3	=S3+U2:U3	=V3-V2
3				=D4+273.15	700	220		=10^(-H4)	=J3*(218/220)	=J4*C4/100	=10^(-(1.17+0.012*D4))	=10^(-(6.4883-0.0054*D4))	=10^(-(10.5495-0.0087*D4))	=K4*L4	=O4*(1+(M4/I4)+(M4*N4/(I4*I4)))	=P4*F4/1000	=K4*(G4/1000)/(0.08205*E4)	=R4+Q4	=S4*12.01*1000	=2/220*R4	=S4+U2:U4	=V4-V2
4				=D5+273.15	700	220		=10^(-H5)	=J4*(218/220)	=J5*C5/100	=10^(-(1.17+0.012*D5))	=10^(-(6.4883-0.0054*D5))	=10^(-(10.5495-0.0087*D5))	=K5*L5	=O5*(1+(M5/I5)+(M5*N5/(I5*I5)))	=P5*F5/1000	=K5*(G5/1000)/(0.08205*E5)	=R5+Q5	=S5*12.01*1000	=2/220*R5	=S5+U2:U5	=V5-V2
5				=D6+273.15	700	220		=10^(-H6)	=J5*(218/220)	=J6*C6/100	=10^(-(1.17+0.012*D6))	=10^(-(6.4883-0.0054*D6))	=10^(-(10.5495-0.0087*D6))	=K6*L6	=O6*(1+(M6/I6)+(M6*N6/(I6*I6)))	=P6*F6/1000	=K6*(G6/1000)/(0.08205*E6)	=R6+Q6	=S6*12.01*1000	=2/220*R6	=S6+U2:U6	=V6-V2
6				=D7+273.15	700	220		=10^(-H7)	=J6*(218/220)	=J7*C7/100	=10^(-(1.17+0.012*D7))	=10^(-(6.4883-0.0054*D7))	=10^(-(10.5495-0.0087*D7))	=K7*L7	=O7*(1+(M7/I7)+(M7*N7/(I7*I7)))	=P7*F7/1000	=K7*(G7/1000)/(0.08205*E7)	=R7+Q7	=S7*12.01*1000	=2/220*R7	=S7+U2:U7	=V7-V2
7				=D8+273.15	700	220		=10^(-H8)	=J7*(218/220)	=J8*C8/100	=10^(-(1.17+0.012*D8))	=10^(-(6.4883-0.0054*D8))	=10^(-(10.5495-0.0087*D8))	=K8*L8	=O8*(1+(M8/I8)+(M8*N8/(I8*I8)))	=P8*F8/1000	=K8*(G8/1000)/(0.08205*E8)	=R8+Q8	=S8*12.01*1000	=2/220*R8	=S8+U2:U8	=V8-V2

Table A4.2 Spreadsheet used for CO_2 calculations in quartz tube experiments

A	B	C	D	E	F	G	H	I	J	K	L	M	N	O	P	Q	R	S	T	U	V
Sample No.	Hours	CO_2 %	°C	Kelvins	Liq. (ml)	Gas (ml)	pH	[H+]	P (atm)	p(CO2)	Kh	K1	K2	molality	Conc Aq CO2	n(aq)	n(g)	n(total)	mg C	note	n(net)
1				=D2+ 273.15				=10^ (-H2)	1	=J2*C2 /100	=10^(- (1.17+0.012 *D2))	=10^(- (6.4883- 0.0054*D2))	=10^(- (10.5495- 0.0087*D2))	=K2*L2	=O2*(1+(M2/ I2)+(M2*N2/(I2*I2)))	=P2*F 2 /1000	=K2*(G2/1000)/(0.08205*E2)	=R2+Q2	=S2*12. 01*1000		=S2- (0.00000149 214 /69*F2)- (0.00000039 3785 /18*G2)
2				=D3+ 273.15				=10^ (-H3)	1	=J3*C3 /100	=10^(- (1.17+0.012 *D3))	=10^(- (6.4883- 0.0054*D3))	=10^(- (10.5495- 0.0087*D3))	=K3*L3	=O3*(1+(M3/ I3)+(M3*N3/(I3*I3)))	=P3*F 3/1000	=K3*(G3/1000)/(0.08205*E3)	=R3+Q3	=S3*12. 01*1000		=S3- (0.00000149 214 /69*F3)- (0.00000039 3785 /18*G3)
3				=D4+ 273.15				=10^ (-H4)	1	=J4*C4 /100	=10^(- (1.17+0.012 *D4))	=10^(- (6.4883- 0.0054*D4))	=10^(- (10.5495- 0.0087*D4))	=K4*L4	=O4*(1+(M4/ I4)+(M4*N4/(I4*I4)))	=P4*F 4/1000	=K4*(G4/1000)/(0.08205*E4)	=R4+Q4	=S4*12. 01*1000		=S4- (0.00000149 214 /69*F4)- (0.00000039 3785 /18*G4)
4				=D5+ 273.15				=10^ (-H5)	1	=J5*C5 /100	=10^(- (1.17+0.012 *D5))	=10^(- (6.4883- 0.0054*D5))	=10^(- (10.5495- 0.0087*D5))	=K5*L5	=O5*(1+(M5/ I5)+(M5*N5/(I5*I5)))	=P5*F 5/1000	=K5*(G5/1000)/(0.08205*E5)	=R5+Q5	=S5*12. 01*1000		=S5- (0.00000149 214 /69*F5)- (0.00000039 3785 /18*G5)
5				=D6+ 273.15				=10^ (-H6)	1	=J6*C6 /100	=10^(- (1.17+0.012 *D6))	=10^(- (6.4883- 0.0054*D6))	=10^(- (10.5495- 0.0087*D6))	=K6*L6	=O6*(1+(M6/ I6)+(M6*N6/(I6*I6)))	=P6*F 6/1000	=K6*(G6/1000)/(0.08205*E6)	=R6+Q6	=S6*12. 01*1000		=S6- (0.00000149 214 /69*F6)- (0.00000039 3785 /18*G6)

Appendix 5

Conversion from headspace O_2 to total O_2

A5.1 Theory

The calculation of total O_2 is less complicated than the calculation of total CO_2 from a headspace gas measurement. Calculations are again based on a Henry's Law description of the partitioning of the gas between the headspace and the water, but in this case the complications of a series of equilibrium reactions that follow dissolution are not involved. In this case Henry's law was used in the form

$$K_H = \frac{c_{aq}}{\rho_{O_2}} \qquad \text{Equation A5.1}$$

Where c_{aq} is the aqueous concentration of O_2, and ρ_{O_2} is the partial pressure of O_2 in the headspace. The temperature dependence of the relationship is taken into account by using the following equation for the Henry's Law constant, K_H.

$$K_H = K_H^\theta \times \exp\left(\frac{-\Delta_{soln}H}{R}\left(\frac{1}{T} - \frac{1}{T^\theta}\right)\right) \qquad \text{Equation A5.2}$$

Where K_H is the constant at the temperature of interest, T; K_H^θ is the constant at a standard temperature, T^0; and $\Delta_{soln}H$ is the enthalpy of the solution. R is the gas constant. These equations and the constants used in the spreadsheets were obtained from (Sander 1999).

A5.2 Calculations for photochemical reactor and quartz tube experiments

The spreadsheet used to calculate total O_2 in the photochemical reactor experiments is shown in Table A5.1. Blank spaces are for the entry of experimental data. Column F calculates the pressure in the photochemical reactor at the time of sampling, assuming an initial pressure of 1 atm, and taking into account the removal of gas during the previous sampling events. Column H uses Equation A5.2 to calculate the value of Henry's Constant for the given temperature, and Column I calculates c_{aq} using equation A5.1. Column K uses the ideal gas law to calculate the number of moles of O_2

in the headspace. Column N estimates the number of moles of O_2 removed with the gas sample and Column O calculates the total O_2, including the amount removed during all previous sampling events. All other columns are self-explanatory.

A similar spreadsheet (Table A5.2) was used for quartz tube experiments, but in this case each line of the spreadsheet represented a different tube. The notable difference in this spreadsheet is Column O, which uses the average molality and partial pressure of O_2 in the 0-time samples to estimate the initial amount of O_2 in each tube.

A5.3 Reference

Sander, R. 1999, Compilation of Henry's Law Constants for Inorganic and Organic Species of Potential Importance in Environmental Chemistry. Version 3. April 8, 1999. http://www.mpch-mainz.mpg.de/~sander/res/henry.html

Table A5.1 Spreadsheet used for oxygen calculations in experiments using photochemical reactor.

A	B	C	D	E	F	G	H	I	J	K	L	M	N	O	P	Q
Sample No.	Hours	O_2 %	°C	Kelvins	P(total)	p(O2)	Henry's Constant	molality	n(aq)	n(g)	n(total)	mg O	Removed	Cumulativ e	Total mg O	Net O2 Consumption
1				=D2+273. 15	= 0.99090909^ A2	=F2*C2/10 0	=0.0013*EXP(- 1700*(1/E2-1/298.15))	=G2*H2	=I2*0.7	=G2*0.22/(0.082 05*E2)	=K2+J2	=L2*15.9994* 1000*2	=K2*0.0090 909	=L2+N2	=O2*15.9994* 1000*2	=O2-O2
2				=D3+273. 15	= 0.99090909^ A3	=F3*C3/10 0	=0.0013*EXP(- 1700*(1/E3-1/298.15))	=G3*H3	=I3*0.7	=G3*0.22/(0.082 05*E3)	=K3+J3	=L3*15.9994* 1000*2	=K3*0.0090 909	=L3+N2: N3	=O3*15.9994* 1000*2	=O3-O2
3				=D4+273. 15	= 0.99090909^ A4	=F4*C4/10 0	=0.0013*EXP(- 1700*(1/E4-1/298.15))	=G4*H4	=I4*0.7	=G4*0.22/(0.082 05*E4)	=K4+J4	=L4*15.9994* 1000*2	=K4*0.0090 909	=L4+N2: N4	=O4*15.9994* 1000*2	=O4-O2
4				=D5+273. 15	= 0.99090909^ A5	=F5*C5/10 0	=0.0013*EXP(- 1700*(1/E5-1/298.15))	=G5*H5	=I5*0.7	=G5*0.22/(0.082 05*E5)	=K5+J5	=L5*15.9994* 1000*2	=K5*0.0090 909	=L5+N2: N5	=O5*15.9994* 1000*2	=O5-O2
5				=D6+273. 15	= 0.99090909^ A6	=F6*C6/10 0	=0.0013*EXP(- 1700*(1/E6-1/298.15))	=G6*H6	=I6*0.7	=G6*0.22/(0.082 05*E6)	=K6+J6	=L6*15.9994* 1000*2	=K6*0.0090 909	=L6+N2: N6	=O6*15.9994* 1000*2	=O6-O2
6				=D7+273. 15	= 0.99090909^ A7	=F7*C7/10 0	=0.0013*EXP(- 1700*(1/E7-1/298.15))	=G7*H7	=I7*0.7	=G7*0.22/(0.082 05*E7)	=K7+J7	=L7*15.9994* 1000*2	=K7*0.0090 909	=L7+N2: N7	=O7*15.9994* 1000*2	=O7-O2
7				=D8+273. 15	= 0.99090909^ A8	=F8*C8/10 0	=0.0013*EXP(- 1700*(1/E8-1/298.15))	=G8*H8	=I8*0.7	=G8*0.22/(0.082 05*E8)	=K8+J8	=L8*15.9994* 1000*2	=K8*0.0090 909	=L8+N2: N8	=O8*15.9994* 1000*2	=O8-O2
8				=D9+273. 15	= 0.99090909^ A9	=F9*C9/10 0	=0.0013*EXP(- 1700*(1/E9-1/298.15))	=G9*H9	=I9*0.7	=G9*0.22/(0.082 05*E9)	=K9+J9	=L9*15.9994* 1000*2	=K9*0.0090 909	=L9+N2: N9	=O9*15.9994* 1000*2	=O9-O2
9				=D10+273 .15	= 0.99090909^ A10	=F10*C10/ 100	=0.0013*EXP(- 1700*(1/E10-1/298.15))	=G10*H 10	=I10*0. 7	=G10*0.22/(0.08 205*E10)	=K10+J 10	=L10*15.9994 *1000*2	=K10*0.009 0909	=L10+N2: N10	=O10*15.9994 *1000*2	=O10-O2
10				=D11+273 .15	= 0.99090909^ A11	=F11*C11/ 100	=0.0013*EXP(- 1700*(1/E11-1/298.15))	=G11*H 11	=I11*0. 7	=G11*0.22/(0.08 205*E11)	=K11+J 11	=L11*15.9994 *1000*2	=K11*0.009 0909	=L11+N2: N11	=O11*15.9994 *1000*2	=O11-O2
11				=D12+273 .15	= 0.99090909^ A12	=F12*C12/ 100	=0.0013*EXP(- 1700*(1/E12-1/298.15))	=G12*H 12	=I12*0. 7	=G12*0.22/(0.08 205*E12)	=K12+J 12	=L12*15.9994 *1000*2	=K12*0.009 0909	=L12+N2: N12	=O12*15.9994 *1000*2	=O12-O2

Table A5.2 Spreadsheet used to calculate O_2 in quartz tube experiments.

A	B	C	D	E	F	G	H	I	J	K	L	M	N	O	P
Sample No.	Hours	O2 %	oC	Kelvins	Volume Liquid	Volume Gas	P(total)	p(O2)	Henry's constant	molality	n(aq)	n(g)	n(total)	n(initial)	n(net)
1				=D2+273.15			1	=H2*C2/100	=0.0013*EXP(-1700*(1/E2-1/298.15))	=I2*J2	=K2*F2/1000	=I2*(G2/1000)/(0.08205*E2)	=M2+L2	=F2/1000*0.000229414+0.1907001*(G2/1000)/(0.08205*294.15)	=N2-O2
2				=D3+273.15			1	=H3*C3/100	=0.0013*EXP(-1700*(1/E3-1/298.15))	=I3*J3	=K3*F3/1000	=I3*(G3/1000)/(0.08205*E3)	=M3+L3	=F3/1000*0.000229414+0.1907001*(G3/1000)/(0.08205*294.15)	=N3-O3
3				=D4+273.15			1	=H4*C4/100	=0.0013*EXP(-1700*(1/E4-1/298.15))	=I4*J4	=K4*F4/1000	=I4*(G4/1000)/(0.08205*E4)	=M4+L4	=F4/1000*0.000229414+0.1907001*(G4/1000)/(0.08205*294.15)	=N4-O4
4				=D5+273.15			1	=H5*C5/100	=0.0013*EXP(-1700*(1/E5-1/298.15))	=I5*J5	=K5*F5/1000	=I5*(G5/1000)/(0.08205*E5)	=M5+L5	=F5/1000*0.000229414+0.1907001*(G5/1000)/(0.08205*294.15)	=N5-O5
5				=D6+273.15			1	=H6*C6/100	=0.0013*EXP(-1700*(1/E6-1/298.15))	=I6*J6	=K6*F6/1000	=I6*(G6/1000)/(0.08205*E6)	=M6+L6	=F6/1000*0.000229414+0.1907001*(G6/1000)/(0.08205*294.15)	=N6-O6
6				=D7+273.15			1	=H7*C7/100	=0.0013*EXP(-1700*(1/E7-1/298.15))	=I7*J7	=K7*F7/1000	=I7*(G7/1000)/(0.08205*E7)	=M7+L7	=F7/1000*0.000229414+0.1907001*(G7/1000)/(0.08205*294.15)	=N7-O7
7				=D8+273.15			1	=H8*C8/100	=0.0013*EXP(-1700*(1/E8-1/298.15))	=I8*J8	=K8*F8/1000	=I8*(G8/1000)/(0.08205*E8)	=M8+L8	=F8/1000*0.000229414+0.1907001*(G8/1000)/(0.08205*294.15)	=N8-O8
8				=D9+273.15			1	=H9*C9/100	=0.0013*EXP(-1700*(1/E9-1/298.15))	=I9*J9	=K9*F9/1000	=I9*(G9/1000)/(0.08205*E9)	=M9+L9	=F9/1000*0.000229414+0.1907001*(G9/1000)/(0.08205*294.15)	=N9-O9
9				=D10+273.15			1	=H10*C10/100	=0.0013*EXP(-1700*(1/E10-1/298.15))	=I10*J10	=K10*F10/1000	=I10*(G10/1000)/(0.08205*E10)	=M10+L10	=F10/1000*0.000229414+0.1907001*(G10/1000)/(0.08205*294.15)	=N10-O10